

第 51 回 フラーレン・ナノチューブ・グラフェン 総合シンポジウム

The 51st Fullerenes–Nanotubes–Graphene General Symposium



講演要旨集

Abstracts

2016年9月7日（水）～9日（金）
北海道立道民活動センター かでる2・7
Hokkaido citizens actives center kaderu 2・7

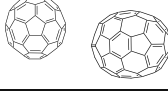
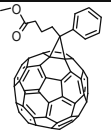
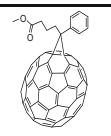
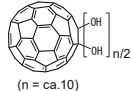
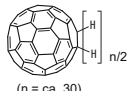
主催 フラーレン・ナノチューブ・グラフェン学会
The Fullerenes, Nanotubes and Graphene Research Society

共催 日本化学会 The Chemical Society of Japan

協賛 日本物理学会 The Physical Society of Japan
応用物理学会 The Japan Society of Applied Physics
高分子学会 The Society of Polymer Science, Japan
電気化学会 The Electrochemical Society of Japan


Research Society

nanom フロンティアカーボンのフラーレン製品

銘柄	分子構造	純度(HPLC面積%、代表値) 内容他	最低数量 (g)
nanom purple フラーレンC60		99	10
		99.5	2
		99.5/昇華精製品	2
		99.9/昇華精製品	1
		99.9/昇華精製/単結晶品	1
nanom orange フラーレンC70		97	1
		98/昇華精製品	0.5
nanom mix 混合フラーレン		C60,C70,その他高次 フラーレンの混合物 ※微粒化品(ST-F)もあります	50
nanom spectra [60]PCBM (phenyl C61-butrylic acid methyl ester)		99	1
		99.5	1
		99.9	0.5
nanom spectra [70]PCBM (phenyl C71-butrylic acid methyl ester)	 主成分	99/異性体トータル ※位置異性体の混合物	0.5
		99.5/異性体トータル ※位置異性体の混合物	0.5
nanom spectra Q100 [60]インデン付加体		99	0.5
nanom spectra Q400 [60]インデン2付加体		99/異性体トータル ※位置異性体の混合物	1
nanom spectra D100 水酸化フラーレン	 (n = ca. 10)	C ₆₀ OH _n n=10を主成分とする混合物	1
nanom spectra A100 水素化フラーレン	 (n = ca. 30)	C ₆₀ H _n n=30を主成分とする混合物	1

※銘柄、取扱数量等は予告無く変更する場合がございます。 ※試験研究用途向けです。

当社製品は、下記から購入いただけます。直接お問い合わせください。

・関東化学株式会社 試薬事業本部

〒103-0022 東京都中央区日本橋室町2-2-1 TEL:03-6214-1090 FAX:03-3241-1047

<http://www.kanto.co.jp> E-mail:reag-info@gms.kanto.co.jp

・中山商事株式会社 筑波営業所 (担当 落合敬宝)

〒300-2651茨城県つくば市鬼ヶ窪1139-1 TEL:029-847-7355 FAX:029-847-1923

E-mail:nst15@nakayama-co.jp

<本資料に関するお問い合わせ先>

フロンティアカーボン株式会社【担当:梶原】

〒100-8086 東京都千代田区丸の内2-6-1丸の内パークビルディング24階

TEL:03-3210-2620 FAX:03-3210-4606 <http://www.f-carbon.com>

※弊社へのお問い合わせはHPよりお願いいたします。

Abstract of The 51st Fullerenes-Nanotubes-Graphene General Symposium

Sponsored by : The Fullerenes, Nanotubes and Graphene Research Society
Co-Sponsored by : The Chemical Society of Japan
Supported by : The Physical Society of Japan
The Japan Society of Applied Physics
The Society of Polymer Science, Japan
The Electrochemical Society of Japan

Date : September 7th (Wed.) – 9th (Fri.), 2016
Place : Hokkaido citizens actives center kaderu 2・7, Kita2, Nishi7,
Chuo-ku, Sapporo, Hokkaido, 060-0002, Japan

Presentation Time : Plenary Lecture (40 min presentation + 5 min discussion)
Special Lecture (25 min presentation + 5 min discussion)
General Lecture (10 min presentation + 5 min discussion)
Poster Preview (1 min presentation without discussion)

第 51 回フラーレン・ナノチューブ・グラフェン総合シンポジウム 講演要旨集

主催：フラーレン・ナノチューブ・グラフェン学会
共催：日本化学会
協賛：日本物理学会、応用物理学会、高分子学会、電気化学会

日時：平成 28 年 9 月 7 日（水）～ 9 日（金）

場所：北海道立道民活動センター かでる 2・7
〒060-0002 北海道札幌市中央区北 2 条西 7 丁目

発表時間：基調講演（発表 40 分＋質疑応答 5 分）
特別講演（発表 25 分＋質疑応答 5 分）
一般講演（発表 10 分＋質疑応答 5 分）
ポスタープレビュー（発表 1 分・質疑応答 なし）

展示団体御芳名 (五十音順、敬称略)

(株) シンキー

(株) 島津製作所

(株) セントラル科学貿易

田中貴金属工業 (株)

(株) ニューメタルスエンドケミカルスコーポレーション

ハイソル (株)

(株) 堀場エステック

(株) 名城ナノカーボン

広告掲載団体御芳名 (五十音順、敬称略)

(株) 池田理化

(株) システムブレイン

(株) セントラル科学貿易

ソーラボジャパン (株)

(株) 東陽テクニカ

ナノフォトン (株)

日本ゼオン (株)

日本電子 (株)

日立工機 (株)

ビタミン C60 バイオリサーチ (株)

フロンティアカーボン (株)

北海道エア・ウォーター (株)

北海道和光純薬 (株)

(株) ムトウ

Contents

Time Table	i
Chairperson	iii
Program	Japanese iv
	English xviii
Abstracts	Plenary Lecture & Special Lecture 1
	General Lecture 9
	Poster Preview 43
Author Index	161

目次

早見表	i
座長一覧	iii
プログラム	和文 iv
	英文 xviii
講演予稿	基調講演&特別講演 1
	一般講演 9
	ポスター発表 43
発表索引	161

プログラム早見表

9月7日 (水)		9月8日 (木)		9月9日 (金)	
9:00	受付開始 9:00 ~ 開場 9:30 ~	9:00	受付開始 9:00 ~ 開場 9:15 ~ 講演開始 9:45 ~	9:00	受付開始 9:00 ~ 開場 9:15 ~ 講演開始 9:45 ~
10:00	講演開始 10:00 ~ 基調講演 (河野 淳一郎) 10:00-10:45	10:00	基調講演 (Jin Zhang) 9:45-10:30	10:00	特別講演 (久 英之) 9:45-10:15
11:00	一般講演 3件 (ナノチューブの物性・ナノチューブの応用) 10:45-11:30	11:00	一般講演 3件 (ナノチューブの物性・ナノチューブの生成と精製) 10:30-11:15	11:00	一般講演 3件 (ナノチューブの物性・グラフェンの応用) 10:15-11:00
12:00	休憩 11:30-11:45	12:00	休憩 11:15-11:30	11:00	休憩 11:00-11:15
13:00	一般講演 3件 (ナノチューブの応用・グラフェン生成・グラフェンの物性) 11:45-12:30	12:00	一般講演 3件 (大澤賞・飯島賞受賞対象者講演) 11:30-12:30	12:00	特別講演 (齋藤 直人) 11:15-11:45
13:00	昼食 (幹事会) 12:30-13:45	13:00	昼食 12:30-13:45	13:00	一般講演 3件 (グラフェンの物性) 11:45-12:30
14:00	特別講演 (宮田 耕充) 13:45-14:15	14:00	若手奨励賞表彰式 13:45-14:00	13:00	昼食 12:30-13:45
15:00	一般講演 4件 (原子層) 14:15-15:15	14:00	総会 14:00-14:30	14:00	ポスタープレビュー (3P-1 ~ 3P-39) 13:45-14:25
16:00	休憩 15:15-15:30	15:00	特別講演 (Don Futaba) 14:30-15:00	15:00	ポスターセッション (展示ホール) 14:25-16:00
17:00	特別講演 (安食博志) 15:30-16:00	15:00	一般講演 3件 (グラフェンの応用) 15:00-15:45	16:00	特別講演 (山越 葉子) 16:00-16:30
18:00	一般講演 3件 (原子層・ナノホーン・ナノワイヤー) 16:00-16:45	16:00	休憩 15:45-16:00	17:00	一般講演 3件 (内包ナノチューブ・フラーレンの化学・フラーレン) 16:30-17:15
19:00	ポスタープレビュー (1P-1 ~ 1P-40) 16:45-17:25	17:00	一般講演 2件 (グラフェンの物性・その他) 16:00-16:30	17:15	
	ポスターセッション (展示ホール) 17:25-19:00	18:00	ポスタープレビュー (2P-1 ~ 2P-39) 16:30-17:10		
		18:45	ポスターセッション (展示ホール) 17:10-18:45		
		19:00	懇親会 (ホテル札幌ガーデンパレス、2F丹頂) 19:00-21:00		
		21:00			

基調講演: 発表40分+質疑5分【2件】
 特別講演: 発表25分+質疑5分【6件】
 賞対象者講演: 発表10分+質疑10分【3件】
 一般講演: 発表10分+質疑5分【30件】
 ポスタープレビュー: 発表1分【118件】

Time table

September 7th (Wed)		September 8th (Thu)		September 9th (Fri)	
9:00	Registration begins at 9:00 KADERU Hall opens at 9:30 Lectures begins at 10:00	9:00	Registration begins at 9:00 KADERU Hall opens at 9:15 Lectures begins at 9:45	9:00	Registration begins at 9:00 KADERU Hall opens at 9:15 Lectures begins at 9:45
10:00	Plenary Lecture (Junichiro Kono) 10:00-10:45	10:00	Plenary Lecture (Jin Zhang) 9:45-10:30	10:00	Special Lecture (Hideyuki Hisashi) 9:45-10:15
11:00	General Lectures [3] (Properties of nanotubes·applications of nanotubes) 10:45-11:30	11:00	General Lectures [3] (Properties of nanotubes·Formation and purification of nanotubes) 10:30-11:15	11:00	General Lectures [3] (Properties of nanotubes·Applications of graphene) 10:15-11:00
	Coffee Break 11:30-11:45	11:00	Coffee Break 11:15-11:30	11:00	Coffee Break 11:00-11:15
12:00	General Lectures [3] (Applications of nanotubes·Graphene synthesis· Properties of graphene) 11:45-12:30	12:00	General Lectures [3] (Lectures of Osawa Award and Iijima Award Nominees) 11:30-12:30	12:00	Special Lectures (Naoto Saito) 11:15-11:45
13:00	Lunch (Administrative meeting) 12:30-13:45	13:00	Lunch 12:30-13:45	13:00	General Lectures [3] (Properties of graphene) 11:45-12:30
14:00	Special Lecture (Yasumitsu Miyata) 13:45-14:15	14:00	Award Ceremony 13:45-14:00	14:00	Lunch 12:30-13:45
15:00	General Lectures [4] (Atomic layers) 14:15-15:15	14:00	General meeting 14:00-14:30	14:00	Poster Preview (3P-1 through 3P-39) 13:45-14:25
	Coffee Break 15:15-15:30	15:00	Special Lecture (Don. Futaba) 14:30-15:00	15:00	Poster Session (Exhibition Hall) 14:25-16:00
	Special Lecture (Hiroshi Ajiki) 15:30-16:00	15:00	General Lectures [3] (Applications of graphene) 15:00-15:45	16:00	Special Lecture (Yoko Yamakoshi) 16:00-16:30
16:00	General Lectures [3] (Atomic layers·Nanohorns· Nanowires) 16:00-16:45	16:00	Coffee Break 15:45-16:00	16:00	General Lectures [3] (Endohedral nanotubes·Chemistry of fullerenes·Fullerenes) 16:30-17:15
17:00	Poster Preview (1P-1 through 1P-40) 16:45-17:25	17:00	General Lectures [2] (Properties of graphene·Other topics) 16:00-16:30	17:00	
18:00	Poster Session (Exhibition Hall) 17:25-19:00	17:00	Poster Preview (2P-1 through 2P-39) 16:30-17:10	17:15	
19:00		18:00	Poster Session (Exhibition Hall) 17:10-18:45		
		18:45			
		19:00	Banquet 2F, Tancho, Hotel Sapporo Garden Palace 19:00-21:00		
		21:00			

Plenary Lecture:40 min + 5 min [2]
 Special Lecture:25 min + 5 min [6]
 Award Nominee Lecture:10 min + 10 min [3]
 General Lecture:10 min + 5 min [30]
 Poster Preview:1 min [118]

座長一覧 (Chairpersons)

9月7日 (水)

セッション	時間	座長
基調講演 (河野 淳一郎)	10:00 ~ 10:45	丸山 茂夫
一般講演 3件	10:45 ~ 11:30	松田 一成
一般講演 3件	11:45 ~ 12:30	大野 雄高
特別講演 (宮田 耕充)	13:45 ~ 14:15	齋藤 理一郎
一般講演 4件	14:15 ~ 15:15	北浦 良
特別講演 (安食 博志)	15:30 ~ 16:00	齋藤 晋
一般講演 3件	16:00 ~ 16:45	保田 諭
ポスタープレビュー	16:45 ~ 17:25	野々口 斐之 大町 遼

9月8日 (木)

セッション	時間	座長
基調講演 (Jin Zhang)	9:45 ~ 10:30	片浦 弘道
一般講演 3件	10:30 ~ 11:15	宮内 雄平
大澤賞受賞対象者講演	11:30 ~ 11:50	中嶋 直敏
飯島賞受賞対象者講演	11:50 ~ 12:30	
特別講演 (Don Futaba)	14:30 ~ 15:00	野田 優
一般講演 3件	15:00 ~ 15:45	宮本 良之
一般講演 2件	16:00 ~ 16:30	秋田 成司
ポスタープレビュー	16:30 ~ 17:10	南本 大穂 蓬田 陽平

9月9日 (金)

セッション	時間	座長
基調講演 (久 英之)	9:45 ~ 10:15	篠原 久典
一般講演 3件	10:15 ~ 11:00	岡田 晋
特別講演 (齋藤 直人)	11:15 ~ 11:45	湯田坂 雅子
一般講演 3件	11:45 ~ 12:30	佐野 正人
ポスタープレビュー	13:45 ~ 14:25	弓削 亮太 小林 慶太
特別講演 (山越 葉子)	16:00 ~ 16:30	前田 優
一般講演 3件	16:30 ~ 17:15	小久保 研

9月7日(水)

基調講演：発表40分+質疑応答5分
特別講演：発表25分+質疑応答5分
一般講演：発表10分+質疑応答5分
ポスタープレビュー：発表1分、質疑応答なし

基調講演 (10:00-10:45)

- 1S-1 Wafer-Scale Monodomain Films of Spontaneously Aligned Single-Wall Carbon Nanotubes
* 河野 淳一郎 1

一般講演 (10:45-11:30)

ナノチューブの物性・ナノチューブの応用

- 1-1 円偏光を用いたカーボンナノチューブと遷移金属カルコゲナイド物質の光学的性質
* 齋藤 理一郎, 佐藤 直道, 辰巳 由樹 9
- 1-2 単層カーボンナノチューブの発光特性の制御
* 前田 優, 武埜 祐哉, 西野 朱音, 南 竣, 山田 道夫, 鈴木 光明, 永瀬 茂 10
- 1-3 Application of carbon nanotubes as electrodes and doping methods in photovoltaics
* 田 日, 丸山 茂夫, 松尾 豊 11

>>>>>> 休憩 (11:30-11:45) <<<<<<<

一般講演 (11:45-12:30)

ナノチューブの応用・グラフェン生成・グラフェンの物性

- 1-4 Mechanically durable and stretchable micro-supercapacitors with elastomeric components harmonized with wearable field-effect transistors
* Fumiaki Tanaka, Atsuko Sekiguchi, Karolina Laszczyk, Kazufumi Kobashi, Shunsuke Sakurai, Don Futaba, Takeo Yamada, Kenji Hata 12
- 1-5 架橋グラフェンナノリボンのウェアスケール集積化合物と合成機構
* 鈴木 弘朗, 金子 俊郎, 澁田 靖, 大野 宗一, 前川 侑毅, 加藤 俊顕 13
- 1-6 溶液中に漂うグラフェンの直接観察
松野 豊, 佐藤 雄哉, 佐藤 光, * 佐野 正人 14

>>>>>> 昼食 (12:30-13:45) <<<<<<<

特別講演 (13:45-14:15)

- 1S-2 面内原子層ヘテロ構造の成長と評価
* 宮田 耕充 2

一般講演 (14:15-15:15)

原子層

- 1-7 Visualization of structural modulation in the charge density wave phase of 1T-TaSe₂ by scanning transmission electron microscopy
* 小林 慶太, 保田 英洋 15
- 1-8 一軸歪み印加による h-BN ナノリボンの極性変調
* 山中 綾香, 岡田 晋 16

9月7日(水)

- 1-9 Germanium Sulfide Photodetectors with High Photosensitivity and Broad Spectral Response
* *Dezhi Tan, Xiaofan Wang, Yuhei Miyauchi, Kazunari Matsuda* 17
- 1-10 Current jump and memory effect in MoS₂ transistor operated at high temperature
* *Tomoki Yamanaka, Masahiro Matsunaga, Ayaka Higuchi, Yuichi Ochiai, Guanchen He, Jonathan P. Bird, Nobuyuki Aoki* 18

>>>>>> 休憩 (15:15-15:30) <<<<<<<

特別講演 (15:30-16:00)

- 1S-3 単層カーボンナノチューブの光学選択則
* *安食 博志* 3

一般講演 (16:00-16:45)

原子層・ナノホーン・ナノワイヤー

- 1-11 Strain Modulation of Electronic Properties in Hexagonal Boron-Nitride Atomic Layers
* *Yoshitaka Fujimoto, Susumu Saito* 19
- 1-12 カーボンナノホーンとシクロデキストリンのホスト・ゲスト錯体形成
* *原野 幸治, 山田 純也, 熊本 明仁, 柴田 直哉, 中村 栄一* 20
- 1-13 コイル直径に対するカーボンナノコイル抵抗率の依存性
* *須田 善行, 中村 康史, 飯田 民夫, 針谷 達, 滝川 浩史, 植 仁志, 島 弘幸* 21

ポスタープレビュー (16:45-17:25)

ポスターセッション (17:25-19:00) (☆) 若手奨励賞候補

フラーレンの化学

- 1P-1 水酸化フラーレン保護金ナノ粒子の調製
* *佐藤 希, 小久保 研, 櫻井 英博* 43
- 1P-2 ジェナミンとフラーレンの一電子移動と水素移動反応によるピロリジノフラーレンの生成
* *伊熊 直彦, 山本 浩之, 小久保 研, 大島 巧* 44

フラーレンの応用

- 1P-3 皮膚の光老化に対するフラーレンの有効性
* *青島 央江, 伊藤 雅之* 45
- 1P-4 Nanoscale Water Droplet Confined in Fullerene Bilayer Vesicles
☆ * *Sai Prakash Maddala, Tatsuya Homma, Ricardo Gorgoll, Koji Harano, Wasim Abuillan, Alexandra Burk, Motomu Tanaka, Eiichi Nakamura* 46

金属内包フラーレン

- 1P-5 Gd@C₆₀(CF₃)₃ の ESR 測定
* *山口 貴久, 中川 綾乃, 篠原 久典, 古川 貢, 加藤 立久* 47

フラーレン

- 1P-6 電場下における PCBM の電子物性
* *古谷 匠, 岡田 晋* 48

9月7日(水)

ナノチューブの物性

- 1P-7 第一原理 DFT 計算によるカルコゲン内包単層カーボンナノチューブの電子状態
* *Yutaka Sato, Yosuke Kataoka, Eita Yokokura, Hironori Ogata* 49
- 1P-8 高純度(6,5)単層カーボンナノチューブのボロメータ性能
枝 淳子, * 蓬田 陽平, 柳 和宏 50
- 1P-9 Superconductivity in WS₂ chiral nanotube
☆ * *Feng Qin, Wu Shi, Toshiya Ideue, Masaro Yoshida, Alla Zak, Reshef Tenne, Tomoka Kikitsu, Daishi Inoue, Daisuke Hashizume, Yoshihiro Iwasa* 51
- 1P-10 The structural contribution to the electrical character of super-growth SWCNT forest through a height dependent study
* *Takayuki Watanabe, Hiroe Kimura, Shigeki Hano, Shunsuke Sakurai, Motoo Yumura, Kenji Hata, Don Futaba* 52

ナノチューブの応用

- 1P-11 Development of Air-stable n-type Thermoelectric Materials with Benzimidazole derivative-doped Single-walled Carbon Nanotubes
☆ * *Yuki Nakashima, Tsuyohiko Fujigaya, Naotoshi Nakashima* 53
- 1P-12 光による化学結合形成を用いた多層カーボンナノチューブ/ポリスチレン複合材料の作製
* 馬場 拓麻, 高田 知哉 54
- 1P-13 塩に誘導される単層 CNT の n 型ドーピングにおけるパイ拡張アリアルクラウンの役割
☆ * 池田 智博, 野々口 斐之, 河合 壯 55
- 1P-14 Improvement of Single-Walled Carbon Nanotube Cathodes for Perovskite Solar Cells
* *Takahiro Sakaguchi, Hayato Kobayashi, Hiroki Suko, Takeshi Okochi, Taiki Inoue, Rong Xiang, Shohei Chiashi, Esko Kauppinen, Shigeo Maruyama* 56
- 1P-15 繰り返し短時間焼成による鉄配位窒素ドーブ被覆垂直配向カーボンナノチューブ酸素還元電極触媒の作製
☆ * 内堀 揚介, 保田 諭, 村越 敬 57

ナノチューブの生成と精製

- 1P-16 SiC ナノチューブ内の新奇構造を有する多層カーボンナノチューブの創製
* 田口 富嗣, 山本 春也, 大場 弘則 58
- 1P-17 Purification of high purity semiconducting single-wall carbon nanotubes with a large diameter of 1.9 nm by gel filtration
☆ * *Boanerges Thendie, Haruka Omachi, Jun Hirotsu, Yutaka Ohno, Ryo Kitaura, Yasumitsu Miyata, Hisanori Shinohara* 59
- 1P-18 高真空下でのアルコール CVD 法による Ru 触媒からの単層カーボンナノチューブ成長
* 藤井 貴之, 桐林 星光, 小川 征悟, 才田 隆広, 成塚 重弥, 丸山 隆浩 60

9月7日(水)

1P-19	Possible mechanism for selective separation of semiconducting single-walled carbon nanotubes	
☆	* 大園 啓太, 利光 史行, 中嶋 直敏	61
内包ナノチューブ		
1P-20	STM/STS studies on Europium nanowires encapsulated in carbon nanotubes	
	* Terunobu Nakanishi, Ryo Kitaura, Shoji Yoshida, Osamu Takeuchi, Hidemi Shigekawa, Hisanori Shinohara	62
グラフェン生成		
1P-21	2段階の無触媒アルコールCVDによるサファイア基板上へのグラフェン直接成長	
	* 上田 悠貴, 山田 純平, 藤原 亨介, 山本 大地, 丸山 隆浩, 成塚 重弥	63
1P-22	窒化ホウ素をテンプレートとしたグラフェンのCVD成長	
☆	* 小川 峻, 小林 佑, 真庭 豊, 宮田 耕充	64
グラフェン応用		
1P-23	Graphene FET of high photosensitivity using schottky diode between graphene and n-type silicon	
	* 小林 史歩, 安野 裕貴, 竹井 邦晴, 有江 隆之, 秋田 成司	65
1P-24	Catalytic properties of non-metal and platinum supported surface-modified nanocarbon materials	
	* 緒方 啓典, 吉竹 晴彦, 佐藤 豊, 西村 智明, 王志朋, 森本 信吾, 橋本 佳男, 遠藤 守信	66
1P-25	光定在波を用いたグラフェン機械共振の非線形制御	
	* 井上 太一, 安野 裕貴, 竹井 邦晴, 有江 隆之, 秋田 成司	67
1P-26	作動電圧に応じてキャパシタと電池双方の挙動を示すオール酸化グラフェンデバイス	
	* 緒方 盟子, 黒木 るり子, 畠山 一翔, 谷口 貴章, 鯉沼 陸央, 松本 泰道	68
1P-27	Suppression of Electrical Conductivity Deterioration of Cu Nanowire by Coating 2D-layered Materials	
	* Nguyen Thanh Cuong, Susumu Okada	69
1P-28	電気化学的酸化還元サイクルによって作製した酸化グラファイト(GtO)電極の電気化学キャパシタンスの評価	
	* 栗屋 恵介, 畠山 一翔, 鯉沼 陸央, 松本 泰道	70
グラフェンの物性		
1P-29	液中グラフェン観察を可能にする顕微鏡のコントラスト機構	
☆	* 佐藤 光, 松野 豊, 佐藤 雄哉, 佐野 正人	71
1P-30	酸化グラフェンの金属浸透現象	
	* 鯉沼 陸央, 緒方 盟子, 松本 泰道	72
1P-31	Enhanced terahertz-wave absorption in monolayer graphene via evanescent wave coupling	
☆	* 原田 要一, M. Shoufie Ukhtary, Minjie Wang, Sanjay K. Srinivasan, Eddwi H. Hasdeo, Ahmad R. T. Nugraha, Weilu Gao, 酒井 裕司, 齋藤 理一郎, 河野 淳一郎	73

9月7日(水)

原子層

- 1P-32 Transverse Magnetic and Transverse Electric Surface Waves in Silicene
* *M. Shoufie Ukhtary, Ahmad R.T Nugraha, Eddwi H. Hasdeo, Riichiro Saito* 74
- 1P-33 polymethylglutarimide を用いた薄膜転写
☆ * 松前 貴司, 須賀 唯知 75
- 1P-34 Energetics and electronic structures of hexagonal GaN thin films and heterostructures
☆ * *Yanlin Gao, Susumu Okada* 76
- 1P-35 WS₂/MoS₂ ヘテロ構造における一次元閉じ込めポテンシャルの形成
* 小林 佑, 吉田 昭二, 櫻田 龍司, 高島 健悟, 山本 貴博, 齊藤 哲輝, 小鍋 哲, 谷口 尚, 渡邊 賢司, 真庭 豊, 武内 修, 重川 秀実, 宮田 耕充 77
- 1P-36 Fabrication and optical properties of vertical heterostructure of monolayer-WSe₂/MoTe₂
☆ * *Takao Yamaoka, Lim En, Koirala Sandhaya, Yuhei Miyauchi, Kazunari Matsuda* 78

ナノ炭素粒子

- 1P-37 炭化水素ネットワークの電子状態と磁性
* 反町 純也, 岡田 晋 79

バイオ

- 1P-38 二機能性タンパク質によるグラフェン-TiO₂ 複合体の作製
☆ * 橋間 裕貴, 石川 泰明, 上沼 睦典, 岡本 尚文, 山下一郎, 浦岡 行治 80

その他

- 1P-39 アゾベンゼン型分散剤を用いたナノカーボン材料の分散制御
* 神徳 啓邦, 松澤 洋子, 木原 秀元, 吉田 勝 81

グラフェン生成

- 1P-40 Effect of the flow regime on graphene growth
*Ya-Ping Hsieh, * Ching-Hua Shih, Yi-Jing Chiu, Mario Hofmann* 82

9月8日(木)

基調講演：発表 40 分＋質疑応答 5 分
特別講演：発表 25 分＋質疑応答 5 分
大澤賞・飯島賞対象者講演：発表 10 分＋質疑応答 10 分
一般講演：発表 10 分＋質疑応答 5 分
ポスタープレビュー：発表 1 分、質疑応答なし

基調講演 (9:45-10:30)

2S-4 Growth of Single-Walled Carbon Nanotubes with Controlled Structure
* Jin Zhang 4

一般講演 (10:30-11:15)

ナノチューブの物性・ナノチューブの生成と精製

2-1 BN ナノチューブへの不純物ドーピング
* 斎藤 晋, 藤本 義隆 22

2-2 Chirality selective synthesis of single-walled carbon nanotubes with sputtered Co-W catalyst and its possible mechanism
* Hua An, Rong Xiang, Hiroki Takezaki, Shinnosuke Ohyama, Yang Qian, Taiki Inoue, Shohei Chiashi, Shigeo Maruyama 23

2-3 Development of new polymeric gels for the M/S separation of single-wall carbon nanotubes
* Guowei Wang, Xiaojun Wei, Atsushi Hirano, Shunjiro Fujii, Takeshi Tanaka, Hiromichi Kataura 24

>>>>>> 休憩 (11:15-11:30) <<<<<<<<

大澤賞受賞対象者講演 (11:30-11:50)

2-4 金属内包フラーレンの炭素ケージ内電子スピンを利用した分子位置検知
* 高野 勇太, 田下 諒, 鈴木 光明, 永瀬 茂, 今堀 博, 赤坂 健 25

飯島賞受賞対象者講演 (11:50-12:30)

2-5 フラビンモノヌクレオチドを用いた、単層カーボンナノチューブの光学異性体純度評価
* 魏 小均, 蓬田 陽平, 平野 篤, 藤井 俊治郎, 田中 丈士, 佐藤 直道, 齋藤 理一郎, 片浦 弘道 26

2-6 Low temperature growth of ultra-high mass density carbon nanotube forests on conductive supports
* 杉目 恒志, Santiago Esconjauregui, Lorenzo D'Arcié, John Robertson 27

>>>>>> 昼食 (12:30-13:45) <<<<<<<<

若手奨励賞表彰式 (13:45-14:00)

FNTG 学会総会 (14:00-14:30)

特別講演 (14:30-15:00)

2S-5 Super-Growth CVD: Past, Present, and Future
* Don Futaba 5

9月8日(木)

一般講演 (15:00-15:45)

グラフェンの応用

- 2-7 Hydrogenation properties of supported metal nanoparticles on graphene
* *Shigehito Isobe, Kengo Omori, Satoshi Yasuda* 28
- 2-8 金属フタロシアニン/還元酸化グラフェンハイブリッド酸素還元触媒の作製
* *村上 慎一, 鯉沼 陸央, 松本 泰道* 39
- 2-9 銅埋込型カーボン電極触媒による酸素還元
* *加藤 優, 武藤 鞠佳, 八木 一三* 30

>>>>>> 休憩 (15:45-16:00) <<<<<<<

一般講演 (16:00-16:30)

グラフェンの物性・その他

- 2-10 酸化グラフェンを用いた新規プロトン/電子混合伝導体
* *畠山 一翔, 鯉沼 陸央, 木田 徹也, 速水 真也, 松本 泰道* 31
- 2-11 陽極酸化によるダイヤモンド電解質溶液ゲート電界効果トランジスタのしきい値シフト
* *稲葉 優文, 五十嵐 圭為, 檜村 卓朗, 阿部 修平, 柴田 将暢, 新谷 幸弘, 平岩 篤, 川原田 洋* 32

ポスタープレビュー (16:30-17:10)

ポスターセッション (17:10-18:45) (☆) 若手奨励賞候補

フラーレンの化学

- 2P-1 種々の置換基を有するトリアゾリウムフラーレンの合成と自己集合性
* *岡田 俊彦, 稲場 沙織, 伊熊 直彦, 櫻井 英博* 83
- 2P-2 Supramolecular Differentiation for Construction of Anisotropic C₆₀ Nanostructures by Time-Programmed Control of Interfacial Growth
☆ * *Kosuke Minami, Partha Bairi, Jonathan P. Hill, Waka Nakanishi, Lok Kumar Shrestha, Liu Chao, Koji Harano, Eiichi Nakamura, Katsuhiko Ariga* 84

フラーレンの応用

- 2P-3 フラーレンカテコールの自己組織化単分子膜を用いた逆型有機太陽電池におけるフィルファクタの向上
* *田 日, 小汲 佳祐, 中川 貴文, 松尾 豊* 85
- 2P-4 固体NMR分光法によるバルクヘテロ接合型有機薄膜太陽電池の局所構造解析
* *河野 紗希, 緒方 啓典* 86

金属内包フラーレン

- 2P-5 open C₆₀ 中の酸素分子の三重項状態
* *加藤 梓, 二子石 師, 村田 靖次郎, 加藤 立久* 87

ナノチューブの物性

- 2P-6 カーボンナノチューブと芳香族アミノ酸の相互作用
* *平野 篤, 岩下 和輝, 白木 賢太郎, 桜庭 俊, 亀田 倫史, 石井 梨恵子, 田中 丈士* 88

9月8日(木)

2P-7	Synthesis of local phenylboronic acid-modified single-walled carbon nanotubes and its PL behavior	
☆	* Hisashi Onitsuka, Tomohiro Shiraki, Naotoshi Nakashima	89
2P-8	二硫化モリブデンナノチューブの構造と物性	
	* 大島 駿太郎, 豊田 雅之, 斎藤 晋	90
2P-9	Theory of optimized power factor of low-dimensional semiconductors and application to semiconducting carbon nanotubes	
	* グエン タン フン, アフマド リドワン トレスナ ヌグラハ, 齋藤 理一郎	91
ナノチューブの応用		
2P-10	Effect of internal structure on the electrical performance of MWCNT-Cu wires	
☆	* Rajyashree Sundaram, Atsuko Sekiguchi, Takeo Yamada, Kenji Hata	92
2P-11	Measurement of photoinduced force acting on polystyrene microsphere by carbon nanotube mechanical resonator	
	* 安田 正明, 竹井 邦晴, 有江 隆之, 秋田 成司	93
2P-12	Photothermoelectric properties of carbon nanotubes terahertz imagers and inspection applications	
☆	* 鈴木 大地, 小田 俊理, 河野 行雄	94
2P-13	Flexible heater and temperature sensor for temperature range higher than 100 °C using multiwall carbon nanotube	
	* Daiki Kobayashi, Kuniharu Takei, Takayuki Arie, Seiji Akita	95
2P-14	Novel method to detect dopamine with high sensitivity based on adsorption onto carbon nanotube surface	
☆	* Takuya Ushiyama, Shigeru Kishimoto, Yutaka Ohno	96
ナノチューブの生成と精製		
2P-15	高真空下でのアルコール CVD 法による Rh 触媒からの単層カーボンナノチューブ成長	
	* 丸山 隆浩, 小澤 顕成, 才田 隆広, 成塚 重弥, 飯泉 陽子, 岡崎 俊也, 飯島 澄男	97
2P-16	二元系触媒のコンビナトリアル探索による単層カーボンナノチューブのカイラリティ選択成長	
☆	* 江戸 倫子, 杉目 恒志, 野田 優	98
2P-17	Substrate design for high efficiency single walled carbon nanotube synthesis	
	* 松本 尚之, 大島 あずさ, 石沢 佐智子, 畠 賢治, フタバ ドン	99
2P-18	Control of catalyst surface states towards synthesis of single chirality single-walled carbon nanotubes using plasma CVD	
☆	* Bin Xu, Toshiro Kaneko, Toshiaki Kato	100
内包ナノチューブ		
2P-19	First-principles calculations of electronic states and solid state NMR parameters in alkali halides encapsulated single-walled carbon nanotubes	
	* 横倉 瑛太, 片岡 洋右, 緒方 啓典	101

9月8日(木)

グラフェン生成

- 2P-20 メラミン蒸気を混合したメタンの CVD による窒素ドーパ多層グラフェンの成長と
キャラクタリゼーション
吉田 貴裕, 土屋 文, * 坂東 俊治 102
- 2P-21 Effect of crystallization of Ni catalyst on low-temperature direct-precipitation of multilayer
graphene
* Jumpei Yamada, Yuki Ueda, Kyosuke Fujiwara, Daichi Yamamoto, Takahiro Maruyama,
Shigeya Naritsuka 103

グラフェンの応用

- 2P-22 グラフェン担体中の非金属元素ドーパントが白金の拡散に与える影響
* 長谷川 瞬, 国貞 雄治, 坂口 紀史 104
- 2P-23 Electrochemical characteristics of enzyme/graphene electrodes
* 中川 典駿, 梁井 皓平, 平野 正浩, 黄 晋二 105
- 2P-24 Electrochemical properties of CVD-grown monolayer graphene oxidized by UV/O₃
treatment
* 梁井 皓平, 中川 典駿, 黄 晋二 106
- 2P-25 細菌や酵母の増殖と生存率に及ぼすグラフェンの効果
* 溝淵 恭平, 中川 典駿, 平野 正浩, 阿部 文快, 黄 晋二 107
- 2P-26 Edge-disorder effect on Id-Vg characteristics of GNR-FETs
☆ * 高島 健悟, 山本 貴博 108

グラフェンの物性

- 2P-27 金属ナノ粒子が吸着したグラフェンの電場応答
* 松原 愛帆, 岡田 晋 109
- 2P-28 Probing interface strain in graphene and boron nitride in-plane heterostructures
☆ * Shintaro Yoshimura, Yu Kobayashi, Shun Ogawa, Shogo Sasaki, Yutaka Maniwa,
Yasumitsu Miyata 110
- 2P-29 トポロジカル欠陥を有するグラフェンの分極と磁性状態
* 丸山 実那, 岡田 晋 111

原子層

- 2P-30 遷移金属ダイカルコゲナイドヘテロ構造のバレー分極マッピング
* 長谷川 勇介, 松田 一成, 宮内 雄平, 毛利 真一郎 112
- 2P-31 Photoluminescence properties of monolayer MoS₂ FETs fabricated by dry-transfer process
☆ * 王 曉凡, 宮内 雄平, 松田 一成 113
- 2P-32 単層 Mo_{1-x}Re_xS₂ 合金の成長と評価
☆ * 森 勝平, 佐々木 将悟, 小林 佑, 劉 崢, 吉田 昭二, 竹内 高広, 重川 秀実,
末永 和知, 真庭 豊, 宮田 耕充 114
- 2P-33 基盤との干渉効果を取り入れた GaTe の光吸収とラマンスペクトルにおける異方性
* 辰巳 由樹, Shengxi Huang, Xi Ling, Huaihong Guo, Teng Yang, Mildred S. Dresselhaus,
齋藤 理一郎 115

9月8日(木)

- 2P-34 電界効果による二層 MoS₂ のバンドギャップ変調
☆ * 齊藤 哲輝, 小林 佑, 渡邊 賢司, 谷口 尚, 真庭 豊, 宮田 耕充 116

ナノワイヤー

- 2P-35 Growth of Diamond Nanocylinder Forest Using Template-Assisted Microwave Plasma
Chemical Vapor Deposition
☆ * Wenxi Fei, Masafumi Inaba, Yu Hirano, Hideki Masuda, Hiroshi Kawarada 117

ナノ炭素粒子

- 2P-36 *In situ* synchrotron X-ray diffraction study of structural changes on neutron-irradiated
highly oriented pyrolytic graphite under static high pressure and temperature
* Tomohiko Hisakuni, Shin-ichi Honda, Masahito Niibe, Mititaka Terasawa,
Yuji Higo, Keisuke Niwase, Hirokazu Izumi, Eiji Taguchi, Tadao Iwata 118

バイオ

- 2P-37 カーボンナノチューブのマウス組織中アップコンバージョン発光イメージング
☆ * 奥平 早紀, 湯田坂 雅子, 飯泉 陽子, 岡崎 俊也, 松田 一成, 宮内 雄平 119

その他

- 2P-38 高分子マトリックス中に炭素繊維を垂直配向・高密度充填した熱界面材料の開発
☆ * 山田 亮, 杉目 恒志, 大沢 利男, 野田 優 120

グラフェンの応用

- 2P-39 Ultrathin graphene-based solar cells
Ya-Ping Hsieh, * Chin-Fu Chen, Mario Hofmann 121

懇親会 (19:00-21:00)

ホテル札幌ガーデンパレス 2F 丹頂

9月9日(金)

特別講演：発表 25 分＋質疑応答 5 分
一般講演：発表 10 分＋質疑応答 5 分
ポスタープレビュー：発表 1 分、質疑応答なし

特別講演 (9:45-10:15)

- 3S-6 カーボンナノチューブの安全性向上検討 ―大気中に殆ど飛散しない CNT の開発―
* 久 英之 6

一般講演 (10:15-11:00)

ナノチューブの物性、グラフェンの応用

- 3-1 Optical Properties of Oxidized (6,5) Single-Wall Carbon Nanotubes
* 大淵 真理, 宮本 良之 33
- 3-2 耐酸性を備えたグラフェン/銀 SERS 基板
* 鈴木 誠也, 吉村 雅満 34
- 3-3 A nanoporous graphene terahertz detector
* Juxian Li, Suzuki Daichi, Shunri Oda, Yoshikazu Ito, Fujita Takeshi, Yukio Kawano 35

>>>>>> 休憩 (11:00-11:15) <<<<<<<<

特別講演 (11:15-11:45)

- 3S-7 カーボンナノチューブの人工関節への応用と安全性
* 齋藤 直人 7

一般講演 (11:45-12:30)

グラフェンの物性

- 3-4 化学変換グラフェン-ピレン連結系の合成と光物性
* 梅山 有和, 白 鎮碩, 今堀 博 36
- 3-5 Diazonium Chemistry for Tunable Grafting and Nanomanipulation
*John Greenwood, Tomoko Inose, Yasuhiko Fujita, Oleksandr Ivasenko, Yoshito Tobe, Steven De Feyter; * Hiroshi Uji-I* 37
- 3-6 ゲート制御型端選択的光酸化によるグラフェンナノリボン形成
* 野内 亮, 松本 守広, 池田 京一郎 38

>>>>>> 昼食 (12:30-13:45) <<<<<<<<

ポスタープレビュー (13:45-14:25)

ポスターセッション (14:25-16:00) (☆) 若手奨励賞候補

フラーレンの化学

- 3P-1 メタノフラーレン誘導体[70]PCBM およびビス[70]PCBM の高選択的合成
* 伊藤 貴敏, 井上 裕太, 岩澤 哲郎, 松元 深, 岩井 利之, 森脇 和之, 高尾 優子, 水野 卓巳, 大野 敏信 122
- 3P-2 C₆₁H₂ および C₇₀ を持つ土星型オリゴチオフェンマクロサイクルの構造決定
* 岡田 洋史, 清水 秀幸, 青柳 忍, 周 彪, 伊與田 正彦, 松尾 豊 123

9月9日(金)

フラーレンの応用

- 3P-3 Preparation of [C₆₀]Fullerene Nanowhisiker-Silver Nanoparticle Composites and Their Catalytic Activity for Oxidation of Tetramethylbenzidine with Hydrogen Peroxide
* Jeong Won Ko, Weon Bae Ko 124
- 3P-4 金属/酸化物多層膜を用いた半透明有機薄膜太陽電池の色制御
* 藤井 俊治郎, 片浦 弘道 125

金属内包フラーレン

- 3P-5 新規 Gd 内包フラーレン誘導体の単離
☆ * 中川 綾乃, 青柳 忍, 大町 遼, 王志永, 石野 勝真, 北浦 良, 篠原 久典 126

ナノチューブの物性

- 3P-6 透過電子顕微鏡その場観察法による多層カーボンナノチューブの通電加熱中の構造と発光に関する研究
☆ * 西川 耕史, 安坂 幸師, 中原 仁, 齋藤 弥八 127
- 3P-7 超音波分散機 PR-1 を用いた CNT 数種の画期的分散ならびに評価手法
* 高塚 隆之 128
- 3P-8 Pyrene dimer and monomer on single-walled carbon nanotubes
☆ * Jinseok Baek, Tomokazu Umeyama, Yuta Sato, Kazu Suenaga, Hiroshi Imahori 129
- 3P-9 マット構造を有する CNT 薄膜の電界下での電子物性
* 古地 健人, 岡田 晋 130

ナノチューブの応用

- 3P-10 Voltage generation by movement of electrolyte solution on carbon nanotube thin film
☆ * Tomohiro Yasunishi, Shigeru Kishimoto, Yutaka Ohno 131
- 3P-11 Controlled n-type doping of carbon nanotube thin-film transistors with salt and crown ether
* Fumiyuki Nihey, Kei Endo, Jiang Pu, Noriyuki Tonouchi, Fusako Sasaki, Yuki Kuwahara, Takeshi Saito, Hiroyuki Endoh 132
- 3P-12 High-yield fabrication of n-type carbon nanotube thin-film transistors on flexible plastic substrate
☆ * Fu-Wen Tan, Jun Hirotani, Tomohiro Yasunishi, Shigeru Kishimoto, Yutaka Ohno 133
- 3P-13 Response to pH of carbon nanotube thin-film transistors for sensor applications
* Kana Hasegawa, Nguyen Viet, Takuya Ushiyama, Shigeru Kishimoto, Yutaka Ohno 134
- 3P-14 1,1'-ビス(ジフェニルホスフィノ)フェロセンを内包した n 型単層カーボンナノチューブの熱電特性
☆ * 飯原 友, 野々口 斐之, 河合 壯 135
- 3P-15 Gradual etching and long-length burning of metallic single-walled carbon nanotubes toward semiconducting nanotube arrays
* Taiki Inoue, Keigo Otsuka, Shohei Chiashi, Shigeo Maruyama 136

ナノチューブの生成と精製

- 3P-16 Effect of 7,8-substituents of Flavin Derivatives on Selective Separation of Single-Walled Carbon Nanotubes
 ☆ * 西村 加奈子, 利光 史行, 中嶋 直敏 137
- 3P-17 Efficient growth and chirality control of single-walled carbon nanotubes by extended alcohol catalytic chemical vapor deposition
 * Bo Hou, Cheng Wu, Yoko Iizumi, Takahiro Morimoto, Toshiya Okazaki, Taiki Inoue, Shohei Chiashi, Rong Xiang, Shigeo Maruyama 138
- 3P-18 Growth of Single-Walled Carbon Nanotubes from Solid-Phase Cobalt Carbide Nanoparticles by Molecular Dynamics Simulations
 * 吉川 亮, 鶴飼 浩行, 高木 勇海, Yann Magnin, 千足 昇平, Christophe Bichara, 丸山 茂夫 139
- 3P-19 In-Plane TEM Imaging of Bimetallic Catalyst for SWNT Growth
 * Rong Xiang, Akihito Kumamoto, Hua An, Taiki Inoue, Shohei Chiashi, Yuichi Ikuhara, Shigeo Maruyama 140

内包ナノチューブ

- 3P-20 カーボンナノチューブの酸化分解反応と内包物質の抽出
 ☆ * 山岸 美保, 大町 遼, 加藤 雅親, 北浦 良, 篠原 久典 141

グラフェン生成

- 3P-21 Growth of Single-Crystal Bi-Layer Graphene Using Alcohol CVD
 * 曾田 将来, Mohamed Atwa, 柏 昂太郎, 上田 直将, 陳 嘯, 井ノ上 泰輝, 項 榮, 千足 昇平, 丸山 茂夫 142
- 3P-22 先進プラズマ CVD によるグラフェンナノリボン合成におけるナノバー触媒種の効果
 ☆ * 和藤 勇太, 鈴木 弘朗, 金子 俊郎, 加藤 俊顕 143

グラフェンの応用

- 3P-23 第一原理計算による、2次元シート材料によるレーザー水分解の促進の研究 II
 * 宮本 良之, Hong Zhang, Xinlu Cheng, Angel Rubio 144
- 3P-24 ゲルクロマトグラフィを用いたグラフェンのサイズによる分離
 * 石黒 駿一, 筈居 高明, 中安 祐太, 田村 直貴, 本間 格 145
- 3P-25 酸化アミンカップリング反応における酸化グラフェン触媒の評価
 * 井坂 琢也, 田嶋 健太郎, 山科 智貴, 太田 豊, 高井 和之 146
- 3P-26 ナノグラフェンホストによる NO_x 吸着の磁気的評価
 西嶋 里美, 山田 朝太郎, * 高井 和之 147
- 3P-27 金電極上のグラフェンへの電気化学的分子修飾
 * 丹野 駿, 佐藤 祐輔, 熊谷 諒太, 中島 浩司, 加藤 優, 保田 諭, 村越 敬, 八木 一三 148
- 3P-28 Fabrication of Graphene Composite Plasmon-Active Photoelectrode
 ☆ * 安田 健介, 南本 大穂, 周 睿風, 保田 諭, 村越 敬 149

9月9日(金)

グラフェンの物性

- 3P-29 時間分解光電子分光法によるグラフェン/SiC(000-1)の超高速キャリアダイナミクスの直接観測
☆ * 染谷 隆史, 吹留 博一, 渡邊 浩, 山本 貴士, 岡田 大, 鈴木 博人, 小川 優, 飯盛 拓嗣, 石井 順久, 金井 輝人, 田島 圭一郎, Baojie Feng, 山本 達, 板谷 治郎, 小森 文夫, 岡崎 浩三, 辛 埴, 松田 巖 150
- 3P-30 化学修飾によるグラフェン端の仕事関数変調
* 平 麗実, 山中 綾香, 岡田 晋 151
- 3P-31 Charge/Covalent Interactions at the Interface between Graphene and Electrolyte
* 鈴木 大輔, 高井 和之 152

原子層

- 3P-32 単層 Nb ドープ WS₂ の成長と光学的性質
☆ * 佐々木 将悟, 小林 佑, 劉 崢, 末永 和知, 真庭 豊, 宮内 雄平, 宮田 耕充 153
- 3P-33 高集積 WS₂ アレイの層数制御合成
☆ * 李 超, 金子 俊郎, 加藤 俊顕 154
- 3P-34 Polarization-resolved photoluminescence spectroscopy on monolayer transition metal dichalcogenides under electrostatic gating
* Wenjin Zhang, Yusuke Hasegawa, Shinichiro Mouri, Kazunari Matsuda, Yuhei Miyauchi 155
- 3P-35 Electron beam lithography induced strain in MoS₂ crystal
☆ * 松永 正広, 樋口 絢香, He Guanchen, 山田 哲史, Krüger Peter, Bird Jonathan, 落合 勇一, 青木 伸之 156

ナノホーン

- 3P-36 Optimization of Preparation Conditions for Fibrous Aggregates of Single-Walled Carbon Nanohorns
* Ryota Yuge, Fumiyuki Nihey, Kiyohiko Toyama, Masako Yudasaka 157

その他

- 3P-37 WS₂ ナノチューブネットワークにおける両極性トランジスタ
☆ * 菅原 光成, 河合 英輝, 蓬田 陽平, 真庭 豊, 岡田 晋, 柳 和宏 158
- 3P-38 Self-assembled nanofibers of fluorinated bisanthene derivatives
* Hironobu Hayashi, Hiroko Yamada 159
- 3P-39 Synthesis of Sulfur-doped Graphene Oxides
* Haruka Omachi, Zois Syrgiannis, Yasuhiro Kinno, Maurizio Prato, Hisanori Shinohara 160

特別講演 (16:00-16:30)

- 3S-8 フラーレン(C₆₀, M₃N@C₈₀)の医薬品応用のための誘導体化
* 山越 葉子 8

一般講演 (16:30-17:15)

内包ナノチューブ・フラーレンの化学・フラーレン

- 3-7 Doping of porous nanostructures
* 塩澤 秀次 39

9月9日(金)

- 3-8 フラーレンカチオン中間体を活用するフラーレンの修飾：転移反応と環化反応
* 松尾 豊 40
- 3-9 A15-structured Cs_3C_{60} : the first non-cubic A_3C_{60} fulleride
* 高林 康裕, *Ruth H. Zadik, Kosmas Prassides* 41

September 7th, Wed.

Plenary Lecture: 40 min (Presentation) + 5 min (Discussion)

Special Lecture: 25 min (Presentation) + 5 min (Discussion)

General Lecture: 10 min (Presentation) + 5 min (Discussion)

Poster Preview: 1 min (Presentation)

Plenary Lecture (10:00-10:45)

- 1S-1 Wafer-Scale Monodomain Films of Spontaneously Aligned Single-Wall Carbon Nanotubes
* *Junichiro Kono* 1

General Lecture (10:45-11:30)

Properties of nanotubes • Applications of nanotubes

- 1-1 Optical Property of Carbon Nanotubes and Low Dimensional Atomic layer materials by using Circular Polarized light
* *Riichiro Saito, Naomichi Sato, Yuki Tatsumi* 9
- 1-2 Control of photoluminescence properties of single-walled carbon nanotubes
* *Yutaka Maeda, Yuya Takehana, Akane Nishino, Shun Minami, Michio Yamada, Mitsuaki Suzuki, Shigeru Nagase* 10
- 1-3 Application of carbon nanotubes as electrodes and doping methods in photovoltaics
* *Il Jeon, Shigeo Maruyama, Yutaka Matsuo* 11

>>>>>> Coffee Break (11:30-11:45) <<<<<<<<

General Lecture (11:45-12:30)

Applications of nanotubes • Graphene synthesis • Properties of graphene

- 1-4 Mechanically durable and stretchable micro-supercapacitors with elastomeric components harmonized with wearable field-effect transistors
* *Fumiaki Tanaka, Atsuko Sekiguchi, Karolina Laszczyk, Kazufumi Kobashi, Shunsuke Sakurai, Don Futaba, Takeo Yamada, Kenji Hata* 12
- 1-5 Wafer-scale integration of suspended graphene nanoribbons and its growth mechanisms
* *Hiroo Suzuki, Toshiro Kaneko, Yasushi Shibuta, Munekazu Ohno, Yuki Maekawa, Toshiaki Kato* 13
- 1-6 Direct observations of graphene and its oxide dispersed in solution
*Yutaka Matsuno, Yu-uya Sato, Hikaru Sato, * Masahito Sano* 14

>>>>>> Lunch Time (12:30-13:45) <<<<<<<<

Special Lecture (13:45-14:15)

- 1S-2 Growth and characterization of in-plane atomic layer heterostructures
* *Yasumitsu Miyata* 2

General Lecture (14:15-15:15)

Atomic layers

- 1-7 Visualization of structural modulation in the charge density wave phase of 1T-TaSe₂ by scanning transmission electron microscopy
* *Keita Kobayashi, Hidehiro Yasuda* 15
- 1-8 Polarity control of h-BN nanoribbons by uniaxial strain
* *Ayaka Yamanaka, Susumu Okada* 16

September 7th, Wed.

- 1-9 Germanium Sulfide Photodetectors with High Photosensitivity and Broad Spectral Response
* *Dezhi Tan, Xiaofan Wang, Yuhei Miyauchi, Kazunari Matsuda* 17
- 1-10 Current jump and memory effect in MoS₂ transistor operated at high temperature
* *Tomoki Yamanaka, Masahiro Matsunaga, Ayaka Higuchi, Yuichi Ochiai, Guanchen He, Jonathan P. Bird, Nobuyuki Aoki* 18

>>>>>> **Coffee Break (15:15-15:30)** <<<<<<<

Special Lecture (15:30-16:00)

- 1S-3 Selection rules of optical excitations for single-walled carbon nanotubes
* *Hiroshi Ajiki* 3

General Lecture (16:00-16:45)

Atomic layers • Nanohorns • Nanowires

- 1-11 Strain Modulation of Electronic Properties in Hexagonal Boron-Nitride Atomic Layers
* *Yoshitaka Fujimoto, Susumu Saito* 19
- 1-12 Host-Guest Complexation of Cyclodextrins on Carbon Nanohorn Particles
* *Koji Harano, Junya Yamada, Akihito Kumamoto, Naoya Shibata, Eiichi Nakamura* 20
- 1-13 Dependence of the resistivity of carbon nanocoils on coil diameter
* *Yoshiyuki Suda, Yasushi Nakamura, Tamio Iida, Toru Harigai, Hirofumi Takikawa, Hitoshi Ue, Hiroyuki Shima* 21

Poster Preview (16:45-17:25)

Poster Session (17:25-19:00) (☆) Candidates for the Young Scientist Poster Award

Chemistry of fullerenes

- 1P-1 Preparation of gold nanoparticles stabilized by water-soluble fullereneol C₆₀(OH)₃₆
* *Nozomi Sato, Ken Kokubo, Hidehiro Sakurai* 43
- 1P-2 Thermal single electron transfer between C₆₀ and dienamines leading to pyrrolidinofullerenes via hydrogen shift of radical intermediates
* *Naohiko Ikuma, Hiroyuki Yamamoto, Ken Kokubo, Takumi Oshima* 44

Applications of fullerenes

- 1P-3 Availability of fullerene for skin photo-aging; Anti-inflammatory and suppression of carboxylated protein generation.
* *Hisae Aoshima, Masayuki Ito* 45
- 1P-4 ☆ Nanoscale Water Droplet Confined in Fullerene Bilayer Vesicles
* *Sai Prakash Maddala, Tatsuya Homma, Ricardo Gorgoll, Koji Harano, Wasim Abuillan, Alexandra Burk, Motomu Tanaka, Eiichi Nakamura* 46

Endohedral metallofullerenes

- 1P-5 ESR measurements of Gd@C₆₀(CF₃)₃
* *Takahisa Yamaguchi, Ayano Nakagawa, Hisanori Shinohara, Ko Furukawa, Tatsuhisa Kato* 47

Fullerenes

- 1P-6 Electronic properties of PCBM under an external electric field
* *Sho Furutani, Susumu Okada* 48

September 7th, Wed.

Properties of nanotubes

- 1P-7 Electronic states of chalcogen encapsulated in single-walled carbon nanotubes studied by First-Principles DFT Calculations
* *Yutaka Sato, Yosuke Kataoka, Eita Yokokura, Hironori Ogata* 49
- 1P-8 Bolometric performance of highly purified (6,5) Single Walled Carbon Nanotubes
*Junko Eda, * Yohei Yomogida, Kazuhiro Yanagi* 50
- 1P-9 Superconductivity in WS₂ chiral nanotube
☆ * *Feng Qin, Wu Shi, Toshiya Ideue, Masaro Yoshida, Alla Zak, Reshef Tenne, Tomoka Kikitsu, Daishi Inoue, Daisuke Hashizume, Yoshihiro Iwasa* 51
- 1P-10 The structural contribution to the electrical character of super-growth SWCNT forest through a height dependent study
* *Takayuki Watanabe, Hiroe Kimura, Shigeki Hano, Shunsuke Sakurai, Motoo Yumura, Kenji Hata, Don Futaba* 52

Applications of nanotubes

- 1P-11 Development of Air-stable n-type Thermoelectric Materials with Benzimidazole derivative-doped Single-walled Carbon Nanotubes
☆ * *Yuki Nakashima, Tsuyohiko Fujigaya, Naotoshi Nakashima* 53
- 1P-12 Fabrication of Multi-walled Carbon Nanotube / Polystyrene Compound Materials through Photo-induced Chemical Bond Formation
* *Takuma Baba, Tomoya Takada* 54
- 1P-13 Role of π -extended Aryl Crown Ethers in the Salt-induced Chemical n-type Doping of Single-walled Carbon Nanotubes
☆ * *Tomohiro Ikeda, Yoshiyuki Nonoguchi, Tsuyoshi Kawai* 55
- 1P-14 Improvement of Single-Walled Carbon Nanotube Cathodes for Perovskite Solar Cells
* *Takahiro Sakaguchi, Hayato Kobayashi, Hiroki Suko, Takeshi Okochi, Taiki Inoue, Rong Xiang, Shohei Chiashi, Esko Kauppinen, Shigeo Maruyama* 56
- 1P-15 Iron-Nitrogen-Doped Vertically Aligned Carbon Nanotube Electrocatalyst Synthesized through Instantaneous and Repetitive Pyrolysis for Oxygen Reduction Reaction
☆ * *Yosuke Uchibori, Satoshi Yasuda, Kei Murakoshi* 57

Formation and purification of nanotubes

- 1P-16 Synthesis of new-structured multi-walled carbon nanotubes inside silicon carbide nanotubes
* *Tomitsugu Taguchi, Shunya Yamamoto, Hironori Ohba* 58
- 1P-17 Purification of high purity semiconducting single-wall carbon nanotubes with a large diameter of 1.9 nm by gel filtration
☆ * *Boanerges Thendie, Haruka Omachi, Jun Hirotani, Yutaka Ohno, Ryo Kitaura, Yasumitsu Miyata, Hisanori Shinohara* 59
- 1P-18 Single-walled carbon nanotube synthesis using Ru catalysts by alcohol catalytic chemical vapor deposition in high vacuum
* *Takayuki Fujii, Hoshimitsu Kiribayashi, Seigo Ogawa, Takahiro Saida, Shigeya Naritsuka, Takahiro Maruyama* 60

September 7th, Wed.

1P-19	Possible mechanism for selective separation of semiconducting single-walled carbon nanotubes	
☆	* Keita Ozono, Fumiyuki Toshimitsu, Naotoshi Nakashima	61
Endohedral nanotubes		
1P-20	STM/STS studies on Europium nanowires encapsulated in carbon nanotubes	
	* Terunobu Nakanishi, Ryo Kitaura, Shoji Yoshida, Osamu Takeuchi, Hidemi Shigekawa, Hisanori Shinohara	62
Graphene synthesis		
1P-21	Two-step growth of graphene directly grown on sapphire substrate by non-catalytic alcohol CVD	
	* Yuki Ueda, Jumpei Yamada, Kyosuke Fujiwara, Daichi Yamamoto, Takahiro Maruyama, Shigeya Naritsuka	63
1P-22	CVD growth of graphene using boron nitride as growth templates	
☆	* Shun Ogawa, Yu Kobayashi, Yutaka Maniwa, Yasumitsu Miyata	64
Applications of graphene		
1P-23	Graphene FET of high photosensitivity using schottky diode between graphene and n-type silicon	
	* Shiho Kobayashi, Yuki Anno, Kuniharu Takei, Takayuki Arie, Seiji Akita	65
1P-24	Catalytic properties of non-metal and platinum supported surface-modified nanocarbon materials	
	* Hironori Ogata, Haruhiko Yoshitake, Yutaka Sato, Tomoaki Nishimura, Zhipeng Wang, Shingo Morimoto, Yoshio Hashimoto, Morinobu Endo	66
1P-25	Control of nonlinearity of suspended graphene resonator by standing of light	
	* Taichi Inoue, Yuki Anno, Kuniharu Takei, Takayuki Arie, Seiji Akita	67
1P-26	All-graphene oxide device with tunable supercapacitor and battery behaviour by the working voltage	
☆	* Chikako Ogata, Ruriko Kurogi, Kazuto Hatakeyama, Takaaki Taniguchi, Michio Koinuma, Yasumichi Matsumoto	68
1P-27	Suppression of Electrical Conductivity Deterioration of Cu Nanowire by Coating 2D-layered Materials	
	* Nguyen Thanh Cuong, Susumu Okada	69
1P-28	Evaluation of the electrochemical capacitance of graphite oxide electrode prepared by the electrochemical oxidation/reduction cycle	
	* Keisuke Awaya, Kazuto Hatakeyama, Michio Koinuma, Yasumichi Matsumoto	70
Properties of graphene		
1P-29	Contrast mechanisms of the fluorescence microscopy that allows direct observations of nanocarbons in solution	
☆	* Hikaru Sato, Yutaka Matsuno, Yu-uya Sato, Masahito Sano	71
1P-30	Metal Permeation into Multi-layered Graphene Oxide Film	
	* Michio Koinuma, Chikako Ogata, Yasumichi Matsumoto	72

September 7th, Wed.

1P-31	Enhanced terahertz-wave absorption in monolayer graphene via evanescent wave coupling	
☆	* Yoichi Harada, M. Shoufie Ukhtary, Minjie Wang, Sanjay K. Srinivasan, Eddwi H. Hasdeo, Ahmad R. T. Nugraha, Weilu Gao, Yuji Sakai, Riichiro Saito, Junichiro Kono	73
Atomic layers		
1P-32	Transverse Magnetic and Transverse Electric Surface Waves in Silicene	
	* M. Shoufie Ukhtary, Ahmad R.T Nugraha, Eddwi H. Hasdeo, Riichiro Saito	74
1P-33	A Scalable Clean Transfer Process with Polymethylglutarimide	
☆	* Takashi Matsumae, Tadatomu Suga	75
1P-34	Energetics and electronic structures of hexagonal GaN thin films and heterostructures	
☆	* Yanlin Gao, Susumu Okada	76
1P-35	Formation of 1D confining potential in MoS ₂ /WS ₂ -based heterostructures	
	* Yu Kobayashi, Shoji Yoshida, Ryuji Sakurada, Kengo Takashima, Takahiro Yamamoto, Tetsuki Saito, Satoru Konabe, Takashi Taniguchi, Kenji Watanabe, Yutaka Maniwa, samu Takeuchi, Hidemi Shigekawa, Yasumitsu Miyata	77
1P-36	Fabrication and optical properties of vertical heterostructure of monolayer-WSe ₂ /MoTe ₂	
☆	* Takao Yamaoka, Lim En, Koirala Sandhaya, Yuhei Miyauchi, Kazunari Matsuda	78
Carbon nanoparticles		
1P-37	Electronic and magnetic properties of porous hydrocarbon networks	
	* Jun-ya Sorimachi, Susumu Okada	79
Bio		
1P-38	Construction of graphene – TiO ₂ hybrid nano-material using bifunctional protein supramolecule	
☆	* Yuki Hashima, Yasuaki Ishikawa, Mutsunori Uenuma, Naofumi Okamoto, Ichiro Yamashita, Yukiharu Uraoka	80
Other topics		
1P-39	Rapid and Reversible Dispersibility Tuning of Carbon Nanomaterials by the Photoisomerisation of an Azobenzene-derived dispersant	
	* Hirokuni Jintoku, Yoko Matsuzawa, Hideyuki Kihara, Masaru Yoshida	81
Graphene synthesis		
1P-40	Effect of the flow regime on graphene growth	
	Ya-Ping Hsieh, * Ching-Hua Shih, Yi-Jing Chiu, Mario Hofmann	82

September 8th, Thu.

Plenary Lecture: 40 min (Presentation) + 5 min (Discussion)
Special Lecture: 25 min (Presentation) + 5 min (Discussion)
Award Nominee Lecture: 10 min (Presentation) + 10 min (Discussion)
General Lecture: 10 min (Presentation) + 5 min (Discussion)
Poster Preview: 1 min (Presentation)

Plenary Lecture (9:45-10:30)

- 2S-4 Growth of Single-Walled Carbon Nanotubes with Controlled Structure
* *Jin Zhang* 4

General Lecture (10:30-11:15)

Properties of nanotubes • Formation and purification of nanotubes

- 2-1 Doping and electronic properties of BN nanotubes
* *Susumu Saito, Yoshitaka Fujimoto* 22
- 2-2 Chirality selective synthesis of single-walled carbon nanotubes with sputtered Co-W catalyst and its possible mechanism
* *Hua An, Rong Xiang, Hiroki Takezaki, Shinnosuke Ohyama, Yang Qian, Taiki Inoue, Shohei Chiashi, Shigeo Maruyama* 23
- 2-3 Development of new polymeric gels for the M/S separation of single-wall carbon nanotubes
* *Guowei Wang, Xiaojun Wei, Atsushi Hirano, Shunjiro Fujii, Takeshi Tanaka, Hiromichi Kataura* 24

>>>>>>> Coffee Break (11:15-11:30) <<<<<<<<

Osawa Award Nominee Lecture (11:30-11:50)

- 2-4 Utilizing a caged electron spin of an endohedral metallofullerene for molecular location sensing
* *Yuta Takano, Ryo Tashita, Mitsuaki Suzuki, Shigeru Nagase, Hiroshi Imahori, Takeshi Akasaka* 25

Iijima Award Nominee Lecture (11:50-12:30)

- 2-5 Evaluation of Enantiomeric Purity of Single-Wall Carbon Nanotubes using Flavin Mononucleotide
* *Xiaojun Wei, Yohei Yomogida, Atsushi Hirano, Shunjiro Fujii, Takeshi Tanaka, Naomichi Sato, Riichiro Saito, Hiromichi Kataura* 26
- 2-6 Low temperature growth of ultra-high mass density carbon nanotube forests on conductive supports
* *Hisashi Sugime, Santiago Esconjauregui, Lorenzo D'Arciè, John Robertson* 27

>>>>>>> Lunch Time (12:30-13:45) <<<<<<<<

Award Ceremony (13:45-14:00)

General Meeting of the FNTG Society (14:00-14:30)

Special Lecture (14:30-15:00)

- 2S-5 Super-Growth CVD: Past, Present, and Future
* *Don Futaba* 5

September 8th, Thu.

General Lecture (15:00-15:45)

Applications of graphene

- 2-7 Hydrogenation properties of supported metal nanoparticles on graphene
* *Shigehito Isobe, Kengo Omori, Satoshi Yasuda* 28
- 2-8 Metal Phthalocyanine/Reduced Graphene Oxide Hybrid Electrocatalyst for cathodic Oxygen Reduction Reaction
* *Shinichi Murakami, Michio Koinuma, Yasumichi Matsumoto* 29
- 2-9 Oxygen reduction reaction catalyzed by copper-incorporated carbon electrocatalysts
* *Masaru Kato, Marika Muto, Ichizo Yagi* 30

>>>>>> Coffee Break (15:45-16:00) <<<<<<<

General Lecture (16:00-16:30)

Properties of graphene • Other topics

- 2-10 Novel Proton/Electron Mixed Conductor using Graphene Oxide
* *Kazuto Hatakeyama, Michio Koinuma, Tetsuya Kida, Shinya Hayami, Yasumichi Matsumoto* 31
- 2-11 Threshold shift of diamond electrolyte-solution gate field-effect transistor by anodic oxidation
* *Masafumi Inaba, Keisuke Igarashi, Takuro Naramura, Shuhei Abe, Masanobu Shibata, Yukihiro Shintani, Atsushi Hiraiwa, Hiroshi Kawarada* 32

Poster Preview (16:30-17:10)

Poster Session (17:10-18:45) (★) Candidates for the Young Scientist Poster Award

Chemistry of fullerenes

- 2P-1 Synthesis and self-aggregation properties of various triazoliumfullerene
* *Toshihiko Okada, Saori Inaba, Naohiko Ikuma, Hidehiro Sakurai* 83
- 2P-2 Supramolecular Differentiation for Construction of Anisotropic C₆₀ Nanostructures by Time-Programmed Control of Interfacial Growth
☆ * *Kosuke Minami, Partha Baire, Jonathan P. Hill, Waka Nakanishi, Lok Kumar Shrestha, Liu Chao, Koji Harano, Eiichi Nakamura, Katsuhiko Ariga* 84

Applications of fullerenes

- 2P-3 Enhancement of Fill Factor in Inverted Organic Solar Cells using Self-Assembled Monolayer of Fullerene Catechol
* *Il Jeon, Keisuke Ogumi, Takafumi Nakagawa, Yutaka Matsuo* 85
- 2P-4 Solid-State NMR Studies on the Aggregated Structures in Organic Bulk Heterojunction Solar Cells
* *Saki Kawano, Hironori Ogata* 86

Endohedral metallofullerenes

- 2P-5 Triplet state of molecular oxygen in open C₆₀
* *Azusa Kato, Tsukasa Futagoishi, Yasujiro Murata, Tatsuhisa Kato* 87

September 8th, Thu.

Properties of nanotubes

- 2P-6 Interactions between carbon nanotubes and aromatic amino acids
* *Atsushi Hirano, Kazuki Iwashita, Kentaro Shiraki, Shun Sakuraba, Tomoshi Kameda, Rieko Ishii, Takeshi Tanaka* 88
- 2P-7 Synthesis of local phenylboronic acid-modified single-walled carbon nanotubes and its PL behavior
☆ * *Hisashi Onitsuka, Tomohiro Shiraki, Naotoshi Nakashima* 89
- 2P-8 Geometries and electronic properties of MoS₂ nanotube
* *Shuntaro Oshima, Masayuki Toyoda, Susumu Saito* 90
- 2P-9 Theory of optimized power factor of low-dimensional semiconductors and application to semiconducting carbon nanotubes
* *Nguyen Tuan Hung, Ahmad Ridwan Tresna Nugraha, Riichiro Saito* 91

Applications of nanotubes

- 2P-10 Effect of internal structure on the electrical performance of MWCNT-Cu wires
☆ * *Rajyashree Sundaram, Atsuko Sekiguchi, Takeo Yamada, Kenji Hata* 92
- 2P-11 Measurement of photoinduced force acting on polystyrene microsphere by carbon nanotube mechanical resonator
* *Masaaki Yasuda, Kuniharu Takei, Takayuki Arie, Seiji Akita* 93
- 2P-12 Photothermoelectric properties of carbon nanotubes terahertz imagers and inspection applications
☆ * *Daichi Suzuki, Shunri Oda, Yukio Kawano* 94
- 2P-13 Flexible heater and temperature sensor for temperature range higher than 100 °C using multiwall carbon nanotube surface
* *Daiki Kobayashi, Kuniharu Takei, Takayuki Arie, Seiji Akita* 95
- 2P-14 Novel method to detect dopamine with high sensitivity based on adsorption onto carbon nanotube
☆ * *Takuya Ushiyama, Shigeru Kishimoto, Yutaka Ohno* 96

Formation and purification of nanotubes

- 2P-15 Single-walled carbon nanotube synthesis by alcohol catalytic CVD in high vacuum using Rh catalysts
* *Takahiro Maruyama, Akinari Kozawa, Takahiro Saida, Shigeya Naritsuka, Yoko Iizumi, Toshiya Okazaki, Sumio Iijima* 97
- 2P-16 Combinatorial screening of binary metal catalyst for chirality-selective growth of single-wall carbon nanotubes
☆ * *Michiko Edo, Hisashi Sugime, Suguru Noda* 98
- 2P-17 Substrate design for high efficiency single walled carbon nanotube synthesis
* *Naoyuki Matsumoto, Azusa Oshima, Sachiko Ishizawa, Kenji Hata, Don Futaba* 99
- 2P-18 Control of catalyst surface states towards synthesis of single chirality single-walled carbon nanotubes using plasma CVD
☆ * *Bin Xu, Toshiro Kaneko, Toshiaki Kato* 100

September 8th, Thu.

Endohedral nanotubes

- 2P-19 First-principles calculations of electronic states and solid state NMR parameters in alkali halides encapsulated single-walled carbon nanotubes
* *Eita Yokokura, Yosuke Kataoka, Hironori Ogata* 101

Graphene synthesis

- 2P-20 CVD growth of nitrogen doped multilayered graphene by mixing the melamine vapor to methane and their characterization
*Takahiro Yoshida, Bun Tsuchiya, * Shunji Bandow* 102
- 2P-21 Effect of crystallization of Ni catalyst on low-temperature direct-precipitation of multilayer graphene
* *Jumpei Yamada, Yuki Ueda, Kyosuke Fujiwara, Daichi Yamamoto, Takahiro Maruyama, Shigeya Naritsuka* 103

Applications of graphene

- 2P-22 Diffusion of Pt atoms on non-metallic atom-doped graphene support
* *Syun Hasegawa, Yuji Kunisada, Norihito Sakaguchi* 104
- 2P-23 Electrochemical characteristics of enzyme/graphene electrodes
* *Noritoshi Nakagawa, Kouhei Yanai, Masahiro Hirano, Shinji Koh* 105
- 2P-24 Electrochemical properties of CVD-grown monolayer graphene oxidized by UV/O₃ treatment
* *Kouhei Yanai, Noritoshi Nakagawa, Shinji Koh* 106
- 2P-25 The effect of graphene on growth and viability of bacteria and yeast
* *Kyohei Mizobuchi, Noritoshi Nakagawa, Masahiro Hirano, Fumiyoshi Abe, Shinji Koh* 107
- 2P-26 Edge-disorder effect on Id-Vg characteristics of GNR-FETs
☆ * *Kengo Takashima, Takahiro Yamamoto* 108

Properties of graphene

- 2P-27 Effect of metal nanoparticles on carrier accumulation in graphene under an electric field
* *Manaho Matsubara, Susumu Okada* 109
- 2P-28 Probing interface strain in graphene and boron nitride in-plane heterostructures
☆ * *Shintaro Yoshimura, Yu Kobayashi, Shun Ogawa, Shogo Sasaki, Yutaka Maniwa, Yasumitsu Miyata* 110
- 2P-29 Polarity and magnetism of rippled graphene with topological defect
* *Mina Maruyama, Susumu Okada* 111

Atomic layers

- 2P-30 Valley polarization mapping in transition metal dichalcogenides heterostructures
* *Yusuke Hasegawa, Kazunari Matsuda, Yuhei Miyauchi, Shinichiro Mouri* 112
- 2P-31 Photoluminescence properties of monolayer MoS₂ FETs fabricated by dry-transfer process
☆ * *Wang Xiaofan, Yuhei Miyauchi, Kazunari Matsuda* 113

September 8th, Thu.

- 2P-32 Growth and characterization of monolayer $\text{Mo}_{1-x}\text{Re}_x\text{S}_2$ alloys
☆ * Shohei Mori, Shogo Sasaki, Yu Kobayashi, Liu Zheng, Shoji Yoshida, Takahiro Takeuchi, Hidemi Shigekawa, Kazutomo Suenaga, Yutaka Maniwa, Yasumitsu Miyata 114
- 2P-33 Anisotropic optical absorption and Raman spectra in GaTe with the interference effect of the substrates
* Yuki Tatsumi, Shengxi Huang, Xi Ling, Huaihong Guo, Teng Yang, Mildred S. Dresselhaus, Riichiro Saito 115
- 2P-34 Bandgap modulation of bilayer MoS_2 by electric field effect
☆ * Tetsuki Saito, Yu Kobayashi, Kenji Watanabe, Takashi Taniguchi, Yutaka Maniwa, Yasumitsu Miyata 116
- Nanowires**
- 2P-35 Growth of Diamond Nanocylinder Forest Using Template-Assisted Microwave Plasma Chemical Vapor Deposition
☆ * Wenxi Fei, Masafumi Inaba, Yu Hirano, Hideki Masuda, Hiroshi Kawarada 117
- Carbon nanoparticles**
- 2P-36 *In situ* synchrotron X-ray diffraction study of structural changes on neutron-irradiated highly oriented pyrolytic graphite under static high pressure and temperature
* Tomohiko Hisakuni, Shin-ichi Honda, Masahito Niibe, Mititaka Terasawa, Yuji Higo, Keisuke Niwase, Hirokazu Izumi, Eiji Taguchi, Tadao Iwata 118
- Bio**
- 2P-37 Upconversion photoluminescence imaging of carbon nanotubes in mice tissues
☆ * Saki Okudaira, Masako Yudasaka, Yoko Iizumi, Toshiya Okazaki, Kazunari Matuda, Yuhei Miyauchi 119
- Other topics**
- 2P-38 Thermal interface materials of vertically aligned carbon fibers embedded densely in polymer matrix
☆ * Ryo Yamada, Hisashi Sugime, Toshio Osawa, Suguru Noda 120
- Applications of graphene**
- 2P-39 Ultrathin graphene-based solar cells
Ya-Ping Hsieh, * Chin-Fu Chen, Mario Hofmann 121

Banquet (19:00-21:00)

2F, Tancho, Hotel Sapporo Garden Palace

September 9th, Fri.

Special Lecture: 25 min (Presentation) + 5 min (Discussion)
General Lecture: 10 min (Presentation) + 5 min (Discussion)
Poster Preview: 1 min (Presentation)

Special Lecture (9:45-10:15)

- 3S-6 A Study about improving Safety of Carbon Nanotube - Development of Non-airborne type Carbon Nanotube -
* *Hideyuki Hisashi* 6

General Lecture (10:15-11:00)

Properties of nanotubes • Applications of graphene

- 3-1 Optical Properties of Oxidized (6,5) Single-Wall Carbon Nanotubes
* *Mari Ohfuchi, Yoshiyuki Miyamoto* 33
- 3-2 Graphene coated silver substrate for SERS with acid tolerance
* *Seiya Suzuki, Masamichi Yoshimura* 34
- 3-3 A nanoporous graphene terahertz detector
* *Juxian Li, Suzuki Daichi, Shunri Oda, Yoshikazu Ito, Fujita Takeshi, Yukio Kawano* 35

>>>>>>> **Coffee Break (11:00-11:15)** <<<<<<<<

Special Lecture (11:15-11:45)

- 3S-7 Carbon nanotube application and safety in artificial joints
* *Naoto Saito* 7

General Lecture (11:45-12:30)

Properties of graphene

- 3-4 Synthesis and Photophysical Properties of Chemically Converted Graphene–Pyrene Linked Systems
* *Tomokazu Umeyama, Jinseok Baek, Imahori Hiroshi* 36
- 3-5 Diazonium Chemistry for Tunable Grafting and Nanomanipulation
*John Greenwood, Tomoko Inose, Yasuhiko Fujita, Oleksandr Ivasenko, Yoshito Tobe, Steven De Feyter, * Hiroshi Uji-I* 37
- 3-6 Graphene Nanoribbon Fabrication by Gate-Controlled Edge-Selective Photo-Oxidation
* *Ryo Nouchi, Morihiro Matsumoto, Keiichiro Ikeda* 38

>>>>>>> **Lunch Time (12:30-13:45)** <<<<<<<<

Poster Preview (13:45-14:25)

Poster Session (14:25-16:00) (★) Candidates for the Young Scientist Poster Award

Chemistry of fullerenes

- 3P-1 Preparation of methanofullerene derivatives: [70]PCBM and bis-[70]PCBM with high regioselectivity
* *Takatashi Ito, Yuta Inoue, Tetsuo Iwasawa, Fukashi Matsumoto, Toshiyuki Iwai, Kazuyuki Moriwaki, Yuko Takao, Takumi Mizuno, Toshinobu Ohno* 122
- 3P-2 Structure Determination of Saturn-Like Oligothiophene Macrocyclic with C₆₁H₂ and C₇₀
* *Hiroshi Okada, Hideyuki Shimizu, Shinobu Aoyagi, Biao Zhou, Masahiko Iyoda, Yutaka Matsuo* 123

September 9th, Fri.

Applications of fullerenes

- 3P-3 Preparation of [C₆₀]Fullerene Nanowhisker-Silver Nanoparticle Composites and Their Catalytic Activity for Oxidation of Tetramethylbenzidine with Hydrogen Peroxide
* *Jeong Won Ko, Weon Bae Ko* 124
- 3P-4 Color tuning of semitransparent organic solar cells using oxide/metal/oxide transparent anode
* *Shunjiro Fujii, Hiromichi Kataura* 125

Endohedral metallofullerenes

- 3P-5 Isolation of a missing Fullerenes Gd@C_{2n} derivatives
☆ * *Ayano Nakagawa, Shinobu Aoyagi, Haruka Omachi, Zhiyong Wang, Katsuma Ishino, Ryo Kitaura, and Hisanori Shinohara* 126

Properties of nanotubes

- 3P-6 *In-situ* TEM study on structure and optical emission during Joule heating of a multiwall carbon nanotube
☆ * *Koushi Nishikawa, Koji Asaka, Hitoshi Nakahara, Yahachi Saito* 127
- 3P-7 Novel Dispersion and Evaluation Method for CNTs by Using Ultrasonic Mixer,PR-1
* *Takatsuka Takayuki* 128
- 3P-8 Pyrene dimer and monomer on single-walled carbon nanotubes
☆ * *Jinseok Baek, Tomokazu Umeyama, Yuta Sato, Kazu Suenaga, Hiroshi Imahori* 129
- 3P-9 Electronic structure of CNT thin films with nanoscale interfaces under an electronic field
* *Taketo Kochi, Susumu Okada* 130

Applications of nanotubes

- 3P-10 Voltage generation by movement of electrolyte solution on carbon nanotube thin film
☆ * *Tomohiro Yasunishi, Shigeru Kishimoto, Yutaka Ohno* 131
- 3P-11 Controlled n-type doping of carbon nanotube thin-film transistors with salt and crown ether
* *Fumiyuki Nihey, Kei Endo, Jiang Pu, Noriyuki Tonouchi, Fusako Sasaki, Yuki Kuwahara, Takeshi Saito, Hiroyuki Endoh* 132
- 3P-12 High-yield fabrication of n-type carbon nanotube thin-film transistors on flexible plastic substrate
☆ * *Fu-Wen Tan, Jun Hirotsu, Tomohiro Yasunishi, Shigeru Kishimoto, Yutaka Ohno* 133
- 3P-13 Response to pH of carbon nanotube thin-film transistors for sensor applications
* *Kana Hasegawa, Nguyen Viet, Takuya Ushiyama, Shigeru Kishimoto, Yutaka Ohno* 134
- 3P-14 n-Type Thermoelectric Properties of Single-walled Carbon Nanotubes encapsulating 1,1'-Bis(diphenylphosphino)ferrocene
☆ * *Yu Iihara, Yoshiyuki Nonoguchi, Tsuyoshi Kawai* 135
- 3P-15 Gradual etching and long-length burning of metallic single-walled carbon nanotubes toward semiconducting nanotube arrays
* *Taiki Inoue, Keigo Otsuka, Shohei Chiashi, Shigeo Maruyama* 136

September 9th, Fri.

Formation and purification of nanotubes

- 3P-16 Effect of 7,8-substituents of Flavin Derivatives on Selective Separation of Single-Walled Carbon Nanotubes
☆ * *Kanako Nishimura, Fumiyuki Toshimitsu, Naotoshi Nakashima* 137
- 3P-17 Efficient growth and chirality control of single-walled carbon nanotubes by extended alcohol catalytic chemical vapor deposition
* *Bo Hou, Cheng Wu, Yoko Iizumi, Takahiro Morimoto, Toshiya Okazaki, Taiki Inoue, Shohei Chiashi, Rong Xiang, Shigeo Maruyama* 138
- 3P-18 Growth of Single-Walled Carbon Nanotubes from Solid-Phase Cobalt Carbide Nanoparticles by Molecular Dynamics Simulations
* *Ryo Yoshikawa, Hiroyuki Ukai, Takagi Yukai, Yann Magnin, Shohei Chiashi, Christophe Bichara, Shigeo Maruyama* 139
- 3P-19 In-Plane TEM Imaging of Bimetallic Catalyst for SWNT Growth
* *Rong Xiang, Akihito Kumamoto, Hua An, Taiki Inoue, Shohei Chiashi, Yuichi Ikuhara, Shigeo Maruyama* 140

Endohedral nanotubes

- 3P-20 Oxidative Decomposition of Carbon Nanotubes and Extraction of Encapsulated Materials
☆ * *Miho Yamagishi, Haruka Omachi, Masachika Kato, Ryo Kitaura, Hisanori Shinohara* 141

Graphene synthesis

- 3P-21 Growth of Single-Crystal Bi-Layer Graphene Using Alcohol CVD
* *Masaki Sota, Mohamed Atwa, Kotaro Kashiwa, Naomasa Ueda, Xiao Chen, Taiki Inoue, Rong Xiang, Shohei Chiashi, Shigeo Maruyama* 142
- 3P-22 Effects of nanobar-catalyst types on structure of graphene nanoribbon grown with advanced plasma CVD
☆ * *Yuta Wato, Hiroo Suzuki, Toshiro Kaneko, Toshiaki Kato* 143

Applications of graphene

- 3P-23 Enhancement of laser-induced water decomposition by 2D sheets studied by first-principles simulations II
* *Yoshiyuki Miyamoto, Hong Zhang, Xinlu Cheng, Angel Rubio* 144
- 3P-24 Size separation of graphene nanosheets by gel chromatography
* *Shunichi Ishiguro, Takaaki Tomai, Yuta Nakayasu, Naoki Tamura, Itaru Honma* 145
- 3P-25 Evaluation of GO Catalyst regarding oxidative amine coupling reaction
* *Takuya Isaka, Kentaro Tajima, Tomoki Yamashina, Yutaka Ohta, Kazuyuki Takai* 146
- 3P-26 Magnetic Characterization of NO_x adsorption by Nanographene Host Material
*Satomi Nishijima, Asataro Yamada, * Kazuyuki Takai* 147
- 3P-27 Electrochemical grafting of aryl molecules onto graphene on Au
* *Shun Tanno, Yusuke Sato, Ryota Kumagai, Koji Nakashima, Masaru Kato, Satoshi Yasuda, Kei Murakoshi, Ichizo Yagi* 148
- 3P-28 Fabrication of Graphene Composite Plasmon-Active Photoelectrode
☆ * *Kensuke Yasuda, Hiro Minamimoto, Ruifeng Zhou, Satoshi Yasuda, Kei Murakoshi* 149

September 9th, Fri.

Properties of graphene

- 3P-29 Direct observation of ultrafast carrier dynamics in graphene on SiC(000-1) studied by time- and angle-resolved photoemission spectroscopy
☆ * *Takashi Someya, Hirokazu Fukidome, Hiroshi Watanabe, Takashi Yamamoto, Masaru Okada, Hakuto Suzuki, Yu Ogawa, Takushi Iimori, Nobuhisa Ishii, Teruto Kanai, Keiichiro Tashima, Baojie Feng, Susumu Yamamoto, Jiro Itatani, Fumio Komori, Kozo Okazaki, Shik Shin, Iwao Matsuda* 150
- 3P-30 Work function modulation of edge functionalized graphene nanoflakes
* *Remi Taira, Ayaka Yamanaka, Susumu Okada* 151
- 3P-31 Charge/Covalent Interactions at the Interface between Graphene and Electrolyte
* *Daisuke Suzuki, Kazuyuki Takai* 152

Atomic layers

- 3P-32 Growth and optical properties of Nb-doped WS₂ monolayers
☆ * *Shogo Sasaki, Yu Kobayashi, Zheng Liu, Kazutomo Suenaga, Yutaka Maniwa, Yuhei Miyauchi, Yasumitsu Miyata* 153
- 3P-33 Layer number controlled synthesis of integrated WS₂ array
☆ * *Li Chao, Kaneko Toshiro, Kato Toshiaki* 154
- 3P-34 Polarization-resolved photoluminescence spectroscopy on monolayer transition metal dichalcogenides under electrostatic gating
* *Wenjin Zhang, Yusuke Hasegawa, Shinichiro Mouri, Kazunari Matsuda, Yuhei Miyauchi* 155
- 3P-35 Electron beam lithography induced strain in MoS₂ crystal
☆ * *Masahiro Matsunaga, Ayaka Higuchi, Guan Chen He, Tetsushi Yamada, Peter Krüger, Jonathan Bird, Yuichi Ochiai, Nobuyuki Aoki* 156

Nanohorns

- 3P-36 Optimization of Preparation Conditions for Fibrous Aggregates of Single-Walled Carbon Nanohorns
* *Ryota Yuge, Fumiyuki Nihey, Kiyohiko Toyama, Masako Yudasaka* 157

Other topics

- 3P-37 Ambipolar transistors based on random networks of WS₂ nanotubes
☆ * *Mitsunari Sugahara, Kawai Hideki, Yohei Yomogida, Yutaka Maniwa, Susumu Okada, Kazuhiro Yanagi* 158
- 3P-38 Self-assembled nanofibers of fluorinated bisanthene derivatives
* *Hironobu Hayashi, Hiroko Yamada* 159
- 3P-39 Synthesis of Sulfur-doped Graphene Oxides
* *Haruka Omachi, Zois Syrgiannis, Yasuhiro Kinno, Maurizio Prato, Hisanori Shinohara* 160

September 9th, Fri.

Special Lecture (16:00-16:30)

- 3S-8 Functionalization of C₆₀ and M₃N@C₈₀ for bioapplication
* *Yoko Yamakoshi* 8

General Lecture (16:30-17:15)

Endohedral nanotubes • Chemistry of fullerenes • Fullerenes

- 3-7 Doping of porous nanostructures
* *Hidetsugu Shiozawa* 39
- 3-8 Fullerene Modification by Using Fullerene Cation Intermediate: Migration and Cyclization
* *Yutaka Matsuo* 40
- 3-9 A15-structured Cs₃C₆₀ : the first non-cubic A₃C₆₀ fulleride
* *Yasuhiro Takabayashi, Ruth H. Zadik, Kosmas Prassides* 41

基調講演・特別講演
Plenary & Special Lectures

1S-1 ~ 1S-3

2S-4 ~ 2S-5

3S-6 ~ 3S-8

Wafer-Scale Monodomain Films of Spontaneously Aligned Single-Wall Carbon Nanotubes

Weilu Gao¹, Xiaowei He¹, and Junichiro Kono^{1,2,3}

¹*Department of Electrical & Computer Engineering, Rice University, Houston, Texas, USA*

²*Department of Physics & Astronomy, Rice University, Houston, Texas, USA*

³*Department of Materials Science & NanoEngineering, Rice University, Houston, Texas, USA*

One of the grand challenges in nanoscience and nanotechnology is how to create macroscopic devices by assembling nano-objects while preserving their rich variety of extraordinary properties. For example, the one-dimensional character of electrons, phonons, and excitons in individual single-wall carbon nanotubes (SWCNTs) leads to extremely anisotropic electronic, thermal, and optical phenomena that have stimulated much interest in diverse disciplines, but their macroscopic manifestations have been limited. Therefore, worldwide efforts are in progress to develop ways to produce large-scale architectures of aligned SWCNTs.

Here, we report a simple and robust method for preparing exceptionally large ($> \text{cm}^2$) monodomain films of aligned SWCNTs based on spontaneous alignment that occurs during slow vacuum filtration. The produced films are globally aligned within $\pm 1.5^\circ$ (the nematic order parameter ~ 1) and are highly packed, containing 10^6 nanotubes in a cross-sectional area of $1 \mu\text{m}^2$. The film thickness is controllable from a few nm to ~ 100 nm; sufficiently thick films act as ideal polarizers in the terahertz frequency range. This method is universally applicable to SWCNTs synthesized by various methods.

Moreover, by combining this method with recently developed sorting techniques, we fabricated highly aligned and chirality-enriched SWCNT thin-film devices. Semiconductor-enriched devices exhibited polarized light emission, polarization-dependent photocurrent, and anisotropic conductivities and transistor action with high on/off ratios. These results significantly advance the frontier of research toward scalable carbon-based electronics and photonics.

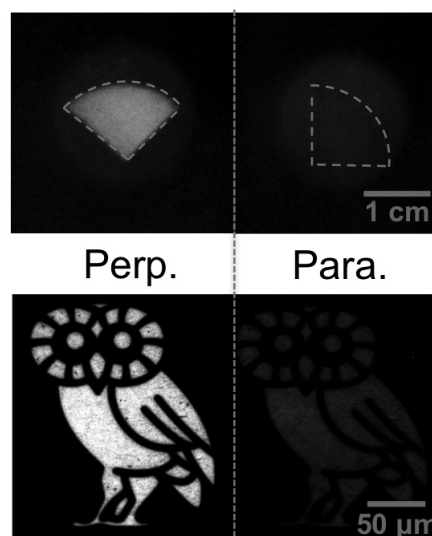


Fig.1: The film is opaque to light polarized parallel to the SWCNT alignment direction and transparent to light polarized perpendicular to the alignment direction on a macroscopic scale (top) and a microscopic scale (bottom). Note also that the film can be easily patterned using conventional photolithography techniques (bottom).

[1] X. He, W. Gao, L. Xie, B. Li, Q. Zhang, S. Lei, J. M. Robinson, E. H. Háróz, S. K. Doorn, R. Vajtai, P. M. Ajayan, W. W. Adams, R. H. Hauge, and J. Kono, *Nature Nanotechnology* **11**, 633 (2016).

Corresponding Author: Junichiro Kono

Tel: +1-713-348-2209, Fax: +1-713-348-3091

E-mail: kono@rice.edu

Growth and characterization of in-plane atomic layer heterostructures

○Yasumitsu Miyata^{1,2}

¹ *Department of Physics, Tokyo Metropolitan University, Hachioji 192-0397, Japan*

² *JST-PRESTO, Kawaguchi, Saitama 332-0012, Japan*

Semiconductor heterojunction interfaces have been an important topic, both in modern solid state physics and in electronics and optoelectronics applications. Recently, the in-plane heterostructures of atomically-thin transition metal dichalcogenides (TMDCs, Fig.1a) are expected to realize one-dimensional (1D) electronic systems at their heterointerface due to their tunable electronic properties. Even though there have been several reports on the growth and device studies, it is still an important challenge to develop the microscopic basis of electronic properties of such atomic-layer heterojunction interfaces. For this purpose, we have fabricated high-quality TMDC atomic layers and various heterostructures based on TMDCs [1-5]. Herein, we report on unique electrical potential modulations of heterojunction interfaces based on TMDC atomic layers [5].

Chemical vapor deposition (CVD) was used to prepare high-quality TMDC samples on exfoliated graphite flakes, as reported in our previous paper [1]. As shown in Fig. 1b, WS₂ (or MoS₂) grains are initially synthesized on the graphite, after which the second growth process of another TMDCs is conducted with firstly-grown grains. Scanning tunneling microscopy/spectroscopy (STM/STS) analyses revealed that the monolayer systems have atomically-sharp interface structure, and form conventional type II heterojunction with staggered gap [3]. Interestingly, we found that the bilayer samples showed the formation of 1D confining potential (potential barrier) in the valence (conduction) band around the heterointerface [5]. The present findings indicate that the atomic layer heterojunctions provide a novel approach to realizing tunable 1D electrical potential for embedded quantum wires and ultrashort barriers of electrical transport.

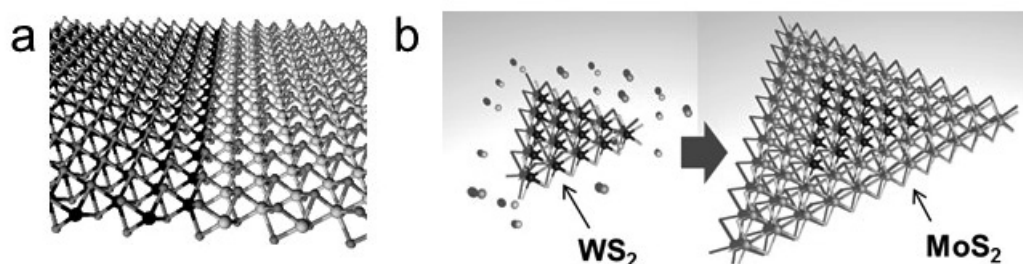


Figure 1. (a) Structure model of in-plane MoS₂/WS₂ heterostructure and (b) its growth process by chemical vapor deposition.

[1] Y. Kobayashi *et al.*, *ACS Nano*, 9, 4056 (2015).

[2] Y. Kobayashi *et al.*, *Nano Res.*, 8, 3261 (2015).

[3] S. Yoshida, *et al.*, *Sci. Rep.*, 5, 14808 (2015).

[4] S. Sasaki *et al.*, *Appl. Phys. Express* 9, 071201 (2016).

[5] Y. Kobayashi *et al.*, *Sci. Rep.*, in press.

Corresponding Author: Y. Miyata

Tel: +81-42-677-2508, E-mail: ymiyata@tmu.ac.jp

Selection rules of optical excitations for single-walled carbon nanotubes

Hiroshi Ajiki

School of Science and Engineering, Tokyo Denki University, Hatoyama 350-0394, Japan

A single-walled carbon nanotube (SWNT) has cylindrical structure of a seamlessly rolled-up graphene. Because of its characteristic structure, the SWNT can be a metal or a semiconductor whose bandgap is inversely proportional to the diameter, and the bandgap can be changed by applying a magnetic flux passing through the tube axis due to the Aharonov-Bohm (AB) effect [1]. These attractive properties can be directly observed from optical spectra. To analyze the electronic states from the optical spectra, it is necessary to know optical selection rules. The selection rules of a SWNT depend on the direction of light polarization because of its cylindrical structure [1]. Interestingly, spectral peaks corresponding to optically allowed transitions do not appear for light polarization perpendicular to the tube axis [1]. This fact comes from the depolarization field arising from induced charge density on the cylindrical surface.

An optically excited electron-hole pair forms a bound state called an exciton. The exciton effects are significant in low dimensional systems such as the SWNT. In fact, the binding energy of the exciton in a SWNT reaches a few hundred millielectronvolts, and thus the excitons can be observed at room temperature [1]. Because of the exciton effects, spectral peaks become large and narrow for light polarization parallel to the tube axis, and small but well-defined peaks appear in spite of the depolarization effect for perpendicular polarization. The small peaks originate from the bonding states (bright states) of degenerate excitons around the K and K' points, which is formed via an electron-hole exchange interaction. The anti-bonding states of the K and K' excitons are optically inactive states (dark states) [1]. As a matter of fact, the dark states have a slight oscillator strength (quasidark states) because the degeneracy of the K and K' excitons is lifted due to the intrinsic band asymmetry of the electron and hole [2]. The band asymmetry parameters can be evaluated by observing intensity ratio of the quasidark to bright states in photo-luminescence excitation spectra.

The optical selection rules are valid when the light wavelength is much larger than the diameter of a SWNT, and this condition is fully satisfied in the usual situation. This means that the selection rules are violated for a high-gradient light field, that is, the field intensity significantly changes across the diameter of the SWNT. Such a high-gradient light field is generated by exciting surface plasmons. We have shown the selection-rule breakdown for perpendicular polarization of an isolated SWNT placed in a nanogap of a metallic nanodimer [3]. Although the Raman signal for the perpendicular polarization is weak, we can detect the signal because of the strong enhancement of the light field due to the surface plasmons. The breakdown of the selection rules has been numerically simulated [3]. This study indicates that the metallic nanostructures not only enhances the light intensity, but increases the optical excitation channels beyond the selection rules.

[1] H. Ajiki, *J. Phys.: Cond. Matt.* **24**, 483001 (2012) and referecnes therein.

[2] Y. Miyauchi, H. Ajiki, and S. Maruyama, *Phys. Rev. B* **81**, 121415(R).

[3] M Takase, H.Ajiki, Y.Mizumoto, K. Komeda, M. Nara, H. Nabika, S. Yasuda, H. Ishihara, and K. Murakoshi, *Nat. Photonics*, **7**, 550 (2013).

Corresponding Author: H. Ajiki

Tel: +81-49-296-2912, Fax: +81-49-296-5720,

E-mail: ajiki@mail.dendai.ac.jp

Growth of Single-Walled Carbon Nanotubes with Controlled Structure

Jin ZHANG

Center for Nanochemistry, College of Chemistry and Molecular Engineering, Peking University, Beijing, 100871, P.R. China
Email: jinzhang@pku.edu.cn

In this talk, we will focus on the controlled growth of SWNTs arrays with ultra-high density, high ratio semiconducting properties and special chiral angles. For the SWNTs arrays with ultra-high density, Trojan catalysts (released from substrate) was developed and the density can be as high as 150 tubes/ μm . Combining Trojan catalysts with Mo nanoparticles as cooperating catalysts, the ultra-high density SWNTs arrays with wafer-scale area can be obtained. For the SWNTs arrays with semiconducting properties, oxides catalysts with oxygen vacancy, bimetal catalysts and uniform Mo_2C catalyst were used to grow semiconducting SWNTs arrays and ratio of semiconducting tubes can be higher than 95%. For the SWNTs arrays with special chiral angles, based on the analysis the thermodynamics and kinetics of SWNTs growth, horizontally (2m, m) SWNT arrays with chiral angle of 19.1° , tubes arrays with small chiral angles (less than 10°) and near-armchair tubes ((n, n-1) or (n, n-2)) can be grown under different conditions.

Reference:

- [1] Chemical Vapor Deposition Synthesis of Near Zigzag Single-walled Carbon Nanotubes with Stable Tube-Catalyst Interface, *Science Advance*, 2016, 2, e1501729.
- [2] Growth of High-Density Horizontally Aligned SWNT Arrays using Trojan Catalysts, *Nat. Commun.* 6 (2015), 6099.
- [3] Growth of Horizontal Semiconducting SWNT Arrays with Density Higher than 100 tubes/ μm using Ethanol/Methane Chemical Vapor Deposition, *J. Am. Chem. Soc.* 2016, 138, 6727-6730.
- [4] Diameter-Specific Growth of Semiconducting SWNT Arrays Using Uniform Mo_2C Solid Catalyst, *J. Am. Chem. Soc.* 137(28) (2015), 8904-8907.
- [5] Selective Scission of C–O and C–C Bonds in Ethanol using Bimetal Catalysts for the Preferential Growth of Semiconducting SWNT Arrays, *J. Am. Chem. Soc.*, 137 (3) (2015), 1012-1015.

Super-Growth CVD: Past, Present, and Future

○ Don N. Futaba^{1,2}

¹ *National Institute of Advanced Industrial Science and Technology (AIST), Central 5, 1-1-1-Higashi, Tsukuba, Ibaraki, 305-8565, Japan.*

² *2Technology Research Association for Single Wall Carbon Nanotubes (TASC), Central 5, 1-1-1 Higashi, Tsukuba, Ibaraki, 305-8565, Japan.*

Over two decades have passed since the discovery and structural elucidation of the carbon nanotube (CNT), however industry has yet to fully realize the promise of their unique properties. For single wall carbon nanotubes (SWCNTs), one of the major obstacles has been the low cost, industrial availability. Twelve years ago, water-assisted chemical vapor deposition (Super-growth CVD) was developed which demonstrated the highly efficient synthesis of high purity SWCNTs, and recently, an industrial production plant, based on this technology went into operation to realize the industrial use of SWCNTs.

This presentation will provide an overview of our recent progress in the synthesis and application of millimeter-scale, vertically-aligned SWNTs using Super-growth CVD. First, I will provide a brief description of the day Super-Growth CVD was serendipitously discovered. Second, I will describe the current state. Finally, I will present our future outlook.

This paper is based on results obtained from a project commissioned by the New Energy and Industrial Technology Development Organization (NEDO).

Corresponding Author: D. Futaba

Tel: +81-28-861-4654, Fax: +81-28-861-4851

E-mail: d-futaba@aist.go.jp

A Study about improving Safety of Carbon Nanotube - Development of Non-airborne type Carbon Nanotube -

○Hideyuki Hisashi

*Mitsubishi Corporation, Marunouchi Park Bldg.6-1.Marunouchi 2-chome,
Chiyoda-Ku, Tokyo, 100-8086.Japan*

Carbon Nanotube (CNT) has a light-weight and numerous mechanical properties, such as higher mechanical strength, higher electrical conductivity, higher thermal conductivity and higher heat resistance. So CNT sometimes is described as “Black diamond in 21st century”. Other hand the worldwide demand for CNT has not grown in these 30 years. In spite of those advantages, the worldwide demand volume of CNT is several hundred metric tons per year and is much smaller than that of Carbon Black (ca. 12 million metric tons per year). Except its relatively high price, the main reason for this low-demand of CNT is on the public uncertainties over its safety. Recently several researches comment as follows. “On manufacturing process of CNT and CNT related products, the concern about CNT’s penetration into worker’s abdominal cavity is not realistic. But we must emphasize the inhalation risk.” The bulk density value of CNT is in a smallest-level category among all raw materials. So by handling CNT in manufacturing process, CNT particles are released into the air and remain for a long time. Airborne CNT particle will not settle easily. Then this situation will cause the inhalation risk. Granulation is one of the common methods to increase bulk density of powdery materials. Because the surface of CNT has less activity about chemical reaction and physical interaction with other materials, it is very difficult to granulate CNT by using of typical binders such as water. Then we developed new method of granulating CNT based on CNT’s lipophilicity. As the result we became its bulk density to be more than ten times value. This new granulated CNT powder is suppressed about the ability of its airborne and is also effective to keep the hands clean during treatment of CNT by hands. Furthermore, during compounding of CNT into plastics or rubber matrix, the new granulated CNT powder is easily fed into extruders without bridging in the hopper. In that compounded material, the new granulated CNT particle is highly dispersed into plastics or rubber matrix. And we can select a high concentration of CNT particle. We indicate the new granulated CNT in the pictures, as shown Fig.1(a). The diameter of each particle is 1-2mm, and we can find that each particle is an agglomeration of smaller particles (Fig. 1(b)).

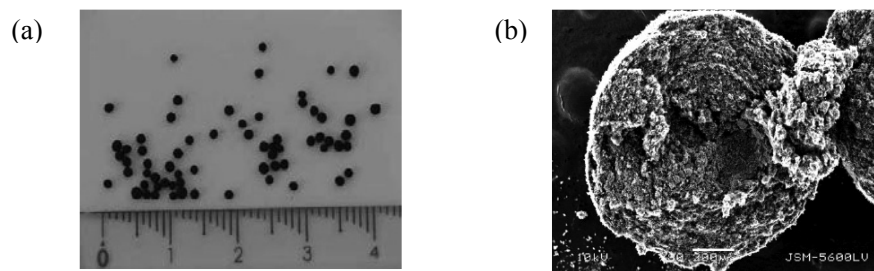


Figure 1. Photographs of (a) Granulated CNT and (b) the enlarged granules.

Carbon nanotube application and safety in artificial joints

Naoto Saito

*Institute for Biomedical Sciences, Interdisciplinary Cluster for Cutting Edge Research,
Shinshu University, Asahi 3-1-1, Matsumoto 390-8621, Japan*

We have been working to conjugate carbon nanotubes (CNTs) to polyethylene for use in sliding and rotating parts of artificial joints. These elements of polyethylene artificial joints wear away with long-term use, leading to breakage of the joint and the need for surgical revision. With this in mind, we are developing more durable artificial joints made of polyethylene and CNTs to reduce the rate of wear loss. As the number of patients receiving artificial joint replacement surgery has been rising worldwide each year, those requiring revision surgery have also increased steadily. Thus, the clinical application of sturdier CNT-based artificial joints is expected to dramatically reduce the need for revision and extend the use of prostheses to younger patients.

Of course, the concerns regarding the safety of CNT inhalation are completely different from those associated with long-term CNT implants. Therefore, safety testing of CNTs and their composites as implantation materials in the body must be performed, including the assessment of inflammatory reactions, acute cytotoxicity, irritation, sensitization, chronic toxicity, and carcinogenicity. Further research and development in this area will lead to the production of superior CNT biomaterials of benefit to a larger number of patients in the near future [1].

[1] N. Saito *et al.* Chem Rev. **123**, 456 (2015).

Corresponding Author: N. Saito

Tel: +81-263-37-2405, Fax: +81-263-37-3549

E-mail: saitoko@shinshu-u.ac.jp

Functionalization of C₆₀ and M₃N@C₈₀ for bioapplication

○Yoko Yamakoshi¹

¹ *Laboratorium für Organische Chemie, ETH Zürich, CH 8093, Switzerland*

Based on the unique physicochemical properties of fullerenes such as photosensitivity and metal encapsulation, bioapplication of fullerenes in areas such as photodynamic therapy and MRI contrast agents have attracted significant attentions in recent decades. Because of their extreme hydrophobicity, the preparation of water-soluble fullerene materials is critical for bioapplications. We have been focusing on the preparation of biocompatible fullerene materials by complexation or conjugation with non-toxic poly(vinylpyrrolidone) (PVP) [1].

In this study, we have developed a bis-carboxylic acid Prato derivative of C₆₀ (**3**) as a useful precursor for further attachment of functional groups such as water-soluble polymers or targeting moieties. A glycine derivative (**1**) was subjected to the 1,3-dipolar cycloaddition (Prato reaction) to C₆₀ in the presence of formaldehyde to provide [6,6]-adduct **2** (Fig. 1, Scheme 1). The deprotection of ^tBu group under acidic condition successfully provided bis-carboxylic acid derivative **3**, which was subjected to the further additions of water-soluble PEG and PVP or solid phase peptide synthesis to provide biocompatible fullerenes such as C₆₀-PEG **4**, C₆₀-peptide **5**, and C₆₀-PVP **7** [2]. A similar Prato reaction was carried out to M₃N@C₈₀ (M = Sc, Lu, Y, Gd) using *N*-ethylglycine as a dipole to evaluate their reactivity (Fig. 1, Scheme 2). In contrast to the result of C₆₀, the [5,6]-adduct (**9a-b**) was obtained as a major product in the reaction of Sc₃N@C₈₀ and Lu₃N@C₈₀, whereas a mixture of [5,6]- and [6,6]-adducts (**9c-d**, **8c-d**) was obtained in the case of Y₃N@C₈₀ and Gd₃N@C₈₀. Further kinetic and computational studies indicated that the kinetic products of Prato reactions of M₃N@C₈₀ (M = Sc, Lu, Y, Gd) were all [6,6]-adducts **8a-d**, which isomerized to the thermodynamic product [5,6]-adducts **9a-d** in a manner dependent on the size of endohedral metal cluster inside C₈₀, which affected the energy level of the adducts due to the pyramidalization and degree of strain of the metal cluster (M₃N). In the presence of excess amount of dipole, the bis-adducts **10c-d** were efficiently obtained from Y₃N@C₈₀ and Gd₃N@C₈₀ [3].

[1] Yamakoshi, Y *et al. J. Chem. Soc., Chem. Commun.* 517 (1994); Iwamoto, Y *et al. Chem. Commun.* 4805 (2006); Oriana, S *et al. Chem. Comm.* **49**, 9302 (2013).

[2] Aroua, S. *et al. Org. Lett.* **16**, 1688 (2014); *Polymer Chem.* **6**, 2616 (2015).

[3] Aroua, S. *et al. J. Am. Chem. Soc.* **134**, 20242 (2012); *Chem. Eur. J.* **20**, 14032 (2014); *J. Am. Chem. Soc.* **137**, 58 (2015).

Corresponding Author: Y. Yamakoshi

Tel: +41-44-633-6420

E-mail: yamakoshi@org.chem.ethz.ch

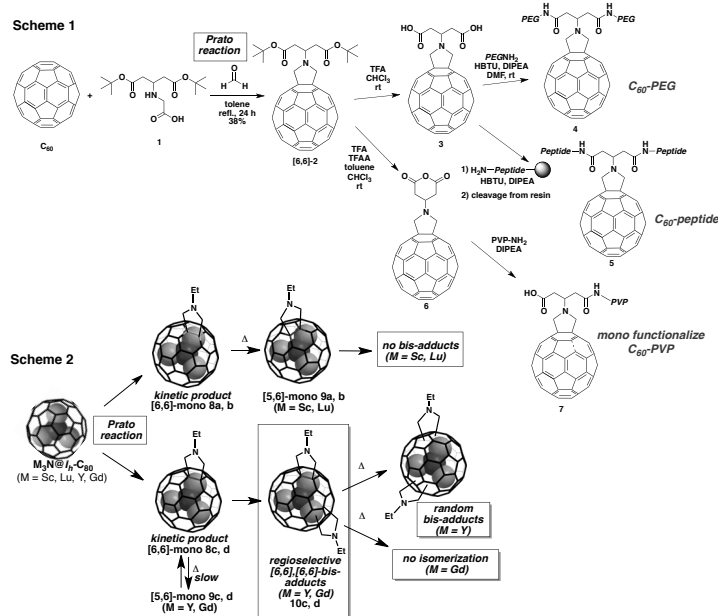


Fig. 1: Prato reactions of C₆₀ and M₃N@C₈₀ (M = Sc, Lu, Y, Gd).

一般講演
General Lectures

1-1 ~ 1-13

2-1 ~ 2-11

3-1 ~ 3-9

Optical Property of Carbon Nanotubes and
Low Dimensional Atomic layer materials
by using Circular Polarized light

Riichiro Saito[○], Naomichi Sato, Yuki Tatsumi

Department of Physics, Tohoku University, Sendai

Circular polarized light has an angular moment which shows unique properties on carbon nanotubes and transition metal dichalcogenide (TMD) atomic layer materials. In the case of carbon nanotubes, we can observe the circular dichroism (CD) for chiral nanotubes. In the case of TMDs, we can observe the valley and spin polarization. In this presentation, we discuss common optical properties by perturbation theory for electro-magnetic fields.

In particular, for the CD of carbon nanotubes, we discuss the selection rule for the circular polarized light. As for valley polarization, spin and valley degree of freedom of TMD are selectively excited by circular polarized light, which are expressed by inner product of the polarization vector and dipole vectors. Within the tight binding method, we calculated dipole vectors for graphene, carbon nanotubes, and TMDs, from which we can see the common physics in the optical properties. The calculated results are compared with the recent experimental results. We would like to propose possible experimental observation in the optical properties with use of circular polarized light.

Corresponding Author: Riichiro Saito

e-mail : rsaito@flex.phys.tohoku.ac.jp

Web: <http://flex.phys.tohoku.ac.jp>

Control of photoluminescence properties of single-walled carbon nanotubes

○Yutaka Maeda¹, Yuya Takehana¹, Akane Nishino¹, Shun Minami¹, Michio Yamada¹,
Mitsuaki Suzuki,¹ Shigeru Nagase²

¹ Department of Chemistry, Tokyo Gakugei University, Tokyo 184-8501, Japan

² Fukui Institute for Fundamental Chemistry, Kyoto University, Kyoto 606-8103, Japan

PL spectroscopy is a very powerful tool for the assignment of semiconducting single-walled carbon nanotubes (SWNTs) because it can be separately observed the E₁₁ PL peaks of individual SWNTs by the excitation of the E₂₂ transitions. Recently, NIR light has received significant attention in bio-imaging applications owing to the high transparency of biological tissues. To improve the performance of SWNTs as biological imaging materials, chirality-separated semiconducting SWNTs have been investigated, and have exhibited superior performance than their non-separated ones. In addition, it was reported that sidewall functionalization of SWNTs results in a new and bright PL peak in the longer wavelength region. Therefore, the sidewall functionalization is an effective method for controlling the PL characteristics of SWNTs for practical applications. We report herein the control of PL properties of SWNTs by chemical functionalization/defunctionalization protocols.

Photoreaction of SWNTs with disulfide in the presence of oxygen afforded oxidized SWNTs. It was revealed that the photoreaction proceeds more favorably in metallic and small-diameter SWNTs than the other types of SWNTs on the basis of their Raman and absorption spectral changing [1]. When (6,5)-SWNT enriched sample was used, the intensity of the characteristic absorption and PL peak at ~976 nm (E₁₁) decreased with an increase of a new PL peak at ~1150 nm. Large Stokes shift allows use of E₁₁ energy for the excitation due to the easy elimination of Rayleigh scattering. It is noteworthy that the excitation of E₁₁ energy increases the excitation efficiency and decreases phototoxicity in their application. To control PL properties, dialkylation of (6,5)-SWNTs enriched sample and subsequent thermal treatment were conducted. Dialkylated SWNTs (R¹-SWNTs-R²) were synthesized using alkyllithium (R¹Li) and alkyl bromide (R²Br) [2,3]. Interestingly, the degree of functionalization is tunable by steric hindrance of alkyl groups used in the reductive alkylation. In addition, the subsequent thermal treatment is effective to control their degree of functionalization. Interestingly, new PL peaks were observed depending on the substituents and condition of the thermal treatment [4]. This methodology has advantages for their productivity, high PL efficiency, and large Stokes shift.

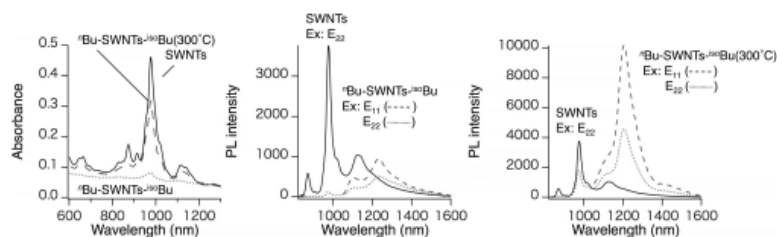


Figure. Absorption and PL spectra of SWNTs and functionalized SWNTs.

[1] Y. Maeda *et al.* *J. Am. Chem. Soc.* **135**, 6356 (2013). [2] Y. Maeda *et al.* *Org. Lett.* **12**, 996 (2010).
[3] Y. Maeda *et al.* *J. Am. Chem. Soc.* **134**, 18101 (2012). [4] Y. Maeda *et al.* *Chem. Commun.* **51**, 13462 (2015).

Corresponding Author: Y. Maeda

Tel: +81-42-329-7512, Fax: +81-42-329-7512

E-mail: ymaeda@u-gakugei.ac.jp

Application of carbon nanotubes as electrodes and doping methods in photovoltaics

○Il Jeon¹, Shigeo Maruyama^{1,2}, Yutaka Matsuo^{1,3}

¹ *Department of Mechanical Engineering, The University of Tokyo, Tokyo 113-8656, Japan*

² *National Institute of Advanced Industrial Science and Technology, Ibaraki 305-8564, Japan*

³ *University of Science and Technology of China, Anhui 230026, China*

Carbon nanotubes (CNTs) have emerged as materials for next-generation electrodes in solar cells (SCs), offering a possible alternative to indium tin oxide (ITO). CNTs have excellent mechanical flexibility and are composed entirely of naturally abundant carbon. Therefore, CNT transparent conductive films in SCs have been the subject of active research.

For the research in SCs, organic SCs and perovskite SCs have attracted a great deal of attention as solution-processable and flexible light-harvesting devices that have the potential to meet the world's energy needs. The efficiency of SCs has increased tremendously with the recent emergence of perovskite SCs. As the result, power conversion efficiency (PCE) has reached as high as 20%. [1] However, SC flexibility is still limited by the use of ITO, which is bendable but not completely flexible like the carbon materials.

We have been working with diverse materials and their applications in solar cells. So far, we have demonstrated applications of CNTs as the transparent electrode, replacing ITO and metal electrodes in SCs. This was done with the doping, which is mandatory to maximize the conductivity and transmittance. We investigated several types of dopants and methods depending on the applications. ITO-free, CNT-based organic SCs showed a PCE of 6.04% with the PTB7:PC₇₁BM photoactive layer, in which MoO_x thermal doping was used. [2] On the other hand, metal-free window-like CNT-based organic SCs produced a PCE of 4.1% [3], because it was transparent solar cells, which could be used for window applications. For this research, we used MoO_x doping and HNO₃ doping, separately. For the application in perovskite SCs, diluted HNO₃ (35 v/v%)-doped CNT-based device produced the highest PCE of 6.32% which was about 70% of the ITO-based device (9.05%). [4] This work opened up the research area of single-walled CNT applied SCs, as similar works have followed up, citing our papers. Especially our first paper on CNT application in organic SCs [1] reached a citation number of 16 in less than a year.

My next step of this research is to use both CNTs and graphene as the electrodes to achieve full carbon SCs. This will be full-carbon SCs, which will again open up a new field of research that many researchers around the globe will follow.

[1] M. Saliba *et al.* *Energ. Environ. Sci.* **9**, 1989 (2016).

[2] I. Jeon, K. Cui, A. Anisimov, A. Nasibulin, E. I. Kauppinen, S. Maruyama, Y. Matsuo
J. Am. Chem. Soc. **137**, 7982 (2015)

[3] I. Jeon, C. Delacou, A. Kaskela, E. I. Kauppinen, S. Maruyama, Y. Matsuo
Scientific Reports, 2016 under revision

[4] I. Jeon, T. Chiba, C. Delacou, Y. Guo, A. Kaskela, O. Reynaud, E. I. Kauppinen, S. Maruyama, Y. Matsuo
Nano Lett. **15**, 6665 (2015)

Corresponding Author: I. Jeon

Tel: +81-3-5841-0978, Fax: +81-3-5841-0696,

E-mail: il.jeon@photon.u.s-tokyo.ac.jp

Mechanically durable and stretchable micro-supercapacitors with elastomeric components harmonized with wearable field-effect transistors

○Fumiaki Tanaka¹, Atsuko Sekiguchi², Karolina U. Laszczyk¹, Kazufumi Kobashi²,
Shunsuke Sakurai², Don N. Futaba², Takeo Yamada², Kenji Hata²

¹ *Technology Research Association for Single Wall Carbon Nanotubes (TASC), Tsukuba
305-8565, Japan*

² *National Institute of Advanced Industrial Science and Technology, Tsukuba 305-8565,
Japan*

Flexibility or stretchability is one of the notable trends in recent electronics towards wearable/implantable systems. Although many flexible/stretchable devices have been proposed so far, mechanical durability is another essential aspect that wearable/implantable devices should possess to keep device performances when exposed to various mechanical stresses occurred in our daily lives.

Here, we developed mechanically durable and stretchable micro-supercapacitors composed of elastomeric materials towards elastomeric electronics possessing both mechanical durability and softness as a system rather than a single device. To this end, we used single-walled carbon nanotubes (SWCNTs), rubber, composite of SWCNT and rubbers, and sulfuric acid electrolytes to make the micro-supercapacitors and demonstrated that elastomeric field effect transistors (FETs) can be driven with them.

The elastomeric micro-supercapacitors had high mechanical durability: the device performances did not degrade even after the severe mechanical stresses including pressures up to 6 MPa or by high-heels step and impact by being struck with a hammer. As well as the mechanical durability, the micro-supercapacitor had stretchability up to 30% and higher energy and power densities (e.g., 16.8 mWh/cm³ and 86.3 W/cm³, respectively, at a current density of 19.2 A/cm²) compared to conventional stretchable supercapacitors. In addition, the elastomeric FETs had the same level of mechanical durability and stretchability.

In both devices, SWCNTs played important roles in mechanical strengths and device performances. The usage of long and pure SWCNTs grown by super-growth method provided a flexible and mechanically durable thin film, which also possessed high electric conductivity and specific surface area, by entangling SWCNTs into deformable network structure. In addition, when mixed with rubbers, the SWCNT network worked as good fillers for conductivity and framework to support the structure of rubber matrix. As a result, SWCNT thin films became good storages for electric double layers in micro-supercapacitors, while the composite of SWCNT and rubber became good electric conductors for current collectors in micro-supercapacitors and electrodes in FETs.

To demonstrate the compatibility between elastomeric micro-supercapacitors and FETs as a system, they are connected with rubbery interconnection of SWCNT-rubber and then the FET was driven by three micro-supercapacitors connected in series. The result clearly showed that elastomeric materials can constitute an electronic system with micro-supercapacitors and FETs beyond a single device.

Our elastomeric system opens up a possibility to realize all-elastomer-state electronics for wearable/implantable systems, providing both softness for wear and mechanical durability for tolerance against the severe mechanical stresses from the environment.

This presentation is based on results obtained from a project commissioned by the New Energy and Industrial Technology Development Organization (NEDO).

Wafer-scale integration of suspended graphene nanoribbons and its growth mechanisms

○Hiroo Suzuki¹, Toshiro Kaneko¹, Yasushi Shibuta², Munekazu Ohno³, Yuki Maekawa², Toshiaki Kato¹

¹Department of Electronic Engineering, Tohoku University, Sendai 980-8579, Japan

²Department of Materials Engineering, The University of Tokyo, Hongo 113-8656, Japan

³Division of Materials Science and Engineering, Faculty of Engineering, Hokkaido University, Sapporo, 060-8628, Japan

Graphene nanoribbons (GNRs) combine the unique electronic and spin properties of graphene with a transport gap that arises from quantum confinement and edge effects. This makes them an attractive candidate material for the channels of next-generation transistors. Although GNRs can be made in a variety of ways, the reliable site and alignment control of GNRs with high on/off current ratios remains a challenge.

Up to now, we developed a novel method based on the advanced plasma CVD method [1] with nano scale Ni catalyst (Ni nanobar) for directly fabricating suspended GNRs devices [2]. However, the growth yield of suspended GNRs is low and understanding the growth mechanism is required to solve this problem.

Based on this background, we attempted to elucidate the growth dynamics of GNRs in our method. Through the comparison of molecular dynamics simulation and phase diagram calculation with the systematically obtained experimental results, it is found that the Ni nanobar becomes liquid state during the high temperature condition (~ 900 °C) and only the Ni nanobar under plasma CVD can maintain its fine structure with liquid phase due to higher carbon composition. Then, phase separation between graphene and Ni happens during the cooling process, which accelerates the dewetting and the destabilization of liquid phase Ni nanobar under the GNR, resulting in the formation of suspended GNR (Fig. 1(a)). By following this growth model, the yield of suspended GNR growth can be drastically improved ($\sim 90\%$) and wafer scale synthesis of 1,000,000 suspended GNRs has been realized. The edge structure of GNRs was also analyzed by polarized Raman measurements, revealing near zigzag edge is dominantly formed with high uniformity in our suspended GNR arrays.

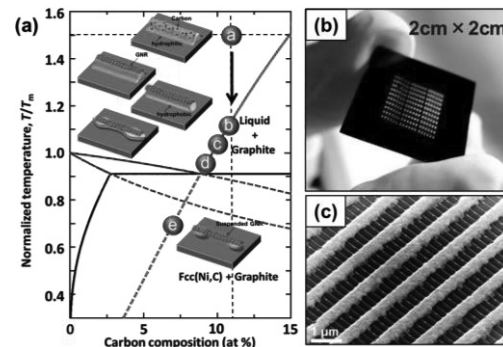


Fig. 1: (a) Growth model of suspended GNR, (b) optical microscope image, and (c) scanning electron microscope image of suspended GNRs array in wafer scale.

[1] H. Suzuki, T. Kato and T. Kaneko, Plasma and Fusion Res. **9**, 1206079 (2014).

[2] T. Kato and R. Hatakeyama, Nature Nanotechnology **7**, 651 (2012).

[3] H. Suzuki, T. Kaneko, Y. Shibuta, M. Ohno, Y. Maekawa and T. Kato, Nature Communications **7**, 11797 (2016).

Corresponding Author: H. Suzuki

Tel: +81-22-795-7046

E-mail: suzuki12@ecei.tohoku.ac.jp

Direct observations of graphene and its oxide dispersed in solution

Yutaka Matsuno, Yu-uya Sato, Hikaru Sato, ○Masahito Sano

Department of Organic Materials Sci., Yamagata University, Yonezawa 992-8510, Japan

A graphene sheet is only one atomic layer thick, yet over several microns wide. This 2D morphology is a main reason that graphene is often placed on a solid substrate for fundamental researches and applications, with a risk of unintentional mechanical strain and chemical doping. Graphene oxide (GO) has many oxygen-containing functional groups, which enable GO to be readily dispersible in various solvents. GO are often used in a form of dispersions for practical applications. Despite of its importance, there has been no practical technique to directly visualize and characterize nanocarbons in liquid environments.

Recently, we have developed a new microscopy that allows direct observation of nanocarbons in solution. In order to visualize atomically thin, 98% transparent graphene in solution, we need to have a very faint illumination compensating for “shooting against the light source”, additional contrast mechanisms besides the small absorption, and orientations facing the wide surface toward an objective lens. These conditions are simultaneously satisfied by dispersing nanocarbons in a fluorescent dye solution near a solid surface. We use the dye fluorescence within a few hundred micrometers from the solid surface as an illumination.

A procedure is simple and quick. A nanocarbon solution is mixed with a dye solution, and is placed on a glass surface. This cell is put on the microscope and an observation is started as if using an ordinary optical microscope. Because the solution is open to the air, it is free to manipulate or perform additional experiments on the solution while observing it in real time.

Sub-micron to sub-millimeter sized GO sheets executing 3D motions are imaged clearly in solution. There are several different mechanisms for contrast. Fluorescence quenching by Dexter electron transfer or Förster resonance energy transfer (FRET) gives dark images. By applying FRET, it is possible to image only an object which has absorbance at the emission wavelengths of the dye. Even then, a large part of the illuminating light is still transmitted through nanocarbons, allowing direct observation of layering and network structures.

Fluorophore properties of many dyes depend on local environments such as solvent, pH, polarity, hydrophobicity, temperature, and concentration. We can create a situation where the dye fluorescence is retarded. If a nanocarbon recovers the fluorescence, it appears bright in a dim background. We show an example of GO appearing bright as a result of adsorption and proton-exchange with dye molecules. Because graphene does not induce such changes, it is possible to differentiate dark graphene from bright GO coexisting in the same solution.

As-synthesized GO itself fluoresces in solution. This autofluorescence can be used to image GO without mixing dyes. A simultaneous acquisition of fluorescence spectra is useful for studying its mechanism. Finally, the viewing object is not limited to nanocarbons. The same contrast mechanisms apply also to various other substances, including living microorganisms.

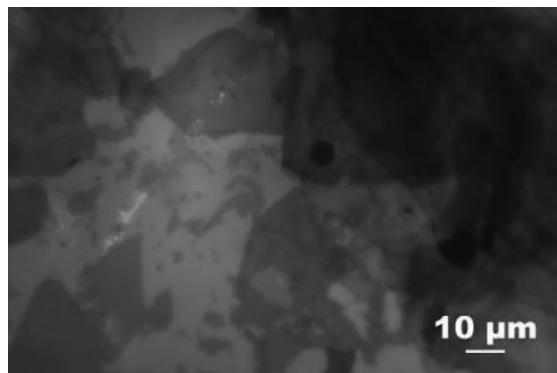


Fig. 1. Image of GO in aq. rhodamine b solution.

Corresponding Author: M. Sano

Tel: +81-238-26-3072 E-mail: mass@yz.yamagata-u.ac.jp

Visualization of structural modulation in the charge density wave phase of 1T-TaSe₂ by scanning transmission electron microscopy

○Keita Kobayashi¹, Hidehiro Yasuda^{1,2}

¹ *Research Center for Ultra-High Voltage Electron Microscopy, Osaka University, 7-1, Mihogaoka, Ibaraki, Osaka 567-0047, Japan*

² *Division of Materials and Manufacturing Science, Graduate School of Engineering, Osaka University, 2-1, Yamadaoka, Suita, Osaka 565-0871, Japan*

Some transition metal dichalcogenides (TMDCs) show a charge density wave (CDW) phase transition due to their low-dimensional electron system [1]. In the CDW phase, the structure of the TMDCs is modulated from that of the normal phase by the periodical displacement of the transition metal atom positions. The formation of supercells in the CDW phase of TMDCs due to the structural modulation has been observed by diffractometry, and models of the displacement of transition metal atoms by the CDW phase transition have been based on these results [1]. To clarify the structural modulation of TMDCs by the CDW phase transition, it is necessary to visualize the displacement of the transition metal atom positions in the CDW phase transition in real space. This would also help clarify the waveform of the CDW, the unique properties of the CDW phase of TMDCs, and the mechanism of the phase transition.

In this study, to clarify the actual structural modulation of TMDCs by the CDW phase transition by experimentally, we attempted to visualize the periodic displacement of Ta atom position in CDW phase of 1T-TaSe₂, which is a typical TMDC that shows a CDW phase at room temperature, by annular dark-field scanning transmission electron microscopy (ADF-STEM). In consequence, we found that the additional periodic image contrast, which was consistent with the periodicity of the supercell of the CDW phase of 1T-TaSe₂, was superimposed on the image contrasts arising from atomic columns in the ADF-STEM image of CDW phase of 1T-TaSe₂ (Figure 1) [2]. We compared experimental and simulated images and found that the periodic image contrast reflects the periodic density fluctuations of Ta atomic columns caused by the static displacement of Ta atom positions. The results confirm that the Ta displacement model predicted by the diffractometric method is correct. Furthermore, we reveal that the CDW has a unique waveform; a coherent CDW is formed on every layer of 1T-TaSe₂.

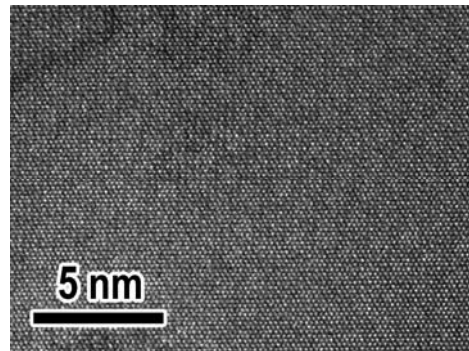


Fig.1: ADF-STEM images of 1T-TaSe₂ acquired from the *c*-axis. A periodic image contrast with six-fold symmetry is seen in addition to the atomic columns.

[1] J. A. Wilson, F. J. Di Salvo, S. Mahajan, *Adv. Phys.* **24**, 117 (1975).

[2] K. Kobayashi, H. Yasuda, Submitted.

Corresponding Author: K. Kobayashi

Tel: +81-6-6879-7941, Fax: +81-6-6879-7942,

E-mail: kobayashi-z@uhvem.osaka-u.ac.jp

Polarity control of h-BN nanoribbons by uniaxial strain

○Ayaka Yamanaka, Susumu Okada

*Graduate School of Pure and Applied Sciences, University of Tsukuba, Tennodai, Tsukuba
305-8577, Japan*

Hexagonal boron nitride (h-BN) is attracting much attention as an insulating version of graphene, due to its unique physical properties, such as mechanically strong hexagonal network, high thermal conductivity, and an insulating electronic structure with wide band gap. Because of these properties, h-BN is regarded as a potential material for the wide areas in the current and future nanotechnologies. Although h-BN possesses the same network topology to the graphene, their physical properties are totally different each other due to the difference in the constituent elements. In our previous works, we demonstrated that the energetics and electronic structure of nanoscale flakes of h-BN are insensitive to their shapes and sizes. On the other hand, edge polarity of the h-BN nanoflakes is sensitive to the edge morphology and chemical functionalization. However, it is still unclear the detailed polar properties of the h-BN nanoflakes in terms of the structural deformations. Thus, in this work, we study the electronic structure of h-BN with uniaxial strain to investigate the effect of strain to polarization of h-BN nanoribbons. All calculations are performed by using the density functional theory (DFT) with the generalized gradient approximation. The effective screening medium (ESM) method is applied to avoid the unintentional dipole interactions with the periodic images.

In this study, we applied tensile and compressive strain parallel to the ribbon direction to h-BN nanoribbons with various edge structures ranging from armchair to zigzag. Figure 1 shows the potential difference between B and N edges of a zigzag h-BN nanoribbon as a function of the strain. We found that the potential difference monotonically increases with increasing the tensile strain and changes its sign at 16 % (Fig. 1). The fact indicates that the ribbon under the 16% tensile strain does not exhibit edge polarization, even though the asymmetrical atomic arrangements at the edges. More interestingly, above the 16% strain, the potential different changes its sign, indicating that the polarity inversion occurs in the uniaxially stretched h-BN ribbons except the armchair ribbons.

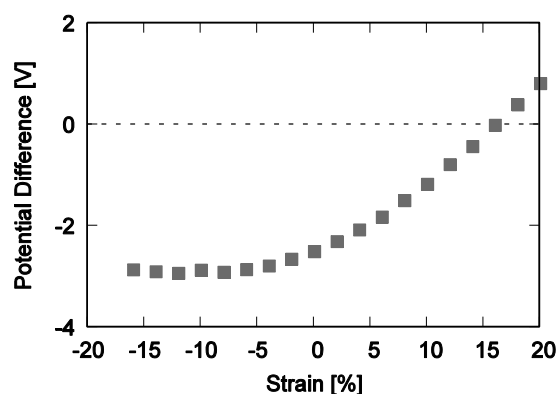


Fig.1: Potential difference of zigzag h-BN nanoribbon as a function of strain. Positive and negative x-axis denote the tensile and compressive strain, respectively.

Corresponding Author: A. Yamanaka
Tel: +81-29-853-5600 (ext. 8233),
Fax: +81-29-853-5924,
E-mail: ayamanaka@comas.frsc.tsukuba.ac.jp

Germanium Sulfide Photodetectors with High Photosensitivity and Broad Spectral Response

○Dezhi Tan, Xiaofan Wang, Yuhei Miyauchi, Kazunari Matsuda

Institute of Advanced Energy, Kyoto University, Uji, Kyoto 611-0011, Japan

Recently, the high-sensitive photodetectors with broad spectral response have been reported using the novel 2D materials, (e.g., graphene, transition metal dichalcogenides and black phosphorus) [1,2]. As a new member of 2D material family, metal monochalcogenides (e.g., GeS and GeSe) have attracted much interests for the highly sensitive photodetector applications. The *p*-type semiconductor 2D GeS with an orthorhombic structure has close direct and indirect optical transitions with small energy difference. Our previous report showed that the GeS exhibits strong light absorption in a broad range from visible to near-infrared spectral regions, which promises GeS as a high-sensitive photodetecting material [3].

Here, the highly sensitive-photodetector based on GeS nanosheets has been demonstrated. We fabricated the GeS nanosheets by using the mechanical exfoliation method and then GeS-based field-effect transistors (GeS-FETs) were prepared using the electron-beam lithography (Inset of Fig. 1(b)). The photo-responses of GeS-FETs were checked with or without light irradiation, where the bias-voltage and light intensity were controlled. Figure 1(a) shows the photocurrent of GeS-FETs with different illuminating light intensity. A nonlinear light-intensity-dependent response is observed (Fig. 1a). The GeS photodetectors exhibited high photoresponsivity R_λ of about 70 A/W under illumination of $0.66 \mu\text{W cm}^{-2}$ at wavelength of 400 nm ($V_g = 0 \text{ V}$, $V_{ds} = 4 \text{ V}$). The specific detectivity, the key figure of merits of a photodetector, is estimated to be 4.8×10^{13} Jones. The photodetecting performance can be enhanced dramatically via increasing the back-gate voltage (V_g) up to 80 V (Fig. 1(b)). R_λ is enhanced to be 600 A/W under the same illumination conditions. Moreover, we revealed that the GeS photodetector shows a broad spectral response in the wavelength range of 400-800 nm along with high photosensitivity. These excellent properties of high photocurrent generation and broad spectral response indicate that the GeS-FET photodetector is a highly qualified candidate for the optoelectronic applications.

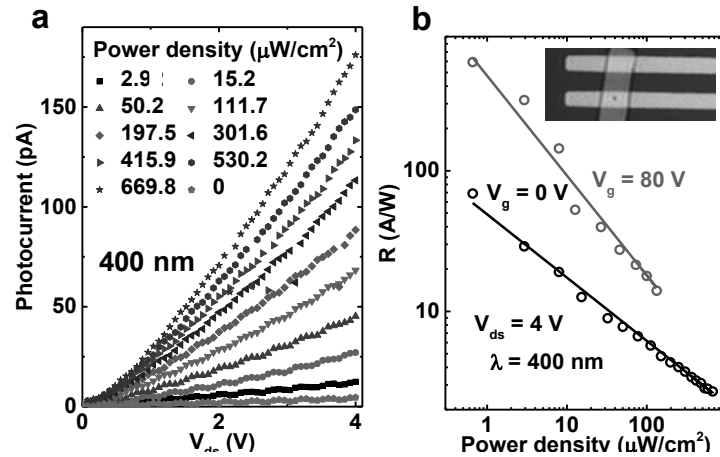


Fig.1 (a) Photocurrent under light (400 nm) irradiation with different power density. (b) Photo-responsivity with $V_g = 0$ and 80 V. Inset shows the optical image of GeS FET.

[1] C. Liu, *et al.*, *Nat. Nanotechnol.* **9**, 273 (2015).

[2] H. Yuan, *et al.*, *Nat. Nanotechnol.* **10**, 707 (2015).

[3] D. Tan, *et al.*, arXiv:1606.06953 (2016).

Corresponding Author: D. Tan

E-mail: tan.dezhi.63m@st.kyoto-u.ac.jp

Current jump and memory effect in MoS₂ transistor operated at high temperature

○Tomoki Yamanaka¹, Masahiro Matsunaga¹, Ayaka Higuchi¹, Yuichi Ochiai¹, Guanchen He², Jonathan P. Bird^{1,2}, and Nobuyuki Aoki¹

¹ Graduate School of Advanced Integration Science, Chiba University,
Chiba 263-8522, Japan

² Department of Electrical Engineering, University at Buffalo, SUNY,
Buffalo, New York 14260-1920, USA

Molybdenum disulfide (MoS₂) have received remarkable attention as new 2D materials with great potentials for future applications [1]. Recently, Jiang *et al.*, reported a kink (memory step) was reproducibly appeared in the transfer curve at high temperature above 450 K [2]. In this study, we attempt to evaluate the memory step by changing the thickness of MoS₂ layers.

MoS₂ FETs were fabricated using exfoliated MoS₂ crystals by well-known scotch tape method. We transferred the crystals onto electrodes pre-fabricated on a SiO₂/Si substrate by dry transfer method using a *h*-BN sheet. The devices form bottom contacted configuration by Au electrodes. Figure 1 shows an optical microscope image of the typical FET. The FET was installed into a vacuum probe station and then it was annealed at 400 K for 20 hours [3] to improve the performance. After the annealing process, additional annealing was performed at 500K for several hours.

After the second annealing process, we measured transfer curves at different temperature between 300 K to 500 K. While no significant change was observed at near room temperature, a current jump was significantly appeared at around zero back gate voltage at high temperature above 400 K. Such a jump was observed at around $V_g = 0$ V in a forward back gate voltage sweep (from -40 to 40 V) while a sudden decrease of the current occurred at around $V_g = -30$ V in the backward sweep. The height of the jump increased with increasing the temperature. Interestingly, the jump became more pronounced with decreasing the MoS₂ thickness. However, the jump is not peculiar effect only in MoS₂ device since a similar trend was observed in a graphene one. Hence, the gate insulator of SiO₂ may act as the origin of the current jump and the memory effect at high temperature. Further discussion will be argued in the presentation.

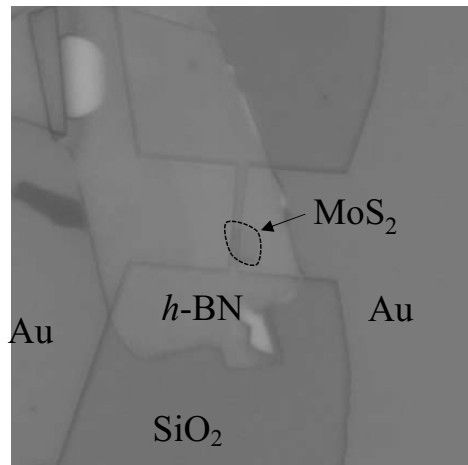


Fig.1. Optical microscope image of a typical MoS₂ FET device. The dashed line shows the shape of the MoS₂ crystal. The top of MoS₂ was covered by a *h*-BN sheet.

[1] Q. H. Wang *et al.*, Nature Nanotech. **7**, 699 (2012).

[2] C. Jiang *et al.*, J. Appl. Phys. **117**, 064301 (2015).

[3] B. W. H. Baugher *et al.*, Nano lett. **13**, 4212 (2013).

Corresponding Author: N. Aoki

Tel:+81-43-290-3430, Fax:+81-43-290-3427

E-mail:n-aoki@faculty.chiba-u.jp

Strain Modulation of Electronic Properties in Hexagonal Boron-Nitride Atomic Layers

○Yoshitaka Fujimoto¹ and Susumu Saito^{1,2,3}

¹*Department of Physics, Tokyo Institute of Technology, Tokyo 152-8551, Japan*

²*International Research Center for Nanoscience and Quantum Physics, Tokyo Institute of Technology, Tokyo 152-8551, Japan*

³*Materials Research Center for Element Strategy, Tokyo Institute of Technology, Kanagawa 226-8503, Japan*

Since the successful exfoliation of graphene from multilayer graphite, hexagonal boron nitride (h-BN) atomic layers have been also regarded as fascinating materials from the viewpoints of fundamental physics and relevant applications in nano/opto-electronics because the structural properties of the h-BN atomic layers are similar to those of graphene. On the other hand, the electronic property of h-BN atomic layers is quite different from that of graphene: graphene exhibits metallic property, while the h-BN layers possess sizable band gap [1]. This sizable band-gap nature of the h-BN atomic layers would provide not only new physical properties but also novel nano- and/or opto-electronics applications.

One of the effective ways to control the electronic properties of nanomaterials is to dope with heteroatoms. Actually, it is reported that the electronic properties of h-BN layers is changed from insulating to metallic properties by doping with carbon atom [2]. Another way to tune the electronic properties is to apply the strains. For example, the band gaps of h-BN atomic layer are tunable by applying strains [3, 4].

In this talk, we report the systematic study that clarifies the strain-induced effects on the stabilities and the electronic properties of h-BN monolayers and bilayers [3-8]. In the former part, we show that the impurity states in the C-doped h-BN monolayers become relatively shallow states when biaxial strains are applied. Furthermore, the compressive strains can induce the new conduction channel (Fig. 1). In the latter part, we show that the band gaps of the h-BN bilayers are tunable by applying strains. We also show that the biaxial strains can produce a transition from indirect to direct band gaps of the h-BN bilayer.

[1] K. Watanabe, T. Taniguchi, and H. Kanda, *Nature Mater.* **3** (2004) 404.

[2] X. Wei, M. Wang, Y. Band, and D. Golberg, *ACS Nano* **5** (2011) 2916.

[3] Y. Fujimoto, T. Koretsune and S. Saito, *J. Ceram. Soc. Jpn.* **122** (2014) 346.

[4] Y. Fujimoto, T. Koretsune and S. Saito, *JPS Conf. Proc.* **1** (2014) 012066.

[5] Y. Fujimoto and S. Saito, *J. Ceram. Soc. Jpn.* **123** (2015) 576.

[6] Y. Fujimoto and S. Saito, *Phys. Rev. B* **93** (2016) 045402.

[7] Y. Fujimoto and S. Saito, *J. Ceram. Soc. Jpn.* **124** (2016) 584.

[8] Y. Fujimoto and S. Saito, to be published.

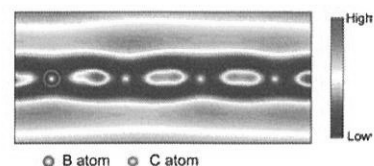


Fig. 1 Nearly free electron state (Ref. [6]).

Corresponding Author: Yoshitaka Fujimoto

TEL: +81-3-5734-2368, FAX: +81-3-5734-2368, E-mail: fujimoto@stat.phys.titech.ac.jp

Host-Guest Complexation of Cyclodextrins on Carbon Nanohorn Particles

○Koji Harano¹, Junya Yamada¹, Akihito Kumamoto², Naoya Shibata², Eiichi Nakamura¹

¹ *Department of Chemistry, The University of Tokyo, Tokyo 113-0033, Japan*

² *Institute of Engineering Innovation, Graduate School of Engineering, The University of Tokyo, Tokyo 113-8656, Japan*

Dispersion of carbon nanomaterials in water is an important technique for enhancement of their processability and medicinal applications. Whereas natural or synthetic surfactants have been widely employed for preparation of water-dispersible nanocarbons, the use of an excess amount of surfactants and their removal by posttreatment are often problematic [1]. Herein we report shape-selective complexation of cyclodextrin (CD), a common host compound for a small hydrophobic molecule, on the surface of carbon nanohorn (CNH) particles through host-guest interaction at a molecular level. We found that CNH particles become dispersed by mixing and heating with cyclodextrins with various diameters (Figure). In contrast, single-walled carbon nanotubes and graphite did not disperse in water by the same treatment, suggesting that the shape-selective interaction of CD molecules with the curved tips of CNH plays a crucial role in formation of highly-dispersible CNH particles. The complexation of CDs on carbon nanohorns was verified by high-resolution transmission electron microscopy (TEM, Figure), in which a trapezoidal contrast of a single cyclodextrin molecule was clearly observed. Such a shape-selective recognition of the nanocarbon surface allows us to separate CNH particles from as-purchased mixture with graphitic particles by mixing with only a small amount (1 wt%) of cyclodextrin, which was confirmed by thermogravimetric analysis and TEM observation.

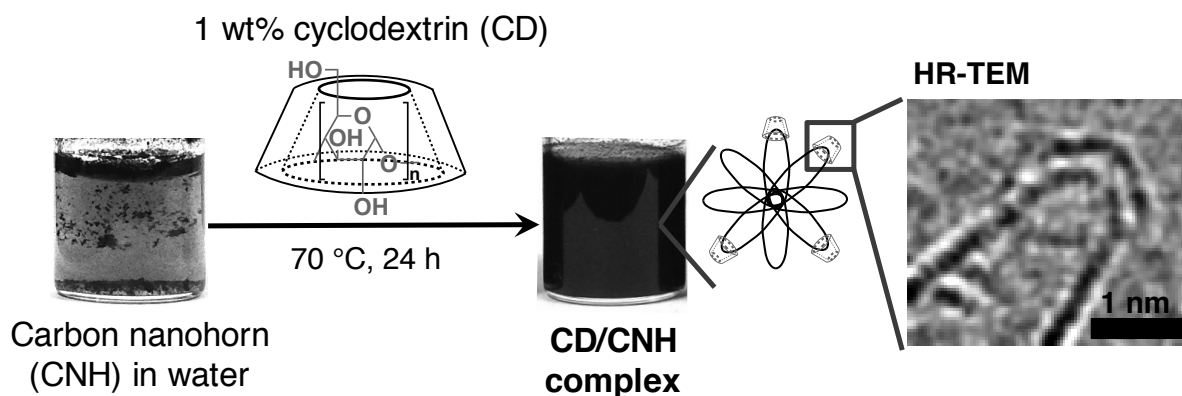


Figure. Dispersion of CNH particles in water through host-guest complexation of cyclodextrin on the tips of nanohorns. A high-resolution TEM image of γ -cyclodextrin on a nanohorn is shown on the right.

A part of this work was conducted in Research Hub for Advanced Nano Characterization, The University of Tokyo, under the support of “Nanotechnology Platform” (project No. 12024046) by MEXT, Japan.

[1] M. Zhang *et al.* *J. Phys. Chem. B* **109**, 22201 (2005).

Corresponding Author: E. Nakamura

Tel: +81-3-5841-4369, Fax: +81-3-5841-4369,

E-mail: harano@chem.s.u-tokyo.ac.jp

Dependence of the resistivity of carbon nanocoils on coil diameter

○Yoshiyuki Suda¹, Yasushi Nakamura¹, Tamio Iida², Toru Harigai¹, Hirofumi Takikawa¹,
Hitoshi Ue³, Hiroyuki Shima⁴

¹ Department of Electrical and Electronic Information Engineering, Toyohashi University of
Technology, Toyohashi, Aichi 441-8580, Japan

² Department of Electrical and Computer Engineering, National Institute of Technology, Gifu
College, Motosu, Gifu 501-0495, Japan

³ Fuji Research Laboratory, Tokai Carbon Co., Ltd., Oyama, Shizuoka 410-1431, Japan

⁴ Department of Environmental Sciences, University of Yamanashi, Kofu, Yamanashi
400-8510, Japan

Carbon nanocoils (CNCs) are an exotic class of low dimensional nanocarbons with helical shape. Typical thicknesses and coil diameters of CNCs fall within the ranges of 100–400 nm and 400–1000 nm, respectively, and their full lengths are on the order of several tens of micrometers [1]. We have developed a precise resistivity measurement system for quasi-one-dimensional nanomaterials using a focused ion beam [2]. The system enables the resistivity of CNCs to be measured and its dependence on coil geometry to be elucidated. Low-temperature resistivity measurements performed on the CNCs revealed that electron transport through the helical axis is governed by the variable range hopping mechanism. The characteristic temperature in variable range hopping theory was found to systematically increase with coil diameter, which supports our theory that the population of sp^2 -domains in CNCs decreases considerably with coil diameter.

CNCs samples were synthesized by catalytic chemical vapor deposition [1]. After the synthesis, a portion of the CNCs was graphitized to obtain graphitized CNCs (G-CNCs) by heat treatment in Ar atmosphere at 2873K for 30 min using a Tammann oven. We then cut off a single CNC from an as-grown aggregate and made the measurement sample using FIB technique [2]. Figure 1 shows the relationship between the coil diameter and resistivity at room temperature: 15 single CNCs and three single G-CNCs were examined. For reference, the resistivities of four single linear-shaped CNFs with fiber diameters of 407–1258 nm are also plotted on the vertical axis. The resistivity of the CNCs was found to increase with their coil diameter, although certain sample-dependent fluctuation was observed. In contrast, the resistivity of G-CNCs was almost invariant to changes in coil diameter. Electron transport through the helical axis will be discussed in the presentation.

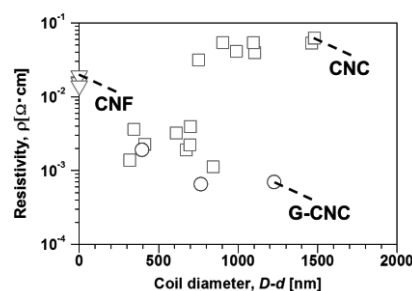


Fig.1: Relationship between resistivity and coil diameter: 15 CNCs, three G-CNCs, and four CNFs were examined.

[1] Taiichiro Yonemura, *et al.*, Carbon, **83** (2015) 183-187

[2] Yasushi Nakamura, *et al.*, Applied Physics Letters, **108**
(2016) 153108-1-4

Corresponding Author: Y. Suda

Tel: +81-532-44-6726, Fax: +81-532-44-6757,

E-mail: suda@ee.tut.ac.jp

Doping and electronic properties of BN nanotubes

○Susumu Saito¹⁻³, Yoshitaka Fujimoto¹

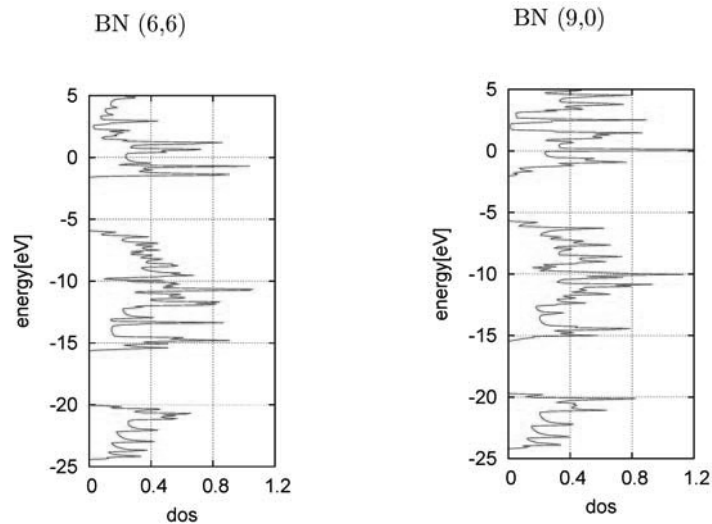
¹*Department of Physics, Tokyo Institute of Technology, Tokyo 152-8551, Japan*

²*International Research Center for Nanoscience and Quantum Physics,
Tokyo Institute of Technology, Tokyo 152-8551, Japan*

³*Materials Research Center for Element Strategy, Tokyo Institute of Technology,
Yokohama, Kanagawa 226-8503, Japan*

Bulk hexagonal boron nitride (h-BN) and h-BN atomic layers are structurally similar to graphite and graphene respectively, but possess fundamental gap in their electronic structure and are interesting future device materials. Although the doping into h-BN monolayer induces rather deep donor and acceptor states, external strain is found to modify the electronic structure and reduce the ionization energy of the impurity induced states [1]. Also the interlayer interaction in the h-BN bilayer gives sizable reduction of the fundamental-gap value. Here we study the electronic properties of BN nanotubes to clarify the curvature effect on the electronic structure of h-BN layers.

We first review the electronic structure of the zigzag BN nanotubes studied in the framework of the density functional theory [2]. Their fundamental gap is found to decrease in the case of thin nanotubes. We next discuss the electronic properties of thin BN nanotubes. We study a series of zigzag nanotubes, armchair nanotubes, and finally the chiral nanotubes, and show that the gap value depends not only on the diameter but also on the helicity of the nanotube [3]. Finally, we discuss the electronic properties of C doped zigzag BN nanotubes. The C atom is doped at the B site of the nanotube and therefore induces the donor state. We discuss the ionization energy of the donor state and its nanotube-radius dependence.



Density of states of BN nanotubes

[1] Y. Fujimoto and S. Saito, *Physical Review B* **93**, 045402 (2016).

[2] S. Okada, S. Saito, and A. Oshiyama, *Physical Review B* **65**, 165410 (2002).

[3] M. Toyoda, Y. Uchida, and S. Saito, to be published.

Corresponding Author: Susumu Saito

E-mail: saito@stat.phys.titech.ac.jp

Fax: +81-3-5734-2739

Chirality selective synthesis of single-walled carbon nanotubes with sputtered Co-W catalyst and its possible mechanism

oHua An¹, Rong Xiang¹, Hiroki Takezaki¹, Shinnosuke Ohyama¹, Yang Qian¹,

Taiki Inoue¹, Shohei Chiashi¹, Shigeo Maruyama^{1,2}

1. *Department of Mechanical Engineering, the University of Tokyo, 7-3-1 Hongo, Bunkyo, Tokyo, 113-8656, Japan*

2. *Energy NanoEngineering Laboratory, National Institute of Advanced Industrial Science and Technology (AIST), 1-2-1 Namiki, Tsukuba, 305-8564, Japan*

The excellent electrical properties have made single-walled carbon nanotubes (SWNTs) one of the most of promising building blocks for future electronics and optics. However, the potential industrial applications are impeded by the mixed chiralities of as-grown SWNT assemblies. Direct synthesis of SWNTs with single chirality is challenging but always attracts considerable attention. Recently, Co₇W₆ clusters were reported to structurally match and thus successfully growing a single chirality SWNT (12, 6), with over 90% and a zigzag SWNT (16, 0), with near 80%, by controlling the catalyst structure and growth conditions with a high-temperature reduction and growth [1, 2].

In this report, we show that (12, 6) can be selectively grown at lower temperatures and with better spatial uniformity by using a sputtered bimetallic Co-W in alcohol catalytic chemical vapor deposition [3]. The enrichment of (12, 6) is 50-70% according to the statistical Raman mapping analysis and optical absorption spectrum. Reduction temperature before growth is found to be critical for the selectivity. At high reduction-temperatures, selective area electron diffraction identified an intermediate structure of Co₆W₆C, which is associated with the selectivity [4]. The details of catalyst structure, and time-dependent selectivity from 10 s to normally 5 min will be discussed.

[1] F. Yang et al., *Nature* **510**, 522 (2014).

[2] F. Yang et al., *J. Am. Chem. Soc.* **137**, 8688 (2015).

[3] S. Maruyama et al., *Chem. Phys. Lett.* **360**, 229 (2002).

[4] H. An et al., *Nanoscale*, (2016), in press, doi: 10.1039/C6NR02749K

Corresponding Author: Shigeo Maruyama

Tel: +81-3-5841-6421, Fax: +81-3-5800-6983

E-mail: maruyama@photon.t.u-tokyo.ac.jp

Development of new polymeric gels for the M/S separation of single-wall carbon nanotubes

○Guowei Wang, Xiaojun Wei, Atsushi Hirano, Shunjiro Fujii,
Takeshi Tanaka, and Hiromichi Kataura*

Nanomaterials Research Institute, National Institute of Advanced Industrial Science and Technology (AIST), Tsukuba, Ibaraki 305-8565, Japan

The metal/semiconductor (M/S) or single-chirality separation of single-wall carbon nanotubes (SWCNTs) is important for the electronic or biomedical applications. Among various separation methods [1, 2], the gel column chromatography shows a great potential for scalable production [3]. However, the available gels have been limited to agarose and allyl dextran-based gels. The current gels are not optimized for the separation of SWCNTs and face the problem of high cost. Moreover, two gels are far from enough for studying the microscopic separation mechanism. Thus, more efforts are needed in developing new polymeric gels.

In this study, we will introduce the latest results in finding novel polymeric gels that can be used for the separation of SWCNTs. Considering the current two gels are polysaccharides, we focused our screening on polysaccharide polymers. Several kinds of water soluble polysaccharides were cross-linked to get their corresponding gels. The gels were proved to be effective for the M/S separation. Fig. 1 shows the optical absorption spectra of M- and S-SWCNTs that were separated by the newly developed guar gum gel. In contrast, water insoluble polysaccharides were examined to be ineffective for the M/S separation. This research reveals the importance of gel wettabilities and provides us a general strategy to modify water soluble polymers for M/S separation. The variety of the newly developed gels will contribute to both scientific researches and industrial applications.

This work was supported by JSPS KAKENHI, grant no. 25220602.

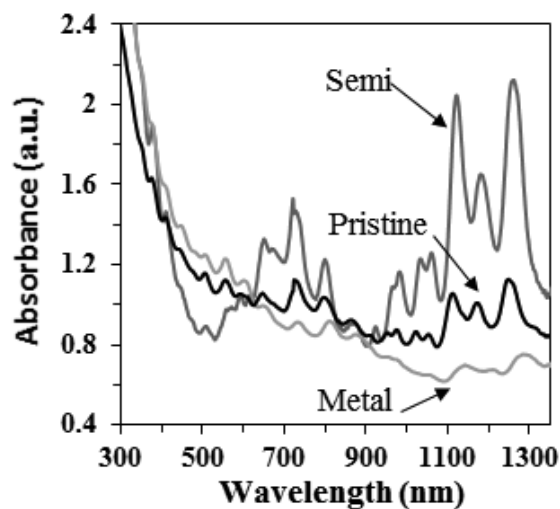


Figure 1. Normalized optical absorption spectra of pristine SWCNTs and separated M- and S-SWCNTs using a new guar gum gel.

[1] C. Y. Khripin et al. *J. Am. Chem. Soc.* **135**, 6822-6825 (2013).

[2] S. Ghosh et al. *Nat. Nanotechnol.* **5**, 443-450 (2010).

[3] H. Liu et al. *Nat. Commun* **2**, 309 (2011).

Corresponding Author: H. Kataura

Tel: +81-29-861-2551, Fax: +81-29-861-2786, E-mail: h-kataura@aist.go.jp

Utilizing a caged electron spin of an endohedral metallofullerene for molecular location sensing

○Yuta Takano¹, Ryo Tashita², Mitsuaki Suzuki^{2,3,4}, Shigeru Nagase⁵, Hiroshi Imahori^{1,6}, Takeshi Akasaka^{2,3,7,8}

¹Institute for Integrated Cell-Material Sciences (WPI-iCeMS), Kyoto University, Kyoto 606-8501, Japan. ²Life Science Center of Tsukuba Advanced Research Alliance, University of Tsukuba, Ibaraki 305-8577, Japan. ³Department of Chemistry, Tokyo Gakugei University, Tokyo 184-8501, Japan. ⁴Department of Chemistry, Josai University, Saitama 350-0295, Japan. ⁵Fukui Institute for Fundamental Chemistry, Kyoto University, Kyoto 606-8103, Japan. ⁶Department of Molecular Engineering, Graduate School of Engineering, Kyoto University, Kyoto 615-8510, Japan. ⁷Foundation for Advancement of International Science, Ibaraki 305-0821, Japan. ⁸State Key Laboratory of Materials Processing and Die & Mould Technology, School of Materials Science and Technology, Huazhong University of Science and Technology, Wuhan 430074, China.

Location recognition in molecular-scale provides valuable information on positional relationship, absolute conformation and dynamics of molecules. This information is critical to elucidating biological processes and understanding the nature of functional molecular materials.

Endohedral metallofullerenes are promising nano-materials including that for spatial location recognition [1], because the caged metal is uniquely isolated from the outer environment and rarely escapes from the fullerene cage even in extreme conditions, such as strongly acidic media and high temperature. Such stability makes them the preferred molecular probes in a variety of materials ranging from biological systems to industrial chemicals.

In this study, we present a novel molecular location sensing approach based on an endohedral metallofullerene, Ce@C₈₂, using its anisotropic magnetic properties which lead to temperature-dependent paramagnetic shifts in ¹H-NMR spectra [2] (Fig.1). To achieve this concept, five site-isomers of Ce@C₈₂CH₂-3,5-C₆H₃Me₂ (**1a-e**) were chemically synthesized by a radical coupling reaction [3]. The temperature-dependent shifts, which are induced by the magnetic anisotropy of the caged Ce, in ¹H-NMR spectra of the isomers were clearly characterized by means of experimental molecular structural analysis and theoretical calculations using density functional theory. Detailed numerical analysis of the shifts using suitable statistic criteria successfully located the relative position of the nearby hydrogen atoms from the inside Ce atom. These results evidenced that the paramagnetic shifts based on the anisotropic magnetism of the encapsulated metal atom can be used for molecular location recognition.

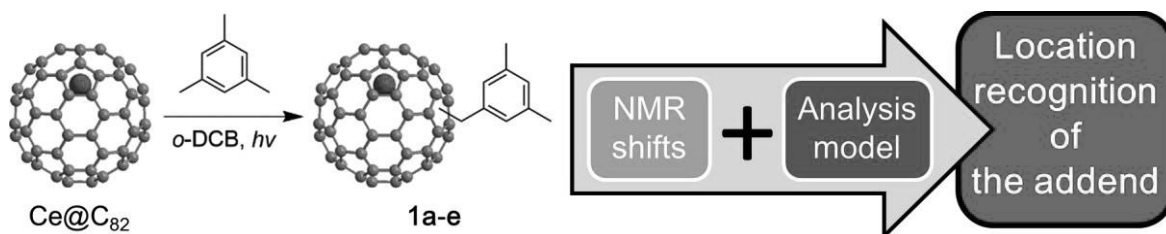


Fig. 1 Schemes for (left) synthesizing Ce@C₈₂CH₂C₆H₃Me₂ and (right) location sensing by the fullerene.

References: [1] For a review; M. Yamada *et al.*, *Bull. Chem. Soc. Jpn.*, 2014, **87**, 1289. [2] Y. Takano *et al.*, *J. Am. Chem. Soc.*, 2016, **138**, 8000. [3] Y. Takano *et al.*, *J. Am. Chem. Soc.*, 2008, **130**, 16224.

Corresponding Author: Yuta Takano

Tel: +81-75-383-2494, Fax: +81-75-383-2571, E-mail: ytakano@icems.kyoto-u.ac.jp

Evaluation of Enantiomeric Purity of Single-Wall Carbon Nanotubes using Flavin Mononucleotide

○Xiaojun Wei¹, Yohei Yomogida¹, Atsushi Hirano¹, Shunjiro Fujii¹, Takeshi Tanaka¹, Naomichi Sato², Riichiro Saito², and Hiromichi Kataura¹

¹ *Nanomaterials Research Institute, National Institute of Advanced Industrial Science and Technology (AIST), Tsukuba, Ibaraki 305-8565, Japan*

² *Department of Physics, Tohoku University, Sendai 980-8578, Japan*

Recently, we separated 12 (*n,m*) enantiomers of single-wall carbon nanotubes (SWCNTs) [1], which showed two times higher circular dichroism (CD) intensities than the reported value in the previous work [2]. However, we could not estimate the enantiomeric purity (EP) of SWCNTs because the available evaluation method was not reported to date.

In this study, we report an available evaluation for the EP of (6,5) SWCNTs using chiral flavin mononucleotide (FMN) [3] for the first time. Two (6,5) enantiomers (defined as (+) with a negative E₂₂ CD signal and (-) with a positive one), which were separated by gel chromatography, were dispersed in FMN solution after removing the initial dispersant. Figure 1 shows the optical absorption spectra and photoluminescence (PL) excitation-emission maps of (+)- and (-)-(6,5) SWCNTs dispersed in FMN solution.

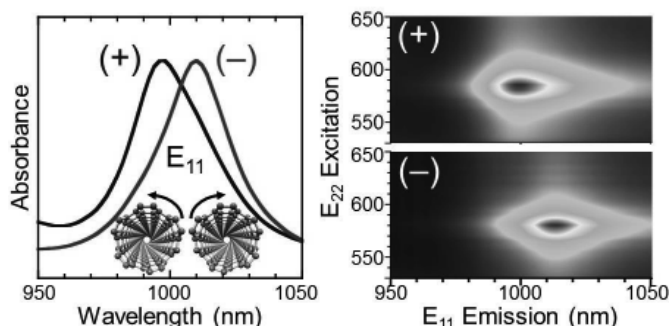


Figure 1. Optical absorption spectra (left) and PL excitation-emission maps (right) of (+)- and (-)-(6,5) SWCNTs dispersed in FMN solution.

Difference in E₁₁ wavelength between (+)- and (-)-(6,5) was clearly observed. This is probably attributed to the non-equivalent local environments induced by the chiral FMN which possessed unequal affinities for (+)- and (-)-(6,5) SWCNTs. This difference enables us to distinguish (+)- and (-)-compositions contained in enantiomeric mixture. By a conventional peak decomposition procedure, the EP of (6,5) SWCNTs was successfully estimated based on the integrated intensities of the fitted E₁₁ optical absorption peaks of (+)- and (-)-compositions (78% and 75% for (+)- and (-)-(6,5) samples, respectively, shown in Figure 1). Furthermore, we confirmed that the estimated EP is proportional to the CD intensity, which allows us to estimate the EP of (6,5) SWCNTs simply from the CD intensity. Because we know that CD intensity depends on the diameter of SWCNT and wavelength of the incident light, we can try to estimate the EP of the other chiral (*n,m*) SWCNTs using present result for (6,5).

This work was supported by KAKENHI No. 25220602.

[1] X. Wei et al. 49th FNTG Symposium 2-5, p28 (2015), X. Wei et al. (2016) submitted.

[2] S. Ghosh et al. Nat. Nanotechnol. 5, 443-450 (2010).

[3] S. Ju et al. J. Am. Chem. Soc. 134, 13196-13199 (2012).

Corresponding Author: H. Kataura

Tel: +81-29-861-2551, Fax: +81-29-861-2786, E-mail: h-kataura@aist.go.jp

Low temperature growth of ultra-high mass density carbon nanotube forests on conductive supports

○Hisashi Sguime^{1,2}, Santiago Esconjauregui², Lorenzo D'Arsi², John Robertson²

¹ Waseda Institute for Advanced Study, Waseda University, Tokyo 169-8050, Japan

² Department of Engineering, University of Cambridge, Cambridge CB3 0FA, UK

Growth of dense carbon nanotube (CNT) forest on conductive supports by chemical vapor deposition (CVD) is of great importance for variety of applications such as sensors, interconnects in LSI, and heat dissipation devices. The growth on conductive supports is generally more challenging than that on insulating supports. This mainly comes from the difficulties of the formation of catalyst nanoparticles, therefore we need to engineer the catalyst/support systems. On the other hand, lowering the process temperature during CVD, which is typically ~ 800 °C, is another key issue since versatile substrates are available.

Here we report low temperature (450 °C) growth of dense CNT forests on Cu conductive layers using two types of catalyst/support systems. One is the CNT forests with a record high mass density of 1.6 g cm^{-3} by Co-Mo catalyst on Ti supports (Fig. 1a, b) [1, 2]. The density is controllable with Mo thickness, and the forests can be patterned with a pitch of ~ 400 nm and a line width of ~ 200 nm due to their highly packed morphology (Fig. 1c). The growth kinetics is investigated in detail, and it has been found that the morphology of the forests change drastically before the growth termination. The morphology change comes from the structure change of catalyst nanoparticles.

The other dense CNT forest is the one grown by Co/Al/Mo multilayer catalyst system (Fig. 2) [3]. The 0.5 nm Al layer between Co and Mo acts as a barrier layer partially preventing Co-Mo interdiffusion. The CNT forests consist of tubes with extremely narrow inner spacing. The forest shows the thermal effusivity of $1840 \text{ J m}^{-2} \text{ s}^{-0.5} \text{ K}^{-1}$ and the thermal conductivity of $4.0 \text{ J s}^{-1} \text{ m}^{-1} \text{ K}^{-1}$, suggesting the forest is potentially useful for the heat dissipation devices. The growth mechanism and the kinetics of dense CNT forests will be discussed.

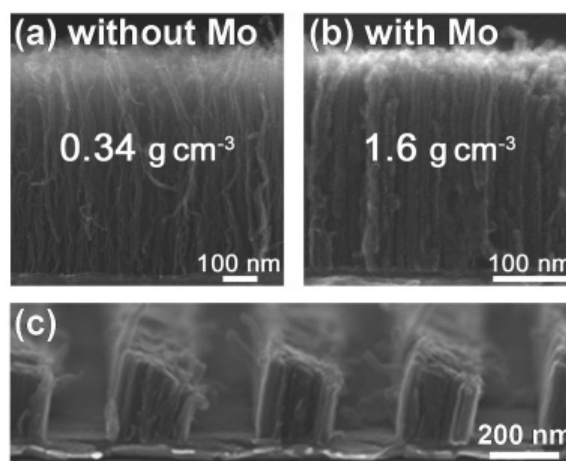


Fig. 1: CNT forests grown at 450 °C on Ti-coated Cu layer with (a) Co catalyst and (b) Co-Mo catalyst. (c) Patterned CNT forest with the pitch of 400 nm and a line width of 200 nm.

[1] H. Sugime et al., *Appl. Phys. Lett.* **103**, 073116 (2013).

[2] H. Sugime et al., *ACS Appl. Mater. Interfaces* **6**, 15440 (2014).

[3] H. Sugime et al., *ACS Appl. Mater. Interfaces* **7**, 16819 (2015).

Corresponding Author: H. Sugime

Tel: +81-3-5286-2769

E-mail: sugime@aoni.waseda.jp

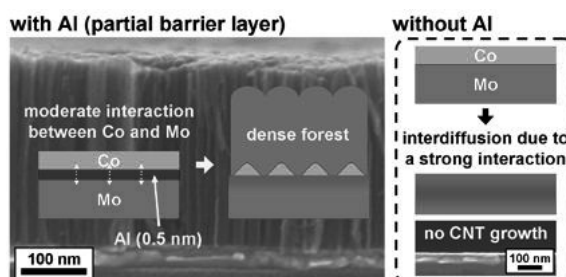


Fig. 2: SEM image and schematic of dense CNT forests with Co/Al/Mo catalyst.

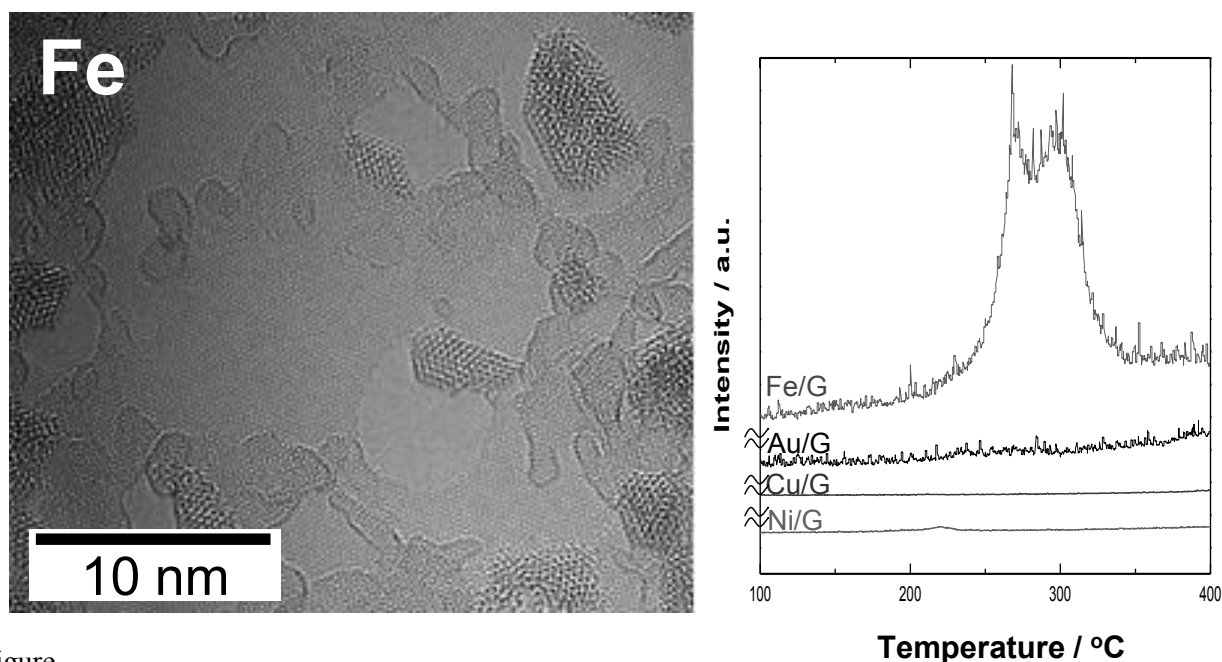
Hydrogenation properties of supported metal nanoparticles on graphene

○Shigehito Isobe¹, Kengo Omori¹, Satoshi Yasuda²

¹ Graduate school of Engineering, Hokkaido University, Sapporo 060-8628, Japan

² Department of Chemistry, Hokkaido University, Sapporo 060-0810, Japan

We have reported that Fe nanoparticles on graphene can absorb hydrogen at low temperature by density functional theory (DFT) calculation [1]. In this work, we have experimentally investigated the hydrogenation properties of metal nanoparticles of Fe, Ni, Cu and Au on graphene. The metal nanoparticles were evaporated on single layer graphene on Cu substrate by vacuum evaporation method. The samples were hydrogenated under 1.0 MPa of H₂, for 10 min, at -196 °C, 100 °C, and dehydrogenated from R.T. to 400 °C and analyzed using mass spectrometer (MS). The hydrogen desorption was observed around 1600 °C for Fe, around 150 °C for Ti, and not observed for Au. Observed hydrogen desorption was caused by metal nanoparticles because we could not observed hydrogen desorption when we performed same experiment to graphene on Cu substrate.



Figure

TEM image of Fe nanoparticles on graphene (left)

Hydrogen MS profiles of each Fe, Au, Cu and Ni nanoparticles on graphene (right)

[1] K. Takahashi et al., Low temperature hydrogenation of iron nanoparticles on graphene, Scientific reports, 4: 4958 (2014)

Corresponding Author: S. Isobe

Tel: +81-11-706-6771, E-mail:isobe@eng.hokudai.ac.jp

Metal Phthalocyanine/Reduced Graphene Oxide Hybrid Electro-catalyst for cathodic Oxygen Reduction Reaction

○Shinichi Murakami¹, Michio Koinuma¹, Yasumichi Matsumoto¹

¹ Graduate School of Science and Technology, Kumamoto University
2-39-1 Kurokami, Chuo-ku, Kumamoto, 860-8555, Japan

Pt/C is the best electrocatalyst for cathodic oxygen reduction reaction (ORR) in fuel cells and metal-air batteries. However, high cost and limited reserve will be problem in the mass production. Therefore, development of highly efficient and stable Pt-free electrocatalyst is required. MPcs exhibit positive charge and have attracted a great deal of attention for a wide variety of applications owing to their versatile functional properties, which depend on the central metal ion. We proved that an iron phthalocyanine (FePc)-based catalyst exhibits high activity for ORR at an alkaline condition[1]. GO exhibit negative charge and have electric insulation owing large amount of oxygen functional groups, while removal of these groups by a reduction process. Reduction changes insulating GO into conductive rGO that have graphene-like sp^2 domains. In this work, presents the electrocatalytic activity for ORR of MPcs/GO hybrid catalyst.

GO was prepared by Hummers' method. A GO dispersed (0.5 g L^{-1}) in N,N-dimethylformamide. A solution of MPcs (0.5 g L^{-1}) was prepared by adding FePc powder to chloroform and subjecting the resulting mixture to ultrasonic treatment for 30 min. The mixed solutions were dipped on glassy carbon electrode, and vacuum drying. Then, the MPcs/GO/GC electrodes were reduced for 10 min at -1.1 V (vs. Ag/AgCl) in $0.1 \text{ M Na}_2\text{SO}_4$. Samples were tested as electrodes for the ORR in 0.1 M KOH saturated with O_2 . Pt wire and Ag/AgCl electrodes were used as the counter and reference electrodes, respectively.

The CV results (Fig.1) shows that the FePc/rGO hybrid offered a higher peak reduction potential than 20 wt% Pt/C. Moreover, the onset potential of FePcOC₆H₆/rGO and FePcOCH₃/rGO were observed at $+0.06 \text{ V}$ and $+0.02 \text{ V}$ (vs Ag/AgCl), respectively. These results suggested that FePcOC₆H₆/rGO and FePcOCH₃/rGO indicated high ORR catalytic activity in alkaline electrolyte. XPS results showed that most of Fe where complex were central metal was left in FePcOC₆H₆/rGO and FePcOCH₃/rGO by electrochemical reduction of the samples. Furthermore, Fe in the FePcOC₆H₆/rGO and FePcOCH₃/rGO was confirmed that the Fe^{2+} is dominant. However, this problem need more investigation and is still open to discuss.

Funding and sample offer form ADEKA corporation are gratefully acknowledged.

[1]T. Taniguchi *et al.* Part. Part. Syst. Charact. **30**, 1063 (2013).

Corresponding Author: S. Murakami

Tel: +81-96-342-3659, Fax: +81-96-342-3679,

E-mail: 157d8344@st.kumamoto-u.ac.jp

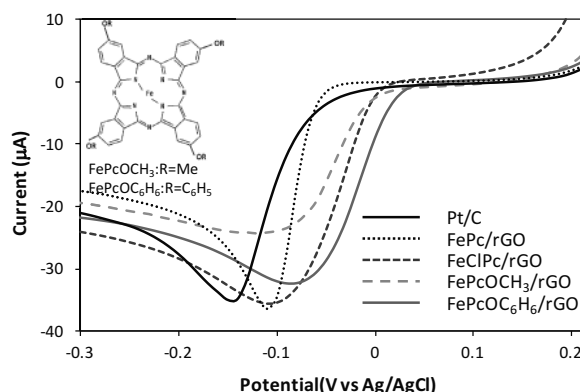


Fig.1: CV results in O_2 -saturated 0.1 M KOH .

Oxygen reduction reaction catalyzed by copper-incorporated carbon electrocatalysts

○Masaru Kato^{1,2}, Marika Muto², Ichizo Yagi^{1,2}

¹ Faculty of Environmental Earth Science, Hokkaido University, Sapporo 060-0810, Japan

² Graduate School of Environmental Science, Hokkaido University, Sapporo 060-0810, Japan

Oxygen reduction reaction (ORR) is a key reaction in energy conversion devices such as polymer electrolyte fuel cells (PEFCs). In PEFCs, platinum group metals (PGMs) are widely used as cathode materials to electrochemically catalyze the ORR. PGMs, however, are rare and expensive, and should be replaced by non-PGM electrocatalysts for the widespread commercialization of PEFCs. Intensive efforts have been devoted to developing non-PGM ORR electrocatalysts such as Fe- and Co-based electrocatalysts and one of the promising synthetic approaches to them is pyrolysis of metal, nitrogen and carbon precursors.^[1,2] Compared with Fe- and Co-based electrocatalysts, much less Cu-based electrocatalysts have been reported,^[3-5] even though an enzyme of Laccase efficiently catalyzes the ORR at the active center of a trinuclear copper complex.^[6]

Herein we report synthesis, characterization and ORR catalytic activity of a Cu,N-codoped carbon electrocatalyst (r[Cutrz/GO]) synthesized in pyrolysis from a trinuclear copper complex with a nitrogen-rich ligand of 1,2,4-triazole (Cutrz)^[7] as the metal and nitrogen source and graphene oxide (GO) as an carbon source (Fig. 1). Cutrz, which has a trinuclear metal core, was inspired by the catalytic active site of Laccase. We used GO because we expected that the heating treatment reduced GO involving incorporation of copper active sites into conductive carbon sheets.^[1,8]

Linear sweep voltammetry of r[Cutrz/GO] recorded in a pH range from pH 1 to pH 13 under oxygen revealed that the ORR activity of r[Cutrz/GO] increased with increasing pH and the activity at pH 13 was higher than that of Pt/C. Physical chemical measurements including X-ray photoelectron spectroscopy and X-ray absorption fine structure spectroscopy demonstrated that the pyrolysis process involved not only the reduction of graphene oxide but also incorporation of unsaturated copper cores into sp² carbon networks.

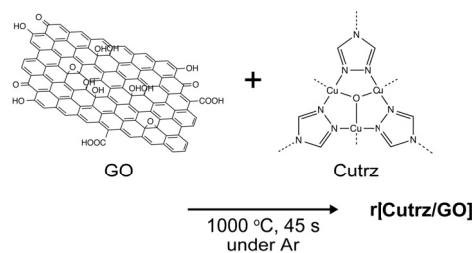


Fig.1: Synthetic procedure of r[Cutrz/GO]

[1] M. Lefèvre *et al.*, *Science*. **324**, 71 (2009). [2] G. Wu, K.L. More, C.M. Johnston, P. Zelenay, *Science*. **332**, 443 (2011). [3] M.S. Thorum, J. Yadav, A.A. Gewirth, *Angew. Chem. Int. Ed.* **48**, 165 (2009). [4] M. Kato *et al.*, *J. Phys. Chem. C*, *in press*. DOI: 10.1021/acs.jpcc.5b11663. [5] M. Kato *et al.*, *Phys. Chem. Chem. Phys.* **17**, 8638 (2015). [6] N. Mano, V. Soukharev, A. Heller, *J. Phys. Chem. B.* **110**, 11180 (2006). [7] T. Yamada, G. Maruta, S. Takeda, *Chem. Commun.* **47**, 653 (2011). [8] K. Kamiya, K. Hashimoto, S. Nakanishi, *Chem. Commun.* **48**, 10213 (2012).

Corresponding Authors: M. Kato and I. Yagi

Tel: +81-11-706-2276, Fax: +81-11-706-4529,

E-mails: masaru.kato@ees.hokudai.ac.jp (MK); iyagi@ees.hokudai.ac.jp (IY)

Novel Proton/Electron Mixed Conductor using Graphene Oxide

○Kazuto Hatakeyama¹, Michio Koinuma¹, Tetsuya Kida¹, Shinya Hayami¹,
Yasumichi Matsumoto¹

¹ Graduate School of Science and Technology, Kumamoto University
2-39-1 Kurokami, Chuo-ku, Kumamoto, 860-8555, Japan

Proton/electron mixed conductors with high electrical and protonic conductivities enable various applications such as fuel cells, supercapacitors and gas separation membranes. Perovskite-type oxides such as BaCeO₃, LaYbO₃ and La₆WO₁₂ are most commonly used as mixed conductors. However, these materials only act at higher temperatures (> 650 °C). To overcome these problems, heterogeneous mixtures of electron and proton conductors have been reported to produce mixed conductors that function at room temperature. A Nafion based membrane hybridized with carbon showed proton and electron conductivities of $\sim 10^{-6}$ - 10^{-4} S cm⁻¹ and $\sim 10^{-3}$ S cm⁻¹, respectively, at room temperature. However, in such heterogeneous mixed conductors, carrier transport is limited by phase boundaries, making it substantially difficult to obtain high mixed conductivities. Thus, it is desirable to develop single phase mixed conducting materials where diffusion paths of charged carriers are interconnected in the molecular scale.

Graphene oxide (GO), the oxidized form of graphene, shows high proton conductivity because of its large amount of oxygen functional groups. While it is well-known that reduced GO (r-GO) acts a good electron conductor because its sp² domains gradually expand by reduction process. Herein, we demonstrate the successful control of the proton and electron conductivities of GO using the photoirradiation and thermal reduction processes [1]. The proton conductivity decreased when the layer distance decreased, whereas the electron conductivity drastically increased with decreasing oxygen content. We also discovered that photo or thermally reduced r-GO films act as a good proton/electron mixed conductor at room temperature. In this case, electrons transfer through r-GO planes, while protons diffuse into the interlayer (Fig. 1). This single phase mixed conductor showed both the proton and electron conductivities of $\sim 10^{-4}$ S cm⁻¹ under high humidity conditions. Moreover, we were successful to increase these conductivities ~ 2 -3 order magnitudes by introducing sulfate ions into r-GO interlayers [2]. Among mixed conductors reported, the developed r-GO films exhibited the best performance at room temperature, demonstrating their feasibility for various applications such as fuel cells, supercapacitors and gas separation membranes.

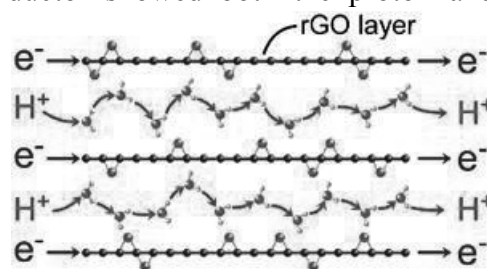


Fig. 1 Schematic model of electron and proton mixed conduction in r-GO film.

[1] K. Hatakeyama *et al.* Chem. Mater. **26**, 5598 (2014).

[2] K. Hatakeyama *et al.* J. Mater. Chem. A **3**, 20892 (2015).

Corresponding Author: K. Hatakeyama

Tel: +81-96-342-3659, Fax: +81-96-342-3679,

E-mail: kazuto@kumamoto-u.ac.jp

Threshold shift of diamond electrolyte-solution gate field-effect transistor by anodic oxidation

○Masafumi Inaba¹, Keisuke Igarashi¹, Takuro Naramura¹, Shuhei Abe¹, Masanobu Shibata¹, Yukihiko Shintani², Atsushi Hiraiwa¹, Hiroshi Kawarada¹

¹ Graduate School of Advanced Science and Engineering, Waseda University, Tokyo 169-8555, Japan

² Yokogawa Electric Corp., Tokyo 180-8750, Japan

Diamond surface has wide potential window and is biocompatible, it is useful for bio- and chemical- sensing. We have investigated the electrolyte-solution gate field-effect transistors (SGFETs) with diamond channel^[1]. Hydrogen terminated (C-H) diamond surface have two dimensional hole gas layer (2DHG) due to the dipole of surface C-H bond, where H is slight positive. Hole carriers are induced by surface negative charges in electrolyte solution across electric double layer (EDL) on the surface. To form EDL on diamond surface, negative bias over threshold voltage is necessary. When the surface is partially oxidized, threshold voltage should shift to negative because the surface potential shifted to negative. In this study, we investigated the threshold shift by anodic oxidation of diamond surface^[2]. This process might be useful for controlling the device parameter of nanocarbon FET-type sensors.

Fig. 1 shows the schematic image of the SGFET on diamond. Initially, the channel was terminated by hydrogen, and source and drain electrodes (Ti/Au) were passivated by epoxy resin. Here, C-H diamond channel is directly contact to solution, and the surface EDL works as gate dielectric. Gate bias was applied from the reference electrode. We used phosphorus buffer solution (PBS) as electrolyte solution. Fig. 2 shows the typical I_{DS} - V_{DS} characteristics. Good modulation was observed. Anodic oxidation was performed by applying positive bias to source and drain. Fig. 3 shows the $\sqrt{I_{DS}}$ - V_{GS} characteristics by changing applied voltage for anodic oxidation. As the applied voltage increased over 1.1 V, the threshold shifted to negative. By anodic oxidation, surface C-H was partially oxidized and the intensity of C-O or C=O bond increased in X-ray photospectroscopy (XPS). The detail oxidation mechanism will be shown on site.

[1] A.R. Ruslinda, H. Kawarada et al., J. Electrochem. Soc. 159, J182 (2012).

[2] T.N. Rao and A. Fujishima, Diam. Relat. Mater. 9, 384 (2000).

Corresponding Author: M. Inaba

Tel&Fax: +81-3-5286-3391

E-mail: inaba-ma@ruri.waseda.jp

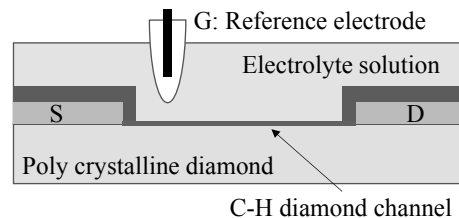


Fig. 1. Schematic image of diamond SGFET

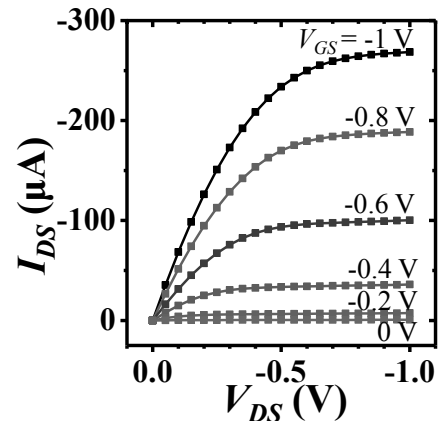


Fig. 2. Typical I_{DS} - V_{DS} characteristics of C-H diamond SGFET

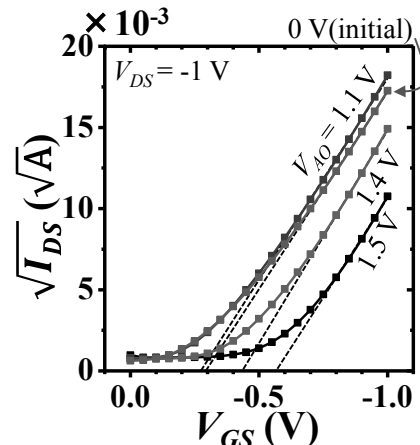


Fig. 3. $\sqrt{I_{DS}}$ - V_{GS} characteristics by changing anodization voltage

Optical Properties of Oxidized (6,5) Single-Wall Carbon Nanotubes

○Mari Ohfuchi¹, Yoshiyuki Miyamoto²

¹ *Fujitsu Laboratories Ltd., Atsugi 243-0197, Japan*

² *Research Center for Computational Design of Advanced Functional Materials, National Institute of Advanced Industrial Science and Technology (AIST), Tsukuba 305-8568, Japan*

Optical properties of oxidized single-wall carbon nanotubes (SWCNTs) have attracted much attention because of the greater luminescence quantum yield than that of pristine CNTs. To advance the fundamental understanding of the optical properties of oxidized SWCNTs, we theoretically investigated the energetics and the optical transitions for complex oxygen (O) adsorption structures on (6,5) CNTs, including adsorption of two O atoms.

As shown in Fig. 1, we obtained four groups of optical transition levels below E_{11} for CNTs adsorbed by isolated O atoms, including the levels known as E_{11}^* and E_{11}^{*-} . The most stable O-adsorption structure is ether structure, which corresponds to the E_{11}^* level. The epoxy structure that produces the E_{11}^{*-} level is much more exothermic than the ether structure. We found two additional groups of optical transition levels for adsorption structures of two O atoms. The most stable adsorption structure for two O atoms is two parallel ether structures, whose transition energy appear between E_{11}^* and E_{11}^{*-} , and more endothermic than two isolated ether structures. The second most stable structure is neighboring ether and epoxy structures, whose O-adsorption energy is also much stronger than the sum of those of isolated ether and epoxy structures. The transition energy is only 0.02eV lower than the E_{11}^{*-} level that is produced by the isolated epoxy structure. There are no dark states below the level, which would work as intrinsic non-radiative decay paths and reduce the luminescence quantum yield.

These results explain the recent bioimaging experiments where the E_{11}^{*-} emission increases its intensity with respect to E_{11}^* as the ultraviolet/ozone irradiation time increases [1]. It also seems that we well understand the multiple emission peaks in the low-temperature PL measurements of SWCNTs oxidized by O_3 [2] and those in the PL spectra of SWCNTs oxidized by O_2 molecules during single chirality separation processes [3], by taking adsorption structures of two O atoms into consideration.

This comprehensive understanding is essential for further applications of oxidized SWCNTs.

[1] Y. Iizumi *et al.*, The 50th FNTG General Symposium, **1-10** (2016).

[2] X. Ma *et al.*, ACS Nano **8**, 10782 (2014).

[3] X. Wei *et al.*, J. Phys. Chem. C **120**, 10705 (2016).

Corresponding Author: M. Ohfuchi

E-mail: mari.ohfuti@jp.fujitsu.com

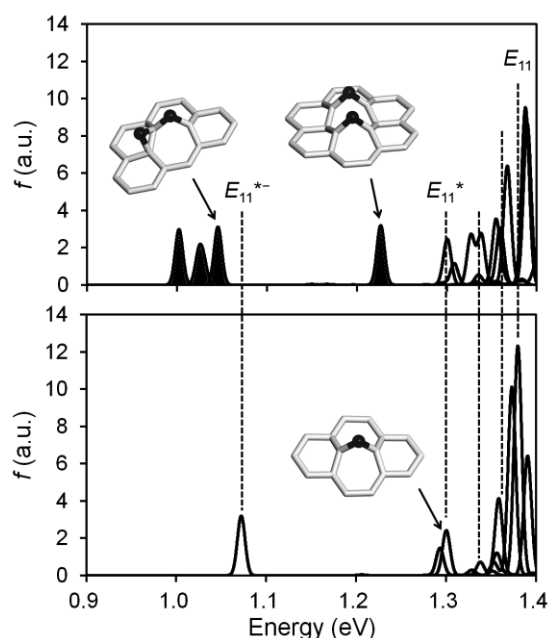


Fig.1: Optical transitions for (6,5) CNTs adsorbed by one O atom (lower panel) or two O atoms (upper panel). The oscillator strengths are plotted with 5-meV width around the transition energies. The insets are the schematic diagrams for the related O-adsorption structures. The gray sticks and black spheres represent C-C bonds and O atoms, respectively.

Graphene coated silver substrate for SERS with acid tolerance

○Seiya Suzuki, Masamichi Yoshimura

Graduate School of Engineering, Toyota Technological Institute, Nagoya 468-8511, Japan

Surface enhanced Raman scattering (SERS) technique is a novel method to sense molecular and lattice vibrations. Although nanostructured silver (Ag) surface provides the most intense SER signals [1], the use of the Ag surface is limited under acidic environment which dissolves Ag. Graphene, a single atomic carbon layer, has a prominent stability for chemical agent, and its honeycomb lattice completely prevents the penetration of small molecules like hydrogen and water [2]. Here, we report development of the SERS substrate consisting of nanostructured Ag and millimeter-scale single-crystal graphene (gSERS). The durability of the gSERS substrate for acidic conditions was demonstrated.

The gSERS substrate was prepared on a SiO₂ (300 nm)/Si substrate. A 6 nm thick Ag was deposited by sputtering on the SiO₂/Si, and then millimeter-scale single-crystal graphene, as grown by chemical vapor deposition [3], was transferred onto the substrate by wet transfer.

Figure 1 shows Raman spectra of Ag/SiO₂/Si, graphene/SiO₂/Si, and graphene/Ag/SiO₂/Si (gSERS) substrates in air. The sputtered Ag showed strong Raman peaks of adventitious carbon, indicating SERS. While graphene/SiO₂/Si shows small G and G' peaks, the gSERS substrate showed strong peaks, indicating SERS.

Subsequently, the SERS substrate was embedded in hydrochloric acid (0.1 ~ 1 × 10⁻⁴ M) to test the durability for acid. Then, rhodamine 6G (R6G) in aqueous solution was dropped on the substrate, and was dried in air. Figure 2(a) shows an optical microscope image of the substrate surface where hexagonal graphene is visible (guided by broken lines). Figure 2(b) shows a Raman mapping of R6G peak (~1650 cm⁻¹) overlapped on the optical image taken at around the upper left corner of the hexagonal graphene. Figure 2(c) indicates Raman spectra taken at the circles in Fig. 2(b). The Raman spectra at the bright spots on graphene (Fig. 2(b)) show strong R6G peaks like the spectrum 1 in Fig. 2(c), indicating hot spots of SERS. R6G peaks can also be observed on the inside of the graphene domain (spectrum 2 in Fig. 2(c)) but not on the outside (spectrum 3). This indicates that nanostructured Ag on the inside (outside) of the graphene has (not) existed under hydrochloric acid, indicating gSERS substrate can be used in acid environment. We expect that the present advanced technique will further enhance the potential of SERS applications.

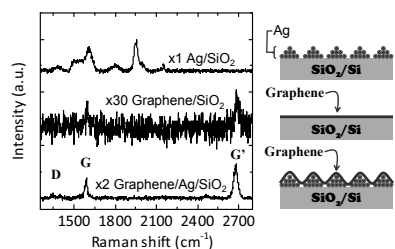


Fig. 1. Comparison of Raman spectra with laser wavelength of 532 nm.

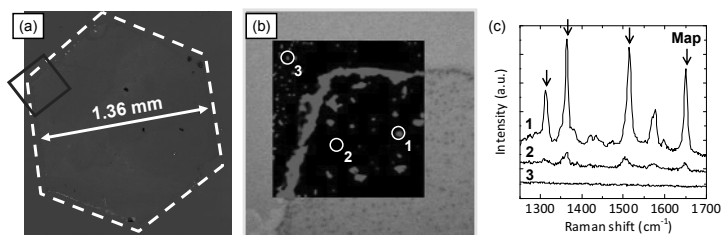


Fig. 2. (a) Optical microscope image of the SERS substrate. (b) Raman mapping of R6G and (c) Raman spectra in (b).

[1] K. Kneipp *et al.*, “*Surface-Enhanced Raman Scattering*”, Springer (2006).

[2] S. C. O’Hern *et al.*, *Nano Lett.* **14**, 1234 (2014).

[3] S. Suzuki *et al.*, *e-J. Surf. Sci. Nanotech.* **13**, 404 (2015).

Corresponding Author: Seiya Suzuki

Tel: +81-52-809-1852, E-mail: seiya09417@gmail.com

A nanoporous graphene terahertz detector

○Juxian Li¹, Daichi Suzuki¹, Shunri Oda¹, Yoshikazu Ito², Takeshi Fujita², Yukio Kawano¹

¹ QNERC and Dept. of EE, Tokyo Institute of Technology, Tokyo 152-8552, Japan

² WPI Advanced Institute for Materials Research, Tohoku University, Sendai 980-8577, Japan

Terahertz (THz) wave is an electromagnetic wave having a wavelength of around several hundreds micrometers and is promising for various fields such as medical and security imaging, astronomy, agriculture, etc [1]. However it is difficult to detect THz wave because of its low photon energy. Here, we developed a THz detector based on a novel nanocarbon material, nanoporous graphene, and achieved highly sensitive and high speed THz detection operating in room temperature.

Nanoporous graphene is synthesized by a new chemical vapor deposition process in which single layers or a few layers graphene grow on a cheese-like nickel template full filled with porous of various size [2]. This material possesses the characteristic of single layer graphene, and at the same time has a 3D configuration, which means the mechanical strength is enough to accomplish bulk application of marvel character of graphene without substrate such as broadband light absorption spectrum and Dirac cone energy dispersion [2]. Differently from single layer graphene, the nanoporous graphene has broadband absorption spectrum with absorption rate over 90%, covering even THz range. It also has large Seebeck coefficient making it possible to convert thermal energy, obtained from THz radiation, into electrical signal.

We have fabricated a device by a pristine nanoporous graphene sample with averaged porous size around 100-300 nm. As shown in Fig.1, the THz response of this device was observed even without external electric field. This device has an advantage that the fabrication does not need complicated semiconductor fine process.

Because of the high thermal conductivity and the low specific heat [3], which determine the transient speed of thermal energy, our detector speed is relatively fast even for the detection mechanism based on thermoelectric effect.

For further improvement we are making a PN junction device.

This work was supported in part by the Japan Science and Technology Agency, MEXT/JSPS KAKENHI Grant Numbers JP26286005, JP16H00798, JP16H00906, and Support for Tokyotech Advanced Researchers (STAR).

[1] Y. Kawano, Contemporary Physics. **54**, 143 (2013).

[2] Y. Ito, *et al.* Angew. Chem. **53**, 4822 (2014).

[3] Y. Ito, *et al.* Adv. Mater. **27**, 4302(2015).

Corresponding Author: Y. Kawano

Tel: +81-3-5734-3811, Fax: +81-3-5734-3811,

E-mail: kawano@pe.titech.ac.jp

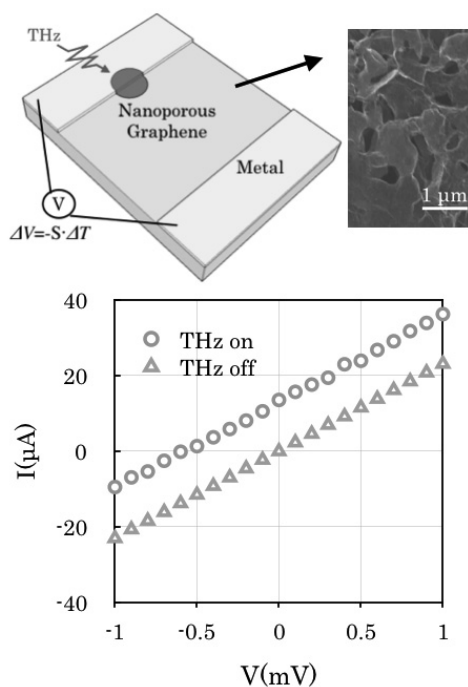


Fig.1: Device Structure and THz response.

Synthesis and Photophysical Properties of Chemically Converted Graphene–Pyrene Linked Systems

○Tomokazu Umeyama¹, Jinseok Baek¹, Junya Mihara¹, Hiroshi Imahori^{1,2}

¹ Graduate School of Engineering, Kyoto University, Kyoto 615-8510, Japan

² Institute for Integrated Cell-Material Sciences, Kyoto University, Kyoto 615-8510, Japan

In this study, pyrene dimer and monomer are covalently linked onto the chemically converted graphene (CCG) to investigate the dimerization effect on the optical and photophysical properties of the pyrene–graphene covalently linked systems.

Formation of dimeric and monomeric pyrenes standing on sp^2 carbon network of graphene has been achieved by one- and two-step methods as recently conducted using single-walled carbon nanotubes (SWNTs).^[1] As illustrated in Fig. 1 (upper), dimeric pyrenes were attached to CCG by one-step method, i.e., direct addition reaction of 4-(1-pyrenyl)phenyl (PP) radical onto the graphene plane of CCG (Py-1-CCG). We also synthesized monomeric pyrenes on CCG

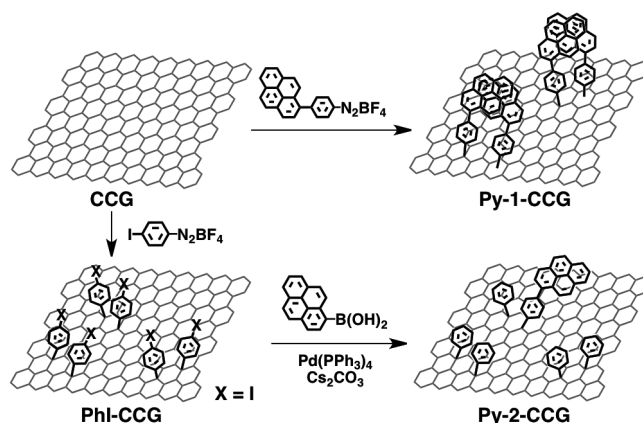


Fig. 1 Synthesis of Py-1-CCG and Py-2-CCG.

selectively by the stepwise additions consisting of the first addition of the iodinephenyl (PhI) radical onto CCG to yield the PhI-functionalized CCG (PhI-CCG), followed by the second Suzuki coupling between PhI-CCG and pyrene boronic ester (Py-2-CCG) (Fig. 1, lower). The low yield (ca. 15%) of the Suzuki coupling reaction rendered the PP groups monomeric in Py-2-CCG, even if the PhI groups in PhI-CCG formed paired structures on CCG.

The dimeric and monomeric structures on CCG in Py-1-CCG and Py-2-CCG, respectively, were substantiated by UV-vis absorption measurements. The spectrum of Py-2-CCG consists of those of PhI-CCG and Py-ref (1-phenylpyrene), i.e., a pyrene π - π^* band at 350 nm in addition to the broad structureless absorption of CCG extending to the near-infrared (NIR) region. This is consistent with the presence of the monomeric pyrenes on CCG in Py-2-CCG. In contrast, the spectrum of Py-1-CCG shows a new band at 450 nm. This emerging shoulder can be rationalized by the dimeric interaction between the pyrene rings in Py-1-CCG.

Upon excitation of Py-1-CCG and Py-2-CCG at 350 nm, where the absorbance of the pyrene moiety was adjusted to be identical to that of Py-ref, the fluorescence from pyrene moieties on CCG was quenched nearly quantitatively in comparison with Py-ref. This result implies that the pyrene excited states are quenched efficiently by CCG. In the presentation, we will show the results of transient absorption measurements to discuss the pyrene dimerization effect on the interaction between pyrene and CCG in the excited states in detail.

[1] T. Umeyama, J. Baek, Y. Sato, K. Suenaga, F. Abou-Chahine, N. V. Tkachenko, H. Lemmetyinen and H. Imahori, *Nat. Commun.* **6**, 7732 (2015)

Corresponding Author: T. Umeyama

Tel: +81-75-383-2568, Fax: +81-75-383-2571, E-mail: umeyama@scl.kyoto-u.ac.jp

Diazonium Chemistry for Tunable Grafting and Nanomanipulation

John Greenwood², Tomoko Inose¹, Yasuhiko Fujita², Oleksandr Ivasenko², Yoshito Tobe³,
Steven De Feyter², Hiroshi Uji-i^{1,2}

¹ *RIES, Hokkaido University, Sapporo 001-0020, Japan*

² *Department of Chemistry, KU Leuven-University of Leuven, Leuven 3001, Belgium*

³ *Division of Frontier Materials Science, Osaka University, Osaka 560-8531, Japan*

Graphene, a single atom thick sheet of sp² hybridized carbon, is the focus of intense research efforts because of its unique electronic, optical, mechanical, and thermal characteristics. Despite these exceptional qualities, however, the gapless band structure of pristine graphene leads to low on/off ratios in the application of field effect transistors (FET), hindering the development of graphene based devices. To take full advantage of the properties of graphene, therefore, it is important to develop a method to modify its electronic properties. For instance, chemical defects in the sp² hybridized surface lattice of graphene are known to promote bandgap opening, one of the requirements for the efficient operation of FETs. Covalent modification of graphene and HOPG from radicals produced from diazonium reagents is the most commonly used method to introduce chemical defect. However, this method is rather limited in terms of the grafting density due to multilayer formation and/or dendritic growth of adsorbates during the diazonium chemistry.

Here we selected 3,5-bis-*tert*-butylbenzenediazonium (3,5-TBD) as a sterically hindered reagent and succeeded in monolayer grafting with a high density.¹

We have used high-resolution scanning tunneling microscopy (STM) measurements to directly observe graphite lattice buckling at the site of covalent attachment to a previously defect-free HOPG and graphene surface for the first time, demonstrating the value of STM for characterizing systems. Using suitable tunneling parameters, we have demonstrated STM nanoshaving of grafted molecules for the first time under ambient conditions, which allows complex topographic patterns to be created in high density grafted layers. Importantly, using Raman spectroscopy and STM, we have proven that the pristine sp² carbon lattice is restored on removal of grafted species. Raman spectroscopy also indicates change in the electronic properties of graphene and possibility of tunable band gap opening following grafting of 3,5-TBD by varying the diazonium reagent concentration.

Our results settle several long-standing controversies regarding the details of diazonium modification of carbon surfaces, while high density monolayer grafting opens the way for efficient graphene-based devices.

[1] H. Uji-i *et al.* ACS Nano **9**, 5520 (2015).

Corresponding Author: H. Uji-i

Tel: +81-11-706-9409, Fax: +81-11-706-9406,

E-mail: hiroshi.ujii@es.hokudai.ac.jp

Graphene nanoribbon fabrication by gate-controlled edge-selective photo-oxidation

○Ryo Nouchi, Morihiko Matsumoto, Keiichiro Ikeda

*Nanoscience and Nanotechnology Research Center, Osaka Prefecture University, Sakai
599-8570, Japan*

All carbon atoms in graphene belong to its surface, leading to controllability of surface chemical phenomena by a configuration of a field-effect transistor (FET). In line with this “field-effect surface chemistry” concept, we have shown that photo-oxidation of graphene can be controlled by the FET configuration, especially by the polarity of the gate voltage (Fig. 1) [1]. The gate-controlled photo-oxidation occurs selectively at the edges of the graphene channel of the FET, and proceeds into the channel center. The formed graphene oxide is an insulator, and thus narrowing of a conducting graphene channel becomes possible by this method. Although graphene is unsuitable for switching/digital device applications because of no band gap, a finite band gap is known to be introduced by narrowing it down to nanometer scale. In this presentation, we report a conversion of a conductive wide graphene channel into a semiconducting narrow graphene ribbon by means of the gate-controlled edge-selective photo-oxidation.

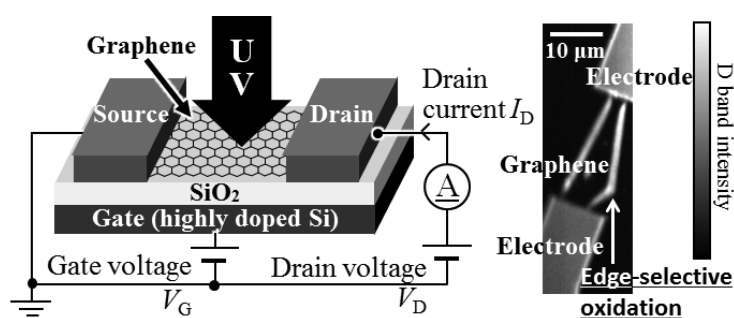


Fig. 1: Gate-controlled edge-selective photo-oxidation of graphene. The UV photo-oxidation was found to occur only under the negative gate voltage [1].

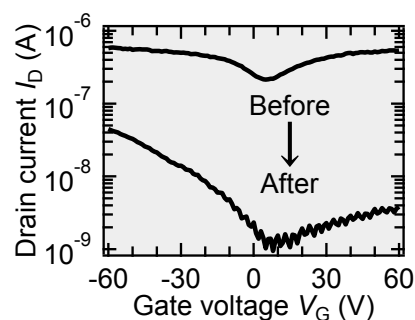


Fig. 2: Change in the transfer characteristics by the narrowing. The drain voltage was set to 5 mV.

Mechanically exfoliated graphene flakes were formed on a highly doped Si substrate with a 300-nm-thick thermal oxide layer. A FET structure shown in Fig. 1 was obtained by fabricating Au electrodes (with Cr adhesion layers) by electron beam lithography processes. Under application of the gate voltage of -60 V by using the FET configuration, the graphene channel was irradiated by ultraviolet (UV) light (Ushio UXM-Q256BY, ~ 2 W/cm²) in air (27°C, relative humidity of 60%). A comparison of transfer characteristics (gate-voltage dependence of the drain current) of the FET before and after the UV irradiation shows that the current on/off ratio at room temperature largely increased from 3 to 50, which indicates a successful conversion of a conductive wide graphene channel into a semiconducting narrow graphene ribbon.

[1] N. Mitoma and R. Nouchi, *Appl. Phys. Lett.* **103**, 201605 (2013).

Corresponding Author: R. Nouchi

Tel: +81-72-254-8394, Fax: +81-72-254-8394,

E-mail: r-nouchi@21c.osakafu-u.ac.jp

Doping of porous nanostructures

○Hidetsugu Shiozawa

¹ Faculty of Physics, University of Vienna, Boltzmannngasse 5, 1090 Vienna, Austria

In the interior of porous nanostructures, such as carbon nanotubes (CNTs) and metal-organic frameworks (MOFs), atoms and molecules can be arranged in 1D arrays and nanoclusters that could outperform their bulky counterparts. Our experiments using Raman, UV-Vis, photoemission, SQUID, electron microscopy and magnetotransport measurements elucidate electronic and magnetic interactions at guest-host molecular interfaces that are responsible for their unique physical properties [1,2]. We show that encapsulated inside single-wall carbon nanotubes (SWCNTs), nickel clusters behave as stable single-domain magnets exhibiting large coercive fields as the cluster size becomes as small as the exchange length. In MOFs, metal ions are coordinated to form metal arrays and nanovoids. Magnetic transition metal arrays in MOFs are ideal systems in which we study anisotropic magnetic coupling. Metal ions exposed to the interior voids react with infiltrating molecules, leading to MOF's sensing abilities. We show that the MOF's electrical conduction and magnetic ordering temperature can be tuned by molecular doping.

[1] H. Shiozawa *et al.* Sci. Rep. **5**, 15033 (2015).

[2] M. Kharlamova *et al.* Nanoscale **7**, 1383 (2015).

Corresponding Author: H. Shiozawa

Tel: +43-1-4277-72628, Fax: +43-1-4277-9726,

E-mail: hidetsugu.shiozawa@univie.ac.at

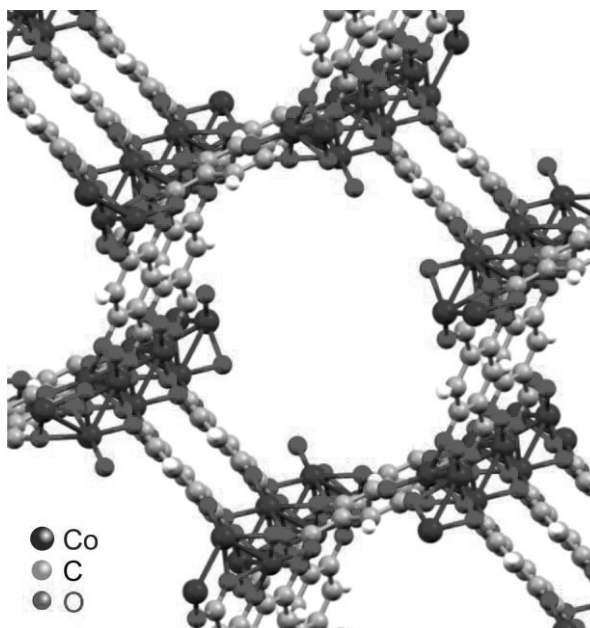


Fig.1: A metal-organic framework (Co-MOF-74) with a honeycomb nanostructure.

Fullerene Modification by Using Fullerene Cation Intermediate: Migration and Cyclization

○Yutaka Matsuo^{1,2}

¹*Hefei National Laboratory for Physical Sciences at Microscale, University of Science and Technology of China, Hefei, Anhui 230026, China*

²*Department of Mechanical Engineering, School of Engineering, The University of Tokyo, Bunkyo-ku, Tokyo 113-8656, Japan*

Fullerene cation, which is reactive and has an ability to rearrange, is of great interest and can serve as a versatile platform for functionalization of fullerene. A number of functionalized fullerenes which are difficult to synthesize otherwise, have been successfully obtained by the rearrangement of a fine-designed fullerene derivatives cation. For example, 1,2-dihydromethano[60]fullerene was synthesized in nearly quantitative yield by using a γ -silyl fullerene cation.^[1] A series of non-cyclic 1,2-diorgano[60]fullerene derivatives have been synthesized in good to excellent yield through an intramolecular Friedel–Crafts reaction of an arylsilylmethyl[60]fullerene cation derived from oxidation of an organo[60]fullerene dimer or mono(organo)[60]fullerene anion.^[2]

Fullerene cation, however, had been considered to be difficult to generate because the electronegative nature of the fullerene moiety. Thus, substrate scope and application has still been limited so far. We employed fullerene anions or fullerene radicals as starting materials to obtain key intermediate fullerene cations through oxidation using appropriate oxidants such as copper(II) halides. In this presentation, we summarize various reactions using fullerene cations, those are migration reactions and cyclization reactions to produce new fullerene-based electron-acceptors for organic solar cells application. In addition, in some reactions, additive plays important role to control the reaction. We will also disclose such examples to understand reaction mechanisms of fullerene cations-based fullerene modification reactions.

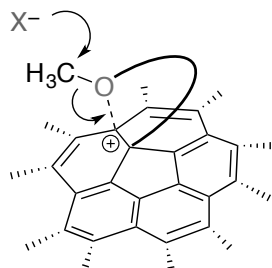


Figure. An example for fullerene cation-mediated cyclization reaction to produce a cyclo[60]fullerene derivative

References

- [1] Y. Matsuo, J. Kawai, H. Inada, T. Nakagawa, H. Ota, S. Otsubo, E. Nakamura, *Adv. Mater.* **2013**, *25*, 6266–6269.
 [2] Y. Zhang, Y. Matsuo, E. Nakamura, *Org. Lett.* **2011**, *13*, 6058–6061.

Corresponding Author: Y. Matsuo

Tel: +81-3-5841-0978, E-mail: matsuo@ustc.edu.cn; matsuo@photon.t.u-tokyo.ac.jp

A15-structured Cs_3C_{60} : the first non-cubic A_3C_{60} fulleride

○Yasuhiro Takabayashi¹, Ruth H. Zadik², Kosmas Prassides^{1,3}

¹ WPI - Advanced Institute for Materials Research (WPI-AIMR), Tohoku University, Sendai 980-8577, Japan

² Department of Chemistry, Durham University, Durham DH1 3LE, UK

³ Japan Science and Technology Agency, ERATO Isobe Degenerate π -Integration Project, Tohoku University, Sendai 980-8577, Japan

C_{60} -based solids with stoichiometry A_3C_{60} are archetypal examples of unconventional molecular superconductors in which electronic correlations play a dominant role. They are known to adopt cubic crystal structures based either on fcc or bcc packing. The bcc-derived A15-structured Cs_3C_{60} fulleride is an antiferromagnetic ($S = \frac{1}{2}$) Mott-Jahn-Teller insulator (MJTI) with a Néel temperature, T_N of 46 K (Fig. 1b) [1]. It is the parent of the superconductors with the highest T_c ($= 38$ K) found for any molecular solid [2]. Superconductivity emerges from the MJTI by applying hydrostatic pressure. Here, we present the results of a detailed investigation of the crystal structure of A15 Cs_3C_{60} at ambient pressure using high-resolution synchrotron X-ray powder diffraction (SXRPD).

Peak broadening of selected Bragg reflections due to anisotropic lattice microstrain was observed in the SXRPD data of A15 Cs_3C_{60} below T_N . Careful consideration of the broadened peaks allowed us to identify the presence of compression of the cubic unit cell along its body diagonal, consistent with the occurrence of a rhombohedral distortion (inset Fig. 1a). Rietveld refinements of the SXRPD data allowed a full characterization of the low-temperature crystal structure. The temperature dependence of the rhombohedral angle, α mirrors the temperature evolution of the magnetization (Fig. 1). A15-structured Cs_3C_{60} emerges as the first fulleride in which breaking of the spin rotational symmetry (spin ordering) is accompanied by simultaneous symmetry-breaking of the lattice and orbital degrees of freedom.

[1] Y. Takabayashi, *et al.*, *Science* **323**, 1585 (2009).

[2] A. Y. Ganin, *et al.* *Nat. Mater.* **7**, 367 (2008).

Corresponding Author: Yasuhiro Takabayashi

Tel: +81-22-217-5953, Fax: +81-22-217-5995

E-mail: yasuihiro.takabayashi.e4@tohoku.ac.jp

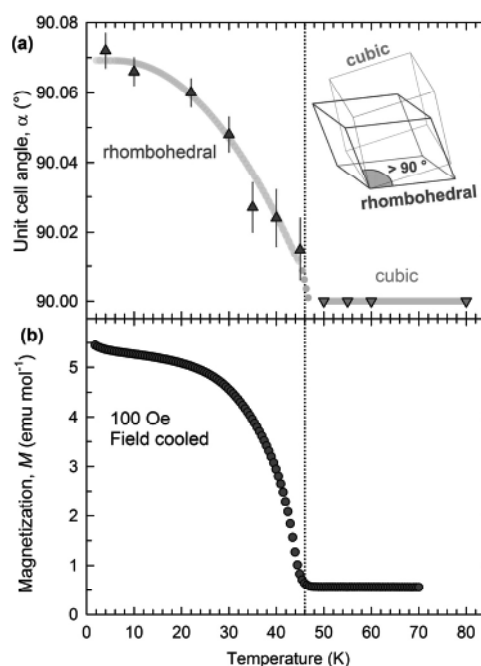


Fig.1 (a) Evolution of the unit cell angle with temperature. The solid line is a guide to the eye. Inset shows a distortion from cubic to rhombohedral symmetry. (b) Temperature dependence of the magnetization.

ポスター発表
Poster Presentations

1P-1 ~ 1P-40

2P-1 ~ 2P-39

3P-1 ~ 3P-39

Preparation of gold nanoparticles stabilized by water-soluble fullereneol $C_{60}(OH)_{36}$

○Nozomi Sato, Ken Kokubo, Hidehiro Sakurai

*Division of Applied Chemistry, Graduate School of Engineering, Osaka University,
Osaka 565-0871, Japan*

Properties of gold nanoparticles (AuNPs) can be controlled by the design of their protecting ligands that stabilize the nanoparticles from their undesired aggregation [1]. Water-soluble polymer such as poly(vinylpyrrolidone) (PVP) is one of the representative protecting ligands of AuNPs in aqueous solution. We have found that a naturally abundant polymer, chitosan, as a protecting ligand improved the catalytic activity [2]. However, because of the sterically regulated polymeric chain structure, the polymer ligands generally require a large excess amount to stabilize AuNPs (colloidal size is ca. 10–100 nm). In addition, much stronger molecular-sized ligand instead of polymers, which can reduce the amount of use, may decrease the catalytic activity by complete covering of the Au surface.

To improve the ligand system, water-soluble carbon nanomaterials, which are well known to form a nano-sized aggregation, can be good candidates for a newly designed ligand. Indeed, some examples on Au nanocomposites with C_{60} have been reported [3]. In order to prepare the quasi-homogeneous colloidal dispersion of Au/fullerene composites in aqueous solution, water-soluble fullerenes are used. We have explored a series of polyhydroxylated fullerenes, $C_{60}(OH)_n$ ($n = 10, 12, 24, 36, 44$ etc), and among them, $C_{60}(OH)_{36}$ exhibits high water solubility up to 17.5 mg/mL with high dispersion on a molecular level [4].

The AuNPs stabilized by $C_{60}(OH)_{36}$, $Au:C_{60}(OH)_{36}$, was prepared by common reduction method with an excess amount of $NaBH_4$ from $HAuCl_4$ aqueous solution in the presence of $C_{60}(OH)_{36} \cdot 8H_2O$. The colloidal particles were homogeneously dispersed in water and were stable for months. Its core size (measured by TEM) and colloid size (by IG [4]) were 3.7 ± 0.8 nm and 12.2 ± 4.5 nm, respectively. XPS and XAS measurements revealed that $Au:C_{60}(OH)_{36}$ was negatively charged in total, but rather positively charged on the surface. It also exhibited the catalytic activity toward the reduction of 4-nitrophenol in the presence of $NaBH_4$.

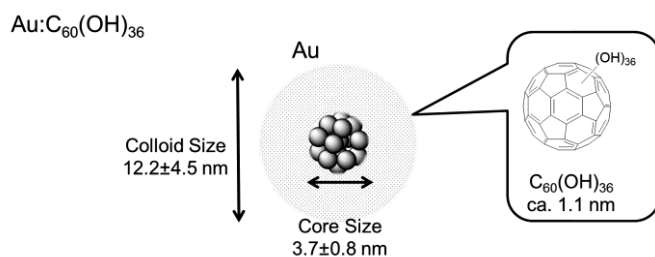


Fig.1 Image and the size of $Au:C_{60}(OH)_{36}$.

- [1] D. Li, Q. He, J. Li, *Adv. Colloid Interface Sci.* **149**, 28 (2009).
 [2] R. N. Dhital, A. Murugadoss, H. Sakurai, *Chem. Asian J.* **7**, 7325 (2011).
 [3] M. Geng, Y. Zhang, Q. Huang, B. Zhang, Q. Li, W. Li, J. Li, *Carbon* **48**, 3570 (2010).
 [4] K. Kokubo, K. Matsubayashi, H. Tategaki, H. Takada, T. Oshima, *ACS Nano* **3**, 237 (2008).

Corresponding Author: K. Kokubo, H. Sakurai
 Tel: +81-6-6879-4592, Fax: +81-6-6879-4593,
 E-mail: kokubo@chem.eng.osaka-u.ac.jp, hsakurai@chem.eng.osaka-u.ac.jp

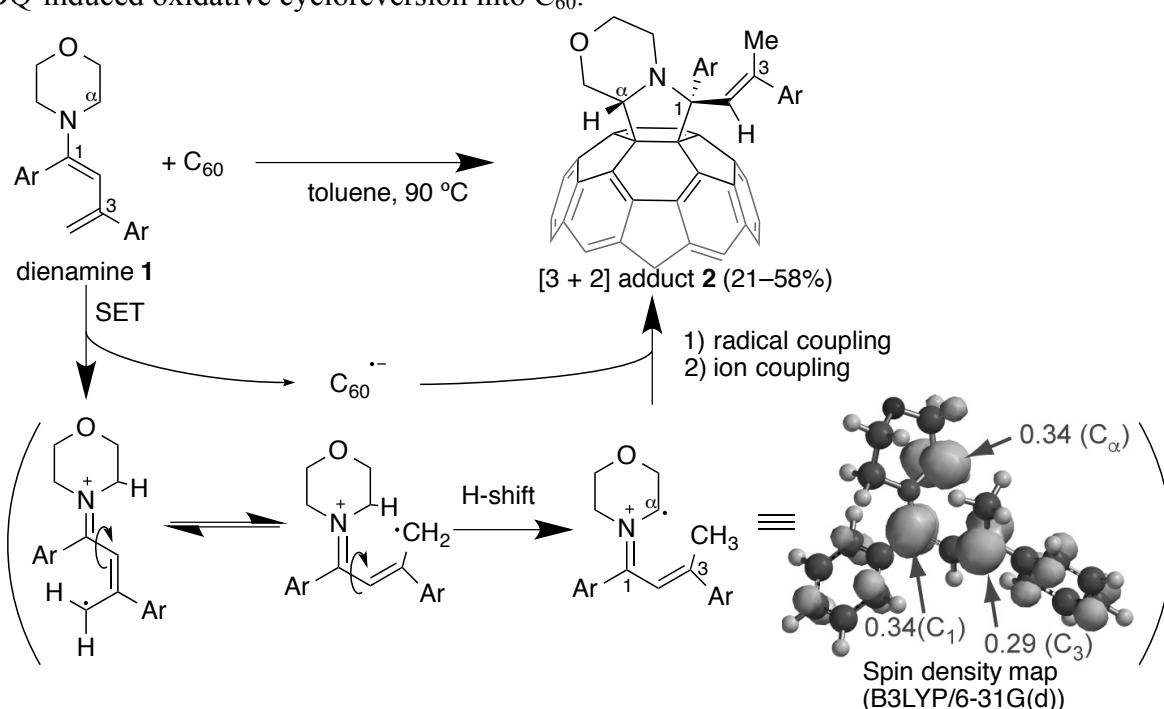
Thermal single electron transfer between C₆₀ and dienamines leading to pyrrolidinofullerenes via hydrogen shift of radical intermediates

○Naohiko Ikuma, Hiroyuki Yamamoto, Ken Kokubo, Takumi Oshima

*Division of Applied Chemistry, Graduate School of Engineering,
Osaka University, Suita 565-0871, Japan*

Single electron transfer (SET) reaction of donor reagents with C₆₀ is a useful procedure for formation of fullerene monoadducts via radical or ionic coupling because the reduced electrophilicity of monoadduct inhibits further addition. Previously we have reported the selective [2+2] monoaddition of enamines with C₆₀ [1]. Here, we present the SET reaction of dienamines with C₆₀ followed by unexpected hydrogen shift to give pyrrolidinofullerenes [2,3].

Aryl-substituted dienamines **1** with variously substituents were reacted with C₆₀ under dark condition to give pyrrolidinofullerenes **2** in 21–58 % yields. The reaction mechanism includes SET of diaryldienamines to C₆₀ and the following consecutive 1,6-hydrogen shift and the [3 + 2] cycloaddition of the generated radical ion pair, clarified by DFT calculations and EPR measurement with a spin-trapping agent (nitrosobenzene). The LUMO levels of pyrrolidinofullerenes were ca. 0.1 eV higher than that of C₆₀, consequently suppressing the bisadduct formation. The phenyl-substituted pyrrolidinofullerene **2a** representatively exhibited the protic acid-catalyzed intramolecular Friedel–Crafts cyclization and the DDQ-induced oxidative cycloreversion into C₆₀.



[1] T. Mikie, H. Asahara, K. Nagao, N. Ikuma, K. Kokubo, T. Oshima, *Org. Lett.* **13**, 4244 (2011).

[2] N. Ikuma, H. Yamamoto, K. Kokubo, T. Oshima, *Chem. Lett.*, **43**, 1648 (2014).

[3] N. Ikuma, H. Yamamoto, K. Kokubo, T. Oshima, *Heterocycles*, **90**, 1168 (2015).

Corresponding Author: N. Ikuma

Tel: +81-6-6879-4592, Fax: +81-6-6879-4593, E-mail: ikuma@chem.eng.osaka-u.ac.jp

Availability of fullerene for skin photo-aging; Anti-inflammatory and suppression of carboxylated protein generation.

○Hisae Aoshima, Masayuki Ito

*Vitamin C60 BioResearch Corporation,
Tatsunuma Bldg. 9F 1-3-19 Yaesu Chuo-ku, Tokyo 103-0028, Japan*

Fullerene is a carbon allotrope with a unique structure in which the carbon atoms are bonded with each other to form soccer ball-like structure. The efficient radical scavenging/anti-oxidant properties as part of a new class of carbon materials has attracted considerable attention for companies innovating in the cosmetic and pharmaceutical sectors.

Fullerene as a cosmetic ingredient composed with polyvinylpyrrolidinone (PVP) has been on the market since 2005 (Fig.1).

We examined the effect of fullerene on UV induced prostaglandin E₂ (PGE₂) and interleukin-8 (IL-8) productions in reconstructed human epidermis (RhE). The UV induced PGE₂ [1] and IL-8 productions were significantly suppressed by the addition of fullerene.

Carboxylated proteins are known as cause of skin dullness. They are produced by UV irradiation and generate radicals in the stratum corneum. We examined the effect of fullerene on UV induced carboxylated proteins production in human stratum corneum. The UV induced carboxylated proteins were remarkably inhibited by the addition of fullerene.

In this conference, we will show the radical scavenging properties, anti-inflammatory effects, and the suppression of carboxylated protein generation by fullerene. In addition, we will introduce the results of safety evaluation tests of fullerene for human skin applications [2, 3].

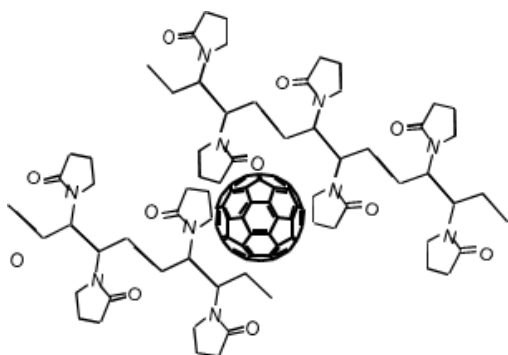


Fig.1: Fullerene composed with PVP.

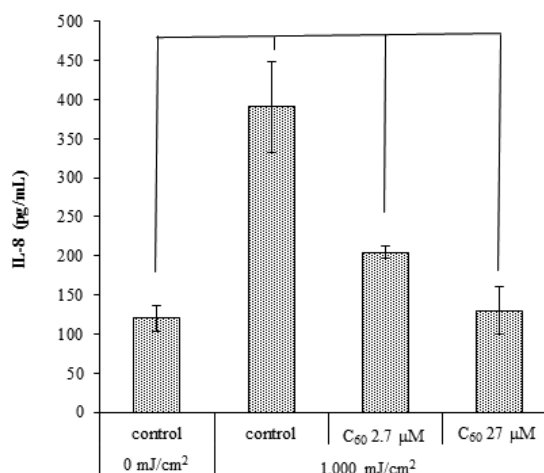


Fig.2: Suppression of IL-8 by fullerene.

[1] S. Inui *et al.* J. Nanobiol. **12**:6, Open Access (2014).

[2] H. Aoshima *et al.* J. Toxicol. Sci. **34**:5, 555 (2009).

[3] H. Aoshima *et al.* J. Toxicol. Sci. **35**:3, 401 (2010).

Corresponding Author: Hisae Aoshima
Tel: +81-3-3517-3253, Fax: +81-3-3517-3260
E-mail: hisae.aoshima@vc60.com

Nanoscale Water Droplet Confined in Fullerene Bilayer Vesicles

○ Sai Prakash Maddala¹, Tatsuya Homma¹, Ricardo M. Gorgoll¹, Koji Harano¹, Wasim Abuillan², Alexandra Burk², Motomu Tanaka², Eiichi Nakamura¹

¹ Department of Chemistry, The University of Tokyo, Tokyo 113-0033, Japan

² Institute of Physical Chemistry, University of Heidelberg, D69120 Heidelberg, Germany

Understanding the behaviour of water confined on nano- and mesoscales is a key to gaining complete understanding of diverse biophysical phenomena such as water transport in cells, protein folding etc.¹ However, conventional lipid or polymer vesicles lack the robustness necessary to isolate and characterize confined water. Herein we report that highly robust containers for the entrapment of water molecules at nano and mesoscale (> 100 nm) were prepared by the self-assembly of potassium salt of functionalized fullerene molecules $R_5C_{60}^- K^+$, where R = Ph (**PhK**), *p*-C₂₀H₄₁C₆H₄ (**C20K**) and *p*-C₈F₁₇C₆H₄ (**F8K**), respectively (Figure 1). The vesicles were prepared by injecting monomer solution, in THF, into water. Through careful variation of the injection rate, stirring rate and reaction volume, we were able to control the monomer self-assembly and achieved highly monodisperse bilayer vesicles on nano and meso length scales. The presence of water in vesicles deposited on solid substrate was determined using SEM/EDAX analysis (Figure 2A). Despite the ultrahigh vacuum conditions (10⁻⁵ pa), we were able to demonstrate by the presence of oxygen signals (water is the sole source of oxygen in the vesicles). Quantitative evaluation of total oxygen content was performed for **F8K**, using fluorine atom as the internal standard. Finally, we were able to visualize additive mediated controlled disruption and release of water from the **F8K** vesicles using STEM (Figure 2B). Small Angle Neutron Scattering analysis was used to probe the vesicle morphology and permeability of the bilayers. The vesicles had a permeability of 2.6 x 10⁻¹³ m/s, which is 10⁹ times lower than that of lipid bilayers. Thus making these vesicles among the most robust bilayer materials known.

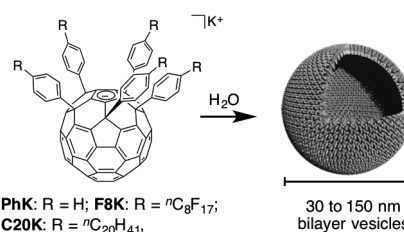


Figure 1: Schematic representation of preparation of fullerene bilayer vesicles

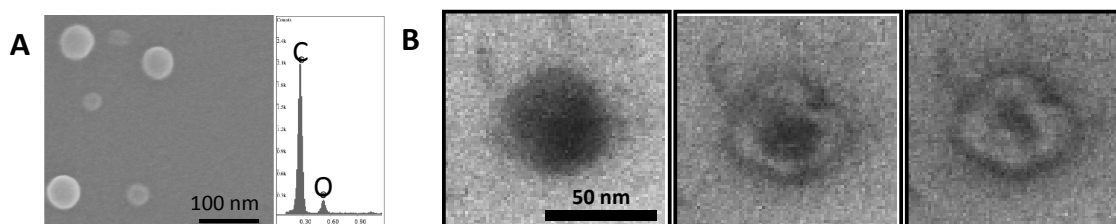


Figure 2: A) SEM image and EDX of **C20K** vesicle showing the presence of oxygen; B) Controlled water release (STEM images from **F8K** vesicles following the addition of C₈F₁₈)

[1] a) L.Barros da Silva, *J. Nanostruct. Chem.*, 2014, **4**, 104. b) V.V. Chaban, V.V. Prezhdo and O.V. Prezhdo, *ACS Nano*, 2012, **6**, 2766-2773. c) D. Chandler, *Nature*, 2005, **437**, 640-647.

Corresponding Author: E. Nakamura

Tel: +81-3-5841-4369, Fax: +81-3-5841-4369,

E-mail: s.p.maddala@chem.s.u-tokyo.ac.jp

ESR measurements of $\text{Gd@C}_{60}(\text{CF}_3)_3$

○Takahisa Yamaguchi¹, Ayano Nakagawa³, Hisanori Shinohara³,
Ko Furukawa⁴, Tatsuhisa Kato^{1,2}

¹Graduate School of Human and Environmental Studies, Kyoto University, Kyoto 606-8501,
Japan

²Institute for Liberal Arts and Sciences, Kyoto University, Kyoto 606-8501, Japan

³Department of Chemistry, Nagoya University, Nagoya 464-8602, Japan

⁴Department of Chemistry, Niigata University, Niigata 950-2181, Japan

The Nagoya group of authors succeeded to produce trifluoromethyl derivatives of Gd@C_{60} by the arc discharge of a metal/graphite composite rod with polytetrafluoroethene as source for functional group.^[1] The electron spin state of the major isolated component of $\text{Gd@C}_{60}(\text{CF}_3)_3$ was investigated by ESR spectroscopy.

$\text{Gd@C}_{60}(\text{CF}_3)_3$ exhibited the ESR spectrum shown in Fig. 1, which was observed by X-band ESR spectrometer at 4K and well reproduced by the computer simulation using positive value of zero field splitting $D = 0.2365 \text{ cm}^{-1}$, $E = 0.0000 \text{ cm}^{-1}$, and the spin quantum number $S=7/2$. The $S=7/2$ spin state was attributed to seven radical electrons on the 4f orbital of an endohedral gadolinium ion with the closed-shell electronic structure of carbon cage. Considering the computer simulation for W-band ESR measurement, as shown in Fig. 2, the quantum number of $S=7/2$ would be confirmed by the clear structure of W-band spectrum, and the positive sign of D would be determined by W-band measurement at low temperature. The zero value of parameter E suggested the uniaxial symmetric structure of $\text{Gd@C}_{60}(\text{CF}_3)_3$. It is noticeable that the value of D is comparable with those for $S=7/2$ states of Gd@C_{82} ,^[2] and topological isomers of Eu@C_{82} .^[3]

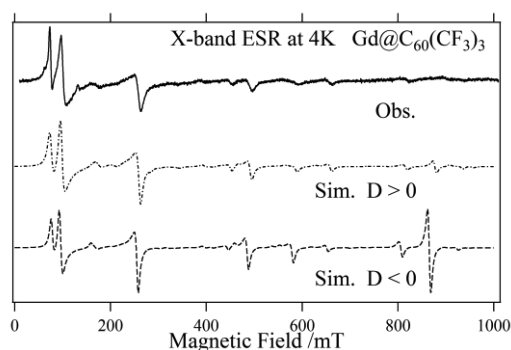


Fig. 1. X-band ESR observed (Obs.) and simulated (Sim.) spectra of $\text{Gd@C}_{60}(\text{CF}_3)_3$.

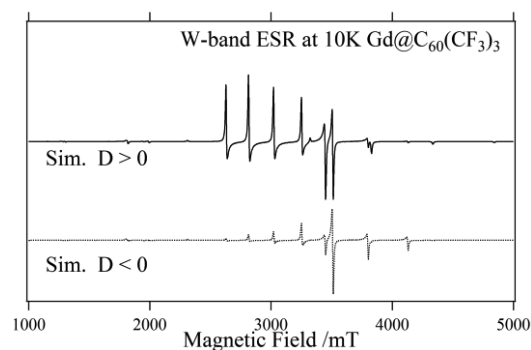


Fig. 2. W-band ESR simulated spectra $\text{Gd@C}_{60}(\text{CF}_3)_3$.

References

- [1] Z. Wang et al., *Angew. Chem. Int. Ed.* **52**, 11770-11774 (2013).
[2] K. Furukawa et al., *J. Phys. Chem.* **107**, 10933-10937 (2003).
[3] H. Matsuoka et al., *J. Phys. Chem.* **108**, 13972-13976 (2004).

Corresponding Author: Tatsuhisa Kato

Tel: +81-75-753-6695, Fax: +81-75-753-6695, E-mail: kato.tatsuhisa.6e@kyoto-u.ac.jp

Electronic properties of PCBM under an external electric field

Sho Furutani and Susumu Okada

*Graduate School of Pure and Applied Sciences, University of Tsukuba, 1-1-1 Tennodai, Tsukuba, Ibaraki
305-8571, Japan*

Functionalized fullerenes are known to possess unusual electronic structure, which is totally different from that of the pristine fullerene, making them constituent materials of the optical, optoelectronic, magnetic, and photovoltaic devices. Since fullerene and functionalized fullerene possess the deep lowest unoccupied states, they act as n-type semiconducting constituent materials of organic thin film solar cells with high conversion efficiency. [6,6]-phenyl-C₆₁-butyric acid methyl ester (PCBM) and silylmethylfullerenes (SIMEF) are widely used for the electron acceptors of the organic photovoltaic devices. However, microscopic mechanism of the electron accumulation in this molecule by the electric field is not elucidated yet. Therefore, in the present work, we aim to investigate the electronic properties of PCBM under an external electric field by using the density functional theory combined with the effective screening medium method to give theoretical insight into the microscopic mechanism of the carrier accumulation in PCBM. To investigate the effect of the molecular arrangement on the carrier accumulation, we consider two different molecular arrangements with respect to the gate electrode.

Figure 1 shows the electrostatic properties of PCBM under the zero electric field. As shown in Fig. 1, the potential at the tail region of PCBM is lower by 0.32 V than that at the head region, indicating that PCBM possess electric dipole moment, because of the asymmetric shape and attached functional group onto C₆₀ cage. The dipole moment is expected to affect the carrier injection into PCBM with respect to their mutual molecular arrangement to the electrode. In fact, we find that the accumulated electrons are localized on the bowl region under the head-to-tail arrangement with respect to the electrode, while they are extended throughout the molecule in the tail-to-head arrangement. In accordance with the carrier distribution, induced electric field around the PCBM under the external electric field also depends on the molecular arrangement. The accumulated electrons on the molecular feathers lead to the substantial electric field concentration around them because of its sharpen shape. The present results give a guiding principle for designing the p-n junction of organic photovoltaic devices.

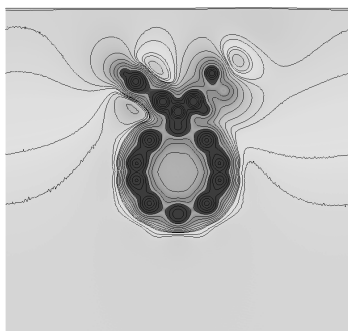


Fig.1 Contour plot of the electrostatic potential of PCBM without the external electric field.

Corresponding author: S. Furutani

Tel: +81-29-853-5600 (ext.8233), Fax: +81-29-853-5924,

E-mail: sfurutani@comas.frsc.tsukuba.ac.jp

Electronic states of chalcogen encapsulated in single-walled carbon nanotubes studied by First-Principles DFT calculations

○¹Yutaka Sato, ²Yosuke Kataoka, ¹Eita Yokokura and ^{1,2,3} and Hironori Ogata

¹ Graduate School of Science and Engineering, Hosei University, Koganei 184-8584, Japan

²Department of Faculty of Bioscience and Applied Chemistry, Hosei University, Koganei, 184-8584, Japan

³Research Center for Micro-Nano Technology, Hosei University, Koganei 184-0003, Japan

Single-walled carbon nanotubes (SWNTs) have a hollow space in the nanometer size that can be encapsulated various functional molecules. The confined molecular assemblies is expected to exhibit unique low-dimensional structures and solid state properties that can not be realized in the bulk states. Recently, syntheses of sulfur encapsulated SWNTs or selenium encapsulated DWNTs and unique one-dimensional conductive sulfur chain structure or double-helices selenium structure were reported. In this study, we report the effects of chirality and diameter of CNTs on the local structure and molecular structure and electronic states of the chalcogens encapsulated by SWNTs by using first-principles DFT calculations. We calculated the band structures and solid ³³S- NMR parameters (NMR chemical shift tensors and electric field gradient (EFG) tensors). All of the calculations were done by using a Open-Source computer code package PWscf and GIPAW in Quantum ESPRESSO. Table 1 shows the EFG tensors at S-sites in S@(5,5)SWNT and S@(7,0)SWNT. The detailed results including both band structures and ³³S-NMR chemical shift tensors in S@SWNT with different chiral structures will be presented.

	$e^2qQ/h(\text{MHz})$		η	
	S@(5,5)SWNT	S@(7,0)SWNT	S@(5,5)SWNT	S@(7,0)SWNT
S1	-33.904	-17.262	0.553	0.091
S2	-35.106	-15.628	0.554	0.340
S3	-20.728	-17.220	0.029	0.253
S4	-21.460	-15.971	0.030	0.198

Table 1. EFG tensors at S-sites in S@(5,5)SWNT and S@(7,0)SWNT.

References

- [1] Toshihiko Fujimori et al. Nature Communications4(2013)2162.
- [2] Frank H.Stillinger et al. J.Phys.Chem85(1986)6460.
- [3] Frank H.Stillinger et al. J.Phys.Chem.1987, 91 (19), pp4899-4907.
- [4] Toshihiko Fujimori et al. ACS Nano vol.7 No.6(2013)5067-5613.
- [5] T.A wagler et al. Journal of Magnetic resonance 161 (2003) 191-197.
- [6] L.A. O'Dell, I.L. Moudrakovski. Journal of Magnetic Resonance 207 (2010) 345-347.
- [7] P. Giannozzi et al., J.Phys.:Condens.Matter, 21(2009)395502.

Corresponding Author: H. Ogata Tel: +81-42-387-6229, Fax: +81-42-387-6229, E-mail: hogata@hosei.ac.jp

Bolometric performance of highly purified (6,5) Single Walled Carbon Nanotubes

Junko Eda, Yohei Yomogida, and Kazuhiro Yanagi

Department of Physics, Tokyo Metropolitan University, Tokyo 192-0397, Japan

Because of the smallness of specific heat and the large optical absorption in far-infra red region of single walled carbon nanotubes (SWCNTs), the bolometric performance of SWCNTs and their applications for temperature sensors have been intensively studied. Previously, we have proposed the importance of preparation of high-purity semiconducting SWCNT samples for improving the performance due to their intrinsically large resistance change by the shift of the temperature. Recent progress of purification techniques enables us to prepare single-chiral semiconducting SWCNTs with purity more than 99% on the basis of analyses of their optical absorption spectra. Here we demonstrate how the purity significantly influences the bolometric performance of their thin film devices. We prepared two types of purified (6,5) SWCNTs with different purity. Here the purity was tentatively evaluated from the ratio of optical absorption intensities at around (6,5) peak and 450 nm (Fig. 1(a)). The one, which is called as P-(6,5), is 0.19, and the other, which is called as HP-(6,5) is 0.07, indicating that the amount of amorphous carbon and metallic nanotubes in HP-(6,5) would be less than the half of that in P-(6,5). We fabricated thin films on parylene substrates and measured the resistance changes upon the illumination of black body radiation (BBR) with different temperature. In the case of HP-(6,5), we observed clear resistance change when the BBR temperature is 30 °C at room temperature, 20°C. The ratio of resistance change by the illumination of BBR as a function of BBR temperature is plotted in Fig. 1(c). The sensitivity of HP-(6,5) was 10 times better than that of P-(6,5). The noise equivalent temperature was significantly reduced from 1.1 °C in P-(6,5) to 0.1 °C in HP-(6,5). These results clearly indicate the importance of high-purity semiconducting SWCNTs for their bolometric applications.

This work is supported by Huawei Innovation Research Program (HIRP)

References:[1] He et al., *Adv. Optical. Mater.* 3, 989 (2015), [2] Yanagi et al, *ACS Nano* 4, 4027 (2010), [3] Yomogida et al., *Nat. Comm.* 7, 12056 (2016).

Corresponding Author: Kazuhiro Yanagi
e-mail: yanagi-kazuhiro@tmu.ac.jp

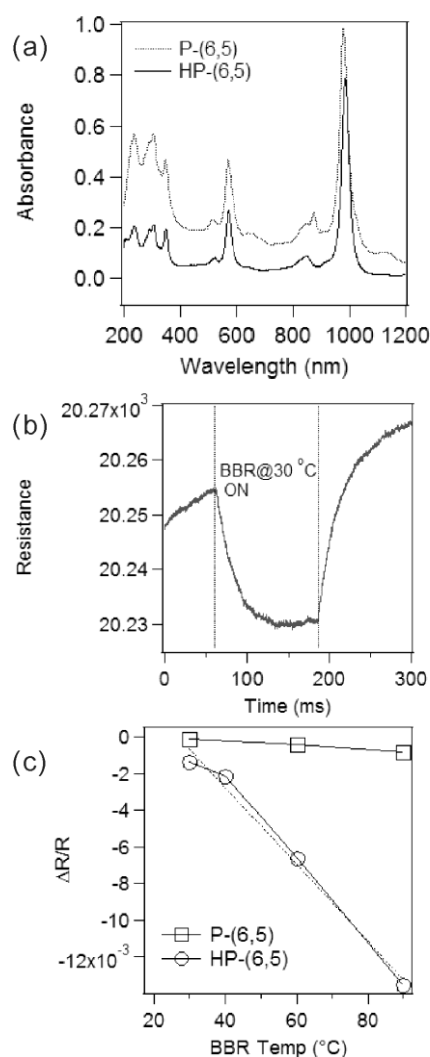


FIG1 : (a) Optical absorption spectra, (b) responses to the BBR with temperature of 30 °C, (c) relationship between resistance change and BBR temperature.

Superconductivity in WS₂ chiral nanotube

○Feng Qin¹, Wu Shi^{1,2}, Toshiya Ideue¹, Masaro Yoshida¹, Alla Zak³, Reshef Tenne⁴,
Tomoka Kikitsu⁵, Daishi Inoue⁵, Daisuke Hashizume⁵, Yoshihiro Iwasa^{1,5}

¹ *Quantum Phase Electronics Center (QPEC) and Department of Applied Physics,
The University of Tokyo, Tokyo 113-8656, Japan*

² *Materials Science Division, Lawrence Berkeley National Laboratory, Berkeley, CA 94720,
USA*

³ *Faculty of Sciences, Holon Institute of Technology, 52 Golomb Street, P. O. Box 305, Holon,
Israel*

⁴ *Department of Materials and Interfaces, Weizmann Institute of Science, Rehovot 76100,
Israel*

⁵ *RIKEN Center for Emergent Matter Science (CEMS), Wako, Saitama 351-0198, Japan*

Superconductivity characteristic in low dimensional structures, such as nanotubes (NTs), is of great interest, because of their uniqueness in geometry. Despite the intensive studies of superconductivity in carbon NTs[1], properties reflecting its peculiar cylindrical/chiral geometries[2] have remained elusive. One of the manifestations of the chiral structure in the electronic transport is the nonreciprocal resistance[3]. As shown in Fig. 1, the two directions of current injection are not identical due to the chiral nature of the conducting substance when the magnetic field is applied parallel to the tube.

Here we report the first observation of superconductivity in individual multi-walled tungsten disulfide (WS₂) chiral nanotubes[4] induced by ionic gating. The interference of supercurrent along the tube circumference was proved by the periodic magnetoresistance oscillation with the period of a flux quantum inside the tube[5]. More importantly, the observation of antisymmetric second harmonic signal in AC resistance provides unambiguous evidence of unprecedented nonreciprocal superconducting transport originating from the tube chirality[6], consistent with electron diffraction analysis as shown in Fig. 2. In view of the wealthy family of materials[7,8], the present result indicates that chiral nanotubes should be a new platform for the nanoscaled superconductivity with broken inversion symmetry.

- [1] M. Koiciak *et al.*, *Phys. Rev. Lett.* **86**, 2416-2419 (2001)
 [2] S. Iijima, *Nature* **354**, 56-58 (1991)
 [3] G. L. J. A. Rikken *et al.*, *Phys. Rev. Lett.* **87**, 236602 (2001)
 [4] R. Tenne *et al.*, *Nature* **360**, 444-460 (1992)
 [5] W. A. Little *et al.*, *Phys. Rev. Lett.* **9**, 9 (1962)
 [6] V. Krstić *et al.*, *J. Chem. Phys.* **117**, 11315 (2002)
 [7] L. S. Panchakarla *et al.*, *J. Phys. Chem. Lett.* "Perspectives" **5**, 3724-3736 (2003)
 [8] C. N. R. Rao *et al.*, *Dalton Trans.* **1**, 1-24 (2003)

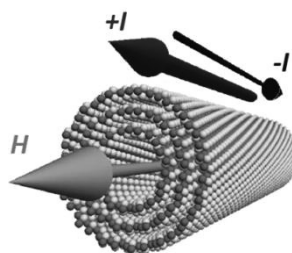


Fig. 1: Nonreciprocal superconductivity in WS₂ chiral nanotube

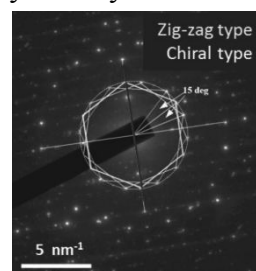


Fig. 2: Electron diffraction analysis of WS₂ chiral nanotube

Corresponding Author: F. Qin

Tel: 03-5841-6822(26822), Fax: 03-5841-6822(26822),

E-mail: qinfeng@mp.t.u-tokyo.ac.jp

The structural contribution to the electrical character of super-growth SWCNT forest through a height dependent study

○Takayuki Watanabe², Hiroe Kimura^{2,4}, Shigeki Hano^{2,4}, Shunsuke Sakurai^{1,2}, Motoo Yumura^{1,2}, Kenji Hata^{1,2,3,4} and Don N. Futaba^{1,2}

¹*CNT Application Research Center, National Institute of Advanced Industrial Science and Technology (AIST), Tsukuba, 305-8565, Japan*

²*Technology Research Association for Single Wall Carbon Nanotubes (TASC), Tsukuba, 305-8565, Japan*

³*Japan Science and Technology Agency, c/o AIST, 34 Miyukigaoka, Tsukuba, Ibaraki 305-8501, Japan*

⁴*Tsukuba University, Department of Pure and Applied Sciences, Tsukuba University, Tsukuba, 305-8573, Japan*

We report an electrical investigation of super-growth SWCNT forests where we have succeeded in elucidating the electrical contributions of the forest surface (cap) and vertically aligned (body) structures of the assembly [1]. We applied an electrical characterization method to SWCNT forests patterned into a Hall bar-like configuration to reliably evaluate the lateral (i.e. in-plane) resistance for a series of SWCNT forests spanning three orders of magnitude, 0.3 to 700 μm , in height while avoiding direct mechanical contact to the measurement region.

Figure 1 shows the measured resistivities along lateral direction of forests at each forest height and fitting curve. A simple model based on treating the forests as two parallel resistors was used to explain the observed behavior of the lateral resistivity and forest height. The model well explains the behavior of the measurement data. Fitting results also showed that there is a large difference between the cap and body resistivity, which ranges 20~700 times.

In summary, we showed that the forests resistivity could be simply described electrically by two structural features, the cap and body, through 0.3 ~ 700 μm height range. In addition, our analysis found that the resistivity of the body was about 20 ~ 700 times higher than that of the cap.

[1] T. Watanabe *et al.* Carbon. **108**, 106(2016).

Corresponding Author: DN. Futaba

E-mail: d-futaba@aist.go.jp

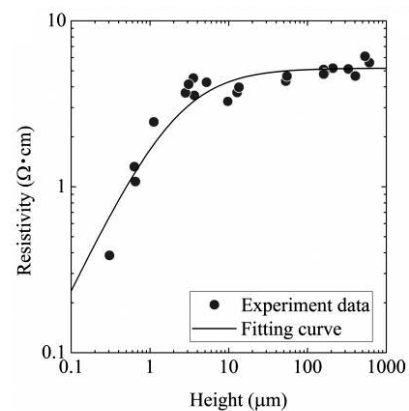


Fig.1 Height dependence of super-growth SWCNT forest resistivity.

Development of Air-stable n-type Thermoelectric Materials with Benzimidazole derivative-doped Single-walled Carbon Nanotubes

○Yuki Nakashima¹, Tsuyohiko Fujigaya^{1,2,3}, Naotoshi Nakashima^{1,2}

¹ Graduate School of Engineering, Kyushu University, 744 Motoooka, Nishi-ku, Fukuoka, 819-0395, Japan ² World Premier International (WPI), International Institute for Carbon-Neutral Energy Research ³ Precursory Research for Embryonic Science and Technology (PRESTO), Japan Science and Technology Agency (JST)

Despite the remarkable growth of microelectronics such as wearable and portable devices, remote sensors, etc. on the market in recent years, most of the microelectronics are still powered by batteries that are required to recharge and replace at stated periods. One possible solution for powering these wireless microelectronics without a battery is to harvest energy from the human body by using thermoelectric (TE) generation which generates electricity especially from temperature difference. To generate electricity via Seebeck effect is promising. Seebeck effect is the phenomenon that a temperature difference between hot and cold ends of the TE generators that produces a voltage. To fabricate the TE devices, p- and n-type materials are necessary and the study of TE materials using inorganic semiconductors such as Bi₂Te₃ have been done for a long time as they illustrate high efficiency. However, these materials contain rare elements which show toxicity and poor processability. Therefore among the several candidates including conducting polymers, transition metal dichalcogenide and carbon nanotubes (CNTs), single-walled CNTs (SWNTs) are emerged as the promising candidate due to their non-toxicity, processability, abundant resources together with the remarkable electrical conductivity, potentially large Seebeck coefficient and light weight. However, due to the air oxidation, SWNTs only show p-type semiconducting property in air. In the development of the CNT-based TE devices, instability of the n-type CNT has been a central issue, since n-type SWNT are easily oxidized due to an electrophilic chemisorption of oxygen.[1] Previously, we reported n-type SWNT by encapsulating cobaltcence to SWNT, however, n-type stability lasts only 30 days in air.[2] Therefore, in this study we explored an air-stable n-type thermoelectric material by covering the anion part of the SWNT surface by using cationic molecules as a dopant (n-type dopant). In this strategy, 2-(2-methoxyphenyl)-1,3-dimethyl-2,3-dihydro-1H-benzo [d] imidazole (DMBI) was chosen, since it is stable in the atmosphere, forms a stable cationic state by hydride transfer[3] and is known as n-type dopant for other carbon materials, such as graphene and fullerene.[4] We evaluated the air stability of SWNT doped by DMBI and found that the n-type nature of the DMBI-doped SWNT was stable at least for 170 days at room temperature.[5]

[1] Cheng, J.-P et al. *J. Am. Chem. Soc.* **2008**, 130, 2501.

[2] Nakashima, N et al. *Sci. Rep.* **2015**, 5, 7951.

[3] Bao, Z et al. *J. Am. Chem. Soc.* **2010**, 132, 8852.

[4] Bao, Z. et al. *Nano Lett.* **2013**, 13 (5), 1890.

[5] Nakashima, Y. Nakashima, N. Fujigaya, T. *submitted*.

Corresponding Author: Fujigaya, T.

Tel: + 81-92-802-2842, Fax: +81-92-802-2842, E-mail: fujigaya.tsuyohiko.948@m.kyushu-u.ac.jp

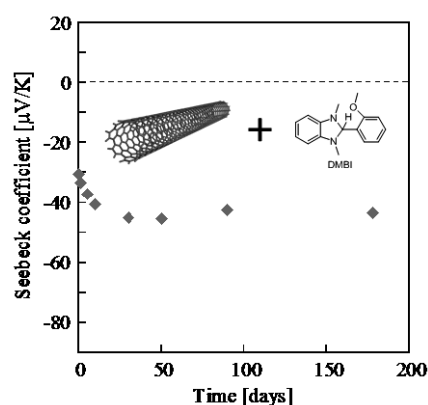


Fig. 1 Time course of Seebeck coefficient of DMBI-doped SWNT measured at 320 K

Fabrication of Multi-walled Carbon Nanotube / Polystyrene Compound Materials through Photo-induced Chemical Bond Formation

○Takuma Baba¹, Tomoya Takada²

¹ Graduate School of Photonics Science, Chitose Institute of Science and Technology, Chitose 066-8655, Japan

² Department of Applied Chemistry and Bioscience, Chitose Institute of Science and Technology, Chitose 066-8655, Japan

Modification of polymers with carbon nanotubes (CNTs) is important for fabrication of functional materials containing CNTs. In this work, we prepared multi-walled carbon nanotubes (MWCNTs) / polystyrene derivatives compound materials through photochemical covalent bond formation induced by UV light irradiation (Scheme 1). In addition, photothermal conversion characteristics of the materials obtained were evaluated by means of thermography observation.

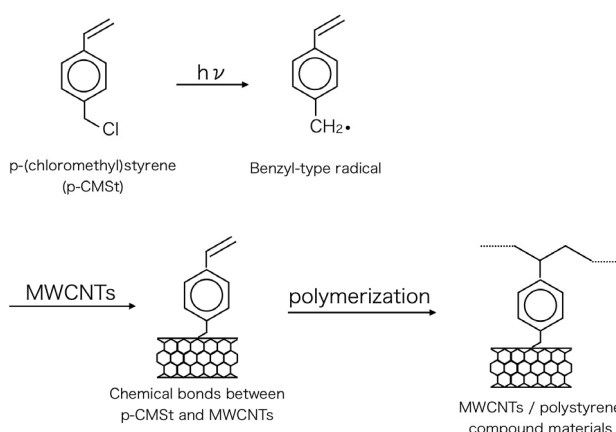
Firstly, p-(chloromethyl)styrene and MWCNTs were mixed in *N*-methylpyrrolidone and irradiated with UV light (250 – 385 nm) from a xenon light source at room temperature for 3 hours. Then, the resultant product was polymerized using azobisisobutyronitrile radical initiator. The obtained viscous polymer solution was diluted with solvent, and then polymer films were made by spin-coating on glass pieces. Chemical structure of the composite materials was analyzed by means of some spectroscopic techniques (¹H NMR, Raman, XPS, and so on). In order to evaluate photothermal conversion property of the materials, the materials were irradiated with infrared light (IR) from a xenon light source and the temperature change during the irradiation was observed by using a thermal imaging camera.

According to the NMR spectroscopy, decrease of –CH₂Cl groups of p-(chloromethyl)styrene and formation of alkyl groups from vinyl groups were confirmed. Structural change of MWCNTs before and after the irradiation was also observed by means of Raman spectroscopy. These results confirmed the covalent bond formation and subsequent polymerization. Other results such as the XPS analysis and the observation of infrared-induced temperature change will be shown at the symposium.

This work was supported by Nanotechnology Platform Program of the MEXT, Japan, and JSPS KAKENHI. The authors acknowledge the Laboratory of XPS analysis (technical staff: Mr. Keita Suzuki), Hokkaido University.

Corresponding Author: T. Takada

Tel: +81-123-27-6056, Fax: +81-123-27-6056, E-mail: t-takada@photon.chitose.ac.jp



Scheme 1 Fabrication of MWCNTs / polystyrene compound materials.

Role of π -extended Aryl Crown Ethers in the Salt-induced Chemical n-type Doping of Single-walled Carbon Nanotubes

○Tomohiro Ikeda¹, Yoshiyuki Nonoguchi¹, Tsuyoshi Kawai¹

¹ Graduate School of Materials Science, Nara Institute of Science and Technology, Ikoma 630-0192, Japan

Due to an increased demand for ambient thermal energy harvesting, the thermoelectric properties of light-weight flexible conductors including single-walled carbon nanotubes (SWNTs) have recently been evaluated. The construction of high-performance bipolar modules requires both p-type and n-type materials. It is recognized that SWNTs can be n-doped by efficient electron donors including alkali metals and polyamines. However, a challenge in the rational design of air-stable n-type SWNTs has long remained to be addressed. We have very recently proposed the electrostatic compensation of negatively-charged carriers in n-type SWNTs using large cationic complexes [1,2]. SWNTs are converted to n-type conductors by doping with salt-crown ether complexes, and large cationic complexes effectively stabilize the negatively-charged n-type products.

Here we explore limiting factors governing the salt-induced n-type doping by using synthetic π -extended aryl crown ethers as host dopants. Prior to thermoelectric evaluation, parent SWNT buckypapers were dipped in the 0.01 M stock solution of KOH and crown ether derivatives: 18-crown, benzo-18-crown, 2,3-naphtho-18-crown, and 1,2-naphtho-18-crown. All treated SWNTs showed the negative Seebeck coefficient and increased electrical

conductivity, indicating efficient n-type doping (Fig. 1). Importantly, π -extended host dopants such as naphtho-crown ethers enabled relatively-deep doping and its stabilization, as suggested by the conductivity exceeding 2000 S/cm in air. The n-type doping of SWNTs was further characterized using vis-NIR, Raman, and photoelectron spectroscopy. We will discuss the chemical origin of the highly-stable n-type doping of SWNTs, by considering the electrostatic interaction of n-type SWNTs with cationic potassium-crown ether complexes (Fig. 2).

[1] Y. Nonoguchi *et al.* *Sci. Rep.* **3**, 3344 (2013).

[2] Y. Nonoguchi *et al.* *Adv. Funct. Mater.* **26**, 3021 (2016).

Corresponding Author: Y. Nonoguchi

Tel: +81-743-72-6181, Fax: +81-743-72-6179,

E-mail: nonoguchi@ms.naist.jp

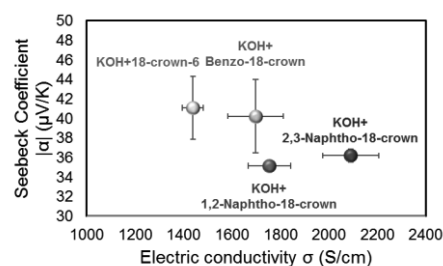


Fig.1: The Seebeck coefficient and electrical conductivity of n-type SWNTs.

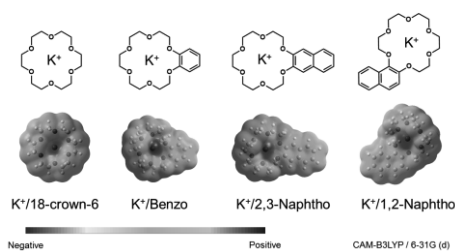


Fig.2: Electrostatic potential mapping of crown ether host dopants.

Improvement of Single-Walled Carbon Nanotube Cathodes for Perovskite Solar Cells

○Takahiro Sakaguchi¹, Hayato Kobayashi¹, Hiroki Suko¹, Takeshi Okochi¹, Taiki Inoue¹, Rong Xiang¹, Shohei Chiashi¹, Esko I. Kauppinen², Shigeo Maruyama^{1,3}

¹ Department of Mechanical Engineering, The University of Tokyo, Tokyo 113-8656, Japan

² Department of Applied Physics, Aalto University School of Science, Espoo 15100, Finland

³ Energy NanoEngineering Lab, National Institute of Advanced Industrial Science and Technology (AIST), Ibaraki 305-8564, Japan

Perovskite solar cells [1] are attracting a lot of attention due to their high power conversion efficiency (PCE) with low-cost materials. The PCE was 3.8 % in 2009 [1] and has drastically increased to 22.1 % [2]. As cathodes, gold electrodes and Spiro-MeOTAD are used in conventional perovskite solar cells. Both gold and Spiro-MeOTAD are expensive, and the latter is unstable in ambient. Single-walled carbon nanotubes (SWNTs) have been reported to act as cathodes in perovskite solar cells by substituting gold and Spiro-MeOTAD [3]. However, PCEs of perovskite solar cells with SWNT cathodes have not yet attained those with conventional cathodes.

In this study, we developed a novel fabrication method of perovskite solar cells using SWNTs as cathodes to realize improved interface between perovskite crystals and SWNTs. Dry-deposited SWNT films [4] were employed, and solar cell structures were fabricated by deposition of TiO₂ layers, perovskite crystals, and SWNT films on FTO/glass substrates in ambient air. While SWNT films are usually transferred on perovskite crystals at the last step (type 1 cell), we inserted the transfer process of SWNT films between two-step spin coating of perovskite crystal precursors (type 2 cell). Figure 1 shows the J - V characteristics of the type 1 and the type 2 cells. The type 2 cell achieved better fill factor than the type 1 cell. This indicates the contact between SWNTs and perovskite crystals is considerably improved. We further increased the PCE of the type 2 cell by adding PMMA layers on top of the SWNT films (Fig. 2).

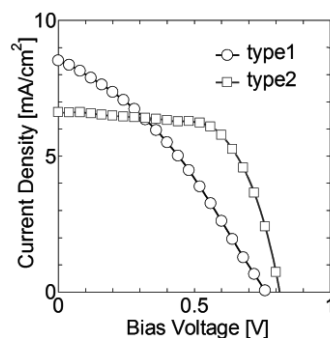


Fig. 1 J - V characteristics of type 1 and type 2 cells.

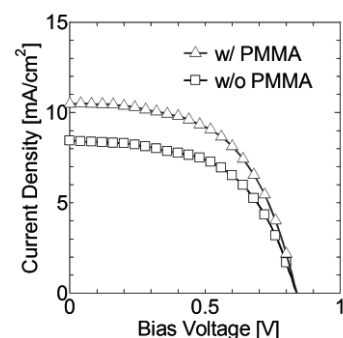


Fig. 2 J - V characteristics of w/ PMMA and w/o PMMA cells.

[1] A. Kojima *et al.*, *J. Am. Chem. Soc.*, **131**, 6050 (2009).

[2] http://www.nrel.gov/ncpv/images/efficiency_chart.jpg

[3] Z. Li *et al.*, *ACS Nano*, **8**, 6797 (2014).

[4] A. Kaskela *et al.*, *Nano Lett.*, **10**, 4349 (2010).

Corresponding Author: S. Maruyama

Tel: +81-3-5841-6421, Fax: +81-3-5841-6421,

E-mail: maruyama@photon.t.u-tokyo.ac.jp

Iron-Nitrogen-Doped Vertically Aligned Carbon Nanotube Electrocatalyst Synthesized through Instantaneous and Repetitive Pyrolysis for Oxygen Reduction Reaction

○Yosuke Uchibori, Satoshi Yasuda, Kei Murakoshi

¹ *Department of Chemistry, Faculty of science, Hokkaido University, Sapporo, 060-0810, Japan*

Development of alternatives to costly and limited reserves Pt-based catalysts for oxygen reduction reaction (ORR) has become one of the hot topics in polymer electrolyte fuel cells (PEFC) field. Among the various Pt replaced candidates, Fe coordinated to nitrogen functionalized graphitic carbon (Fe-N-C) catalysts have been attracted much attention due to their high ORR activities in acid solution. Although various approaches have been performed to enhance ORR activity, the resultant catalysts still suffers from limited activity presumably due to low density of the Fe-N-C catalytic sites. To resolve the issue, we developed abundant active Fe-N-C sites attached to a vertically aligned carbon nanotube (VA-CNT), which has a high specific surface area, by pyrolyzing iron phthalocyanine (FePc) molecules adsorbed on VA-CNTs.¹ In this study, we explored an influence of the pyrolysis process upon the ORR activity to realize the further activation.

Fe-N-C coated VA-CNTs catalyst was synthesized by pyrolyzing FePc molecules adsorbed on VA-CNTs. Instantaneous and repetitive pyrolysis (several times at the pyrolysis condition of 900 °C under Ar atmosphere for 1minute) were employed to inhibit ORR inactive Fe nanoparticle formation. Ring rotating disk electrode (RRDE) voltammetry in oxygen saturated 0.5 M H₂SO₄ solution was performed to evaluate the ORR activities.

The catalyst synthesized by the process exhibited high ORR activity of half-wave potentials of 0.79 V versus the reversible hydrogen electrode (RHE), high selectivity 3.96 electron transferred number in oxygen-saturated 0.5 M H₂SO₄ solution (“Short” in Fig. 1), compared to a conventional catalyst (half-wave potentials of 0.76 V) synthesized by continuous pyrolysis process (“Long” in Fig. 1). These results strongly indicate that the instantaneous and repetitive pyrolysis process enables to inhibit the Fe nanoparticle, resulting in formation of dense Fe-N-C active site on VA-CNT surface.

Reference

[1] S. Yasuda, A. Furuya, Y. Uchibori, K. Murakoshi, *Adv. Funct. Mater.*, **2016**, 26, 738-744.

Corresponding Author: S. Yasuda

TEL: +81-(0)11-706-4811,

FAX: +81-(0)11-706-4811

E-mail: satoshi-yasuda@sci.hokudai.ac.jp

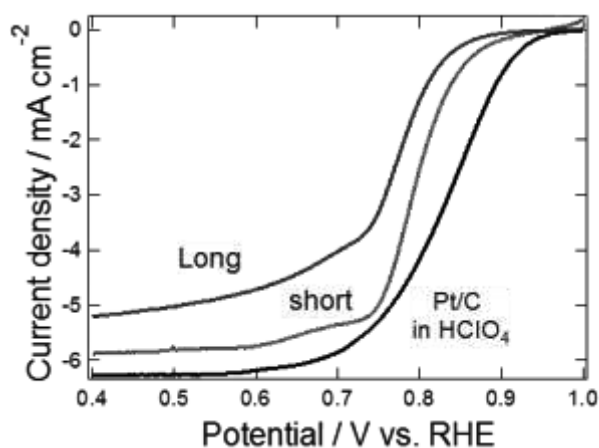


Fig. 1 RRDE polarization curves of Fe-N-C/VA-CNT in an O₂-saturated 0.5 M H₂SO₄ solution.

Synthesis of new-structured multi-walled carbon nanotubes inside silicon carbide nanotubes

○Tomitsugu Taguchi¹, Shunya Yamamoto¹, Hironori Ohba¹

¹Quantum Beam Science Research Directorate, National Institutes for Quantum and Radiological Science and Technology, Tokai-mura, Ibaraki 319-1106, Japan

Carbon nanomaterials such as fullerenes, carbon nanotubes, and graphene have attracted particular attention due to their fascinating geometries and physical properties. In particular, carbon nanotubes represent an interesting and important class of carbon based nanomaterials with wide-ranging applications. It is, therefore, required to synthesize the carbon nanotubes with new structure in order to develop and broaden the application of carbon nanotubes.

Multi-walled carbon nanotubes (GSI creos Corporation, Tokyo, Japan) were used as template materials. The C-SiC coaxial nanotubes were synthesized by heating multi-walled carbon nanotubes with Si powder at 1200 °C for 100 h in a vacuum [1, 2]. The C-SiC coaxial nanotubes were irradiated with 340 keV Si⁺ ions from 400 kV ion implanter at room temperature. The ion fluence was 2.4×10^{20} ions/m², and the corresponding irradiation damage (displacement per atom, dpa) was calculated by SRIM 2008) to be 6.8 dpa [3].

Figure 1 shows the typical TEM image and selected area electron diffraction (SAED) patterns of the irradiated C-SiC coaxial nanotube. According to high-resolution (HR) TEM image, the amorphous structure is observed in the SiC layer of C-SiC coaxial nanotube. The orientation of the graphitic shells in the C-SiC coaxial nanotubes before ion irradiation was almost parallel to the length directions of the nanotubes. However, HR-TEM observation and SAED result indicate that the orientation of graphitic shells after ion irradiation changes such that they are completely parallel to the radial directions of the nanotubes. The graphite (002) spots in the SAED image are clearly observed even after ion irradiation up to 6.8 dpa, indicating the certain crystallinity of the carbon layer in the C-SiC coaxial nanotube. In this study, the multi-walled carbon nanotubes with graphitic shells completely oriented parallel to the radial direction of the nanotube inside amorphous SiC nanotube was synthesized by ion irradiation technique for the first time [3]. Such a multi-walled carbon nanotubes with this new structure may be expected to find new applications.

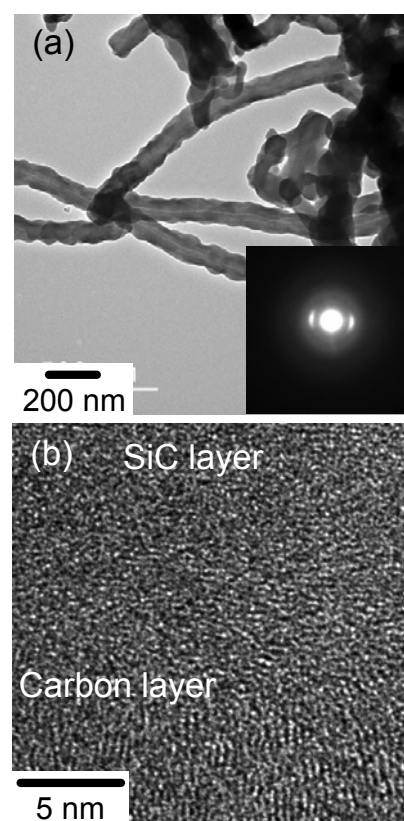


Fig.1: (a) Low-magnification TEM image and SAED pattern, and (b) high-resolution TEM image of new structured multi-walled carbon nanotube inside SiC nanotube.

[1] T. Taguchi *et al.* J. Am. Ceram. Soc. **88**, 459 (2005).

[2] T. Taguchi *et al.* Physica E **28**, 431 (2005).

[3] T. Taguchi *et al.* Carbon **95**, 279 (2015).

Corresponding Author: T. Taguchi

Tel: +81-70-3943-3446,

E-mail: taguchi.tomitsugu@qst.go.jp

Purification of high purity semiconducting single-wall carbon nanotubes with a large diameter of 1.9 nm by gel filtration

○Boanerges Thendie¹, Haruka Omachi¹, Jun Hirotani², Yutaka Ohno², Ryo Kitaura¹, Yasumitsu Miyata³, and Hisanori Shinohara¹

¹Department of Chemistry and Institute of Advanced Research, Nagoya University, Nagoya, 464-8602

²Department of Quantum Engineering, School of Engineering, Nagoya University, Nagoya, 464-8603

³Department of Physics, Tokyo Metropolitan University, Tokyo, 192-0397

Single-wall carbon nanotubes (SWCNTs) have broad diversities on its structure and properties which should be separated and purified prior to application such as electronic devices. Gel filtration is one of the most powerful separation methods of SWCNTs, capable of purify SWCNTs based on electronic-type, diameter, and length. However, although many satisfactory reports on gel filtration of SWCNTs have been published, few to no report was found on the successful electronic-type purification of SWCNTs with diameter larger than 1.4 nm.

Here, we demonstrate the purification of semiconducting SWCNTs (s-SWCNTs) with a diameter of as large as 1.9 nm by using gel filtration. Combination of increased column temperature and elution with gradient concentration are critical for the purification. Optical absorption and Raman spectra indicate the high purity s-SWCNTs with diameter around 2.0 nm, which was confirmed by transmission electron microscopy (TEM) images as shown in fig. 1.

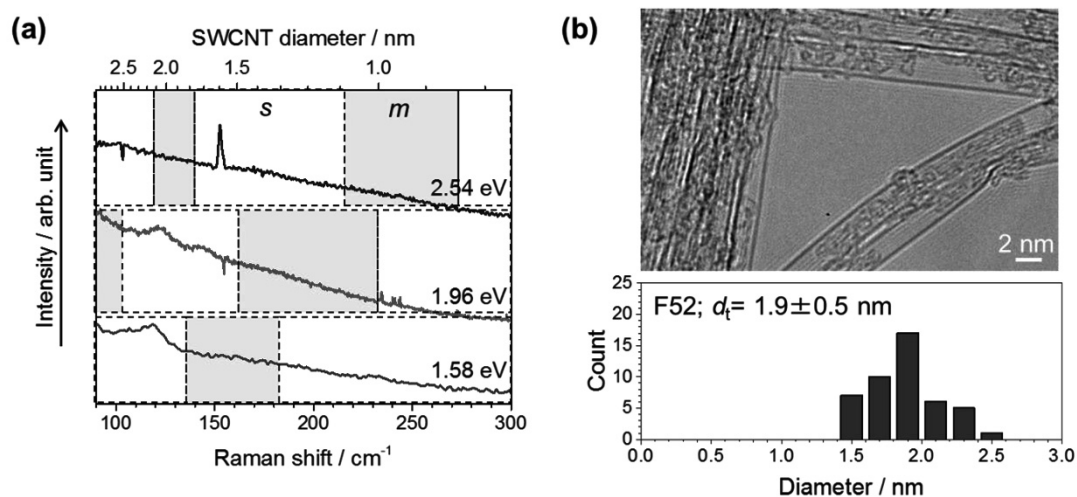


Figure 1 (a) Raman spectra of the purified s-SWCNTs fraction using 3 different laser excitation: 2.54, 1.96, and 1.58 eV. No peak of m-SWCNTs (gray shaded) was observed. (b) TEM images and diameter distribution of the purified fraction showing s-SWCNTs with large diameter of 1.9 nm.

Corresponding author: Hisanori Shinohara

Tel: (+81) 52-789-2482, **Fax:** (+81) 52-747-6442, **E-mail:** noris@nagoya-u.jp

Single-walled carbon nanotube synthesis using Ru catalysts by alcohol catalytic chemical vapor deposition in high vacuum

○Takayuki Fujii¹, Hoshimitsu Kiribayashi¹, Seigo Ogawa¹, Takahiro Saida²,
Shigeya Naritsuka¹, Takahiro Maruyama²

¹ Department of Materials Science and Engineering, Meijo University, 1-501 Shiogamaguchi, Tempaku, Nagoya 468-8502, Japan

² Department of Applied Chemistry, Meijo University, 1-501 Shiogamaguchi, Tempaku, Nagoya 468-8502, Japan

Single-walled carbon nanotube (SWNT) have various excellent electrical characteristics for applications to electronics. So far, we have conducted SWNT growth using platinum-group metals as catalysts. Previously, we have reported SWNT growth using Pt and Rh catalysts [1] [2]. These catalysts are one of the most expensive metals, which are disadvantages for practical applications. In this study, we focused on Ru as catalysts for SWNT growth. Although Ru belongs to platinum-group elements, it is not so expensive, compared to Rh and Pt. Using Ru as a catalyst, we succeeded in growing SWNTs. In addition, effects of feedstock gas pressure on SWNT growth was investigated.

Al₂O₃ was deposited on SiO₂/Si substrates by rf sputtering. Ru catalysts were deposited on them using a pulsed arc plasma gun, and they were used as substrates for SWNT growth. The growth temperature was 700 °C, and the ethanol pressure was varied between 1×10⁻⁴ and 1×10⁻² Pa. The grown SWNTs were characterized by scanning electron microscope and Raman spectroscopy.

Fig. 1 shows the Raman spectra of SWCNTs grown from Ru catalysts at 700 °C under an ethanol pressure of 1×10⁻⁴, 1×10⁻³ and 1×10⁻² Pa, when the catalyst thickness was 0.2 nm. At 1×10⁻² Pa, strong RBM peaks and G-band peaks appeared, indicating that SWNT yield was enhanced under this ethanol pressure. Our results show that Ru is useful for growth of SWNT.

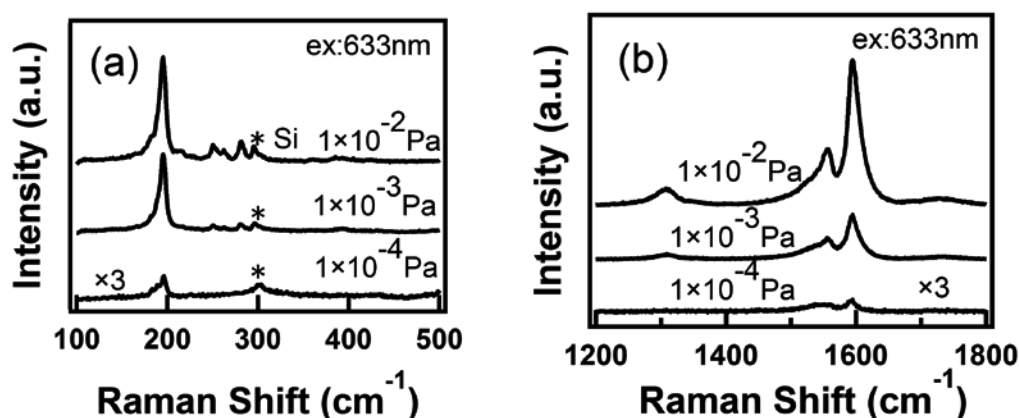


Fig. 1 Raman spectra of SWCNTs grown at 700 °C from Ru catalysts under an ethanol pressure of 1×10⁻⁴, 1×10⁻³ and 1×10⁻² Pa. Ru catalyst film thickness was 0.2 nm.

[1] T. Maruyama et al. Carbon 96 (2016) 6.

[2] A. Kozawa et al. Diamond Relat. Mater. 63 (2016) 159.

Corresponding Author: T. Maruyama

Tel: +81-52-838-2386, Fax: +81-52-832-1179, E-mail: takamaru@meijo-u.ac.jp

Possible mechanism for selective separation of semiconducting single-walled carbon nanotubes

○Keita Ozono¹, Fumiyuki Toshimitsu¹, Naotoshi Nakashima^{1,2}

¹ Department of Applied Chemistry, Graduate School of Engineering, Kyushu University, 744, Motooka Nishi-ku Fukuoka, Japan

² WPI-I2CNER, Kyushu University, 744, Motooka Nishi-ku Fukuoka, Japan

Single-walled carbon nanotubes (SWNTs) have superior physical and electronic properties and are promising nanomaterials for the next generation. However, SWNTs have two major problems; one is that SWNTs can't dissolve in solvents, and another is that they are synthesized as mixtures of semiconducting- and metallic-SWNTs. In order to use them for many applications, their efficient chirality separation is highly demanded.

Several efficient sorting methods including gel chromatography method [1], density gradient ultracentrifugation method [2,3], use of oligo DNA [4], aqueous two-phase extraction method [5], and use of dynamic coordination [6] and hydrogen polymer-based supramolecular chemistry [7] have been reported.

We have already reported that a flavin derivative can selectively solubilize semiconducting-SWNTs from the pristine SWNTs [8]. At this meeting, we focus on mechanism for this separation by means of experiments and MD simulation.

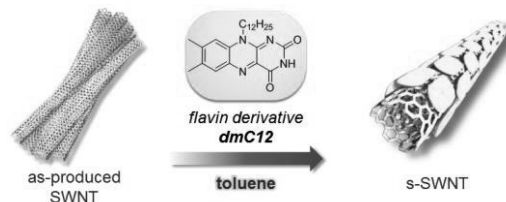


Fig 1: Scheme of semiconducting-SWNTs separation using flavin derivative.

This poster is based on results obtained from a project commissioned by the New Energy and Industrial Technology Development Organization (NEDO).

- [1] H. Liu, D. Nishide, T. Tanaka, H. Kataura, Nat. Commun. **2**, 309 (2011).
- [2] M. S. Arnold, A. A. Green, J. F. Hulvat, S. I. Stupp, M. C. Hersam, Nat. Nanotechnol. **1**, 60 (2006)
- [3] Ghosh, S.; Bachilo, S. M.; Weisman, R. B. Nat. Nanotechnol. **5**, 443 (2010)
- [4] Zheng, M.; Jagota, A.; Strano, M. S.; Santos, A. P.; Barone, P.; Chou, S. G.; Diner, B. A.; Dresselhaus, M. S.; McLean, R. S.; Onoa, G. B.; et al., **302**, 1545 (2003)
- [5] Gui, H.; Streit, J. K.; Fagan, J. a.; Hight Walker, A. R.; Zhou, C.; Zheng, M. Nano Lett. **15**, 1642 (2015)
- [6] Toshimitsu, F.; Nakashima, N. Nat. Commun. **5**, 5041 (2014)
- [7] Toshimitsu, F.; Nakashima, N. Sci. Rep. **5**, 18066 (2015)
- [8] Y Kato, M Fukuzawa, F Toshimitsu, N Nakashima, Chem. Lett. **44**, 556 (2015)

Corresponding Author: Naotoshi Nakashima
 Tel: +81-92-802-2840, Fax: +81-92-802-2840,
 E-mail: nakashima.naotoshi.614@m.kyushu-u.ac.jp

STM/STS studies on Europium nanowires encapsulated in carbon nanotubes

○Terunobu Nakanishi¹, Ryo Kitaura¹, Shoji Yoshida²,
Osamu Takeuchi², Hidemi Shigekawa², Hisanori Shinohara¹

¹ *Department of Chemistry and Institute for Advanced Research, Nagoya University, Nagoya, 464-8602, Japan*

² *Faculty of Pure and Applied Sciences, University of Tsukuba, Tsukuba, 305-8573, Japan*

The discovery of carbon nanotubes (CNTs) and their fascinating properties have ignited intense research interests on one-dimensional nanosystems. Although metal nanowires, whose diameter is one to several atoms, are one of the most ideal one-dimensional nanosystems, the preparation and characterization of these have been difficult because of their high reactivity towards air. Previously, we have reported the synthesis of Europium (Eu) nanowires in the interior space of CNTs and characterization of their structure with transmission electron microscopy.^[1-2] Here, we present the preparation and investigation of spatially-resolved electronic structure of Eu nanowires encapsulated in CNT (EuNW@CNT) by scanning tunneling microscopy/spectroscopy (STM/STS).

EuNW@CNT was synthesized by the direct nano-filling method^[1] and dispersed in THF with ammonium carbonate by sonification. Figure 1 shows a STS spectrum of EuNW@CNT. At the location where EuNW are expected to exist (the position ranging from 3 to 15 nm in Fig. 1), we observed that the conduction and valence bands are shifted downward and that bandgap shrinks with the appearance of two localized states in the gap region. These drastic change in electronic structure indicates that EuNW strongly interact with CNT, presumably, via the charge transfer from EuNW to CNT.^[3] The results obtained in this work strongly suggest that one can drastically change CNT's band structures by encapsulation of metal atomic wires.

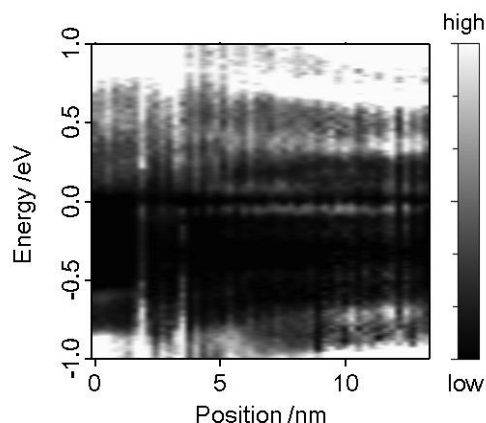


Figure1. STS spectrum of EuNW@CNT. dI/dV mapping taken along CNT axis. The left side is empty CNT area and right side is EuNW encapsulated area.

[1] R.Kitaura *et al.* *Angew.Chem.Int.Ed.* **48**, 8298, (2009).

[2] R.Nakanishi *et al.* *Phys. Rev. B*, **86**, 115445, (2012).

[3] J. Zhou *et al.* *J. Phys. Chem. C*, **114**, (2010),

Corresponding Author: H. Shinohara

Tel: +81-52-789-2477, Fax: +81-52-747-6442, e-mail: r.kitaura@nagoya-u.jp and noris@nagoya-u.jp

Two-step growth of graphene directly grown on sapphire substrate by non-catalytic alcohol CVD

○Yuki Ueda¹, Jumpei Yamada¹, Kyosuke Fujiwara¹, Daichi Yamamoto¹
Takahiro Maruyama², and Shigeeya Naritsuka¹

¹ Department of Materials Science and Engineering, Meijo University, Nagoya 468-8502, Japan

² Department of Applied Chemistry, Meijo University, Nagoya 468-8502, Japan

Chemical vapor deposition (CVD) with metallic catalyst is a conventional method for growing high-quality, large-area graphene. However, it is necessary to transfer the graphene from the surface of the catalyst to a certain substrate for the fabrication of graphene devices. The transfer process is not only complicated but also degrades their performances, such as electron mobility. Therefore, a direct growth of graphene on a substrate is strongly required.

Crystal quality of graphene is in general improved by increasing growth temperature. However, a high-temperature of growth is difficult in a direct growth of graphene on sapphire because C atoms are significantly etched by O atoms decomposed from the substrate. Therefore, we adopted two-step growth that consists of a low-temperature growth of a protection layer for covering the sapphire substrate and a high-temperature growth for a high-quality graphene.

A c-plane sapphire was used as a substrate. Ethanol was supplied to the growth chamber as a source material with bubbled by N₂ gas flow of 7 sccm. And, N₂ gas was flown at 600 sccm as a carrier gas. In a two-step growth, almost 1 layer of graphene was firstly grown at 1180 °C for 1h, and a high-temperature growth was performed at 1400 °C for 1h. H₂ gas was also flown at 10 sccm during the high-temperature growth. A reference sample was grown in a one-step at 1180 °C for 2h.

Figure 1 shows the surface AFM image of reference sample. Many triangular islands, which are found as a graphitic structure by Raman spectroscopy, are observed. Excess supersaturation are thought as a cause, which was brought by the suppression of etching effect of O atoms decomposed from the sapphire substrate after the substrate was covered with a grown graphene. Figure 2 shows (a) a surface AFM image and (b) a Raman spectra of the sample grown by two-step growth. Though graphene wrinkles are observed, the triangular islands are not observed. D/G ratio of 0.3 and a narrow FWHM of G' peak of 58 cm⁻¹ suggest that a high-quality multilayer graphene was grown by the two-step growth.

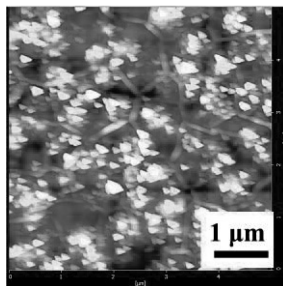


Fig. 1. Surface AFM image of reference sample

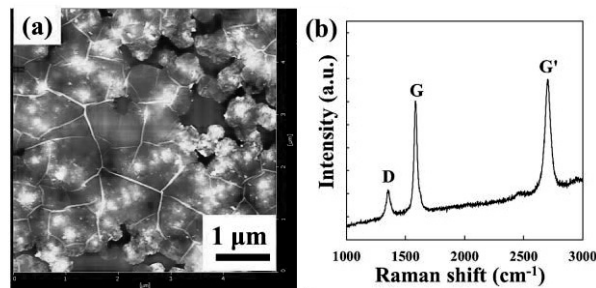


Fig. 2. Sample grown by two-step growth
(a) Surface AFM image and (b) Raman spectra

Corresponding Author: Y. Ueda Tel: +81-52-832-1151 E-mail: 153434003@ccalumni.meijo-u.ac.jp

[Acknowledgment] This work was supported in part by JSPS KAKENHI Grant Numbers 2660089, 15H03558, 26105002, 25000011.

CVD growth of graphene using boron nitride as growth templates

○Shun Ogawa¹, Yu Kobayashi¹, Yutaka Maniwa¹, Yasumitsu Miyata^{1,2}

¹*Department of Physics, Tokyo Metropolitan University, Hachioji 192-0397, Japan*

²*JST, PRESTO, Kawaguchi 332-0012, Japan*

Development of a method to produce structure-controlled graphene nanoribbons (GNRs) has been an important issue to investigate their unique electronic and magnetic properties. In the previous studies, GNRs have been produced by polymerization of organic molecule, anisotropic growth/etching of graphene, and so on. In contrast, we have focus our attention on heteroepitaxial growth of GNRs because of its shape controllability. For example, when hexagonal boron nitride (hBN) is grown from the edge of graphene grains, the hBN films tend to form a ribbon-like shape at an early stage of growth [1]. If graphene were grown from the edge of hBN, GNRs could be formed at an early stage of graphene growth (Fig. 1a). To test this approach, we have investigated chemical vapor deposition (CVD) growth of graphene using hBN grains as growth templates.

Monolayer hBN grains were grown on Cu foil by CVD at 1075 °C using ammonia borane as a precursor. After the hBN growth, graphene was grown on the same Cu foil by supplying methane at high temperature (~1000 °C). The grown films were transferred on SiO₂/Si substrates for Raman measurement. Interestingly, we found that graphene were preferentially grown around the triangle-shaped hBN grains as revealed by 2D-band Raman intensity mapping (Fig. 1b,c). These results suggest that hBN grains can act as growth template during graphene CVD, and could provide a possible way to produce structure-controlled GNRs.

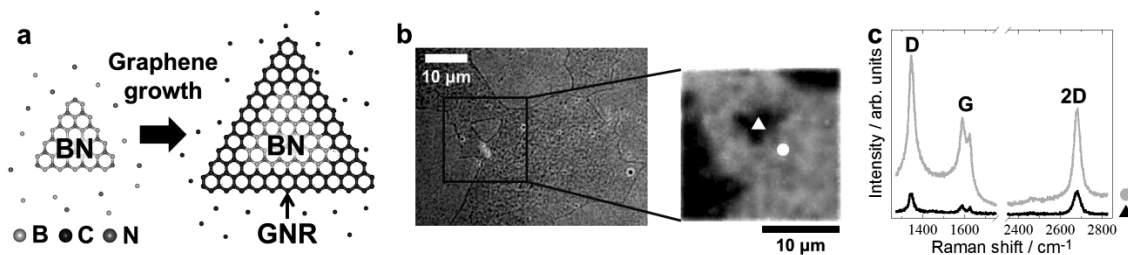


Fig. 1(a) Schematic illustration of epitaxial growth of graphene from the edge of hexagonal boron nitride. (b) Optical (left) and Raman (right) images of CVD-grown graphene on a SiO₂/Si substrate. Gray indicates the Raman intensity of 2D-band. (c) Raman spectra of CVD-grown graphene at different positions in Fig. 1b.

[1] Y. Miyata, *et al.*, Appl. Phys. Express, **5**, 085102 (2012)

Corresponding Author: Yasumitsu Miyata, Tel: +81-42-677-2508, E-mail: ymiyata@tmu.ac.jp

Graphene FET of high photosensitivity using schottky diode between graphene and n-type silicon

○Shiho Kobayashi, Yuki Anno, Kuniharu Takei, Takayuki Arie, Seiji Akita

*Department of Physics and Electronics, Osaka Prefecture University,
Sakai, Osaka 599-8531 Japan*

Graphene/semiconductor heterojunction is one of emerging fields of recent photoelectronic devices due to the low light absorption of graphene of $\sim 2.3\%$, which is appropriate for the window layer of photosensor. Here, we demonstrate the photosensor consisting of graphene field effect transistor (G-FET)/Si heterojunction.

Figure 1 shows the schematic image of the G-FET with the Si depletion layer gate. The channel length and width are 4 and 2 μm , respectively. Unlike common back-gate G-FET, we remove the 300 nm thick SiO_2 layer underneath of the graphene channel by buffered HF. Note that the resistivity of the n-type Si substrate used in this experiment is 0.1~100 Ωcm , so that one can expect that the formation of depletion layer at the interface between the Si and graphene at $V_g > V_{\text{Dirac}}$. Additionally, thin SiO_2 layer was formed after the BHF etching.

Figure 2 shows the transfer characteristics under dark and light irradiation (17.9 pW, 510 nm). The difference between the drain currents (I_d) under dark and illumination are clearly observed at $V_g > V_{\text{Dirac}}$ corresponding to the reverse bias for n-Si/graphene interface. As shown in Fig. 2, the gate leak current $I_g \sim 1$ nA is observed at the $V_g < V_{\text{Dirac}}$, which corresponds to the flat band through accumulation region of Si (forward bias for n-Si/graphene interface) as shown in Fig.3. In this case, the gate capacitance C_g is only formed by the thin native oxide of Si. At $V_g > V_{\text{Dirac}}$ under dark condition corresponding to the reverse bias for n-Si/graphene, the thick depletion layer should be formed, which results in the smaller C_g and low carrier concentration in graphene channel. Under the light irradiation, the thickness of depletion layer is thinner than that at dark condition because of the photoexcited carrier in Si and thus the inversion of n-Si. As a result, sufficient charge is induced in the graphene channel, which contributes to the photoresponse observed in this study.

Acknowledgements This work was partially supported by KAKENHI Grant Number 25286010, 16H00920 and 16H06504. **Corresponding Author:** S. Kobayashi, Tel: +81-72-254- 9261, E-mail: s_kobayashi-4@pe.osakafu-u.ac.jp

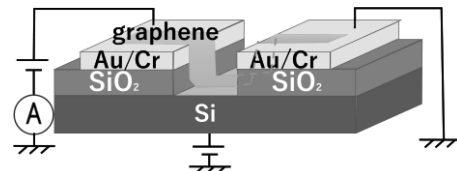


Fig. 1 G-FET with Si depletion layer gate.

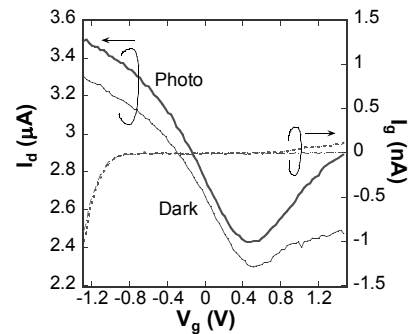


Fig. 2 Transfer characteristic of G-FET with the Si depletion layer gate ($V_d=50$ mV). The gate leak current I_g is also plotted as a function of V_g .

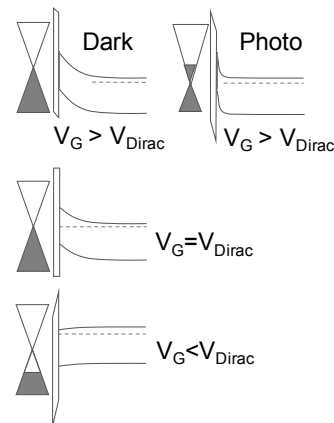


Fig. 3 Band diagram of G-FET with the Si depletion layer gate.

Catalytic properties of non-metal and platinum supported surface-modified nanocarbon materials

○Hironori Ogata^{1,2,3}, Haruhiko Yoshitake¹, Yutaka Sato¹, Tomoaki Nishimura⁴, Zhipeng Wang⁵, Shingo Morimoto⁵, Yoshio Hashimoto⁵, Morinobu Endo⁵

¹Graduate School of Sci. and Engin., Hosei University, Koganei, Tokyo, 184-8584, Japan

²Faculty of Biosci. and Applied Chem., Hosei University, Koganei, Tokyo, 184-8584, Japan

³Research Center Micro-Nano Technol., Hosei University, Koganei, Tokyo 184-0003, Japan

⁴Research Center of Ionbeam Technol., Hosei University, Koganei, Tokyo, 184-8584, Japan

⁵Institute of Carbon Science and Technology, Shinshu University, Nagano 380-8553, Japan

Nanocarbon materials are promising materials for various applications. In recent years, various progress in manufacturing and functionalizing nanocarbon materials has been made to achieve the control of bulk and surface properties. Carbon nanosheets (CNSs), also known as carbon nanowalls which can be described as graphite sheet nanostructures with a large number of edges that are composed of stacks of planar graphene sheets standing almost vertically on the substrate [1]. Direct methanol fuel cells (DMFCs) are one of the most promising transportable power sources which can be used in mobiles, laptops, and small power generation[2]. The basic operation principle of DMFCs involves methanol oxidation and oxygen reduction on the precious metal catalysts, which are loaded on the support surfaces. As is well-known, the dispersion of Pt-based alloys on carbon supports as well as catalyst particle size and shape plays a dominant role in the electrochemical performance for fuel cells[3]. We have explored the electrocatalytic properties of Pt-based nanoparticles supported on the carbon materials by electrodeposition systematically.

In this study, we investigated both the effects of surface modification by ion-irradiation or the radio frequency(RF) O₂ plasma treatments on the surface morphology and oxygen reduction reaction activity of CNSs. We also investigated the dispersion states and electrocatalytic properties of Pt-based nanoparticles supported on the surface modified CNSs by electrodeposition method. The ion beam accelerated with carbon ion source with 200 keV and 400 keV were irradiated to the carbon materials with 1×10^{13} , 1×10^{14} , 1×10^{15} ions/cm².

The detailed results on the morphology, oxygen reduction reaction activity and dispersion state of Pt-based nanoparticles and their electrocatalytic performance for methanol oxidation will be presented.

References:

- [1]M. Hiramatsu, M. Hori, Carbon Nanowalls: Synthesis and Emerging Applications, SpringerWien, New York, 2010.
- [2]J.M.Sieben *et al.*, *J. Appl. Electrochem.* **38**(2008)483-490.
- [3]Zhipeng Wang, Mao Shoji and Hironori Ogata, *Appl. Surf. Sci.* **259**(2012)219-224.
- [4]M.Tsai *et al.*, *ElectroChem. Commun.* **8**(2006)1445-1452.
- [5]S.H.Ahn *et al.*, *Chem. Eng. J.* **181-182**(2012)276-280.
- [6]K. Waki *et al.*, *Energy & Environ. Sci.* **7**(2014)1950-1958.

Corresponding Author: Hironori Ogata

Tel: +81-42-387-6229, Fax: +81-42-387-6229,

E-mail: hogata@hosei.ac.jp

Control of nonlinearity of suspended graphene resonator by standing wave of light

○Taichi Inoue, Yuki Anno, Kuniharu Takei, Takayuki Arie, Seiji Akita

*Department of Physics and Electronics, Osaka Prefecture University,
Sakai 599-8531, Japan*

Graphene mechanical resonator (G-MR) is promising candidate for highly sensitive mass and force sensor because of extremely low mass and high young's modulus. Nonlinearity control is one of key techniques to realize mode exchange of vibration toward practical applications. Here, we demonstrate nonlinearity control of the G-MR by using optical effect.

Monolayer graphene was transferred onto the SiO₂ (300 nm)/Si substrate and was etched by O₂ plasma to form the graphene stripe with the width of 2 μm. Next, the SiO₂ layer underneath of the graphene stripe was etched by buffered HF, and dried by using supercritical drying. As shown in Fig. 1(a), the suspended graphene stripe with the length of 3 μm was successfully fabricated. Resonance properties of the G-MR were measured by optical detection as shown Fig.1 (b), where CW lasers (406 or 521 nm) were used not only to detect the vibration but also to control the nonlinearity. The different detection lasers form the different standing wave profiles between the substrate and the graphene, which induce the different force acting on the G-MR. Note that the G-MR was actuated by photothermal method using 660 nm laser modulated with a certain frequency by illuminating the G-MR support as schematically shown in Fig. 1(b).

Figures 1(c) shows the resonance curves using 406 nm laser. The peak frequency shifts to lower frequency at higher CW laser power, which is so called optical softening. Additionally, the Q-factor increases with increasing the CW laser power. This implies that the 406 nm laser irradiation works as positive feedback for the oscillation, which results in the increase of the vibration amplitude. On the contrary, in the case of 521 nm laser shown in Fig. 1(d), the vibration amplitude increases with decreasing the CW laser power. The stronger nonlinearity is observed at lower laser power. The standing wave profile enhances the nonlinearity of the G-MR. Thus, we successfully demonstrate the nonlinear control of G-MR using the standing wave of the light.

Acknowledgements This work was partially supported by KAKENHI Grant Number 25286010, 16H00920 and 16H06504. **Corresponding Author:** T. Inoue, Tel: +81-72-254-9261, E-mail: t_inoue-4@pe.osakafu-u.ac.jp

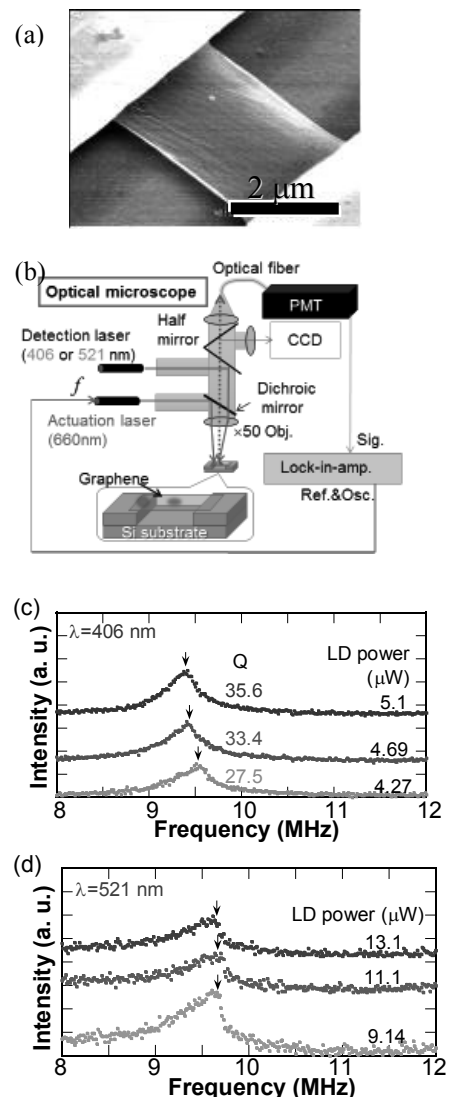


Fig. 1 (a) SEM image of the graphene resonator. (b) Measurement setup. (c) and (d) are CW laser power dependences of frequency responses of G-MR under the illumination of 406 and 521 nm, respectively.

All-graphene oxide device with tunable supercapacitor and battery behaviour by the working voltage

○Chikako Ogata^{1,2}, Ruriko Kurogi¹, Kazuto Hatakeyama^{1,2}, Takaaki Taniguchi³,
Michio Koinuma¹, Yasumichi Matsumoto¹

¹ Graduate School of Science and Technology, Kumamoto University,
2-39-1 Kurokami, Chuo-ku, Kumamoto 860-8555, Japan

² Research Fellow of Japan Society for the Promotion of Science (JSPS Research Fellow)

³ International Center for Materials Nanoarchitectonics (WPI-MANA), National Institute for Materials Science (NIMS), 1-1 Namiki, Tsukuba, Ibaraki 305-0044, Japan

As hydrated Graphene Oxide (GO) is simultaneously a good ionic conductor and an electrical insulator, GO can be used as both a separator and electrolyte. Moreover, reduced GO (rGO) is suitable for electrode materials owing to its high electrical conductivity and high specific surface area. Based on these considerations, the rGO/GO/rGO structure is expected to perform as an electrical device. In this study, we demonstrate a new type of rGO/GO/rGO device that functions as both a supercapacitor (Graphene Oxide Supercapacitor: GOSC) and a battery (Graphene Oxide Redox Battery: GORB), depending on the working voltage [1].

The GO was prepared by Hummers' method. The rGO/GO/rGO device was fabricated by photoirradiation of both surfaces of the GO paper. The electrochemical performance of this device was investigated using CV, galvanostatic charge/discharge measurements and EIS.

The rGO/GO/rGO device operated as a proton-type supercapacitor at working potentials as high as 1.2 V (Fig. 1). The GOSC exhibited high specific area capacitance of 2 mF cm⁻² even when operated at high scan rates of 1,000 mV s⁻¹. We speculate that the charge storage mechanism of GOSC resulted from (1) proton conductivity and (2) polarized/separated water molecules in the interlayer spacing of the nanoscale GO. At potentials greater than 1.5 V, this rGO/GO/rGO device behaved as a battery (Fig. 2). In particular, the GORB, which had a plateau potential of approximately 0.75 V and coulombic efficiency of approximately 53%, exhibited excellent battery behavior at a charge voltage of 1.7 V. The rGO/GO/rGO device, which comprises two different rGO electrodes with redox couples based on two different functional groups with dissimilar reaction potentials, functioned as a battery. We deduced the following two hypotheses for the redox mechanism of the GORB: (1) cathode: C=O + H⁺ + e⁻ ↔ C-OH; anode: CH (defect) + CO₂ ↔ 2C=O (or C-O) + H⁺ + e⁻; or (2) cathode: 4H⁺ + 4e⁻ + O₂ ↔ H₂O; anode: CH (defect) + CO₂ ↔ 2C=O (or C-O) + H⁺ + e⁻.

[1] C. Ogata *et al.* Chem. Commun. **52**, 3919-3922 (2016).

Corresponding Author: C. Ogata

Tel: +81-96-342-3659, Fax: +81-96-342-3659,

E-mail: c-ogata@kumamoto-u.ac.jp

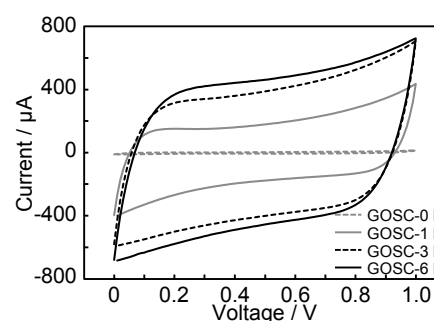


Fig. 1 CV profiles acquired at a scan rate of 0.3 V s⁻¹ for GOSC prepared using various photoreduction times.

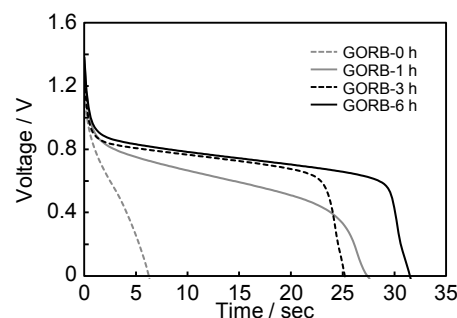


Fig. 2 Discharge profiles of GORB prepared with various photoreduction times at 0.05 mA.

Suppression of Electrical Conductivity Deterioration of Cu Nanowire by Coating 2D-layered Materials

○Nguyen Thanh Cuong¹, Susumu Okada²

¹ *International Center for Young Scientists, National Institute for Materials Science (NIMS), Tsukuba 305-0044, Japan*

² *Graduate school of Pure and Applied Sciences, University of Tsukuba, Tsukuba 305-8571, Japan*

Copper is the crucial material for high efficient interconnections in the semiconductor integrated circuits. Recent advances in the miniaturization progress of electronic devices require the highly conductive Cu wire interconnect at the nano size. Recently, by using graphene as coating layer, the electrical conductivity of Cu nanowires has been enhanced by 15 percent than that of pristine Cu nanowires [1]. However, the physical origin of this high conductivity of graphene-coated Cu nanowires is still unclear. In this work, we explore the electronic structure and transport properties of hybrid-structure between Cu thin films and 2D-layered materials coatings such as boron-nitride and graphene, based on density functional theory and semi-classical Boltzmann transport theory simulations. We find that the unique electrical conduction of graphene-coated Cu nanowire is ascribed to the Shockley surface-states of Cu surfaces. Under realistic environment, the intrinsic Shockley surface-states of Cu surfaces are destroyed by oxygen gas adsorption that lead to the substantial surface scattering decreasing the electrical conductivity. In sharp contrast, these Shockley surface-states of Cu surfaces are preserved by the boron-nitride or graphene coatings, owing to the weak interaction between Cu surface and boron-nitride or graphene layer. Furthermore, the Shockley surface-states with quasi-2D free-electron characteristics exhibit a large conductivity of 1.62×10^7 ($\Omega^{-1} \text{m}^{-1}$) at room temperature. These results indicate the important role of the Shockley surface-states on electrical conductivities of Cu nanowires. Therefore, our work suggest the possibility of using ultra-thin 2D-layered materials: boron-nitride, graphene, etc., as coatings for Cu interconnect in high-performance electronic devices.

[1] R. Mehta, S. Chugh and Z. Chen, Nano Lett. **15**, 2024 (2015).

Corresponding Author: N. T. Cuong

Tel: +81-29-851-3354#4041

E-mail: NGUYEN.Thanhcuong@nims.go.jp

Evaluation of the electrochemical capacitance of graphite oxide electrode prepared by the electrochemical oxidation/reduction cycle

○Keisuke Awaya¹, Kazuto Hatakeyama¹, Michio Koinuma¹, Yasumichi Matsumoto¹

¹ Graduate School of Science and Technology, Kumamoto University
2-39-1 Kurokami, Chuo-ku, Kumamoto, 860-8555, Japan

Graphite oxide (GtO), which is prepared by oxidation of the pristine graphite, has been studied since it showed unique properties (high proton conductivity, hydrophilicity, negative charges on its surface, etc.). Although many chemical oxidation methods have been reported and are used most popularly, they require not only strong acids or oxidants but also dragged reaction time. Therefore, it is generally difficult to control the oxidation degree of graphite. On the other hand, the electrochemical method offers a facile way to control it by operating the applied oxidation potential and oxidizes the electrode directly. The rGtO, reduced GtO electrode, showed high electrochemical capacitance, and it became much higher when the electrode was electrochemically oxidized and reduced repeatedly [1],[2].

Glassy carbon electrode (BAS Ltd.) was employed as the working electrode and various nitrates were chose as electrolyte in aqueous solution (0.1 M NaNO₃+NaOH_{aq}, 0.1 M NaNO₃_{aq}, 0.1 M NH₄NO₃_{aq}, 0.1 M HNO₃_{aq}). Firstly, the electrode was immersed into aqueous solution and were oxidized electrochemically for 5 minutes. And then cyclic voltammogram was measured at the range of from -0.2 V to +0.7 V in 0.1 M Na₂SO₄_{aq}. The subsequent reduction process was carried out in the same way. The potential value of +2.00 V and -1.10 V in 0.1 M NaNO₃_{aq} was set as the standard, the applied potentials in other solution were estimated by the Nernst equation.

The electrochemical capacitance of GtO/rGtO electrodes were showed in Fig. 1. The capacitance showed high values after every reduction processes (denoted as rnGtO in Fig. 1, where n is re-reduction cycle number) and indicated the maximum in 0.1 M NH₄NO₃_{aq} and 0.1 M NaNO₃_{aq}, 119.6 mF/cm² was observed after 16th reduction. The reaction sites on the electrode were easily eroded away and its surface area increased every electrochemical oxidation/reduction cycle. Thus, its capacitance, derived from electric double layer, became higher in accordance with the augmentation of oxidation/reduction cycle. XPS analysis of rGtO revealed that the amount of CH defect also increased with the cycles number. Therefore, it was suggested that CH defect on the electrochemical reduced rGtO surface influenced upon its electrochemical capacitance.

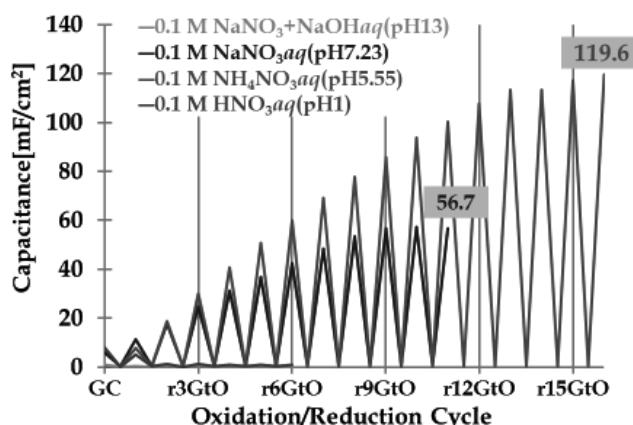


Fig. 1 The electrochemical capacitance of GtO/rGtO electrode prepared by electrochemical oxidation/reduction cycles

[1]H. Tateishi *et al.* Carbon **76**, 40-45 (2014)

[2]H. Tateishi *et al.* J. Electroanal. Chem. **704**, 233-241 (2013)

Corresponding Author: K. Awaya

Tel: +81-96-342-3659, Fax: +81-96-342-3659,

E-mail: 164d8302@st.kumamoto-u.ac.jp

Contrast mechanisms of the fluorescence microscopy that allows direct observations of nanocarbons in solution

○Hikaru Sato, Yutaka Matsuno, Yu-uya Sato, Masahito Sano

Department of Organic Materials Sci., Yamagata University, Yonezawa 992-8510, Japan

We have developed a novel microscopy that visualizes graphene and graphene oxide (GO) dispersed in solution. In order to realize observations, we need to have a very faint illumination for compensating the “shooting against the light source” condition, additional contrast mechanisms besides the small absorption, and orientations facing the larger surface toward an objective lens. These conditions are satisfied simultaneously by dispersing nanocarbons in a fluorescent dye solution near a solid surface. The fluorescence emitted by dye molecules is used as a backlight illumination for the new microscope. Its intensity can be optimized by adjusting the dye concentration and manipulating the excitation beam. Modulations of fluorescence by interactions with nanocarbons give additional contributions to the contrast. Naturally occurring convection current near the solid surface orients graphene sheets parallel to the surface.

Experimentally, a nanocarbon solution is mixed with a dye solution, and is placed on a glass plate. The excitation beam enters the glass from below and irradiates only a region within a few hundred micrometers from the glass/solution interface. Thus, the medium surrounding a graphene sheet fluoresces, but its total intensity is controlled to stay low. Due to the dim illumination, a small change in the light intensity entering the objective lens from a GO sheet causes the sheet to appear either dark or bright relative to the surrounding medium. There are several different mechanisms for this change.

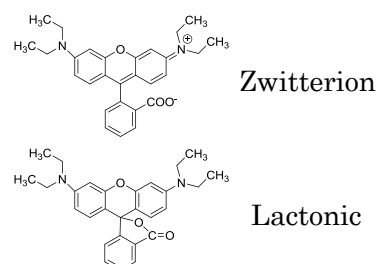
A nanocarbon appears dark if fluorescence around it is quenched by Dexter electron transfer or Förster resonance energy transfer (FRET). The r^{-4} dependence of FRET for molecule-graphene suggests that the dye molecules within 30 nm from a graphene sheet can be quenched. Because FRET efficiency depends on a spectral overlap of the object absorption and the dye emission, it is possible to image an object selectively by choosing an appropriate dye.

The same GO that gives a dark image may appear bright under different conditions. Fluorophore properties of many dyes depends on local environments such as solvent, pH, polarity, hydrophobicity, temperature, and concentration. For instance, rhodamine-b (Rh-b) undergoes chemical conversion from fluorescent zwitterion form to colorless lactonic form in aprotic solvents. Rh-b also forms non-fluorescent H-aggregate as well as fluorescent J-aggregate in water. These states are at equilibrium, which can be shifted by an addition of protic solvents or some solids. When GO is added to NMP solution of Rh-b, a GO sheet appears bright due to either adsorption of Rh-b in a coloring form or shifting the equilibrium by providing proton through hydroxyl groups. Contrarily, graphene has no such group and atomically flat surface, resulting in a dark image. Rh-6G, which cannot be converted into lactonic form but still form H-aggregate, gives bright images of GO due to J-aggregate formation.

In conclusion, it is possible to characterize chemical nature of each GO sheet by analyzing the contrast and fluorescence spectra. These contrast mechanisms indicate that various substances other than nanocarbons become observable by the new microscopy.

Corresponding Author: M. Sano

Tel: +81-238-26-3072 E-mail: mass@yz.yamagata-u.ac.jp



Metal Permeation into Multi-layered Graphene Oxide Film○Michio Koinuma¹, Chikako Ogata^{1,2}, Yasumichi Matsumoto¹¹ *Graduate School of Science and Technology, Kumamoto University,
2-39-1 Kurokami, Chuo-ku, Kumamoto 860-8555, Japan*² *Research Fellow of Japan Society for the Promotion of Science (JSPS Research Fellow)*

Strong adhesion of metals onto graphene oxide (GO) is highly important for building suitable contacts when GO or reduced GO (rGO) is used in electronic and electrochemical devices. Moreover, the metal/graphene oxide (M/GO) interface itself sometimes acts as a catalytic site. The content of oxygenated functional groups at this interface is expected to be strongly affected by the attachment of metals. Thus, understanding M/GO interfaces at atomic and/or electronic scale may bring about the development of new electronic/spintronic, photochemical, and electrochemical devices because their properties are affected by defects and the content of oxygenated functional groups. Here, the unique phenomenon of metal permeation into GO paper bulk (multi-layered GO film) from an M/GO interface is reported.[1] We also demonstrate the importance of the CH defects on the electrochemical capacitance and the dependence of the differences in the functional groups of the rGO samples, particularly the CH defects, on the reduction method.[2]

Metal permeation at M/GO interfaces was observed at 25 °C, where the metals were deposited onto the surface of GO paper by sputtering. In the cases of M = {Cu, Ag, Ni}, the metals were oxidized to the corresponding ions (Cu²⁺, Ag⁺, and Ni²⁺) by redox reactions involving the reduction of GO immediately after metal deposition. These ions then quickly permeated through the interlayers into the GO paper bulk. These reactions and fast permeation occurred with ease under humid conditions but with difficulty under vacuum. Au and Pt atoms also permeated the GO paper bulk, although the permeation rates were low. In these cases, abundant defects and/or edges in the GO paper acted as permeation sites. Other metals are also likely to be able to permeate GO paper bulk as atoms. Consequently, GO paper interlayers have unique properties allowing water, metal ions and other atoms to permeate them while providing a shield against gas molecules. These findings are expected to provide important information about GO used in various (especially electrochemical) devices, where ionic movement potentially affects the functionalities.

[1] C. Ogata *et al. Scientific Reports* **4**, doi:10.1038/srep03647

[2] M. Koinuma *et al. Chem. Lett.* **42** 924-926 (2013).

Corresponding Author: M. Koinuma

Tel: +81-96-342-3660, Fax: +81-96-342-3659,

E-mail: koinuma@chem.kumamoto-u.ac.jp

Enhanced terahertz-wave absorption in monolayer graphene via evanescent wave coupling

Yoichi Harada^{1,2}, M. Shoufie Ukhtary³, Minjie Wang¹, Sanjay K. Srinivasan^{1,4},
Eddwi H. Hasdeo³, Ahmad R. T. Nugraha³, Weilu Gao¹, Yuji Sakai⁵,
Riichiro Saito³, Junichiro Kono¹

¹ *Department of Electrical and Computer Engineering, Rice University,
Houston, Texas 77005, U.S.A.*

² *Department of Engineering, Hokkaido University, Sapporo 060-8628, Japan*

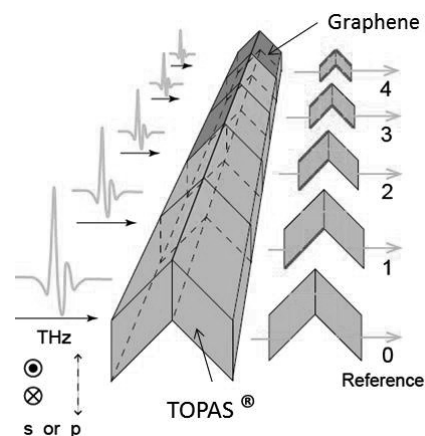
³ *Department of Physics, Tohoku University, Sendai 980-8578, Japan*

⁴ *Department of Physics and Nanotechnology, SRM University, Kancheepuram
District, Chennai, Tamil Nadu, 603203, India*

⁵ *Institute of Laser Engineering, Osaka University, Suita, 565-0871, Japan*

The unique band structure and gate tunability of graphene are expected to result in novel high-frequency and optical phenomena [1]. However, due to the inherently small interaction lengths in monolayer systems, light absorption in graphene is generally small, and simple and robust schemes are being sought for enhancing absorption – particularly, in the terahertz (THz) frequency range.

Here, by using a recently proposed total internal reflection (TIR) geometry [2], we demonstrate significant enhancement of THz-wave absorption in monolayer graphene. Our scheme allows the incident THz beam to be reflected by graphene four times at varying incidence angles, both below and above the critical angle for TIR. We observed extremely large THz absorption, especially for s-polarized radiation. The experimental results are quantitatively consistent with our calculations, incorporating realistic values of carrier scattering time and Fermi energy [2].



[1] R. R. Hartmann, J. Kono, and M. E. Portnoi, *Nanotechnology* **25**, 322001 (2014).

[2] M. Shoufie Ukhtary *et al.* *Appl. Phys. Exp.* **8**, 055102 (2015).

Corresponding Author: Junichiro Kono

Tel: +1-713-348-2109, Fax: +1-713-348-3091

E-mail: kono@rice.edu

Transverse Magnetic and Transverse Electric Surface Waves in Silicene

M. Shoufie Ukhtary, Ahmad R. T. Nugraha, Eddwi H. Hasdeo, Riichiro Saito
Department of Physics, Tohoku University, Sendai 980-8578, Japan

Graphene so far has been the main platform for investigating the surface waves. Surface waves are electromagnetic (EM) waves that propagate on the surface of a material. There are two kinds of surface waves based on their polarizations: transverse magnetic (TM) and transverse electric (TE) surface wave. In the case of TM surface wave, the component of magnetic field is transverse to the propagation direction, while in the case of TE surface wave, the component of electric field is transverse to the propagation direction [see Figs.1 (a) and (b)]. The TM surface wave can be seen as electric dipole oscillation, while the TE surface wave can be seen as magnetic dipole oscillation. It is difficult to integrate graphene with silicon-based optoelectronic devices which utilize the surface waves. On the other hand, silicene, which is a monolayer of silicon atoms arranged in honeycomb lattice similar to graphene structure [see Figs.1 (c) and (d)], is compatible with the silicon technology and might offer more features compared with graphene due to its significant spin orbit coupling and tunable energy gap due to its buckled structure [1]. Silicene has also recently been synthesized experimentally [2,3]. Therefore, it is intriguing to examine the surface waves in silicene.

In this work, we study the characteristics of both TM and TE surface waves in silicene. We determine the dispersion, the confinement length and the wavelength shrinkage for both kinds of surface waves. We also calculate the damping and determine the propagation length of the surface waves. In the case of the TE surface wave in silicene, we find that it exhibits better characteristics compared with that in graphene, in terms of a broader frequency range and more confinement to the surface which originate from the buckled structure of silicene. We find that even undoped silicene can support the TE surface wave. We expect the similar characteristics of TE surface wave in other two-dimensional materials that have slightly buckled honeycomb lattice.

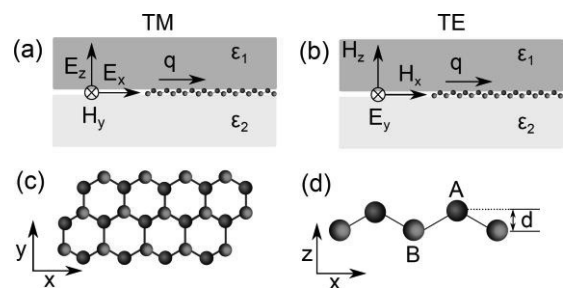


Figure 1: (a) The TM surface wave and its EM field components. (b) The TE surface wave and its EM field components. (c) Honeycomb lattice of silicene. (d) Side view of silicene lattice. Sublattice A and B are separated vertically by $d = 0.46 \text{ \AA}$

[1] C.J. Tabert and E.J. Nicol. PRL 110.197402 (2013).

[2] Lalmi et al. APL 97. 223190 (2010).

[3] Padova et al. APL 96. 261905 (2010).

Corresponding Author: M. Shoufie Ukhtary

TEL: +81-22-795-6442, FAX: +81-22-795-6447, E-mail: shoufie@flex.phys.tohoku.ac.jp

A Scalable Clean Transfer Process with Polymethylglutarimide

○Takashi Matsumae and Tadatomo Suga

Department of Precision Engineering, The University of Tokyo, Tokyo 113-8656, Japan

The practicability of Polymethylglutarimide (PMGI) as a scaffold for a scalable clean transfer is investigated for atomic layers.

Owing to its outstanding electronic¹⁻² properties, graphene has drawn intense research interest for a high speed transistor. A graphene transfer technique using a poly(methyl methacrylate) (PMMA) scaffold has been developed^{3,4} in order to fabricate graphene on an insulating substrate. Nevertheless, it is a great challenge to completely remove the PMMA scaffold without resist residue remaining on the transferred graphene. Extrinsic scattering related to polymer residue limits the performance of CVD graphene films when transferred to insulating substrates.

In this study, a clean graphene transfer process has been achieved by employing a support scaffold composed of a PMGI-based resist. Scanning electron microscopy (SEM) and atomic force microscopy (AFM) observations (Fig. 1) confirmed that the amount of residue on large-area transferred graphene was sufficiently reduced by using PMGI scaffolds in comparison to the traditional technique that uses polymethyl methacrylate (PMMA) scaffolds. The root mean square (RMS) roughness values of graphene surfaces using PMMA and PMGI scaffolds were 6.5 nm and 4.0 nm, respectively. This comparison confirms that a cleaner graphene surface was achieved by using PMGI as a support scaffold. Furthermore, Raman spectroscopy suggests that the quality of the transferred graphene was equivalent to that obtained by the traditional method.

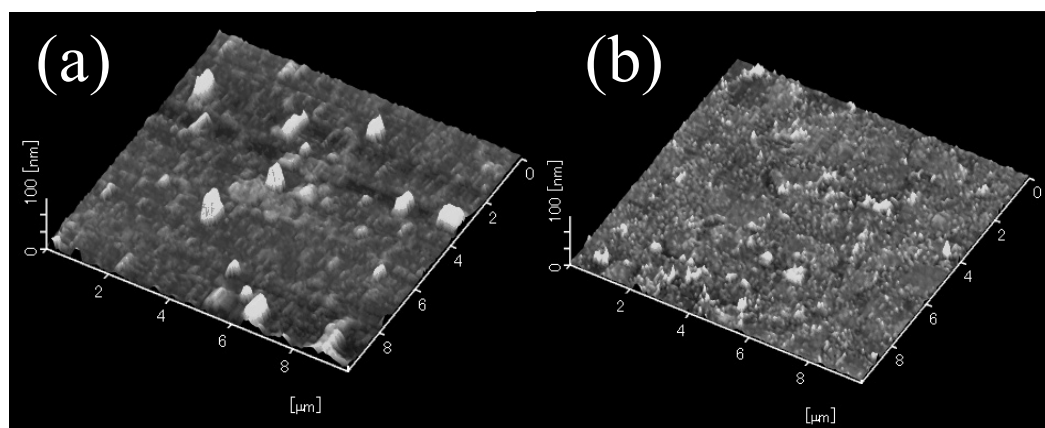


Figure 1: Changes in graphene surface morphology caused by residues from (a)PMMA and (b)PMGI.

- [1] X. Li, *et al. Nano Lett.*, **10**, 4328 (2010).
- [2] H. Cao, *et al., Appl. Phys. Lett.*, **96**, 122106 (2010).
- [3] L.Gao, *et al. Nat. Commun.*, **3**, 699 (2012).
- [4] X.Li, *et al., Nano letters*, **9**(12), 4359 (2009).

Corresponding Author: T. Matsumae

Tel: +81-3-5841-6495, Fax: +81-3-5841-6481,

E-mail: Matsumae.takashi@su.t.u-tokyo.ac.jp

Energetics and electronic structures of hexagonal GaN thin films and heterostructures

○Yanlin Gao, Susumu Okada

*Graduate School of Pure and Applied Sciences, University of Tsukuba,
Tsukuba, 305-8571, Japan*

With their peculiar electronic properties, two-dimensional (2D) materials can be promising candidates for fabricating functionalized devices for the next generation. The electronic structure of 2D materials is sensitive to their consistent elements, network morphology, and interlayer stacking arrangements. In our previous work, we have theoretically demonstrated that the hexagonally bonded GaN (h-GaN) with atomic thickness prefers the planar structure as the case of h-BN, and could be a compound semiconductor with an indirect energy gap of 2.28 eV. In this study, we investigated how the energetics and electronic structures of h-GaN depend on the interlayer interaction and formation of hybrid structures with other 2D materials using the density functional theory with generalized gradient approximation combined with the van der Waals correction.

Our calculations elucidate that h-GaN can form a bilayer structure with AA' stacking arrangement and an interlayer spacing of 2.2 Å at which the interlayer binding energy is 1.18 eV per unit cell. The electronic structure of bilayer h-GaN is slightly modulated owing to a substantial interlayer interaction arising from small interlayer spacing. We also check the geometric and electronic structures of h-GaN thin films with increasing the number of the GaN layer. Interestingly, with increasing the number of the GaN layer, the top of the valence band gradually approaches the Γ point. Then, finally, the bulk h-GaN with the AA' stacking arrangement is a semiconductor with the direct energy gap of 2.78 eV at the Γ point, which is narrower than that of bulk GaN with a Wurtzite structure. We also check the energetics and electronic structures of the h-GaN sheet adsorbed on the other layered materials. We consider graphene and h-BN as representative substrates for h-GaN. Our calculations show that the equilibrium interlayer spacing of h-GaN/graphene and h-GaN/h-BN are both 3.4 Å, indicating that these hybrids are the van der Waals heterostructures, and in each case the electronic structure is almost the simple sum of those of all constituents.

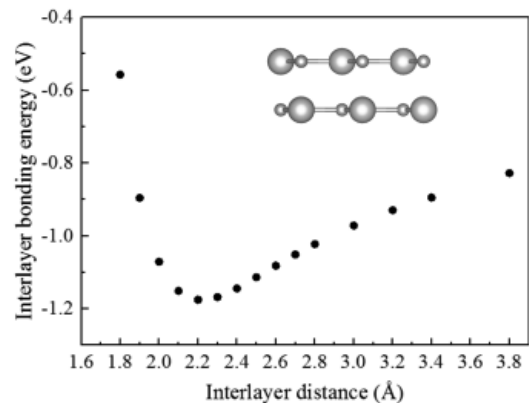


Fig. 1. Interlayer binding energies of bilayer h-GaN versus the interlayer spacing.

Corresponding Author: Y. Gao

TEL: +81-29-853-5921, FAX: +81-29-853-5924

E-mail: ylgao@comas.frsc.tsukuba.ac.jp

Formation of 1D confining potential in MoS₂/WS₂-based heterostructures

○Yu Kobayashi¹, Shoji Yoshida², Ryuji Sakurada², Kengo Takashima³,
Takahiro Yamamoto³, Tetsuki Saito¹, Satoru Konabe⁴, Takashi Taniguchi⁵, Kenji Watanabe⁵,
Yutaka Maniwa¹, Osamu Takeuchi², Hidemi Shigekawa², Yasumitsu Miyata^{1,6,*}

¹Department of Physics, Tokyo Metropolitan University, Hachioji 192-0397, Japan

²Faculty of Pure and Applied Sciences, University of Tsukuba, Tsukuba 305-8573, Japan

³Department of Liberal Arts, Tokyo University of Science, Katsushika 125-8585, Japan

⁴RIST, Tokyo University of Science, Katsushika 125-8585, Japan

⁵National Institute for Materials Science, Tsukuba 305-0044, Japan

⁶JST-PRESTO, Kawaguchi 332-0012, Japan

In-plane atomic layer heterostructures based on transition metal dichalcogenides (TMDCs) are expected to represent ideal systems for the realization of novel confined electronic systems at one-dimensional (1D) interfaces. However, so far, such 1D confined systems have never been observed in the previous studies of TMDC-based monolayer heterostructures [1-3]. Here, we report the formation of confining potential at the heterojunction interface of bilayer WS₂ and MoS₂/WS₂ vertical heterostructure as shown in Fig. 1a [4]. For this bilayer sample, scanning tunneling microscopy/spectroscopy (STM/STS) revealed an upshift in both the valence and conduction band edges at the interface. Notably, the observed band bending can be explained by the presence of 1D fixed charges around the heterointerface as shown in Fig. 1b. The present findings indicate that highly tunable electronic properties of TMDC systems provide an ideal system to realize 1D confined electronic system and the carrier accumulation along the interface.

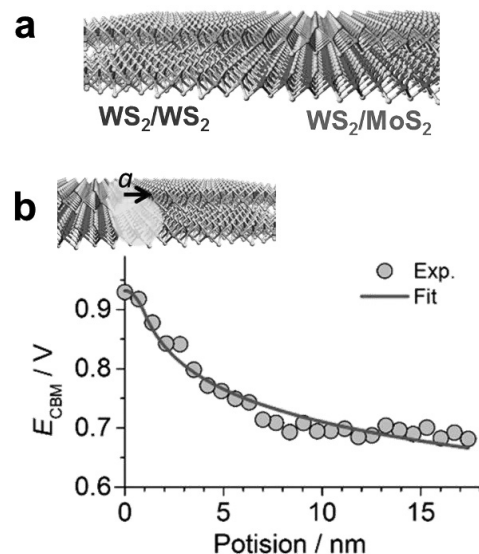


Fig. 1 (a) Structure model of bilayer WS₂ and MoS₂/WS₂ vertical heterostructure. (b) Fitting curve of band bending by cylindrical charge model around the interface of bilayer heterostructure.

[1] Y. Gong, *et al. Nat. Mater.*, 13, 1135 (2014). [2] Y. Kobayashi *et al.*, *Nano Res.*, 8, 3261 (2015).

[3] S. Yoshida, *et al. Sci. Rep.*, 5, 14808 (2015). [4] Y. Kobayashi *et al.*, *Sci. Rep.*, in press.

Corresponding Author: Yasumitsu Miyata, Tel: 042-677-2508, E-mail: ymiyata@tmu.ac.jp

Fabrication and optical properties of vertical heterostructure of monolayer-WSe₂/MoTe₂

○Takao Yamaoka, Lim Hong En, Koirala Sandhaya, Yuhei Miyauchi, Kazunari Matsuda

Institute of Advanced Energy, Kyoto University, Uji, Kyoto 611-0011, Japan

Recently, monolayer transition metal dichalcogenide (1L-TMD) as atomically thin two-dimensional (2D) material has attracted much attention from the viewpoints of fundamental physics and applications [1,2]. The artificial van der Waals heterostructures can be realized by the vertical stacking of different atomically thin 2D TMDs. The van der Waals heterostructures exhibit the intriguing optical and electronic properties, which much differ from their constituting monolayer TMDs [3,4].

In this work, we fabricated the vertical heterostructure of 1L-WSe₂/1L-MoTe₂ on SiO₂/Si substrate by transfer method and also investigated the optical properties of the heterostructure. Figure 1(a) shows the optical microscope image of 1L-WSe₂/1L-MoTe₂ heterostructure, as indicated in the squared region. Figure 1(b) shows Raman scattering spectrum of isolated 1L-MoTe₂, 1L-WSe₂, and 1L-WSe₂/1L-MoTe₂ heterostructure. The Raman peaks at 171 and 235 cm⁻¹ are assigned as A_{1g} and E_{12g} modes in isolated 1L-MoTe₂. In 1L-WSe₂, the Raman scattering peaks of 249 and 261 cm⁻¹ as degenerated A_{1g}, E_{12g} modes and 2nd order Raman process mode are observed. We observe some Raman peaks from each layer of 1L-WSe₂ and 1L-MoTe₂ in the 1L-WSe₂/1L-MoTe₂ heterostructure.

Moreover, the additional peak at 309 cm⁻¹ is appeared, which is assigned as Raman inactive B_{12g} mode in 1L-WSe₂ [5,6]. The out-of-plane B_{12g} mode becomes Raman active in the bi-layer system. Thus, the appearance of out-of-plane B_{12g} mode in 1L-WSe₂/1L-MoTe₂ heterostructure suggests the inter-layer coupling between 1L-WSe₂ and 1L-MoTe₂ in the heterostructure. The detail optical properties including photoluminescence and absorption in the 1L-WSe₂/1L-MoTe₂ heterostructure will be discussed.

- [1] J. C. Shaw *et al.*, *Nano Res.* **7**, 511 (2014).
- [2] N. Dong *et al.*, *Sci. Rep.* **5**, 14646 (2015).
- [3] Y. Gong *et al.*, *Nat. Mater.* **13**, 1135(2014).
- [4] X. Duan. *et al.*, *Nat. Nano.* **9**, 1024 (2014).
- [5] W. Zhao *et al.*, *Nanoscale.* **5**, 9677 (2013).
- [6] M. H. Chu *et al.*, *ACS. Nano.* **8**, 9649 (2014).

Corresponding Author: Kazunari Matsuda

Tel/Fax: +81-774-38-3460

E-mail: matsuda@iae.kyoto-u.ac.jp

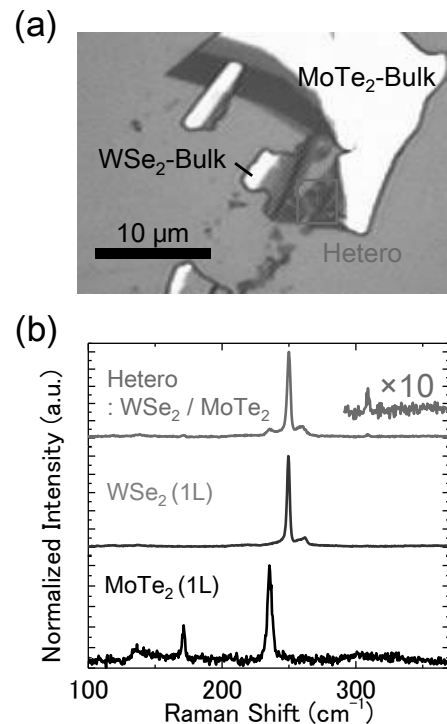


Fig. 1 (a) Optical microscope image of WSe₂/MoTe₂ heterostructure. (b) Raman scattering spectrum of WSe₂/MoTe₂ heterostructure, 1L-WSe₂ and 1L-MoTe₂.

Electronic and magnetic properties of porous hydrocarbon networks

○Jun-ya Sorimachi, Susumu Okada

*Graduate school of Pure and Applied Sciences, University of Tsukuba, Tsukuba
305-8571, Japan*

Electronic structure of hydrocarbon molecules is sensitive to their size and network morphology, making them to be building blocks for the various functional nanomaterials which are applicable for wide area of the modern technology. Among possible morphologies, molecules with a triangular shape occasionally exhibit spin polarization arising from the non-bonding electron states associated with the imbalance between two sublattices. Phenalenyl: $C_{13}H_9$ is the smallest and representative example of such materials with $S=1/2$ polarized spin and could be the constituent unit for 2D porous hydrocarbon networks with magnetic ordering. In this work, we design a novel hydrocarbon molecule with radical spin as the 3D version of phenalenyl molecule (Fig. 1). Furthermore, by assembling this molecule, we also design 2D and 3D porous hydrocarbon network (Fig. 2) and explore their electronic and magnetic properties using the density functional theory with generalized gradient approximation.

In the case of 2D networks, because of a triangular and pyramidal shape of the molecule, we can construct two dimensional honeycomb networks of the molecules. Our calculation shows that one of two networks possesses four magnetic states. In contrast, the other network is a semiconductor with the direct energy gap of 1.2 eV. The 3D network is also a semiconductor with the direct band gap of 1.3 eV. Because of the large spacing arising from the constituent molecule, the 3D porous hydrocarbon network is a low-density material of which density is 40% of that of the diamond. The fact indicates that the 3D network is a plausible candidate for the host materials of the energy storage devices in which a number of atoms or molecules are accommodated in the nanometer scale pore.

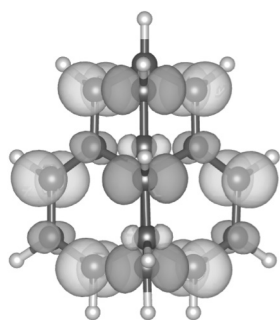


Fig. 1 Geometric structure and spin density of a hydrocarbon molecule with a triangular conical shape.

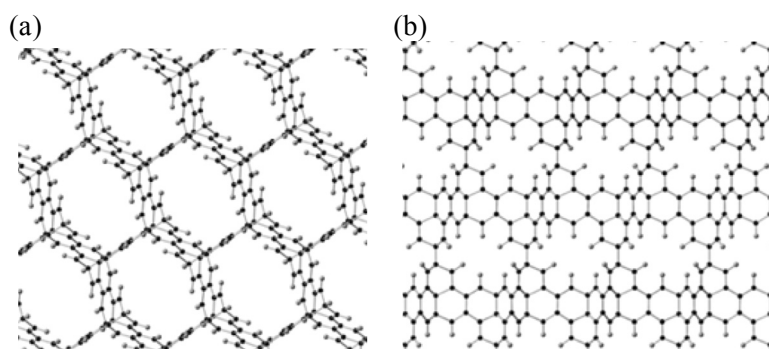


Fig. 2 Geometric structure of (a) 2D and (b) 3D porous hydrocarbon network of pyramidal conical molecules.

Construction of graphene – TiO₂ hybrid nano-material using bifunctional protein supramolecule

○Yuki Hashima, Yasuaki Ishikawa Mutsunori Uenuma, Naofumi Okamoto,
Ichiro Yamashita and Yukiharu Uraoka

¹*Graduate School of Material Science, Nara Institute Science and Technology, 8916-5
Takayama, Ikoma, Nara 630-0192, Japan*

Titanium dioxide (TiO₂) has efficient photoactivity, high photostability, chemical inertness, and nontoxicity as a semiconductor material, which is useful in photovoltaic and photocatalysis. The composite of TiO₂ and graphene would contribute to a hybrid nano-material that combines superior properties for specific device applications. Various TiO₂-graphene composite materials have been produced using “graphene oxides” that were modified with functional polymer [1]. We introduced new TiO₂ composite method using bifunctional protein supramolecule in this study.

We designed and mass-produced Dps displaying carbon nano-horn binding peptide and Ti binding peptide, which named CDT-1. We previously reported that the CDT-1 adsorbed to graphene using carbon nano-horn binding peptide. In this report, TiO₂ was deposited on graphene using Ti binding peptide in Graphene/CDT-1 bio-conjugates.

Experimentally, Graphene/CDT-1 bio-conjugates (50mM phosphate buffer pH 6.0) were then dipped in Titanium precursor solution. Precipitation of graphene – TiO₂ hybrid nano-material was performed by ultracentrifugation. After the process, TEM–EELS mapping was carried out.

The Fig. 1 shows TEM image of graphene - TiO₂ hybrid material and Ti mapping in TEM-EELS image, respectively. In this result, Ti mapping matched with the graphene TEM image, suggesting TiO₂ was deposited on graphene owing to the Ti binding peptide.

We successfully constructed graphene - titanium hybrid nano-material using bifunctional protein supramolecule. All processes were carried out at room temperature, using an environmentally friendly method.

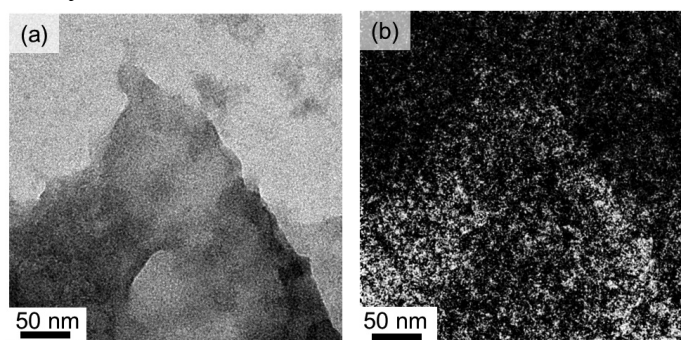


Fig.1 (a) TEM image of the graphene - TiO₂ hybrid material.

(b)EELS mapping of Ti at the same region as (a).

[1] Donghai Wang et al. ACS Nano 3 (4), 907 - 914 2009

Corresponding Author: Yasuaki Ishikawa

Tel:+81-743-72-6064, Fax:+81-743-72-6069,

E-mail:yishikawa@ms.naist.jp

Rapid and Reversible Dispersibility Tuning of Carbon Nanomaterials by the Photoisomerization of an Azobenzene-derived dispersant

○Hirokuni Jintoku, Yoko Matsuzawa,* Hideyuki Kihara,* Masaru Yoshida

Research Institute for Sustainable Chemistry, National Institute of Advanced Industrial Science and Technology (AIST), Tsukuba 305-8565, Japan.

Carbon nanomaterials such as carbon nanotubes (CNTs), graphene, and carbon black find applications in a variety of areas owing to their unique structural, mechanical, and electrical properties. In order to fabricate high-performance carbon nanomaterial-based devices, it is important to not only ensure that the carbon nanomaterials are of good quality, but also remove the organic additives (e.g., solvents and dispersants) that are used during the fabrication process. In particular, the presence of residual organic components in the nanomaterials negatively impacts the electrical properties of electrical devices. Over the past decade, stimuli-responsive dispersants have been investigated for the purification of CNTs and removal of organic components from CNT-based devices.[1] In this work, we report a new photoresponsive dispersant (**AB**) for carbon nanomaterials based on azobenzene and a quaternary ammonium salt, which act as a photosensitive moiety and solubilizing unit in water, respectively (Fig. 1a).

We successfully obtained a well-dispersed SWCNT aqueous dispersion using **AB** as the dispersant with bath sonication followed by centrifugation (solid line, Fig. 1b). The dispersibility of SWCNTs in water changed rapidly upon the photoisomerization of **AB**. Upon irradiation with UV light for a short time (365 nm, 150 mW/cm², 10 min), the SWCNT/**AB** dispersion changed to the agglomerated state (dashed line, Fig. 1b). The reverse photoreaction of the SWCNT/**AB** hybrid resulting in transformation from the agglomerated state to the dispersed state was observed upon irradiation with visible light. When the agglomerate was placed under visible light (436 nm, 25 mW/cm², 20 min), followed by sonication for 5 min, the SWCNT/**AB** hybrid returned to the dispersed state. Over three cycles of switching between the dispersed and agglomerated states by alternate UV and visible irradiation, only a slight spectral change was observed (Fig. 1c).

We would like to discuss about the dispersibility tuning of other carbon nanomaterials (e.g., MWCNT, carbon black and graphene) in presentation.

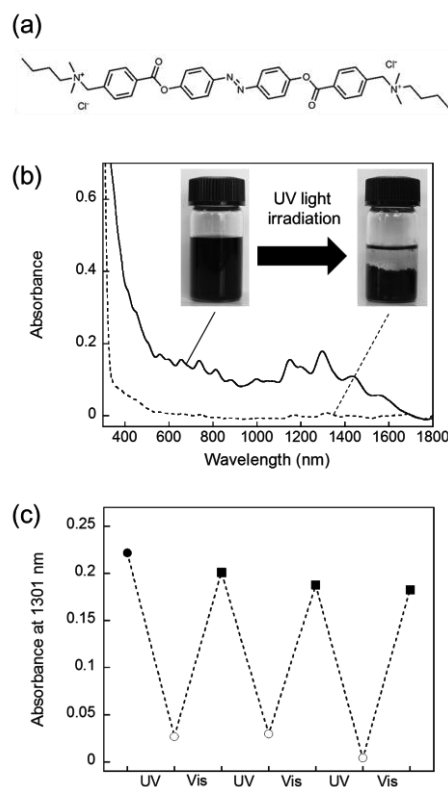


Fig. 1 (a) Chemical Structure of **AB**. (b) UV-Vis-NIR spectra of SWCNT/**AB** in D₂O at 25 °C. (c) Absorbance changes of the SWCNT/**AB** solution before UV irradiation (solid circle), after UV irradiation (open circle) and after Vis irradiation (solid square).

[1] Y. Matsuzawa, M. Yoshida *et al. Adv. Mater.* **23**, 3922 (2011)

Corresponding Author: H. Kihara

Tel: +81-29-861-4442, Fax: +81-29-861-4673

E-mail: h-kihara@aist.go.jp

Effect of the flow regime on graphene growth

Ya-Ping Hsieh¹, Ching-Hua Shih¹, Yi-Jing Chiu¹, and Mario Hofmann²

¹ Graduate Institute of Opto-Mechatronics, National Chung Cheng University and Advanced Institute of Manufacturing with High-Tech Innovations, Chiayi, Taiwan 62102

² Department of Material Science and Engineering, National Cheng Kung University, Tainan, Taiwan 70101

Graphene is a novel 2D material with significant promise for flexible electronics, interconnects, and 3D devices. The most pressing issue for the application of graphene is the scalable production of high quality material. We have recently developed a novel approach to increase the throughput of graphene CVD synthesis. By using closely stacked copper foil substrates, the amount of graphene grown in one batch can be enhanced twenty-fold.

The adjustment of the distance between copper foils allows us to widely tune the fluid dynamical conditions of the graphene growth process. While we observe free flow conditions for large gap sizes, a transition to the molecular flow regime was identified when the gap size is below the mean free path.

By exploring the graphene growth rate we are able to extract the diffusion coefficient for the carbon precursor for each flow condition. The diffusion coefficient was found to decrease with gap size in agreement with the Knudsen condition.

Our analysis of the graphene

quality, as quantified by spectroscopic and electrical transport measurements, indicates the importance of a transport-limited growth process to achieve high quality and uniform graphene growth.

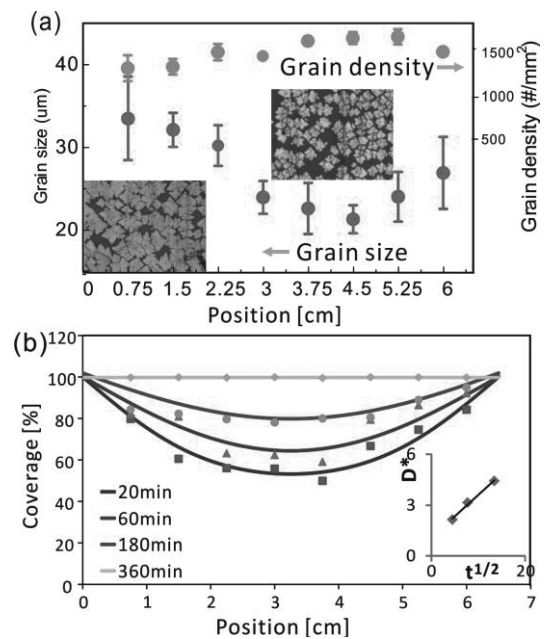


Figure 1. Horizontal growth process (a) distribution of grain size and grain density along one pore, (inset) photographs of graphene grown at the edge and the center of on copper foil, (b) coverage vs. position along one pore for various growth durations, (inset) extracted values of $\sqrt{4Dt}$ vs. \sqrt{t} .

Synthesis and self-aggregation properties of various triazoliumfullerene

○Toshihiko Okada, Saori Inaba, Naohiko Ikuma, Hidehiro Sakurai

*Division of Applied Chemistry, Graduate School of Engineering, Osaka University,
Osaka, 565-0871, Japan*

Ionic fullerenes are useful for medical applications and self-assembly nanocarbon materials based on the amphiphilic intermolecular ionic and hydrophobic interactions [1]. We have prepared ionic triazoliumfullerenes $2^+ \cdot \text{PF}_6^-$ by [3+2] cycloaddition of 1,2-triazadienium salt $1^+ \cdot \text{PF}_6^-$ with C_{60} (Figure 1)[2]. A DFT calculation predicts “periconjugation” between the cationic $\text{N}^1\text{-N}^2\text{-N}^3$ linkage and fullerene sphere and the more reduced LUMO level and molecular dipole moment than pyrrolidiniumfullerene, a conventional ionic fullerene (Figure 2a).

Vesicles (Figure 2b) and crystalline (Figure 2c) self-aggregates were observed by TEM. When $\text{R} = \text{H}$, size of vesicles prepared from THF solution is 21.2 ± 6.4 nm. When $\text{R} = \text{Cl}$, molecular dipole moment decreased and size of vesicles increased to 46.6 ± 13.6 nm.

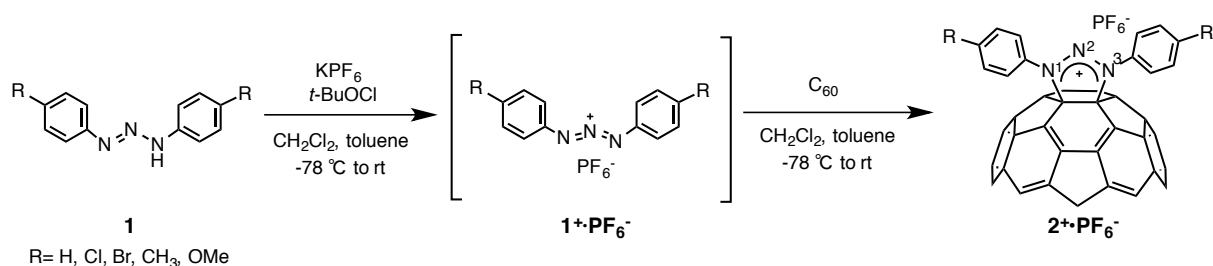


Fig. 1 Synthesis of triazoliumfullerene $2^+ \cdot \text{PF}_6^-$

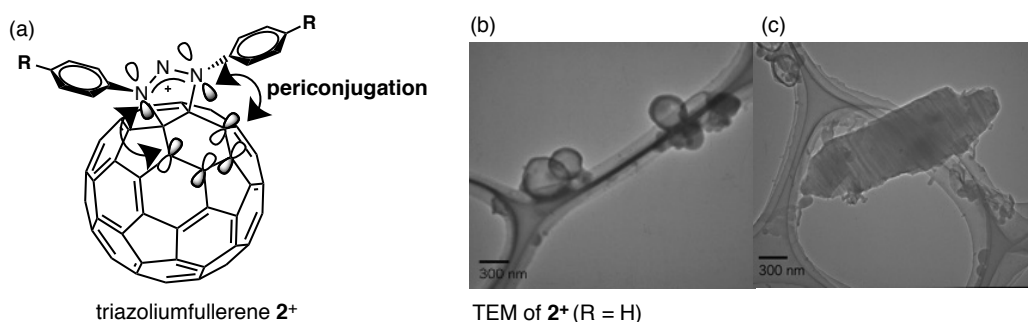


Fig. 2 (a)Molecular structure and (b,c)TEM images of triazoliumfullerene 2^+ prepared from MeOH solution

[1]D. M. Guldi, M. Prato et al., *Acc. Chem. Res.*, 2005, **38**, 38.

[2] N. Ikuma, S. Inaba, K. Kokubo, T. Oshima, *Chem. Commun.*, **2014**, 50, 581.

Corresponding Author: N.Ikuma

Tel: +81-6-6879-4592, Fax: +81-6-6879-4593,

E-mail: ikuma@chem.eng.osaka-u.ac.jp

Supramolecular Differentiation for Construction of Anisotropic C₆₀ Nanostructures by Time-Programmed Control of Interfacial Growth

○Kosuke Minami¹, Partha Bairi¹, Jonathan P. Hill¹, Waka Nakanishi¹, Lok Kumar Shrestha¹, Liu Chao², Koji Harano², Eiichi Nakamura², Katsuhiko Ariga¹

¹International Research Center for Materials Nanoarchitectonics, National Institute for Materials Science, Tsukuba 305-0044, Japan

²Department of Chemistry, The University of Tokyo, Tokyo 113-0033, Japan

Many of the constituents of natural systems including molecules, biomolecules and cells are composed of asymmetric structures. This asymmetry is an extremely important feature and it is maintained even through complex processes. However, processes of self-assembly in chemistry often only yield simple symmetric nanostructures, due to energy minimization processes. The construction of asymmetric nanostructures requires additional information which can be incorporated by applying molecular design principles, such as can be found in finely tuned complex molecules or polymers where phase-separation processes can be affected by designing non-covalent interactions.

Liquid–liquid interfacial assembly has great potential for the synthesis of asymmetric forms [1]. However, there remain some limitations of these approaches in the fabrication of anisotropic nanostructures. Through a combination of the phase-separation and interfacial assembly technique, anisotropic structures containing specifically designed components can be constructed. We have coined the term “supramolecular differentiation” for this process.

Here, we show the synthesis of an anisotropic fullerene nanostructures bearing a single tube-like structure by combining the liquid–liquid interfacial assembly method with local phase-separation of two fullerene derivatives (Figure 1): pentakis(phenyl)fullerene (**PhH**), and pentakis(4-dodecylphenyl)fullerene (**C12H**) [2]. We have finely tuned the local phase-separation by means of time-programmed control of liquid–liquid interfacial assembly and homogeneous growth. Seed particles with a domain structure, which provides a platform for formation of tube-like structures, were prepared by liquid–liquid interfacial precipitation (LLIP) method [3]. After pre-incubation time, sonication was applied to the mixture leading to homogeneous growth process, where the tube-like structures formed on the domain structure on the seed particle. Our technique, which is essentially a combination of the interfacial assembly and phase-separation phenomena, can be used to further enable the construction of anisotropic nanostructures.

[1] W. Li *et al.* *Adv. Mater.* **25**, 5129 (2013).

[2] K. Miyazawa *et al.* *J. Mater. Res.* **17**, 83 (2002).

[3] (a) M. Sawamura *et al.* *JACS* **118**, 12850 (1996);

(b) T. Homma *et al.* *JACS* **133**, 6364 (2011).

Corresponding Author: K. Minami, L. K. Shrestha, K. Ariga

Tel: +81-29-851-3354 (ex. 8456)

E-mail: MINAMI.Kosuke@nims.go.jp (K.M.);

SHRESTHA.lokkumar@nims.go.jp (L.K.S.);

ARIGA.Katsuhiko@nims.go.jp (K.A.)

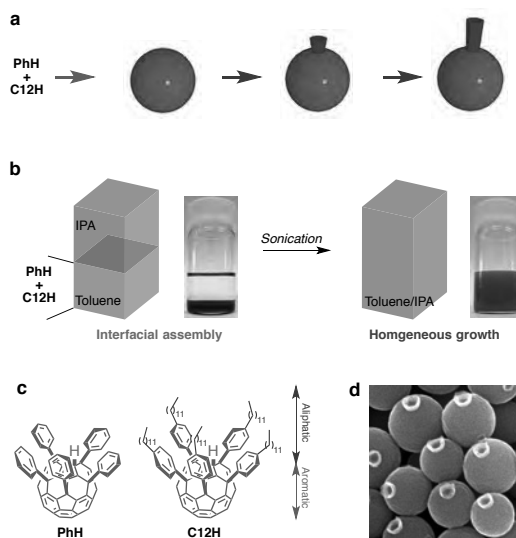


Figure 1. (a) Schematic illustration of supramolecular differentiation of fullerene anisotropic structures. (b) Method of supramolecular differentiation. (c) Structures of fullerene derivatives. (d) An SEM image of fullerene anisotropic nanostructures.

Enhancement of Fill Factor in Inverted Organic Solar Cells using Self-Assembled Monolayer of Fullerene Catechol

○Il Jeon¹, Keisuke Ogumi², Takafumi Nakagawa¹, Yutaka Matsuo^{1,3}

¹ Department of Mechanical Engineering, The University of Tokyo, Tokyo 113-8656, Japan

² Tokyo Metropolitan Industrial Technology Research Institute, Tokyo 135-0064, Japan

³ Hefei National Laboratory for Physical Sciences at Microscale, University of Science and Technology of China, Hefei, 230026, China

The chemical phenomena at the interface of metal oxide are of great importance for organic solar cell performance, because thin-film organic solar cells depend on the interface in facilitating efficient charge extraction. In this regard, inverted organic solar cells (OSCs) can take advantage of the vertical phase separation and concentration gradient in the active layer. Fullerenes as electron acceptors in the photoactive layer have been at the center of OSC technology to date. Fullerene acceptors being near the electron-transporting layer (ETL) has been known to strengthen the charge-carrier transport in an inverted architecture. Thus, technology that can introduce fullerenes on metal oxide can establish the first principles of precise control over the vertical separation.

Self-assembled monolayers (SAMs) with fullerene attached are good motifs for such a prospect. Coating metal oxides or metal with SAMs can change the work function and surface energy of electrodes. There has been a variety of SAMs with fullerenes reported to date. Among those SAMs, catechol-terminated SAMs have attracted the attention owing to their weak diprotic acid nature, which can form bidentate bonding with metal oxide while minimizing damage unlike carboxylic acid- or phosphonic acid-terminated modifiers.

Here, we introduce a simpler catechol-terminated surface modifier that is composed of a catechol end and a fullerene end, which are linked by a simple methylene linker, functioning as effective charge-carrier harvesters. Unlike fulleropyrrolidine, our compound does not contain the nitrogen atom. Catechol, being a weak acid, can bind to TiO_x strongly. Fullerene has high electron mobility and low hole mobility. Therefore, a monolayer of fullerene can function as an additional hole blocker. With fullerene's tendency to attract other fullerene molecules by π - π interactions, the monolayer of fullerene may even induce the vertical separation effect as evidenced by the enhancement of fill factor (FF) in our study. We fabricated an inverted OSC using a mixture of poly(3-hexylthiophene) (P3HT) and phenyl- C_{60} -butyric acid methyl ester (PC₆₁BM) in a structural configuration of glass/ITO/ TiO_x -catechol C_{60} /P3HT:PC₆₁BM/PEDOT:PSS/Au. The catechol C_{60} -treated device gave a PCE of 2.81%, while a non treated device sample gave a PCE of 2.46%, where enhancement of FF was the main reason for the improvement.

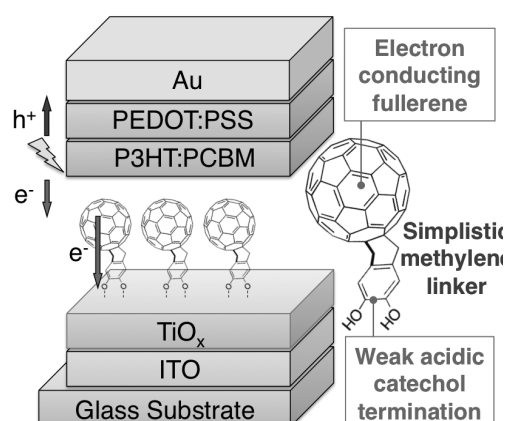


Fig. 1: Concept illustration of this work.

Corresponding Author: Y. Matsuo

Tel: +81-3-5841-0978, E-mail: matsuo@photon.t.u-tokyo.ac.jp

Solid-State NMR Studies on the Aggregated Structures in Organic Bulk Heterojunction Solar Cells

○Saki Kawano¹ and Hironori Ogata^{1,2}

¹Grad. School of Sci. and Engin., Hosei Univ.

²Res.Center for Micro-Nano Technol., Hosei Univ.

Bulk heterojunction (BHJ) organic solar cells are an emerging technology that has the potential to provide a low cost photovoltaic devices. It is well known that the nanomorphology of the polymer:fullerene BHJ is a critical factor which affects the solar cell performance. The addition of processing additives such as 1,8-diiodooctane (DIO) is widely used approach to increase power conversion efficiencies for many organic solar cells^[1-2]. Solid-state solar NMR spectroscopy offers several techniques for the investigation of the morphological, structural, and dynamics properties of BHJ organic solar cells.

We have explored the effects of DIO, 1,8-Octanedithiol(ODT) and 1-Chloronaphthalene(CN) addition of P3HT/PCBM BHJ films on the local crystallinity and morphology by using solid-state NMR spectroscopy. It is reported that the crystallinity of P3HT films also depend on the drying time. In this study, we investigated the change in the crystallinity, morphology, and the properties of molecular motions of P3HT/PCBM BHJ film by changing drying rates by using ¹³C and ¹H solid-state NMR spectroscopy.

Mixed solution of P3HT/PCBM of 1:1(w/w) was prepared by mixing P3HT and PCBM into chlorobenzene at a concentration of 1 wt% for 50 hrs in a glove box under argon atmosphere. Additives were then dropped into the solution and then stirred for 1 hr. The solution was filtered using 0.45μm filter before making films to remove undissolved materials. P3HT/PCBM BHJ films were prepared by dropping the solution in a glass plate and dried in a glove box under argon atmosphere for 40 hrs and then put in the vacuum. Dried film were removed from the glass plate and sealed into 4 mm zirconia NMR rotor. Solid-state NMR spectra (¹³C-CP/MAS-NMR, ¹H-MAS NMR, and their heteronuclear correlation-NMR) and T_1 were measured by using Bruker AVANCE300 spectrometer. The detailed results will be presented.

References:

- 1) J. K. Lee et al., *J. Am. Chem. Soc.*, **130**(2008)3619.
- 2) B.R.Aïch et al, *Organic Electronics*, **13** (2012)1736.
- 3) Ryan C. Nieuwendaal et al., *ACS Macro Lett.* **3**(2014)130–135.

Corresponding Author: Hironori Ogata

Tel: +81-42-387-6229, Fax: +81-42-387-6229,

Triplet state of molecular oxygen in openC₆₀

○Azusa Kato¹, Tsukasa Futagoishi², Yasujiro Murata², Tatsuhisa Kato^{1,3}

¹ Graduate School of Human and Environmental Studies, Kyoto University, Kyoto 606-8501, Japan

² Institute for Chemical Research, Kyoto University, Kyoto 611-0011, Japan

³ Institute for Liberal Arts and Sciences, Kyoto University, Kyoto 606-8501, Japan

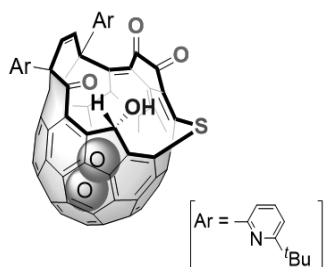


Fig.1 Structure of O₂@openC₆₀

Molecular oxygen (O₂) is the fundamental bi-radical molecule with the electronic ground state $^3\Sigma_g^-$, whose molecular parameters have been studied in gas phase, and well documented. We performed the molecular surgery synthesis of the endohedral fullerene of O₂@openC₆₀, in which O₂ is trapped in an openC₆₀ cage as shown in Fig. 1.^[1] X- and W-band ESR measurements at cryogenic temperatures were carried out to know whether the O₂ molecule trapped in the openC₆₀ cage kept the triplet state of $^3\Sigma_g^-$ in the same condition as gas phase.

O₂@openC₆₀ exhibited spectra as shown in Fig. 2, which were observed by a X-band ESR spectrometer at temperatures from 4K to 32K. The prominent absorption peaks at the magnetic field around 1200mT were well reproduced by the computer simulation using parameters of the g value of 2.0023 and the zero field splitting constants of $D=3.730\text{ cm}^{-1}$ and $E=0.015\text{ cm}^{-1}$. The peak intensities followed the Boltzmann statistics law, the intensity increased with increasing temperature at the temperature range from 1.5 K to 3K, and decreased at the range above 4K. This temperature dependence is consistent with the energy level order among three spin sublevels, $M_s=+1, -1, 0$, which is determined by the zero field splitting constant of positive value of D. Comparing with parameters of O₂ in gas phase, the value of $D=3.730\text{ cm}^{-1}$ is smaller than that of gas phase, 3.963 cm^{-1} .^[2] It's noticeable that O₂@openC₆₀ shows non-zero value of $E=0.015\text{ cm}^{-1}$. These features would attribute to the confinement of the wave function of radical electrons by the openC₆₀ cage.

[1] T.Futagoishi, et al, *Org. lett.* **15**, 2750-2753 (2013).

[2] T. Amano and E. Hirota, *J. Mol. Spectrosc.* **53**, 346-363(1974).

Corresponding Author: Tatsuhisa Kato
Tel: 075-753-6695, Fax: 075-753-6695,
E-mail: kato.tatsuhisa.6e@kyoto-u.ac.jp

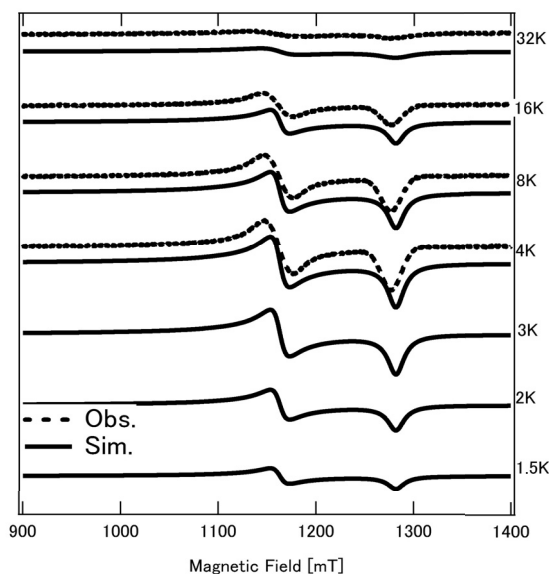


Fig.2 X-band ESR spectra of O₂@openC₆₀ powder observed at 4K, 8K, 16K, and 32K (Obs.). And simulated spectra (Sim.).

Interactions between carbon nanotubes and aromatic amino acids

○Atsushi Hirano¹, Kazuki Iwashita², Kentaro Shiraki², Shun Sakuraba³, Tomoshi Kameda⁴,
Rieko Ishii,¹ Takeshi Tanaka¹

¹ *Nanomaterials Research Institute, National Institute of Advanced Industrial Science and Technology (AIST), Tsukuba, Ibaraki 305-8565, Japan*

² *Faculty of Pure and Applied Sciences, University of Tsukuba, Ibaraki 305-8573, Japan*

³ *Graduate School of Frontier Sciences, The University of Tokyo, Chiba 277-8581, Japan*

⁴ *Artificial Intelligence Research Center, National Institute of Advanced Industrial Science and Technology (AIST), Koto, Tokyo 135-0064, Japan*

Carbon nanotubes are anticipated for use in biological applications such as drug delivery carriers, imaging materials and cancer targeting materials. In these research fields, unspecific interaction between carbon nanotubes and proteins is a crucial factor that affects their functional properties. Fundamental insights into the interaction mechanism should thus be clarified for addressing and controlling the unspecific interaction. Since proteins consist of amino acid residues, the protein–carbon nanotube interaction can be understood in terms of interplays of amino acids with carbon nanotubes. In the present study, we demonstrated that aromatic amino acids, i.e. tryptophan (Trp), tyrosine (Tyr), phenylalanine (Phe), have a high affinity for the single-wall carbon nanotubes (SWCNT) using chromatographic analyses and molecular dynamics simulations.

Fig.1 shows chromatograms of the aromatic amino acids in the column with or without HiPco SWCNTs as ligands. Retention time of the amino acids increased in the order of Phe < Tyr < Trp in the presence of the SWCNTs, meaning that indole has favorable interactions with the SWCNTs [1]. Fig.2 shows binding free energy of the amino acids onto the armchair and zigzag SWCNT sidewalls, which was obtained by the molecular dynamics simulations. The results were consistent with the experimental data. It should be noted that the binding free energy increased monotonously with increasing SWCNT diameter, regardless of the helicity. Thus, SWCNT curvature was found to be a factor that affects the interaction between the amino acids and SWCNTs. On the basis of the knowledge of the interaction, we succeeded to control protein adsorption onto the SWCNTs using arginine [2].

[1] K. Iwashita *et al.* *Langmuir* **31**, 8923 (2015).

[2] K. Iwashita *et al.* *Chem. Lett.* DOI: 10.1246/cl.160390

Corresponding Author: A. Hirano

Tel: +81-29-849-1064, Fax: +81-29-861-2786,

E-mail: hirano-a@aist.go.jp

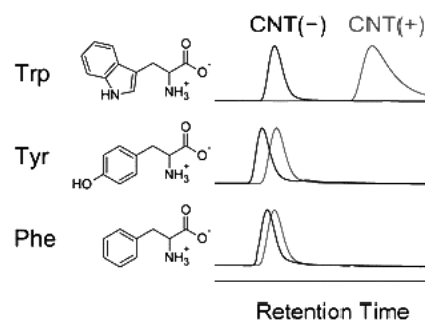


Fig.1: Chromatograms of Trp, Tyr and Phe in the presence and absence of SWCNTs as column ligands.

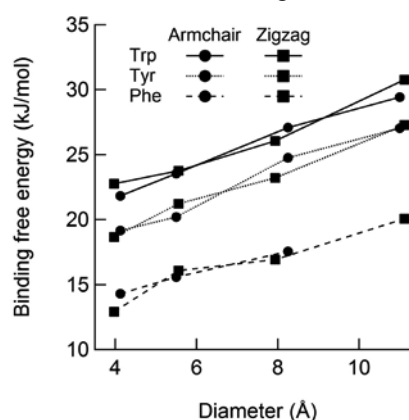


Fig.2: SWCNT-diameter-dependence of the amino acid binding free energy to the SWCNT sidewall.

Synthesis of local phenylboronic acid-modified single-walled carbon nanotubes and its PL behavior

○Hisashi Onitsuka¹, Tomohiro Shiraki^{1,2}, Naotoshi Nakashima^{1,2}

¹*Department of Applied Chemistry, Kyushu University, Fukuoka 819-0395, Japan*

²*WPI-I²CNER, Kyushu University, 744 Motoooka, Fukuoka 819-0395, Japan*

Single-walled carbon nanotubes (SWNTs) emit near-infrared photoluminescence (NIR-PL) that is applicable to advanced optical materials including bio-sensing and imaging applications. Recently, a very small amount of chemical modification on the SWNTs has been reported to enhance their quantum yields dramatically by generation of red-shifted PL (E_{11}^*) compared to PL (E_{11}) of pristine SWNTs [1] and we are elucidating the fundamental properties of the E_{11}^* [2]. Very recently, we reported emergence of new red-shifted SWNT PL based on proximal doped-site design [3].

In this study, we design and synthesized phenylboronic acid-modified SWNTs (BA-SWNTs) and the aqueous dispersion using sodium dodecylbenzenesulfonate (SDBS) showed the E_{11}^* PL at 1138 nm. Interestingly, PL peak shift of the E_{11}^* was observed by adding D-fructose to the BA-SWNTs dispersion. D-glucose also induced similar PL peak shift of the E_{11}^* . However, clear difference between the two sugar was responsiveness to the concentrations of the added sugars, in which D-fructose showed larger peak shift than D-glucose especially at the low concentration region. This spectral change behavior reflects binding constants of phenylboronic acid with sugars (D-fructose: $4370 \text{ M}^{-1} > \text{D-glucose: } 110 \text{ M}^{-1}$) [4]. Therefore, these results strongly support that the observed spectral shift is induced by sugar recognition at the modified site and it induces PL property change of the BA-SWNTs. Moreover, we found that surfactants, which are used as dispersants of SWNTs, can affect sugar recognition on the BA-SWNTs. It indicates that adsorption structures of surfactants on BA-SWNTs can be an important factor of the responsiveness and the sugar recognition behavior would be modified by changing the surfactants. Details in the surfactant effect will be discussed at the symposium.

[1] Y. Wang *et al.*, *Nat. Chem.* **5**, 840 (2013). [2] N. Nakashima *et al.*, *J. Phys. Chem. C*. in press (2015).

[3] N. Nakashima *et al.*, *Sci. Rep.* **6**, 28393 (2016). [4] J. O. Edwards *et al.*, *J. Org. Chem.* **24**, 769 (1959).

Corresponding Author: Naotoshi Nakashima
Tel: +81-92-802-2840, Fax: +81-92-802-2840,
E-mail: nakashima.naotoshi.614@m.kyushu-u.ac.jp

Geometries and electronic properties of MoS₂ nanotube

○Shuntaro Oshima, Masayuki Toyoda, Susumu Saito

Department of Physics, Tokyo Institute of Technology, Meguro-ku, Tokyo 152-8551, Japan

MoS₂ is one of the transition metal dichalcogenides (TMD) with trigonal-prismatic structure [1,2]. Its structure as well as electronic properties has been studied vigorously due to recent experimental realization of various types of atomically-thin layered compounds [3-5]. Contrary to graphene, MoS₂ and other TMD layers are considered to be semiconductors and are attracting attention as future device materials [5,6]. In the present work, we investigate structure and electronic properties of MoS₂ (10,0) single-walled nanotube using local density approximation (LDA) in the framework of density-functional theory.

Prior to the series of studies of MoS₂ nanotube, we have studied bulk MoS₂ with the 2H_b structure and single-layer MoS₂ using LDA. As a result of structural optimization, we have obtained lattice constants of $a = b = 3.14 \text{ \AA}$ for both structures and $c = 12.07 \text{ \AA}$ for the bulk phase. Band structure calculations show direct gap of $E_g = 1.87 \text{ eV}$ at K point and indirect gap of $E_g = 0.74 \text{ eV}$ for monolayer and bulk MoS₂, respectively. Similar trends have been observed in studies of other groups [1,2,7,8].

In the case of the (10,0) nanotube, we obtained $c = 5.25 \text{ \AA}$ for the optimized lattice constant along the tube axis, and 5.74 \AA for the radius of a cylindrical Mo layer. The calculated total energy of this optimized structure is higher than that of single layer structure by 1.2 eV per MoS₂ unit. Band structures for both elongated and shortened (10,0) nanotubes with $c = 5.40 \text{ \AA}$ and 4.60 \AA are calculated, and interestingly the results show metallic gapless properties.

- [1] L. F. Mattheiss, Phys. Rev. B **8**, 3719 (1973).
- [2] R. Coehoorn, C. Haas, J. Dijkstra, C. J. F. Flipse, R. A. de Groot, and A. Wold, Phys. Rev. B **35**, 6195 (1987).
- [3] R. Tenne, L. Margulis, M. Genut, and G. Hodes, Nature **360**, 444 (1992).
- [4] K. S. Novoselov, D. Jiang, F. Schedin, T. J. Booth, V. V. Khotkevich, S. V. Morozov, and A. K. Geim, Proc. Natl. Acad. Sci. U.S.A. **102**, 10451 (2005).
- [5] K. F. Mak, C. Lee, J. Hone, J. Shan, and T. F. Heinz, Phys. Rev. Lett. **105**, 136805 (2010).
- [6] B. Radisavljevic, A. Radenovic, J. Brivio, V. Giacometti, and A. Kis, Nature Nanotechnology **6**, 147 (2011).
- [7] Y. Ding, Y. Wang, J. Ni, L. Shi, S. Shi, W. Tang, Physica B **406**, 2254 (2011).
- [8] W. S. Yun, S. W. Han, S. C. Hong, I. G. Kim, and J. D. Lee, Phys. Rev. B **85**, 033305 (2012).

Corresponding Author: S. Oshima

Tel: +81-3-5734-2703, Fax: +81-3-5734-2739,

E-mail: soshima@stat.phys.titech.ac.jp

Theory of optimized power factor of low-dimensional semiconductors and application to semiconducting carbon nanotubes

○ Nguyen T. Hung, Ahmad R. T. Nugraha, Riichiro Saito
Department of Physics, Tohoku University, Sendai 980-8578, Japan

A good thermoelectric material is characterized by how efficient electricity can be obtained for a given heat source, where two parameters are often evaluated: (1) power factor ($PF = S^2\sigma$, where S is the Seebeck coefficient and σ is the electrical conductivity) and (2) figure-of-merit ($ZT = PF \times T/\kappa$, where T is the average temperature and κ is the thermal conductivity). In applications where the heat source is essentially free of charge (e.g., solar heat), the minimum cost of generating power is achieved by operating at maximum PF [1]. On the other hand, when heat source is expensive (e.g., fossil fuel combustion), obtaining as large ZT as possible is important to reduce the cost of generating power [2]. For obtaining thermoelectric materials having high output power, the PF is a more important parameter rather than ZT [1, 3]. There are many strategies on engineering phonons and electrons to increase ZT over the past two decades [2]. However, enhancement of the PF remains a challenge.

In this work, we theoretically investigate the interplay between the confinement length L and the thermal de Broglie wavelength Λ to optimize the PF. An analytical formula for the PF is derived based on the one-band model assuming non-degenerate and degenerate semiconductors to describe quantum effects on the PF of the low dimensional semiconductors. The PF is enhanced for one- (1D) and two-dimensional (2D) semiconductors when L is smaller than Λ of the semiconductors [Fig. 1]. We apply this theory to semiconducting carbon nanotubes and we find that the PF increases as the tube diameter decreases, which also have the large Seebeck coefficient [5].

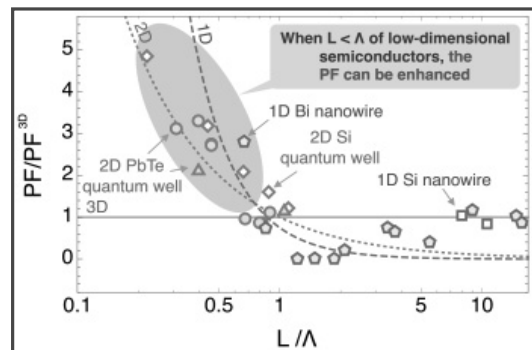


Figure 1 Power factor PF of 1D and 2D systems scaled by power factor of 3D system PF^{3D} as a function of L/Λ ratio of Si, Bi, and PbTe materials. By the PF^{3D} scaling, the PF of different materials can show in the same lines (dashed and dotted lines) for 1D and 2D systems [4].

[1] W. Liu et al., *PNAS* **112**, 3269 (2015).

[2] B. Poudel et al., *Science* **320**, 634 (2008).

[3] W. Liu et al., *Scripta Mater.* **111**, 3 (2016).

[4] N. T. Hung et al., *Phys. Rev. Lett.* in press (2016), arXiv:1604.04353.

[5] N. T. Hung et al., *Phys. Rev. B* **92**, 165426 (2015).

Corresponding Author: Nguyen Tuan Hung

TEL: +81-22-795-6442, FAX: +81-22-795-6447, E-mail: nguyen@flex.phys.tohoku.ac.jp

Effect of internal structure on the electrical performance of MWCNT-Cu wires

○Rajyashree Sundaram¹, Atsuko Sekiguchi^{1,2}, Takeo Yamada^{1,2}, Kenji Hata^{1,2}

¹ *Technology Research Association for Single Wall Carbon Nanotubes (TASC), Central 5, 1-1-1 Higashi, Tsukuba 305-8565, Japan*

² *National Institute of Advanced Industrial Science and Technology (AIST), Central 5, 1-1-1 Higashi, Tsukuba 305-8565, Japan*

Carbon nanotube-copper composites (CNT-Cu), which combine the merits of CNTs and Cu offer many advantages, such as low density, electrical conductivity exceeding Cu at elevated temperatures, high ampacity, metal-like thermal conductivity, and low thermal expansion coefficient [1-3]. Consequently, CNT-Cu can potentially be widely used as a lightweight replacement for Cu. We have previously reported CNT-Cu production as sheets and microfabricated patterns [1-3]. However, there is much demand for CNT-Cu wires from the industry to address the rising need for lightweight conductors in smart fabrics, motor windings, electrical wiring, etc.

Here, we report the electrical properties of multiwalled (MW)CNT-Cu wires fabricated by electrodeposition as a function of internal Cu filling. Our results show that full internal Cu filling throughout the wire-length is essential to maximize the electrical performance of the composite wires.

MWCNT-Cu wires with full internal Cu filling exhibited a combination of (100×) lower resistivity and (3×) higher current carrying capacity than the neat MWCNT wires. These wires also showed lower resistance-change with temperature than Cu and the temperature coefficient of resistance was ½ that of Cu. In comparison, MWCNT-Cu wires with partial and no Cu filling showed inferior electrical properties. Our work indicates that the seamless CNT/Cu structural integration may be crucial to maximize the synergistic contribution from CNTs and Cu to enhance the composite performance.

This presentation is based on results obtained from a project commissioned by the New Energy and Industrial Technology Development Organization (NEDO).

[1] C. Subramaniam *et al.* *Nat. Comm.* **4**, 2202 (2013).

[2] C. Subramaniam *et al.* *Nanoscale* **6(5)**, 2669 (2014).

[3] C. Subramaniam *et al.* *Nanoscale* **8**, 3888 (2016).

Corresponding Author: A. Sekiguchi

Tel: +81-29-861-4551, Fax: +81-29-861-4851

E-mail: atsuko-sekiguchi@aist.go.jp

Measurement of photoinduced force acting on polystyrene microsphere by carbon nanotube mechanical resonator

○Masaaki Yasuda¹, Kuniharu Takei¹, Takayuki Arie¹, Seiji Akita¹

¹ *Department of Physics and Electronics, Osaka Prefecture University, Sakai 599-8531, Japan*

Polystyrene (PS) microspheres are usually used to measure the interaction force between biomolecules with optical tweezers. Although the force acting on the microsphere was estimated from the interaction between the viscous fluid and perfect sphere, it is hard to realize the direct measurements of the optical force which is very small on the order of a few pN or less. Multiwall carbon nanotubes (MWNTs) are one of promising component for nano electro mechanical systems toward minute force sensing [1]. Here, we demonstrate the measurement of photoinduced force on polystyrene sphere by MWNT mechanical resonator.

We fabricated the MWNT - PS sphere composited device as shown in Fig.1 (a) inset. A PS sphere with a diameter of $\sim 3 \mu\text{m}$ was contacted with a very tip of a cantilevered MWNT supported on an Au coated Si substrate under the direct observation of optical microscopy in air. During the contact, a focused laser (power: $>3 \text{ mW}$, spot size: $\sim 1 \mu\text{m}$) beam was irradiated to the MWNT in order to heat the MWNT higher than melting temperature of PS ($\sim 240^\circ\text{C}$). As a result, we successfully welded the target PS sphere to a very tip of the MWNT.

The irradiated laser power dependence of the resonance frequency was measured, where the resonance frequency shift was estimated from the phase change of the resonance characteristic as shown in Fig. 1 (a). Note that the laser was focused on the PS sphere through an x50 objective lens with $\text{NA} = 0.7$ (Fig. 1 (a) inset). Because of the gradient of the laser intensity, the spring constant of the mechanical resonator is modified according to the force gradient induced by the intensity gradient of laser light. Thus, the resonance frequency should be changed by the irradiation of the focused laser beam to the PS sphere. Fig. 1(b) shows the irradiated laser power dependence of the resultant phase change of the fabricated resonator. The phase shift from $1.4 \mu\text{W}$ to $72 \mu\text{W}$ corresponds to $\sim 4 \text{ Hz}$ increase of the resonance frequency, which indicates that $0.1 \mu\text{N/m}$ of the force gradient was acted on PS sphere at $72 \mu\text{W}$. It is well agreed with the theoretical value ($< 0.09 \mu\text{N/m}$ at $72 \mu\text{W}$) of the photon radiation pressure.

Thus, we have successfully measured the gradient force induced by the photon radiation pressure less than $0.1 \mu\text{N/m}$ on the $3 \mu\text{m}$ -diameter PS sphere using the MWNT mechanical resonator.

[1] A. Yoshinaka et al, Appl. Phys. Lett. **98**, 133103 (2011).

Corresponding Author: S. Akita

Tel & Fax: +81-72-254-9261, E-mail: akita@pe.osakafu-u.ac.jp

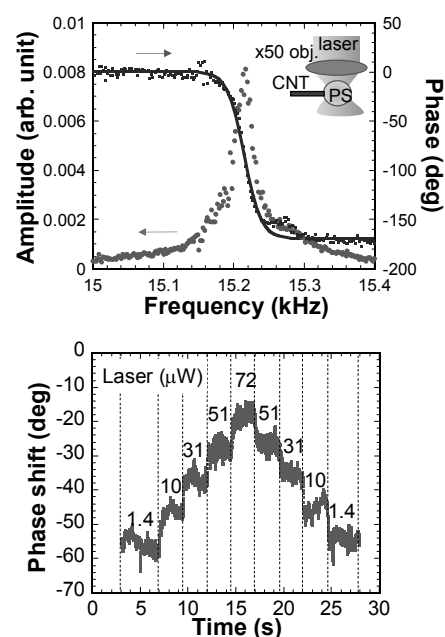


Fig. 1: (a) Drive frequency dependence of the amplitude and the phase of the MWNT mechanical resonator. Inset shows a schematic image of the measurement. (b) Laser power dependence of the phase shift of the resonator.

Photothermoelectric properties of carbon nanotubes terahertz imagers and inspection applications

○Daichi Suzuki^{1,2}, Shunri Oda², Yukio Kawano²

¹ *Research Fellow of Japan Society for the Promotion of Science*

² *QNERC and Dept. of EE, Tokyo institute of Technology, Tokyo 152-8552, Japan*

Imaging and sensing applications based on terahertz (THz) technologies have recently attracted as a powerful tool for non-destructive inspections in a large variety of fields including security, the characterization of organic/inorganic materials, and medical and biological inspection [1]. We previously fabricated a carbon nanotube (CNT) THz detector based on photothermoelectric effect (PTE) and achieved THz detection at room temperature [2][3], but their fabrication process, wet-transfer process, is unsuitable for device integration, hampering practical applications of THz imaging. In this paper, by using a wafer-scale and flexible CNTs film [4], we studied a photothermoelectric properties of integrated THz detector array, and demonstrated inspection applications of THz imaging such as visualizing metals concealed behind opaque objects and a flexible/passive biometric scan of a human hand.

Figure 1 shows the sketch of a CNT THz detector and detected signal under room temperature. The voltage/current signal was generated with THz irradiation via PTE. We then controlled the Fermi level of a CNTs film in order to maximize the Seebeck coefficient, because the sensitivity of PTE is proportional to the Seebeck coefficient. By employing the field-effect techniques, we succeeded in controlling the carrier density of a CNTs film with a few tens micro meter thickness, and in enhancing the THz response. Also we analyzed the thermal conduction in the CNTs film via THz irradiation by both simulation and experiment, enabling us to miniaturize the detector size with keeping its sensitivity.

On the basis of the study about the physical properties of CNTs film, we produced a flexible THz detector array, and demonstrated the inspection applications of THz imaging. We expect that the THz technologies based on the nano-carbon materials will contribute to the field of non-destructive inspections.

We thank ZEON Corporation for giving CNTs film. This work was supported in part by the Japan Science and Technology Agency, MEXT/JSPS KAKENHI Grant Numbers JP26286005, JP16H00798, JP16H00906, JP16J09937, and Support for Tokyotech Advanced Researchers (STAR).

[1] Y. Kawano, *Contemporary Physics*. **54**, 143 (2013).

[2] X. He, *et al.*, *Nano Lett.* **14**, 3953 (2014).

[3] K. J. Erikson, *et al.*, *ACS Nano*. **9**, 11618 (2015).

[4] K. Kobashi, *et al.*, *ACS Appl. Mater. Interfaces*. **5**, 12602 (2013).

Corresponding Author: Y. Kawano

Tel: +81-3-5734-3811, Fax: +81-3-5734-3811,

E-mail: kawano@pe.titech.ac.jp

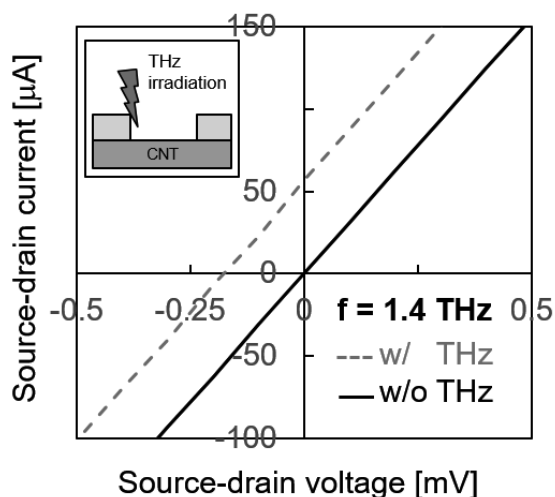


Fig.1: Sketch of THz detector (inset) and detected signal for THz irradiation at 1.4 THz. Voltage/current signal was generated with THz irradiation.

Flexible heater and temperature sensor for temperature range higher than 100 °C using multiwall carbon nanotube

○Daiki Kobayashi, Kuniharu Takei, Takayuki Arie, Seiji Akita

*Department of Physics and Electronics, Osaka Prefecture University,
Sakai, Osaka 599-8531 Japan*

Flexible electronics device is one of emerging fields of recent electronic devices. The research of flexible film heater and thermal sensor can widen possibility of application flexible device. Here, we report on flexible film heaters which can temperature sensing for temperature range higher than 100 °C using multi-wall carbon nanotubes and polyimide film.

The film heater was composed of a sandwich structure of polyimide (PI)-CNT film-PI (total 4.3 μm thick) as shown in Fig. 1, where the PI layers were formed by spin-coating on a Si substrate. Note that multiwall CNT film was formed by spray coating method. Finally, the free standing film heater was obtained by exfoliating the film heater from the substrate.

Figure 2 shows the temperature dependence of electrical resistances measured at heating and cooling process. From the slope, the temperature coefficient of the resistance is ~ 700 ppm/K, which is comparable to that of CNT yarn [1]. One of origins of the temperature dependence is the presence of shallow scattering sites on the current path owing to potential fluctuations. In this case, the scattering probability should decrease at higher temperatures owing to the thermalization of charge carriers. Another possible origin is the decrease in the contact resistance between CNTs. The sheet resistance of our CNT film composite (~ 200 Ω/sq.) is low enough to perform the Joule heating. Here we demonstrate the pressure gauge application based on the heat exchange between the surrounding gases similar to the Pirani gauge. Figure 3 shows gas pressure dependence of the electricity for maintaining the temperature to ~60 °C. The electricity increases with in increasing the surrounding gas pressure, which is most likely due to the heat exchange between the heater and the gas.

Thus, we have successfully fabricated the MWCNT film heater and thermal sensor for temperature range higher than 100 °C through simple fabrication process using spray coating method.

Acknowledgements This work was partially supported by KAKENHI Grant Number 25286010, 16H00920 and 16H06504. **Reference** [1] Y. Wada et al, APEX 9, 085001 (2016). **Corresponding Author:** D.Kobayashi, Tel: +81-72-254-9261, E-mail:kobayashi-4@pe.osakafu-u.ac.jp



Fig. 1 Cross-sectional SEM image of the PI/CNT/PI film sensor/heater.

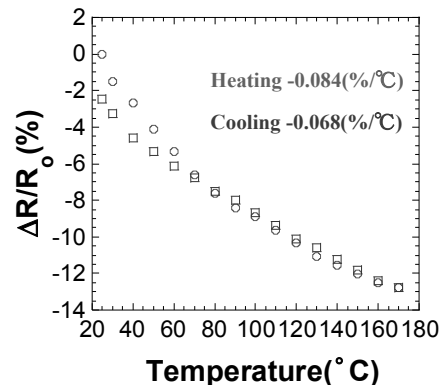


Fig.2 Temperature dependence of the electrical resistance.

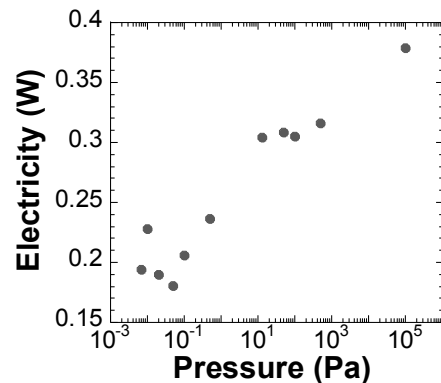


Fig.3 Pressure dependence of the electricity for maintaining the temperature at 60 °C.

Novel method to detect dopamine with high sensitivity based on adsorption onto carbon nanotube surface

○Takuya Ushiyama¹, Shigeru Kishimoto¹, and Yutaka Ohno^{1,2}

¹Graduate School of Engineering, Nagoya University, Nagoya 464-8603, Japan

²Institute of Materials and Systems for Sustainability, Nagoya University, Nagoya 464-8603, Japan

A small amount of neurotransmitters play essential role in brain to convey information from a neuron to neuron. Their unusual concentration, however, causes neuropathies such as Parkinson disease and schizophrenia. Monitoring the concentration of neurotransmitters is helpful to treat patients and to understand the causes of such neuropathies. Carbon nanotube (CNT) is known as an excellent material for electrochemical sensors to detect dopamine (DA), one of important neurotransmitters, because of its electro-catalysis and rapid electron transfer kinetics [1]. Previous electrochemical DA sensors based on CNT have demonstrated the detection of DA in nM regime [2]. In this work, we propose a novel method to detect DA in sub-nM regime on the basis of adsorption of DA onto CNT surface.

We fabricated electrochemical sensors with clean single-walled CNTs on a plastic substrate [3]. After forming a CNT thin film by the dry transfer process based on floating-catalyst CVD [4], the sensor electrodes were fabricated by conventional lithography process. A SiO₂ protection layer was employed to prevent the CNT film from contamination during the fabrication process.

The proposed DA-detection method consists of two steps, that is, the adsorption and detection steps. In the adsorption step, DA is adsorbed onto the CNT surface by applying bias voltage in phosphate buffer saline (PBS) solution containing DA. Here, we applied -0.1 V (vs. Ag/AgCl) to CNT electrode for 600 s. It is known that electrochemically active catechol is adsorbed on activated carbon [5]. After washing CNT electrode by deionized water, the cyclic voltammetry was carried out in 2-M H₂SO₄ solution in the detection step. Figure 1 shows the voltammogram obtained by scanning potential from 0 to 0.5 V (vs. Ag/AgCl). A fine peak corresponding to oxidation current from adsorbing DA was clearly obtained for the 100-pM DA sample (solid line), while no peak was observed for the control sample (dotted line). The result demonstrates higher sensitivity in DA detection than previous reports by factor of 10 [3].

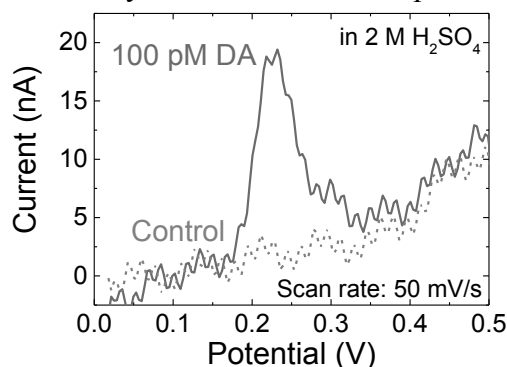


Fig. 1 Voltammogram of DA sample (solid line) and control (dotted line) measured by the novel method.

- [1] C. B. Jacobs *et al.*, *Analyst*, **136**, 3557 (2011)
 [2] Y. Xu *et al.*, *Microchim. Acta*, **182**, 1797 (2015)
 [3] T. Ushiyama *et al.*, *The 50th FNTG General Symp.* 2P-16 (2015)
 [4] A. Kaskela *et al.*, *Nano Lett.*, **10**, 4349 (2010)
 [5] A. S. Kumar *et al.*, *J. Electroanal. Chem.*, **641**, 131 (2010)

Corresponding Author: Y. Ohno
 Phone & Fax: +81-52-789-5387
 E-mail: yohno@nagoya-u.jp

Single-walled carbon nanotube synthesis by alcohol catalytic CVD in high vacuum using Rh catalysts

○Takahiro Maruyama¹, Akinari Kozawa², Takahiro Saida¹, Shigeya Naritsuka²,
Yoko Iizumi,³ Toshiya Okazaki³, Sumio Iijima⁴

¹ *Department of Applied Chemistry, Meijo University, Nagoya 468-8502, Japan*

² *Department of Materials Science and Engineering, Meijo University, Nagoya 468-8502, Japan²*

³ *Nanotube Research Center, National Institute of Advanced Industrial Science and Technology (AIST), Tsukuba 305-8565, Japan*

⁴ *Faculty of Science and Technology, Meijo University, Nagoya 468-8502, Japan*

Single-walled carbon nanotubes (SWCNTs) have been anticipated for applications to electronic devices because of their tremendous electrical properties. To realize SWCNT devices, it is necessary to reduce the growth temperature below 500°C. Previously, we reported SWCNT growth by alcohol catalytic chemical vapor deposition (ACCVD) using Pt catalysts [1]. However, the SWCNT yield from Pt catalysts decreased drastically below 600°C. Recently, theoretical researches showed that there is a low dissociation barrier for ethanol molecules on Rh surface [2]. In this study, we carried out SWCNT growth by a gas source-type ACCVD using Rh catalysts. By controlling the ethanol pressure precisely, we attained SWCNT growth below 500°C.

Rh catalysts were deposited on Al₂O₃/SiO₂/Si substrates using rf sputtering deposition. SWCNT growth was carried out on these substrates using a gas source-type ACCVD system. The grown SWCNTs were characterized using SEM, Raman and photoluminescence.

Fig. 1 shows a SEM image of SWCNTs grown at 460°C. fibrous products were observed on the substrates. Taking into account Raman spectra, these were SWCNTs grown from Rh catalysts and the diameters were distributed between 1.0 and 1.2 nm. Below 600°C, the growth rate decreased with the reduction of the growth temperature, but the SWCNT yield from Rh was higher than that from Pt. The activation energy for SWCNT growth from Rh catalysts estimated from the growth rate was lower than that from Pt, resulting in the higher SWCNT yield in the low temperature region.

This work was partially supported by KAKENHI, a Grant-in-Aid for Challenging Exploratory Research (25600031) from the JSPS and the MEXT Supported Program for the Strategic Research Foundation at Private Universities. Part of this work was conducted at the Institute for Molecular Science (IMS), supported by the “Nanotechnology Platform” of the MEXT.

[1] T. Maruyama *et al.* Carbon **96**, 6 (2016).

[2] J. H. Wang *et al.* J. Phys. Chem. C **113**, 6681 (2009).

Corresponding Author: T. Maruyama

Tel: +81-52-838-2386, Fax: +81-52-832-1179

E-mail: takamaru@meijo-u.ac.jp

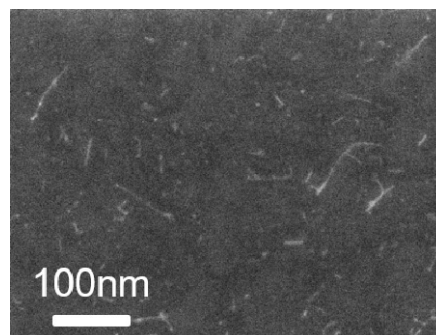


Fig.1: SEM image of SWCNTs grown from Rh catalysts at 460°C.

Combinatorial screening of binary metal catalyst for chirality-selective growth of single-wall carbon nanotubes

○Michiko Edo¹, Hisashi Sugime², and Suguru Noda¹

¹ Department of Applied Chemistry, Waseda University, Tokyo 169-8555, Japan

² Waseda Institute for Advanced Study, Waseda University, Tokyo 169-8050, Japan

Chirality-controlled growth of single-wall carbon nanotubes (SWCNTs) is desired for many applications, especially optoelectronic devices and transistors. Post-growth chirality separation has been extensively studied, however, direct growth of SWCNTs with single chirality is another attractive option. Chirality-controlled growth of SWCNTs was previously reported using cobalt (Co) and tungsten (W) binary catalyst [1]. If both the amount and the composition of the catalyst, chiral selectivity and production yield of SWCNTs will be enhanced further.

In this research, we applied our combinatorial masked deposition (CMD) method [2] to optimize the Co-W catalyst conditions on a single substrate. By placing a physical shadow mask with slit above the substrate during RF sputtering, we changed the nominal thickness of both Co (0.004–1.4 nm) and W (0.006–1.3 nm) by >two orders of magnitude on a 15×15 mm² substrate. Applying this method to *x*- and *y*-axes, we made orthogonal thickness/composition profiles of Co and W on SiO₂(90 nm)/Si substrates (Fig. 1). After annealing them with H₂, we grew SWCNTs via chemical vapor deposition (CVD) by feeding pure ethanol at different pressures (1, 3, 10 Torr) and temperatures (700, 800, 900 and 1000 °C) (total 12 conditions). Each sample was analyzed by Raman spectrum at 10×10 points by automated mapping to roughly search catalyst conditions for narrow chirality distributions, which were then analyzed more carefully using three different wavelengths (488, 514, and 633 nm) to search conditions for single radial breathing mode (RBM) peak.

Fig. 2 shows typical Raman spectra of such careful analysis at nine points with a pitch of 150 μm. In most areas including Area A, multiple RBM peaks were observed (Fig. 2a), whereas an intense RBM peak was observed at 195–197 cm⁻¹ in Area B with 0.47–0.54 nm Co and little W (Fig.2b). According to the Kataura plot [3], it is expected that (12, 6) SWCNTs grew selectively. We will report such analysis for different CVD conditions in the presentation.

[1] F. Yang et al., Nature, 510, 522 (2014).

[2] S. Noda, et al., Carbon 44, 1414 (2006).

[3] H. Kataura, et al, Synthetic Met. 103, 2555 (1999).

Corresponding Author: S. Noda,

Tel&Fax: +81-3-5286-2769, E-mail: noda@waseda.jp

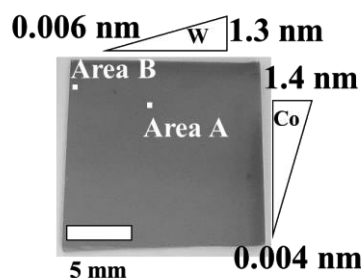


Fig. 1: A combinatorial sample after CVD using 1 Torr ethanol at 900 °C.

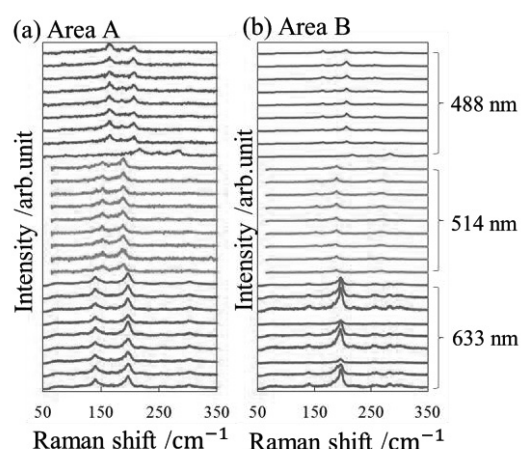


Fig. 2: Raman spectra at Areas A (a) and B (b) in Fig. 1 with three different excitation wavelengths.

Substrate design for high efficiency single walled carbon nanotube synthesis

○Naoyuki Matsumoto¹, Azusa Oshima¹, Sachiko Ishizawa¹, Kenji Hata¹, Don Futaba¹

¹ *CNT-Application Research Center, National Institute of Advanced Industrial Science and Technology (AIST), Tsukuba 305-8565, Japan*

For high efficiency growth for single-walled carbon nanotubes (SWCNTs), immense research has been reported on the ambient, e.g. the hydrocarbon carbon feedstock, additive gases (water and carbon dioxide etc.), plasmas, hot filament, and the substrate-catalyst system, e.g. catalyst buffer materials, porous substrates, alloyed catalysts [1,2]. With the development of the water-assisted (super-growth) method, high yield synthesis for flat substrates could be envisioned [3]. However, uniform source gas delivery to all surfaces of the substrates represents a significant issue in the scaling of uniform height and qualities (SW)CNTs synthesis from flat substrates.

Here, as an alternative to flat substrates, we investigated the use metal (stainless steel) meshes for high efficiency SWCNT synthesis. The (metal) mesh provides a unique substrate structure, which combines both a rounded surface suitable for non-turbulent gas flow, as well as, high surface area compared with a flat substrate. Our results have found the high growth rate synthesis of SWCNT forest with an overall yield surpassing that of flat substrates ($> 4.4 \text{ mg/cm}^2$): long SWCNTs with $\sim 3.0 \text{ mm}$ could be grown in 10 min at the optimum growth conditions (total flow: 1500 sccm, C_2H_2 : 9 sccm, H_2O : 200 sccm, N_2 : 1291 sccm at $775 \text{ }^\circ\text{C}$). Due to the nature of stainless steel meshes, both the diameter and the spacing (open porosity) were used to balance the gas conductance and total surface area on substrate to achieve high efficient SWCNT growths and yields.

Our results showed that although high-speed SWCNT synthesis was possible, abrupt strain-induced growth termination occurred due to the contact between adjacent SWCNT forests. Furthermore, although decrease in spacing was initially expected for higher yield growth, decreased spacing, which caused by CNT growth, led to decreased gas conductance against catalyst on (mesh) substrate and therefore approaching the continuum flat substrate extreme.

This approach demonstrates an alternative to flat substrates as well as rational design of the substrate structure for high efficient (yield) synthesis.

[1] N. Matsumoto *et al.* *Nanomaterials*, **5**, 1200 (2015).

[2] K. Hasegawa *et al.* *ACS Nano*, **2**, 975 (2011).

[3] K. Hata, D. N. Futaba *et al.* *Science*, **306**, 1362 (2004).

Corresponding Author: N. Matsumoto

Tel: +81-29-861-4656, Fax: +81-29-861-4851

E-mail: matsumoto-naoyuki@aist.go.jp

Control of catalyst surface states towards synthesis of single chirality single-walled carbon nanotubes using plasma CVD

○ Bin Xu, Toshiro Kaneko, Toshiaki Kato

Department of Electronic Engineering, Tohoku University, Sendai 980-8579, Japan

Single-walled carbon nanotubes (SWNTs) have many outstanding properties stemming from its unique one dimension structures, which make them as a promising candidate of material for high performance optoelectrical devices. However, as the physical properties of SWNTs strongly depend on the chirality, obtaining specific single chirality SWNTs with high quality is regarded as a critical issue in this scientific community. Recent years, our group has been working on chirality-controlled SWNTs synthesis and we have developed some unique technics towards the growth of narrow chirality-distributed SWNTs using the precise time-controlled synthesis with plasma CVD [1-3], resulting in the controlled synthesis of (6,4) dominant and (6,5) dominant SWNTs (Fig. 1). For the further control of the SWNTs chirality distribution, it is important to elucidate the correlation of catalyst structures and surface states with the chirality species. Based on such background, systematical investigations were carried out aiming for finding out the correlation between catalyst states and chirality distributions for (6,4) dominant and (6,5) dominant samples. The catalyst structures and surface state were analyzed using atomic force microscopy (AFM), X-ray photoelectron spectroscopy (XPS), and transmission electron microscopy (TEM). We find out that there is a clear difference in the catalyst structures between (6,4) dominant and (6,5) dominant SWNTs. Such narrow chirality-distributed SWNTs are very sensitive to the surface state of catalyst, which can be tuned by the appropriate surface treatments. We think that our findings can contribute to the growth of single chirality SWNTs.

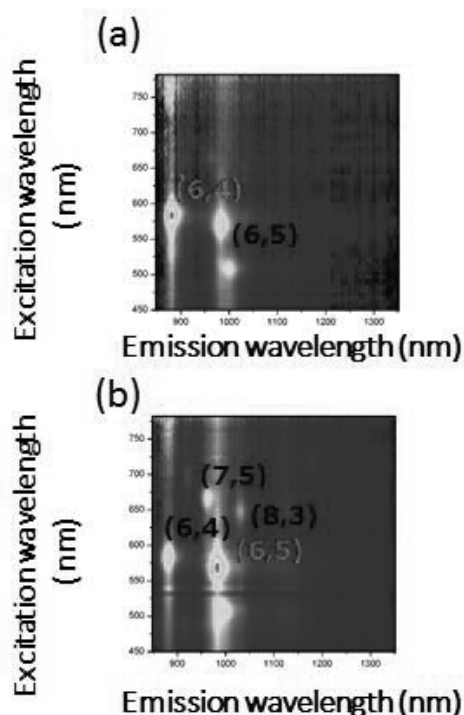


Fig.1: Typical photoluminescence-excitation mapping of (a) (6,4) dominant and (b) (6,5) dominant SWNTs grown by plasma CVD.

[1] Z. Ghorannevis, T. Kato, T. Kaneko, and R. Hatakeyama, *J. Am. Chem. Soc.* **132**, 9570 (2010).

[2] T. Kato and R. Hatakeyama, *ACS Nano* **4**, 7395 (2010).

[3] B. Xu, T. Kato, K. Murakoshi, and T. Kaneko, *J. Plasma Fusion Res.* **9**, 1206075 (2014).

Corresponding Author: B. Xu

Tel: +81-022-795-7046, Fax: +81-022-263-9225

E-mail: xu12@ecei.tohoku.ac.jp

First-principles calculations of electronic states and solid state NMR parameters in alkali halides encapsulated single-walled carbon nanotubes

○Eita Yokokura¹, Yosuke Kataoka¹ and Hironori Ogata^{1,2}

¹ Graduate School of Engineering, Hosei University, Koganei, 184-8584, Japan

² Research Center for Micro-Nano Technology, Hosei University, Koganei, 184-0003, Japan

Single-walled carbon nanotubes (SWNTs) have a hollow space in the nanometer size that can be encapsulated various functional molecules. The confined molecular assemblies may exhibit unique low-dimensional structures and solid state properties that can not be realized in the bulk. Synthesis and structure of alkali halide encapsulated SWNTs have been reported [1-4]. However, the systematic studies of tube diameter dependence, chirality dependence and temperature dependence on the local structures and electronic properties of alkali halides encapsulated in SWNTs have not been reported. In this study, we report the effects of the diameter and chirality of SWNTs on the local structures and electronic properties of the encapsulated alkali halides by using first-principles DFT calculations.

We calculated the band structures and solid ¹³³Cs- or ¹²⁷I-NMR parameters (NMR chemical shift tensors and electric field gradient (EFG) tensors). All of the calculations were done by using a Open-Source computer code package PWscf and GIPAW in Quantum ESPRESSO. We used the pseudo potential methods.

Table 1. shows the chiral vector dependence of ¹³³Cs-NMR chemical shift tensors in CsI@SWNT. Figure 1 shows the band structure and electronic density of states of CsI@(10,10)SWNT.

Detailed results will be presented.

Table 1. ¹³³Cs-NMR chemical shift tensors in CsI@SWNT

Materials	δ_{iso} (ppm)	$\Delta\delta_{anis}=3/2(\delta_{33}-\delta_{iso})$ (ppm)
bulkCsI	0	0
CsI@(6, 6)SWNT	-187.68	786.75
CsI@(8, 8)SWNT	-50.41	591.75
CsI@(9, 9)SWNT	90±5	119±5
CsI@(10, 10)SWNT	9.12	236.75

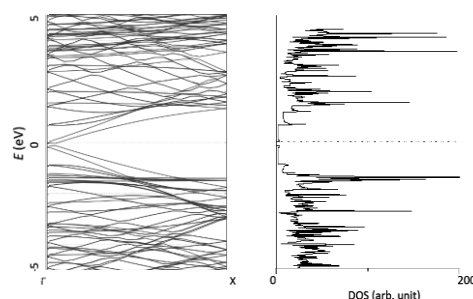


Fig.1 Band structure and DOS of CsI@(10,10)SWNT.

References:

- [1] J. Sloan, M.C. Novotny, *Chem. Phys. Lett.*, **329** (2000)61.
- [2] M. Wilson, P.A. Madden, *J. Am. Chem. Soc.*, **123** (2001)2101.
- [3] Ryosuke Senga, Hannu-Pekka Komsa, Zheng Liu, Kaori Hirose-Takai, Arkady V. Krasheninnikov and Kazu Suenaga, *Nature Materials*, 13(2014)1050.
- [4] ChiYung Yam, ChiChiu Ma, XiuJun Wang and GuanHua Chen . *Appl. Phys. Lett.* 85, 4484 (2004)

Corresponding Author: H. Ogata Tel: +81-42-387-6229, Fax: +81-42-387-6229, E-mail: hogata@hosei.ac.jp

CVD growth of nitrogen doped multilayered graphene by mixing the melamine vapor to methane and their characterization

Takahiro Yoshida¹, Bun Tsuchiya², ○Shunji Bandow¹

*Department of Applied Chemistry, and of General Physics²,
Meijo University, Nagoya 468-8502, Japan*

Several layered (less than 10 layers) graphene was grown on the Cu sheet with a 0.05 mm thick by the chemical vapor deposition of methane including various amounts of melamine vapor. By changing the pressure of melamine vapor, doping amount of nitrogen was controlled in the range of 0 to a few atomic %. Prior to growing the multilayered graphene, Cu sheet was annealed at 1000 °C in one atmospheric pressure of H₂ flow (20 sccm in 30 mm in diameter of quartz tube) for 9 hours. PR gas (10% CH₄ in Ar) was used for the carbon source and the melamine vapor (N source) was controlled at temperature between 150 and 230 °C, corresponding the vapor pressure of 10⁻³ to 1 Torr. Melamine vapor was carried to CVD furnace set at 1000 °C by using a flow of either PR or Ar gas, depending on the mixture ratio of CH₄ and melamine. Additionally a 2 % of H₂ was introduced to CVD furnace during the growth of graphene.

Samples prepared were characterized by the Raman scattering, XPS, RBS, UV-vis, HRTEM and sheet resistivity measurements. By the Raman scattering, we mainly evaluated the sp² bonded carbon network feature from the signals of D, G and G' bands. XPS and RBS were used to determine the doping amount of nitrogen and the chemical bonding nature of N atom. Figure 1 is XPS spectra of samples. From this figure, one can see that the pyridinic N would dominate at higher doping amount of N than that at lower one, where the quaternary (graphitic) N dominates. The number of layers were evaluated by the transmittance of UV-vis at 550 nm and RBS. Sheet resistivity was evaluated at temperatures down to 5 K from RT. Detailed results will be discussed. Here we present some sheet resistivity data in Table 1. It is obvious to see a decrease of sheet resistivity for both N doped m-Gr 1 and m-Gr 2, in which N was quaternary substituted for C.

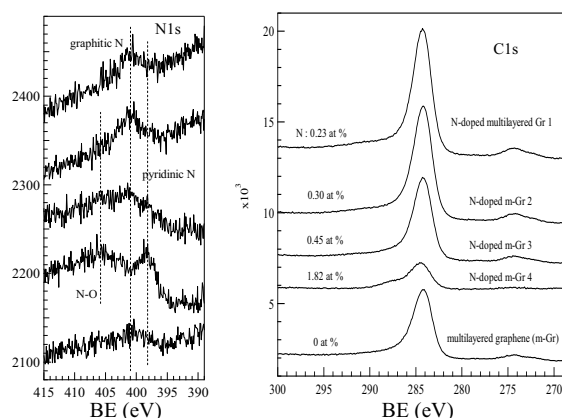


Fig. 1. XPS spectra of N-doped multilayered graphene. Doping amounts of N are indicated with atomic %, which were determined by signal intensity of XPS.

Table 1. Doping amount dependence of N on the sheet resistivity of multilayered graphene at room temperature.

Sample code	Doping amount of N (at%)	Sheet resistivity, Rs (Ω /sq)	Transmittance at 550 nm (%)	Number of layers	Rs / sheet (Ω /sq per sheet)
N doped m-Gr 1	0.23	~2.0 k	81.8	9	~18 k
N doped m-Gr 2	0.30	~2.5 k	85.9	7	~17 k
N doped m-Gr 3	0.45	~67 k	94.5	2	~134 k
m-Gr	0	~14.9 k	89.4	5	~75 k

Corresponding Author: S. Bandow, E-mail: bandow@meijo-u.ac.jp, Tel: +81-52-838-2404

Effect of crystallization of Ni catalyst on low-temperature direct-precipitation of multilayer graphene

○Jumpei Yamada¹, Yuki Ueda¹, Kyosuke Fujiwara¹, Daichi Yamamoto¹,
Takahiro Maruyama², and Shigeya Naritsuka¹

¹*Department of Materials Science and Engineering, Meijo University,
Nagoya 468-8502, Japan*

²*Department of Applied Chemistry, Meijo University, Nagoya 468-8502, Japan*

Because of its outstanding characteristics, graphene is highly expected to apply in a wide range of fields, such as electrical wiring, and transparent electrodes of light emitting diodes (LEDs). In recent years, a direct growth of graphene on a substrate has been studied for the advantages on device applications. We also succeeded in a direct growth of multilayer graphene by precipitation method using W capping layer [1]. In order to avoid a thermal-destruction of devices for the fabrication of opto-electric integrated circuits. It is necessary to lower the process temperature, for example, less than 700 °C. In this study, to directly grow the multilayer graphene at low temperature, the effects of crystallization of Ni catalyst and the cooling rate after growth were studied.

Ni (300 nm) layer was deposited on a sapphire (0001) substrate using electron-beam deposition. After the crystallization of the Ni layer, amorphous carbon (a-C) (1 nm) and W (20 nm) were deposited. Then, the samples were annealed at 700 °C for 30 min in vacuum and cooled with rapid or slow rates.

Fig. 1 shows D/G ratio of Raman spectra of the grown samples, the D/G ratio was successfully decreased by the slow cooling of the Ni crystallization, and it further decreased by the combination of these two processes. The grain size of the graphene was probably increased by the sooth and large-size of grains of the crystallized Ni layer. The small supersaturation during the precipitation by the slow cooling was also beneficial to decrease the density of nucleation. The cause of the quality-improvement of the precipitated graphene will be discussed at the conference site.

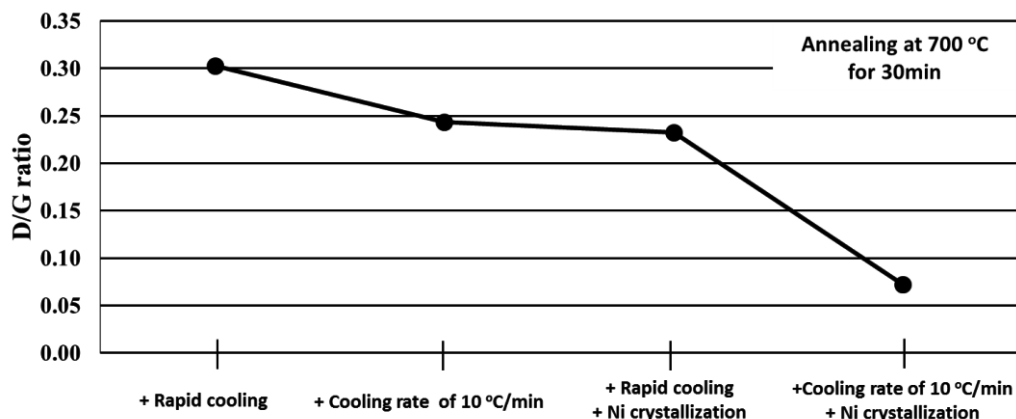


Figure 1. D/G ratio vs. precipitation processes

[1] J. Yamada et al, MRS Fall Meeting & Exhibit, (2015) Q3.69.

Acknowledgement: This work was supported in part by JSPS KAKENHI Grant Numbers 2660089, 15H03558, 26105002, 25000011.

Corresponding Author: J.Yamada, E-mail: jjjjjjyyyyy119@gmail.com

Diffusion of Pt atoms on non-metallic atom-doped graphene support

Syun Hasegawa , Yuji Kunisada , Norihito Sakaguchi

Department of Engineering, Hokkaido University, Sapporo 060-0810, Japan

Introduction Hydrogen is a promising candidate for sustainable energy source. A polymer electrode fuel cell (PEFC) has drawn a great deal of attention because it can generate electricity effectively using hydrogen. It's known that Pt atoms, main catalyst of PEFC, diffuse and aggregate during operation due to weak bonding between Pt atom and carbon support, which causes catalyst degradation. Recently, it has been reported that non-metallic atoms, such as N and B, doped graphene support prevents such diffusion and agglomeration.[1] In this study, we investigate diffusion behaviors of Pt atoms on non-metallic atom-doped graphene support using first principle calculation based on density functional theory (DFT).

Methods DFT calculations were performed using the Vienna ab initio Simulation Package (VASP). A graphene 4×4 supercell with periodic boundary conditions was used. The Pt / graphene systems were separated from their periodic images in the perpendicular direction to a graphene sheet with vacuum space of 15 Å. Non-metallic atom-doped graphene was modeled substituting one carbon atom in graphene with one non-metallic atom, i.e. B, N, Si, P and S.

Results Fig.1 shows the calculated adsorption energy of Pt atoms on non-metallic atom-doped graphene. Fig.2 shows the calculated diffusion barrier of Pt atom on non-metallic atom-doped graphene. Fig.1 and Fig.2 indicate that S, P, Si doped graphene support bonds to Pt atoms more strongly and prevent Pt diffusion more effectively than pristine graphene. These results suggest that S, P, Si doped graphene is promising PEFC support.

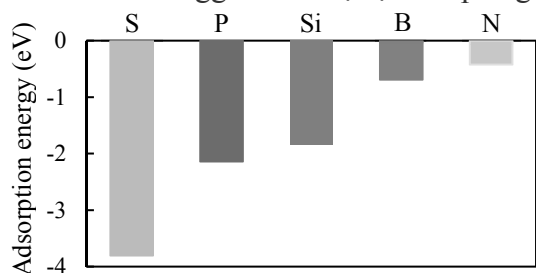


Fig.1 Adsorption energy of Pt atom at the most stable adsorption site on non-metallic atoms doped graphene. The origin of adsorption energy is set to the adsorption energy of Pt atom on pristine graphene.

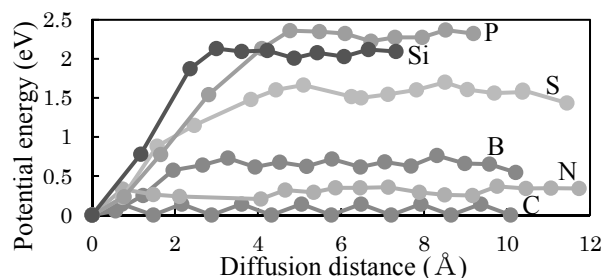


Fig.2 Potential energy change with diffusion of Pt atom on non-metallic atom-doped graphene. The origin of potential energy is set to the energy which Pt atom adsorbs on the most stable site.

[1] L.-S. Zhang, X.-Q. Liang, W.-G. Song, Z.-Y. Wu. Phys. Chem. Chem. Phys. **12**, 12055 (2010).

Corresponding Author: N. Sakaguchi

Tel: 011-706-6768 E-mail: sakaguchi(a)eng.hokudai.ac.jp

Electrochemical characteristics of enzyme/graphene electrodes

○Noritoshi Nakagawa, Kouhei Yanai, Masahiro Hirano, Shinji Koh

*Department of Electrical Engineering and Electronics,
Aoyama Gakuin University, Sagamihara 252-5258, Japan*

Graphene is attractive as electrode materials for biofuel cells because of its high electrical conductivity and chemical stability. The enzyme electrode with high current density and excellent reproducibility can be fabricated by utilizing two-dimensional structure of graphene with a large specific surface area and high uniformity. Stable immobilization of the enzyme is important in applications of enzyme-based biofuel cells. To our knowledge, there are few reports on evaluation of the electrochemical characteristics of enzyme-immobilized graphene planer sheets prepared by chemical vapor deposition (CVD). We focus on CVD-grown graphene sheets as electrode materials for biofuel cells because they are highly uniform, and the shape and size can be accurately controlled by conventional photolithography processes. In this study, we immobilized enzyme on CVD-grown graphene sheets by physical adsorption and evaluated electrochemical characteristics of the enzyme/graphene electrodes.

Graphene sheets were grown by CVD on Cu foil. To evaluate the intrinsic electrochemical characteristics, the graphene sheets were transferred onto electrochemically inert SiO_2/Si substrates by a using polymethyl methacrylate (PMMA) method. The transferred graphene sheets were confirmed to be monolayer by Raman spectroscopy. We immobilized an enzyme, glucose oxidase (GOx), in two ways. One was the easiest procedure, deposition adsorption, in which the graphene sheets were soaked for 12 h in GOx solution [1]. The GOx/graphene electrodes were covered by cellulose membranes to prevent desorption of GOx. The other procedure used noncovalent functionalization of the graphene surface. 1-pyrenebutanoic acid succinimidyl ester (PBSE) was used as a chemical linker on graphene [2]. The pyrenyl group of PBSE interacts strongly with the graphene surface by π -stacking and the succinimidyl ester parts combine with the amino base of GOx. The graphene sheets were soaked in 1 mM PBSE in pure methanol for 3 h followed by soaking in GOx solution for 12 h. Electrochemical characteristics of these electrodes were evaluated by cyclic voltammetry (CV) at a scan rate of 10 mV/s in phosphate buffered saline (PBS:pH 7.0) containing glucose of 25 mM.

Fig. 1 shows the cyclic voltammograms recorded using graphene (dotted line), GOx/graphene (dashed line), and GOx/PBSE/graphene (straight line) electrodes. GOx catalyzes the oxidation reaction of glucose and current due to the oxidation reaction is generated by the addition of glucose. As shown in Fig. 1, the current responses were clearly observed for two enzyme-immobilized electrodes, in which the current density of the GOx/PBSE/graphene electrode had twice as high as that of the GOx/graphene electrode. The result suggested that the immobilization of the enzyme using PBSE formed strong connectivity between graphene and the enzyme, leading to a higher current density.

[1] A. Zebra *et al.*, nature communications. **2**, 370 (2006).

[2] R. J. Chen *et al.*, J. Am. Chem. Soc., **123**, 3838 (2001).

Corresponding Author: Shinji Koh

Tel: +81-42-759-6251, Fax: +81-42-759-6251,

E-mail: koh@ee.aoyama.ac.jp

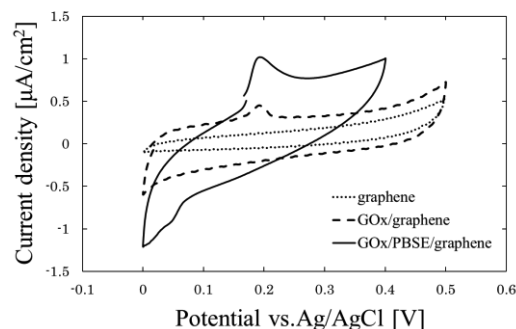


Fig.1: Cyclic voltammograms for 3 electrodes

Electrochemical properties of CVD-grown monolayer graphene oxidized by UV/O₃ treatment

○Kouhei Yanai, Noritoshi Nakagawa, and Shinji Koh

*Department of Electrical Engineering and Electronics,
Aoyama Gakuin University, Sagamihara, 252-5258, Japan*

Electrochemical properties of chemical vapor deposition (CVD) grown monolayer graphene electrodes oxidized by ultraviolet (UV)/ozone (O₃) treatment were studied. Graphene has attracted considerable attention as electrode materials for fuel cells and capacitors due to its high electrical conductivity, chemical and mechanical stability, and high specific surface area. Defects involving edge planes and the oxygen-containing functional groups such as hydroxyl, carboxyl and epoxide groups are key factors that determine electrochemical properties of graphene [1]. This work investigated electrochemical properties of CVD-grown monolayer graphene sheets, in which defects were introduced using UV/O₃ treatment, focusing on its application to electrodes for fuel cells.

Graphene sheets were prepared by CVD on copper foils and transferred onto SiO₂/Si substrates *via* a poly-methyl methacrylate (PMMA) assisted transfer method. Graphene sheets were oxidized by UV/O₃ treatment at room temperature. The presence of defects after oxidization was verified by Raman spectroscopy. The electrochemical properties were evaluated by cyclic voltammetry. We used a hexa-ammine-ruthenium (III) solution containing potassium chloride as a supporting electrolyte, which was degassed with oxygen-free nitrogen. The reaction rate constants k^0 , which allow to categorize reaction rate of graphene electrodes as reversible, quasi-reversible or irreversible systems, were estimated as a functional of redox peak separations ΔE_p from cyclic voltammograms using Nicholson's theorem [2].

Figure 1 shows cyclic voltammograms and Raman spectra of the pristine graphene, 2 min and 9 min UV/O₃ treated graphene. The redox peak separations ΔE_p were 194 mV, 88 mV and 270 mV, respectively. The intensity of D band as shown in the inset of Fig.1, which is ascribed to the structural defects, increased in proportion to the UV/O₃ treatment time. The results showed that 2 min UV/O₃ treatment led to a small ΔE_p , and on the other hands, 9 min treatment increased ΔE_p . The reaction rate constant k^0 of the graphene electrode after 2 min treatment was estimated to be 9.4×10^{-3} cm/s, which was quite close to reversible systems ($k^0 > 10^{-2}$ cm/s) such as platinum electrodes. The electrochemical property was improved due to the edge planes on the graphene surface induced by oxidization. The results suggested that the UV/O₃ treated graphene electrodes have potential for applications to electrodes of fuel cells.

[1] W. Song et al., *Phys. Chem. Chem. Phys.*, **15**, 4799 (2013).

[2] D. Brownson et al., *Nanoscale*, **6**, 1607 (2014).

Corresponding Author: Shinji Koh

Tel: +81-42-759-6251, Fax: +81-42-759-6251,

E-mail: koh@ee.aoyama.ac.jp

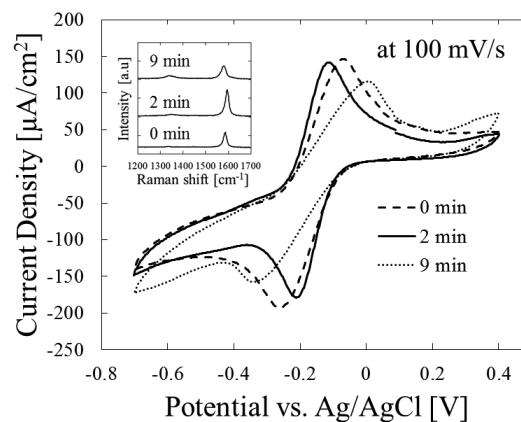


Fig.1 cyclic voltammograms of UV/O₃-treated graphene sheets. Inset shows Raman spectra.

The effect of graphene on growth and viability of bacteria and yeast

○Kyohei Mizobuchi¹, Noritoshi Nakagawa², Masahiro Hirano²,
Fumiyoshi Abe¹, Shinji Koh²

¹ Department of Chemistry and Biological Science,

² Department of Electrical Engineering and Electronics,
Aoyama Gakuin University, Sagamihara 252-5258, Japan

Graphene has attracted much attention for biotechnological applications, such as biosensors and biofuel cells. A significant issue for implementation of these applications is to understand the possible interactions of biological components and living organisms with graphene [1]. Antibacterial activity of graphene oxide [2] and graphene films [3] and toxicity of graphene-related materials [4,5] have been reported. However, the understanding of bio-compatibility and bio-affinity of graphene and its derivatives is still insufficient. In this study, we investigated the occurrence and significance of graphene sheets or powders on growth and viability of gram-negative bacterium *Escherichia coli*, gram-positive bacterium *Bacillus subtilis* and yeast *Saccharomyces cerevisiae*.

Graphene powder, graphene oxide (GO), graphene oxide treated with K_2CO_3 (GO-base) and reduced graphene oxide (rGO) were thoroughly washed with MilliQ water and autoclaved prior to use. Cells of individual species were cultured in growth media with shaking in the presence (800 $\mu\text{g/mL}$) or absence of the graphene derivatives for overnight. Then, small aliquots of the cultures were spread on plates to form colonies for counting. We found that the graphene powder increased the final cell density twofold in *E. coli* while other graphene derivatives slightly reduced it. There was no significant effect of the graphenes on the final cell density in *B. subtilis* and *S. cerevisiae* (Fig. 1). The result suggests that the graphenes do not have an adverse effect on growth and viability of the three microbial species as far as tested under the given conditions.

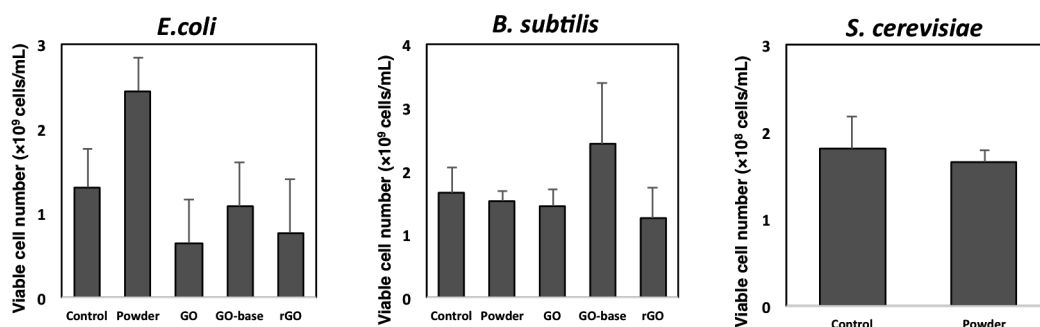


Fig. 1. The effect of graphenes on microbial cell growth

- [1] K. Kostarelos and K. Novoselov, *Science* 344, 261 (2014).
 [2] W. Hu et al, *ACS Nano* 4, 4317 (2010).
 [3] J. Li et al, *Sci. Rep.* 4, 4359 (2014).
 [4] V.C. Sanchez et al, *Chem. Res. Toxicol.* 25, 15 (2012).
 [5] S. Gurunathan and J.H. Kim, *Int. J. Nanomedicine*, 11, 1927 (2016).

Corresponding Author: Shinji Koh

Tel: +81-42-759-6251, Fax: +81-42-759-6251,

E-mail: koh@ee.aoyama.ac.jp

Edge-disorder effect on I_d - V_g characteristics of GNR-FETs

○Kengo Takashima¹, Takahiro Yamamoto^{1,2}

¹ *Department of Engineering, Tokyo University of Science, Tokyo 125-8585, Japan*

² *Department of Liberal Arts, Tokyo University of Science, Tokyo 125-8585, Japan*

Graphene is expected to be a channel material of field effect transistors (FETs) because of its high carrier mobility. However, no band gap of the graphene is a serious problem for its FET application. One possible way to overcome the gap-opening problem is to process it in the form of a nanometer width ribbon, referred as graphene nanoribbons (GNRs). They have been successfully applied to FETs with high on-off ratio. We recently reported that resistance of GNR increase dramatically with edge disorder [1][2]. However, the edge-disorder effect on the GNR-FET properties has not been clarified yet.

In this study, we have theoretically investigated the influence of edge-disorder on I_d - V_g characteristics (I_d : drain current, V_g : gate voltage) of GNR-FETs using the nonequilibrium Green's function method combined with a tight-binding model [3]. In our simulation, edge-disordered armchair GNRs (AGNR) were used as channel materials of FETs, and the edge vacancies were modeled by adding or removing pairs of carbon atoms at the edges (Fig. 1). We have calculated I_d - V_g characteristics of 2.21nm width AGNR-FETs by changing the roughness concentration P from 0% to 30% (Fig. 2). We found that a variance of on current (ΔI_{on}) is independent of I_{on} and ΔI_{on} is constant (universal conductance fluctuation), where P is under 10 %. On the other hand, when P exceeds 10 %, ΔI_{on} and variance of subthreshold become large drastically.

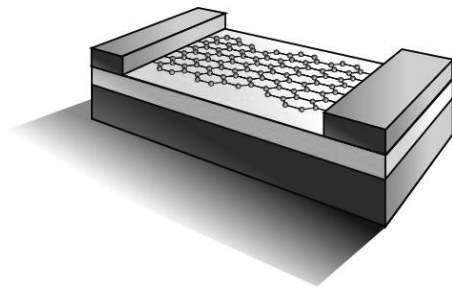


Fig. 1 Edge-disordered AGNR-FET

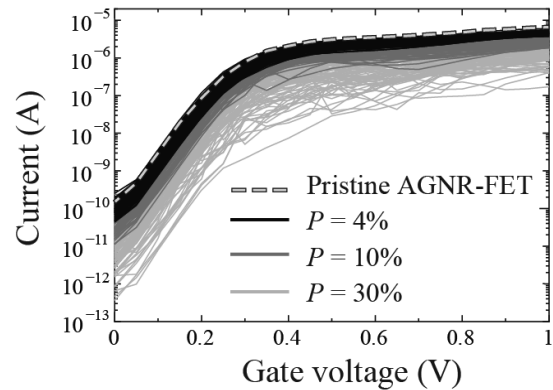


Fig. 2 I_d - V_g curves of edge-disordered AGNR-FETs

References:

- [1] K. Takashima and T. Yamamoto, *APL.*, **104**, 093105 (2014).
- [2] K. Takashima, S. Konabe and T. Yamamoto, *JAP.*, **119**, 024301 (2016).
- [3] P. Koskinen and V. Mäkinen, *Computational Materials Science*, **47**, 237 (2009)

Corresponding Author: T. Yamamoto

E-mail: takahiro@rs.tus.ac.jp

Effect of metal nanoparticles on carrier accumulation in graphene under an electric field

Manaho Matsubara and Susumu Okada

*Graduate School of Pure & Applied Sciences, University of Tsukuba, Tsukuba 305-8571
Japan*

Graphene has been keeping a premier position not only in the field of the low-dimensional sciences but also in the electronic device engineering due to its unique structural and electronic properties. For the fundamental and applied sciences of graphene, it is mandatory to precisely control their electronic structure by external conditions. In particular, the band gap engineering and the Fermi level tuning are highly important. In usual situations, graphene inherently possesses hybrid structure with foreign materials, such as insulating substrate and atoms/molecules. Under such hybrid structures, the microscopic mechanism of the carrier injection into graphene is not fully elucidated yet. Thus, in the present work, we aim to give theoretical insight into the electronic properties of graphene hybrids, which consist of graphene and Al nanoparticles, under the external electric field, using the density functional theory combined with effective screening medium method. To simulate the graphene hybrid under the electric field, we consider a structural model shown in Fig. 1, in which an Al nanoparticle (Al_4) is physically adsorbed on graphene with the optimum spacing as a charged impurity.

Our calculations show that the E_F is located above the Dirac cone, because of the electron transfer from Al nanoparticle to graphene. The characteristic electronic structure indicates that the electrons injected by the electric field is not accumulated into graphene but accommodated into the Al nanoparticle. However, by investigating the distribution of the accumulated electrons under the electric field, we find that the distribution depends on relative arrangement of the gate electrode to the Al nanoparticle (Fig. 2).

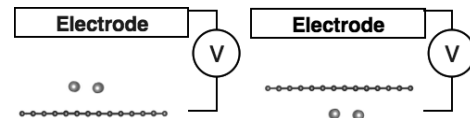


Fig.1: Structural models of graphene adsorbing Al_4 with top (left) and bottom (right) gate electrodes.

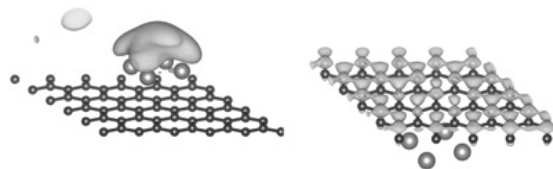


Fig. 2: Isosurfaces of accumulated carriers of graphene adsorbing Al_4 with the top (left) and bottom (right) gate electrodes.

Corresponding author: M. Matsubara

Email: mmatsubara@comas.frsc.tsukuba.ac.jp

Probing interface strain in graphene and boron nitride in-plane heterostructures

○Shintaro Yoshimura¹, Yu Kobayashi¹, Shun Ogawa¹, Shogo Sasaki¹, Yutaka Maniwa¹, Yasumitsu Miyata^{1,2}

¹*Department of Physics, Tokyo Metropolitan University, Hachioji, 192-0397, Japan*

²*JST, PRESTO, Kawaguchi, 332-0012, Japan*

Graphene and hexagonal boron nitride (hBN) in-plane heterostructures have attracted much attention due to their unique physical properties and applications for atomically thin circuitry [1,2]. Because of the presence of lattice mismatch of around 2% between graphene and hBN, the heterostructures should have lattice strain around interface. However, such interface strain has never been observed so far, in spite of its impact on interface properties. To probe the interface strain, we have focused our attention on the Raman spectra of graphene. In particular, it is known that the defect-induced Raman mode (D mode) is selectively enhanced at the edges of graphene grains due to the double resonance processes [3]. For this reason, we can expect that the D mode can be used to probe the structural and electrical properties at the interfaces of graphene-based lateral heterostructures. In this work, we have investigated the interface strain of graphene and hBN in-plane heterostructures by using Raman spectroscopy.

To prepare the in-plane heterostructures, graphene grains were firstly grown on Cu foil by chemical vapor deposition (CVD) with methane, and then, hBN was grown from the graphene edges by CVD of ammonia borane (Fig.1a), as reported in our previous study [1]. The samples were transferred from Cu foil to SiO₂/Si substrates for Raman measurement (Fig. 1b). In Raman spectra (Fig. 1c), we found that the edge and bulk of graphene before hBN growth have almost the same peak positions of D mode. In contrast, only the D-mode of G/hBN interface shows downshift of 6~8 cm⁻¹. This D mode downshift suggests the presence of tensile strain at the heterointerface. In the presentation, the details of the changes in Raman spectra and origin of D mode softening will be discussed.

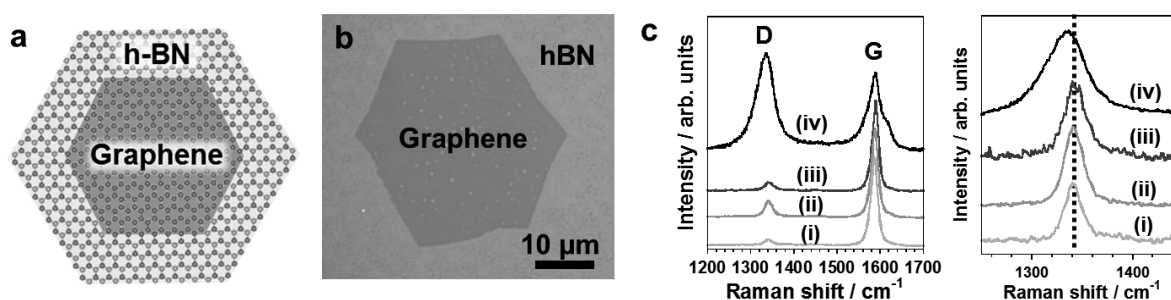


Fig. 1 (a) Structure modal and (b) optical image of CVD-grown graphene/hBN in-plane heterostructure. (c) Normalized Raman spectra of (i) bulk and (ii) edge of graphene before hBN growth, (iii) bulk and (iv) edge of graphene after hBN growth.

[1] Y. Miyata *et al.*, Appl. Phys. Express 5, 085102 (2012), [2] M. Levendorf *et al.*, Nature 488, 627 (2012).

[3] C. Casiraghi *et al.*, Nano Lett. 9, 1433 (2009)

Corresponding Author: Yasumitsu Miyata, Tel: +81-42-677-2508, E-mail: ymiyata@tmu.ac.jp

Polarity and magnetism of rippled graphene with topological defect

○Mina Maruyama and Susumu Okada

Graduate School of Pure and Applied Sciences, University of Tsukuba, Tsukuba 305-8571, Japan

Surfaces and edges of binary compounds induce polarization at or around these imperfections caused by the imbalance of the charge neutrality among constituent elements and the lack of translational symmetry [1,2]. In addition, recently, we demonstrated that the mono-elemental materials, such as graphene and fullerenes, inherently exhibit polarization because of the inhomogeneous charge density of their covalent bonds arising from bond alternation, although they do not possess edges or surfaces. Fullerenes with asymmetric cages possess dipole moment along particular direction depending on the arrangement of 12 pentagonal rings on the cage [3]. The fact indicates that the topological defect on graphene is expected to induce polarization around them. In this work, we aim to investigate geometric and electronic properties of rippled graphene with topological defects using the density functional theory, combined with the effective screening medium method.

Figure 1 shows the structural model of rippled graphene with topological defects which consist of fused pentagons and heptagons. Under the equilibrium lateral lattice constant of 0.87 nm, the sheet is a metal with flat dispersion bands near the E_F leading to the spin polarization with the moment of $1.52 \mu_B/\text{nm}^2$. In addition to the spin polarization, the sheet exhibits electric polarization normal to the sheet with the potential difference of 0.19 V under the equilibrium lattice corresponding to the dipole moment of $0.84 \text{ D}/\text{nm}^2$ (Fig.2). Therefore, the rippled graphene with topological defects possesses both magnetic and electric polarization. We further investigate the stability of the polar properties of the sheet under the biaxial strain. By increasing the lateral lattice parameters, the dipole moment monotonically decreases, while the magnetic moment is insensitive to the strain keeping its value irrespective of the strain except the structure with dangling bonds.

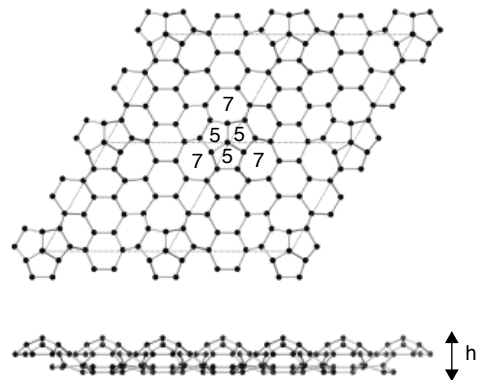


Fig.1: Top and side view of optimized structure of rippled graphene at $a = 8.7 \text{ \AA}$.

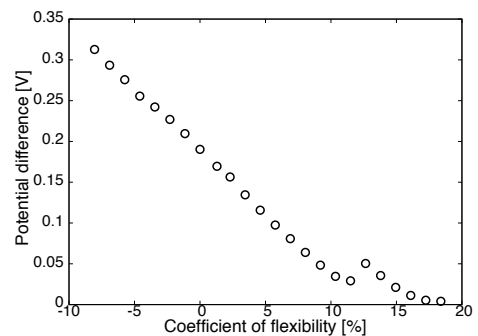


Fig.2: Potential difference of rippled graphene as a function coefficient of flexibility.

References

- [1] A. Yamanaka and, S. Okada, *Carbon* **96**, 351 (2015).
- [2] A. Yamanaka and, S. Okada, in *Abstracts of 50th FNTG symposium*, p. 32 (2016).
- [3] J. Sorimachi and S. Okada, *Chem. Phys. Lett.* **659**, 1 (2016).

Corresponding Author: M. Maruyama

Tel: +81-29-853-5921, Fax: +81-29-853-5924,

E-mail: mmaruyama@comas.frsc.tsukuba.ac.jp

Valley polarization mapping in transition metal dichalcogenides heterostructures

○Yusuke Hasegawa¹, Shinichiro Mouri¹, Kazunari Matsuda¹ and Yuhei Miyauchi¹

¹*Institute of Advanced Energy, Kyoto University, Uji, Kyoto 611-0011, Japan*

Recently, optoelectronic technology relying on valley degree of freedom of electrons, called valleytronics, has attracted increasing attention for developing low energy consumption and high speed optoelectronic devices. One of the possible candidate materials is monolayers of transition metal dichalcogenides (1L-TMDs) such as MoS₂ and WSe₂ [1-3]. These 1L-TMDs are atomic layered materials with hexagonal crystal structures similar to graphene, but semiconductors with finite direct band-gaps. In addition, broken inversion symmetry and strong spin-orbit interaction in these materials enable valley-selective excitation (K or K') in momentum space using circularly polarized light [1,2]. Since the first demonstrations on the optical generation of the valley polarization [1,2], there have been intensive studies on the valley-polarized states in 1L-TMDs. However, it has still remained unclear how the valley polarization properties are affected by various local conditions such as interactions with other 1L-TMDs, inhomogeneous carrier density, local strain, and lattice defects.

Here we examine the effects of the interactions between two different 1L-TMDs artificially stacked with each other (heterostructures) on the valley polarization properties. Various TMDs heterostructures were prepared and photoluminescence (PL) spectra and valley polarization degrees were measured as a function of spatial coordinates using a home-built optical system under excitation photon energy of 1.96 eV.

Figure 1 shows the Atomic Force Microscope (AFM) image and the PL intensity map of 1L-WSe₂ and WSe₂/MoTe₂ at 15 K. The PL intensities of the WSe₂/MoTe₂ heterostructure are lower than 1L-WSe₂ on the SiO₂/Si substrate. This result implies interlayer energy transfer from WSe₂ to MoTe₂, because WSe₂/MoTe₂ is a heterostructure with a straddling gap (type I). We will show the results for various TMDs heterostructures and the spatial dependence of the observed valley polarization under low temperature conditions. The correlations between the local conditions indicated by the PL spectra and the morphologies observed by optical microscope and AFM will be also discussed.

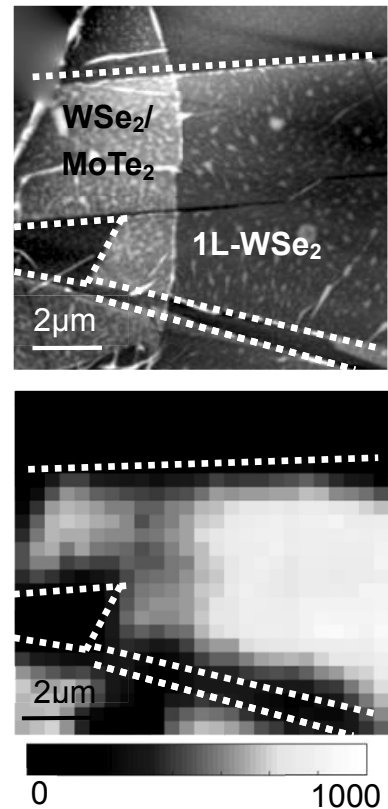


Fig.1 AFM image (top) and PL intensity map (bottom) of 1L-WSe₂ and WSe₂/MoTe₂ (hetero) at 15 K. PL intensities were integrated for the photon energies of 1.74-1.75 eV (exciton PL). White dotted lines indicate the edges of these materials.

- [1] K. F. Mak *et al.*, *Nat. Nanotechnol.* **7**, 494 (2012).
 [2] H. Zeng *et al.*, *Nat. Nanotechnol.* **7**, 490 (2012).
 [3] S. Mouri, Y. Miyauchi, K. Matsuda, *Nano Lett.* **13**, 5944 (2013).
 Corresponding Author: Y. Miyauchi
 Tel/Fax: +81-774-38-3465/+81-774-38-4567
 E-mail: miyauchi@iae.kyoto-u.ac.jp

Photoluminescence properties of monolayer MoS₂ FETs fabricated by dry-transfer process

○Xiaofan Wang, Yuhei Miyauchi, Kazunari Matsuda

Institute of Advanced Energy, Kyoto University, Uji, Kyoto 611-0011, Japan

Recently, transition metal dichalcogenides (TMDs) have attracted much attention as novel two-dimensional semiconductors. These materials are also promising candidate for the future optical and electronic devices, which opens the new research fields [1,2]. The field effect transistors (FETs) fabricated by monolayer TMDs have shown significant potential for enabling new electronic applications [3]. The typical TMD FETs reported to date have been fabricated using conventional electron-beam or photo-lithography technique followed by multiple wet processes. The fabricated TMDs FET with wet process using the polymer may affect the device performance and optical properties [4]. As an alternative method, the multilayer MoS₂ FET fabricated by the dry transfer process has been reported [5].

In this work, we investigated the device performance and optical properties of monolayer MoS₂ FET fabricated by using dry-transfer process. Figure 1(a) shows the optical image of MoS₂ FET fabricated by dry-transfer process. The monolayer FET was annealed in high vacuum condition to improve the contact between the monolayer MoS₂ and the electrode. The inset shows photoluminescence (PL) spectrum of monolayer MoS₂ in this FET device. The PL spectrum shows the A peak at 1.86 eV, composed of exciton and charged exciton emission. Figure 1(b) shows the source-drain current (I_{DS}) as a function of source-drain voltage (V_{DS}) with varying the gate-voltage (V_G). The I_{DS} is clearly modulated by V_G , which shows the characteristic behavior of FET operation. We will discuss the detail device performance and PL properties of monolayer TMDs fabricated by the dry-transfer process.

- [1] Q. H. Wang *et.al.*, Nat. Nanotechnol. **7**, 699 (2012).
- [2] S. Mouri *et.al.*, Nano Lett. **14**, 5944 (2013).
- [3] B. Radisavljevic *et.al.*, Nat. Nanotechnol. **6**, 147(2011).
- [4] A. G. F. Garcia *et.al.*, Nano Lett. **12**, 4449 (2012).
- [5] Rui Yang *et.al.*, J. Vac. Sci. Tech. B **32**, 061203 (2014).

Corresponding Author: Kazunari Matsuda
 Tel/Fax: +81-774-38-3460
 E-mail: matsuda@iae.kyoto-u.ac.jp

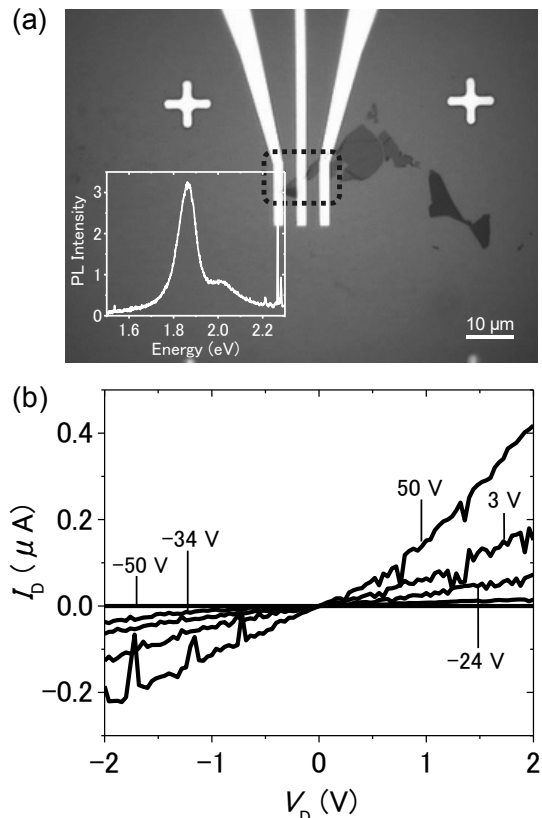


Fig.1 (a) Optical microscope images of device. (b) I_{DS} as a function of V_{DS} of device after 350°C annealing.

Growth and characterization of monolayer $\text{Mo}_{1-x}\text{Re}_x\text{S}_2$ alloys

○Shohei Mori¹, Shogo Sasaki¹, Yu Kobayashi¹, Liu Zheng^{2,3}, Shoji Yoshida⁴, Takahiro Takeuchi⁴, Hidemi Shigekawa⁴, Kazutomo Suenaga³, Yutaka Maniwa¹, Yasumitsu Miyata^{1,5}

¹*Department of Physics, Tokyo Metropolitan University, Hachioji, 192-0397, Japan*

²*Inorganic Functional Materials Research Institute, AIST, Nagoya, 463-8560, Japan*

³*Nanomaterials Research Institute, AIST, Tsukuba, 305-8565, Japan*

⁴*Faculty of Pure and Applied Sciences, University of Tsukuba, Tsukuba 305-8573, Japan*

⁵*JST, PRESTO, Kawaguchi, 332-0012, Japan*

Atomic layers of transition metal dichalcogenides (TMDCs) have attracted much attention because of their unique physical properties and potential applications. To control their electronic properties such as bandgap and carrier concentration, many research groups have studied the growth of TMDC-based alloys so far. In our previous studies, we have also reported the growth and characterization of $\text{Mo}_{1-x}\text{W}_x\text{S}_2$, $\text{Nb}_{1-x}\text{W}_x\text{S}_2$, and $\text{Mo}_{1-x}\text{Re}_x\text{S}_2$ monolayers [1-4]. In this study, we have investigated the structure and electronic properties of $\text{Mo}_{1-x}\text{Re}_x\text{S}_2$ monolayers by using the combination of electron microscopy and scanning tunneling microscopy/spectroscopy (STM/STS).

Monolayer $\text{Mo}_{1-x}\text{Re}_x\text{S}_2$ alloys were formed on graphite and quartz substrates by chemical vapor deposition (CVD) of sulfur, molybdenum oxide, and rhenium oxide. Scanning transmission electron microscope (STEM) observation reveals that Re atoms were substitutionally doped into Mo sites (Fig.1a, b). By using STM/STS, we found that the doped Re sites result in the formation of midgap impurity state as shown in Fig.1c. Such impurity states have never been observed for the W-doped MoS_2 monolayers, and are unique characteristics for Re-doped MoS_2 . In the presentation, we will report the details of composition-dependent structure and electronic properties.

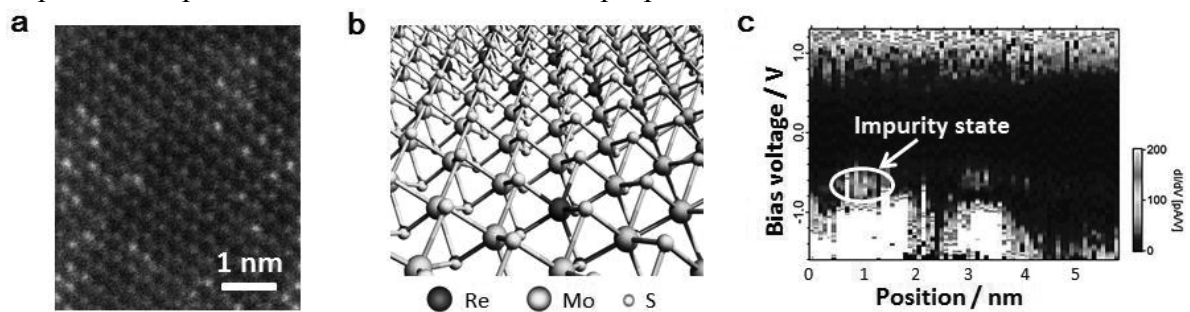


Fig.1 (a) ADF-STEM image and (b) structure model of monolayer $\text{Mo}_{1-x}\text{Re}_x\text{S}_2$. (c) Map of color scale dI/dV curves calculated from the spatially resolved STS spectra of monolayer $\text{Mo}_{1-x}\text{Re}_x\text{S}_2$.

[1] Y. Kobayashi, *et al.*, Nano Res., 8, 3261 (2015). [2] S. Yoshida, *et al.* Sci. Rep., 5, 14808 (2015).

[3] S. Sasaki, *et al.* Appl. Phys. Express, 9, 071201 (2016). [4] S. Mori, *et al.* The 50th FNTG symposium.

Corresponding Author: Yasumitsu Miyata, Tel: +81-42-677-2508, E-mail: ymiyata@tmu.ac.jp

Anisotropic optical absorption and Raman spectra in GaTe with the interference effect of the substrates

○Yuki Tatsumi¹, Shengxi Huang², Xi Ling², Huaihong Guo³, Teng Yang⁴,
Mildred S. Dresselhaus², Riichiro Saito¹

¹Department of Physics, Tohoku University, Sendai 980-8578, Japan

²Department of Electrical Engineering and Computer Science, Massachusetts Institute of Technology, Cambridge, Massachusetts 02139 USA

³College of Science, Liaoning Shihua University, Fushun, 113001, China

⁴Institute of Metal Research, CAS, Shenyang 110016, China

Gallium telluride (GaTe) is one of the atomic layer materials, which consists of 6 Ga and 6 Te atoms in a unit cell as shown in Fig. 1(a). Bulk GaTe is a semiconductor with a direct energy gap ($\sim 1.65\text{eV}$) [1] and can be a good candidate for opto-electronic device applications because of high responsibility (10^4 A/W) and short response time (6 ms) [2]. We have an interest in the low symmetry properties of GaTe (C_{2h}^3 space group in bulk GaTe) and verify the anisotropy of the optical absorption and Raman spectra by (1) calculation of the electron-photon matrix element from DFT, (2) analysis of the group theory, and (3) consideration of the interference effect of the substrate in order to reproduce the experiment.

We evaluate the anisotropy of the absorption probability of GaTe on the 0.5 mm quartz substrate, calculated by transfer matrix method for the optical absorption probability [Fig. 1(b)] and the enhancement factor [3] of GaTe on the $\text{SiO}_2(300\text{nm})/\text{Si}$ substrate for the Raman intensity [Fig. 1(c)] as a function of thickness. We found that the interference effect with the substrates plays an important role in the anisotropy of the optical absorption and Raman intensity. This indicates that the thickness of the GaTe sample and substrate, and the laser energy of incident light are important parameters to give the anisotropy of the optical properties in the experiment.

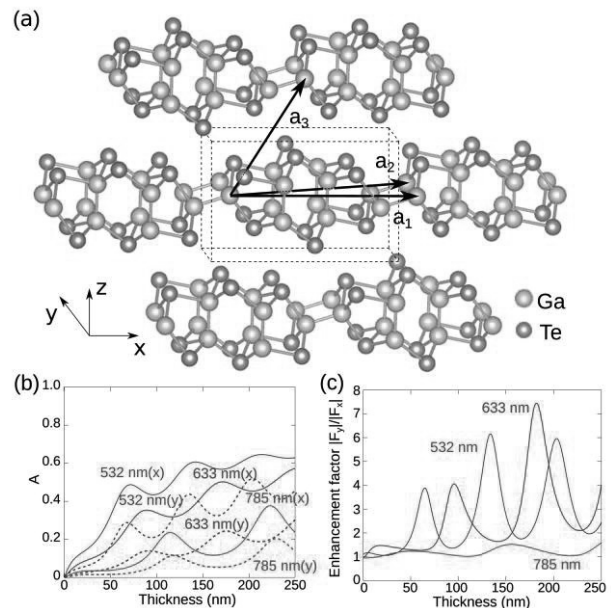


Fig.1: (a) Crystal structure of GaTe. a_1 , a_2 , and a_3 are the primitive lattice vectors. (b) Thickness dependence of the absorption probability of bulk GaTe on the 0.5mm quartz substrate for x- and y-polarized light with three laser wavelength (532, 633, 785 nm). (c) Thickness dependence of the ratio between the Raman enhancement factors [3] on the $\text{SiO}_2(300\text{nm})/\text{Si}$ substrate for x- and y-polarized light with three laser wavelength (532, 633, 785 nm).

[1] P. Hu, *et al.* Nano Res., **7**, 694 (2014)

[2] F. Liu, *et al.* ACS Nano, **8**, 752 (2014)

[3] D. Yoon, *et al.* Phys. Rev. B, **80**, 125422 (2009)

Corresponding Author: Yuki Tatsumi

Tel: +81-22-795-6442, Fax: +81-22-795-6447,

E-mail: tatsumi@flex.phys.tohoku.ac.jp

Bandgap modulation of bilayer MoS₂ by electric field effect

○Tetsuki Saito¹, Yu Kobayashi¹, Kenji Watanabe², Takashi Taniguchi²,
Yutaka Maniwa¹, Yasumitsu Miyata^{1,3}

¹*Department of Physics, Tokyo Metropolitan University, Hachioji, 192-0397, Japan*

²*National Institute for Materials Science, Tsukuba 305-0044, Japan*

³*JST, PRESTO, Kawaguchi, 332-0012, Japan*

Bandgap engineering of transition metal dichalcogenide (TMDC) atomic layers is one of the most important challenges for their potential applications in electronics and optics. In our previous works of WS₂/MoS₂ vertical heterostructures, we reported the bandgap narrowing by interlayer coupling and the observation of interlayer excitons [1]. In contrast, giant Stark effect has been predicted theoretically for similar bilayers of TMDCs [2]. Therefore, it is interesting to investigate the electric field effect of bandgap and optical properties for such bilayer TMDC systems. In this study, we have measured the electric-field dependent photoluminescence (PL) spectra of bilayer MoS₂ by using electric double layer capacitors (EDLCs).

Bilayer MoS₂ were grown on boron nitride (BN) substrates by chemical vapor deposition (CVD) using MoO₃ and sulfurs (Fig. 1a). To study the electric field dependence, Au electrodes were deposited on the bilayer MoS₂, and the MoS₂-based EDLCs with ionic liquid were fabricated (Fig. 1b). Using the EDLC, the PL spectra of bilayer MoS₂ were recorded at different electric field (Fig. 1c). Interestingly, by applying positive gate voltage, we observed a remarkable redshift for the PL peaks derived from indirect transition. Compared to the predictions of first principle calculations [2,3], these results can be explained by the bandgap narrowing due to Stark effect. In the presentation, we will discuss the origin of the peak shift and electric field effect for bilayer TMDCs.

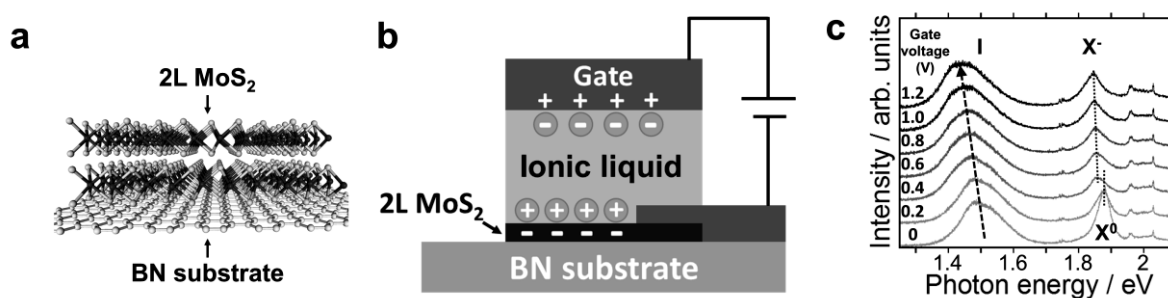


Fig. 1 Schematic illustrations of (a) bilayer MoS₂ on a BN substrate and (b) a bilayer MoS₂ EDLC. (c) PL spectra of bilayer MoS₂ at different gate voltages.

[1] T. Saito, *et al.*, The 50th FNTG symposium.

[2] A. Ramasubramaniam, *et al.*, Phys. Rev., 84, 205325 (2011).

[3] Q. Liu, *et al.*, J. Phys. Chem. C, 116, 21556 (2012).

Corresponding Author: Yasumitsu Miyata, Tel: 042-677-2508, E-mail: ymiyata@tmu.ac.jp

Growth of Diamond Nanocylinder Forest Using Template-Assisted Microwave Plasma Chemical Vapor Deposition

○Wenxi Fei^{1*}, Masafumi Inaba¹, Yu Hirano¹, Hideki Masuda², and Hiroshi Kawarada^{1,3}

¹ Faculty of Science and Engineering, Waseda University, Tokyo 169-8555, Japan

² Department of Applied Chemistry, Tokyo Metropolitan University, Tokyo 192-0397, Japan

³ Kagami Memorial Laboratory for Materials Science and Technology, Tokyo 169-0054, Japan

Recently, great effort has been devoted to the modification of the geometric structures of diamond. Among these structures, cylinder structures are expected to play crucial role in future nanotechnology. For example, diamond nanocylinder forest (DNF) is a promising candidate for electrode materials for fuel cells due to its high surface area, high porosity and electrochemical stability. [1] In the case of transistor, planar boron-doped diamond film is good electrochemical electrode due to the large voltage window. As a result, it is supposed that boron doped DNF (BDDNF) will also show high electrochemical performance. [2]

Various methods have been tried to fabricate well-aligned DNF, including dry air plasma etching [3] and radio frequency Ar/O₂ plasma etching [4]. The common disadvantage for the mentioned etching method is that the quality of DNF will be degenerated by etching. In order to get rid of etching, porous alumina membrane template-assisted microwave plasma chemical vapor deposition (MPCVD) was used to fabricate DNF and two different structures of diamond cylinders have been successfully obtained by optimizing growth conditions in this work. And influence of substrate temperature on the growth process of DNF was studied as well.

Table 1 shows the classification of DNF depending on the morphology. The DNF fabricated with a temperature of 750-900°C were diamond like carbon (DLC) tubes showed in fig.1, while DLC rods were observed with a temperature of 800-950°C. When the temperature was raised up to 1000°C, the obtained DNF were confirmed to be diamond rods. The diamond cylinders with high surface area and porosity fabricated by us is a promising material for applications in electrode and photovoltaic devices.

Table 1. products obtained at different growth temperature

Temperature (°C)	Tube structure	Rod structure
750	●	
800	●	●
900	●	●
950		●
1000		▲

● DLC ▲ Diamond

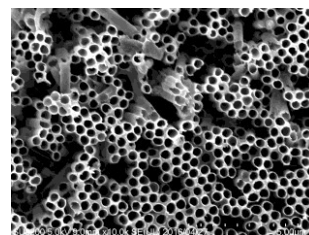


Fig.1:top-view SEM image of DLC tubes obtained at 900 °C

[1] Tang, Jing, et al. Nano Today 9.3 (2014): 305-323.

[2] Luo, Daibing, et al. ACS nano 3.8 (2009): 2121-2128.

[3] Baik, et al Thin solid films 377 (2000): 299-302. 5

[4] Li, C. Y., et al. Thin solid films 515.9 (2007): 4172-4176.

Corresponding Author: Wenxi Fei

Tel: +81-80-6257-5366

E-mail: feiwexi@akane.waseda.jp

***In situ* synchrotron X-ray diffraction study of structural changes on neutron-irradiated highly oriented pyrolytic graphite under static high pressure and temperature**

○T. Hisakuni¹, S. Honda¹, M. Niibe¹, M. Terasawa¹, Y. Higo², K. Niwase³, H. Izumi⁴,
E. Taguchi⁵, T. Iwata⁶

¹University of Hyogo, Himeji, Hyogo 671-2280, Japan

²Japan Synchrotron Radiation Research Institute, SPring-8, Sayo, Hyogo 679-5198, Japan

³Hyogo University of Teacher Education, Kato, Hyogo 673-1494, Japan

⁴Hyogo Prefectural Institute of Technology, Kobe 654-0037, Japan

⁵Osaka University, Ibaraki, Osaka 567-0047, Japan

⁶Japan Atomic Energy Research Institute (JAERI), Naka, Ibaraki 319-1195, Japan

Several methods have been developed for synthesizing diamonds such as direct conversion of graphite under static high pressure and temperature, shock compression, and chemical vapor deposition. Polycrystalline diamond of 10-20 nm across, which exhibits an excellent hardness, was synthesized by direct conversion of graphite under static high pressure and temperature [1]. It was also found that neutron-irradiated graphite can be transformed to amorphous diamond by shock compression and rapid quenching [2], where defects produced by the irradiation are considered to work as the nucleation sites for diamond.

In this study, *in situ* structural analysis for neutron-irradiated and unirradiated HOPG samples under static high pressure and temperature was done, by using a Kawai-type multianvil apparatus with synchrotron X-ray irradiation at BL04B1 of SPring-8. After simultaneous high pressure of 16.4 GPa and high temperature of 1400 °C process, the structural properties of the recovered samples were characterized by optical microscopy, X-ray diffraction, Raman spectroscopy, and transmission electron microscopy (TEM). In addition, soft X-ray absorption spectroscopy (XAS) measurements were performed to characterize electronic states of the recovered samples at BL09 of NewSUBARU.

Figure 1 shows XAS spectra for the recovered sample of neutron-irradiated HOPG with diamond powder as a reference. It was found that the XAS spectra for the neutron-irradiated HOPG exhibited a characteristic dip around 303 eV of diamond. This result indicates that sp³-hybridized carbon atoms increased in the neutron-irradiated HOPG after the simultaneous high pressure and high temperature process. Detailed structural changes for the neutron-irradiated HOPG will be discussed at the conference.

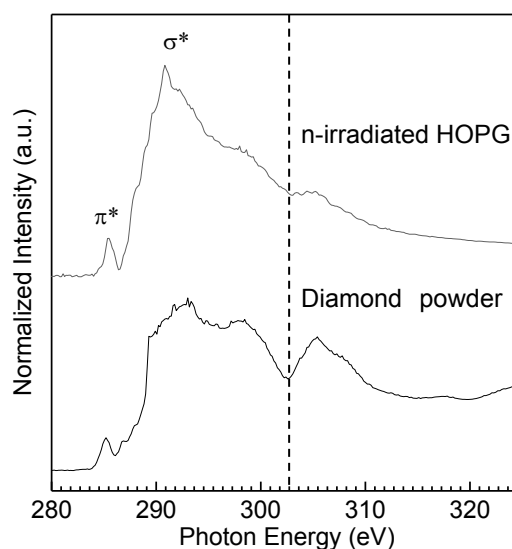


Fig.1: XAS spectra for the recovered sample of neutron-irradiated HOPG with diamond powder as a reference.

[1] T. Irifune et al., Nature **421**, 599 (2003).

[2] K. Niwase et al., Phys. Rev. Lett. **102**, 116803 (2009).

Corresponding Author: S. Honda

Tel: +81-79-267-4922, Fax: +81-79-267-4922,

E-mail: s-honda@eng.u-hyogo.ac.jp

Upconversion photoluminescence imaging of carbon nanotubes in mice tissues

○Saki Okudaira¹, Yoko Iizumi², Masako Yudasaka², Toshiya Okazaki², Kazunari Matsuda¹, and Yuhei Miyauchi¹

¹ Institute of Advanced Energy, Kyoto University, Uji, Kyoto 611-0011, Japan

² National Institute of Advanced Industrial Science and Technology (AIST), Tsukuba, Ibaraki 305-8562, Japan

Single-walled carbon nanotubes (SWNTs) have been considered as promising luminescent probes for deep-tissue bioimaging because of their intrinsic photoluminescence (PL) in the near infrared wavelength range of ~1000-1300 nm called NIR-II [1, 2]. The near infrared light readily penetrates into highly scattering media such as biological tissues; this enables PL imaging of deep inside of them. However, it is necessary to use Stokes PL at longer wavelengths than ~1100 nm to avoid autofluorescence from the biological tissues, and standard Si-based detectors cannot be used in this wavelength range. Recently, efficient upconversion PL (UCPL) of SWNTs has been discovered [3]. The UCPL phenomena enable SWNTs excited at wavelengths longer than ~1050-1200 nm to emit PL shorter than 1000 nm in which standard Si-based detectors have finite sensitivity. The availability of the UCPL thus drastically enhances the usefulness of SWNTs as luminescent probes in their bioimaging applications.

Here we demonstrate the first UCPL imaging of SWNTs in biological tissues of mice with negligible autofluorescence using a Si-based CCD camera. We observed microscopic PL and UCPL images of sectioned liver tissues of mice into which SWNTs were intravenously injected. Figures 1(a)-(c) show an optical transmission image, a Stokes PL image (excited at 658 nm), and a UCPL image (excited at 1064 nm), respectively. Figs. 1(b) and (c) were captured using the same CCD camera. In the case of Stokes PL imaging in Fig. 1(b), PL of both SWNTs (bright spots) and the tissue itself (autofluorescence, bright back ground) were observed. In contrast, only the UCPL of SWNTs (bright spots) was clearly observed in Fig. 1(c); this indicates nearly perfect reduction of the autofluorescence in the UCPL imaging. Results for stained samples will also be discussed.

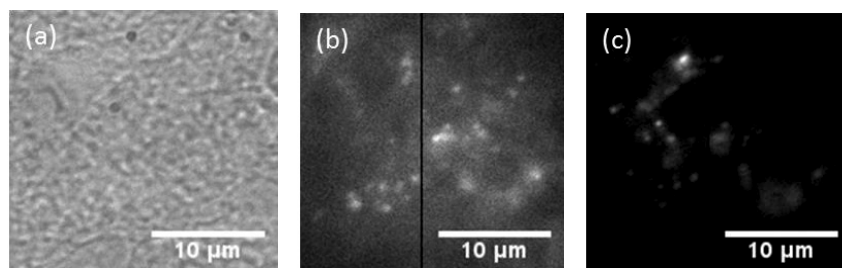


Fig. 1(a) Optical transmission image, (b) Stokes PL image excited at 658 nm, and (c) UCPL image excited at 1064 nm of the sectioned tissue of a mouse liver with the infused SWNTs. In (b) and (c), PL in 950-1000 nm was selectively detected. All images were taken at the same position of the sample.

[1] K. Welsher *et al.*, Nat. Nanotechnol. **4**, 773 (2009), G. Hong *et al.*, Nat. Photon. **8**, 723 (2014)

[2] Y. Iizumi, *et al.*, ACS Appl. Mater. Interfaces **5**, 7665 (2013)

[3] N. Akizuki *et al.*, Nat. Commun. **6**, 8920 (2015)

Corresponding Author: Y. Miyauchi

Tel: 81-774-38-3463, Fax: +81-774-38-4567, E-mail: miyauchi@iae.kyoto-u.ac.jp

Thermal interface materials of vertically aligned carbon fibers embedded densely in polymer matrix

○Ryo Yamada¹, Hisashi Sugime², Toshio Osawa¹, and Suguru Noda¹

¹Department of Applied Chemistry, Waseda University, Tokyo 169-8555, Japan

²Waseda Institute for Advanced Study, Waseda University, Tokyo 169-8050, Japan

The energy consumption of electric devices has been increasing rapidly, and efficient cooling of the devices becomes an important issue. In many devices, thermal interface materials (TIMs) are used to dissipate the heat from substrates to heatsinks, and improving the performance of TIMs is highly required. Because the materials for TIMs should have both good thermal conductivity and softness, carbon fibers (CFs), which individually have axial conductivity as high as 900 W/m K [1], are expected to be the candidate materials for novel TIMs. As the CFs do not form a self-supporting film without binder (e.g. polymer), the method to make a CF/polymer composite is an important issue. Especially, aligning the CFs vertically in the composite film is important for TIMs. For example, TIM with aligned CFs were achieved using electrical field [2]; however, CF content was up to 13.2 wt%.

In this study, TIMs with vertically aligned CFs densely embedded in polymethylmethacrylate (PMMA) matrix are fabricated by a simple process. First, CF/PMMA ink was prepared with toluene as solvent and rod coated on a substrate to make a film. During the rod coating, CFs aligned well to the moving direction of the rod because of the rod-shearing stress (Fig.1). Fabricated CF/PMMA film is then rolled up with the axis parallelly to the CFs alignment and heat pressed to form a rod. The rod is cut to ~100 μm which is proper thickness for the TIMs (Fig.2). We achieved the vertically aligned CFs in the polymer matrix with the CF contents as high as 60 wt%. When the thickness of TIMs become thinner than CFs length, some of individual CFs penetrated the TIMs. Such CFs will greatly enhance the overall thermal conductivity due to the absence of junction resistance between the CFs in vertical direction. The highest conductivity of 35.4 W/m K was achieved so far with 50 wt% CF/PMMA TIM.

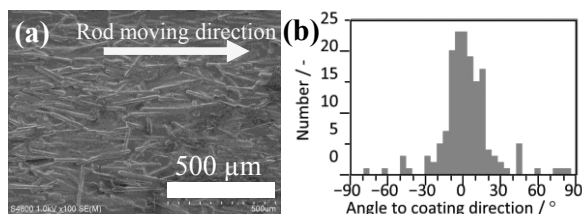


Fig.1 CF/PMMA film

(a) SEM images (b) Alignment histogram

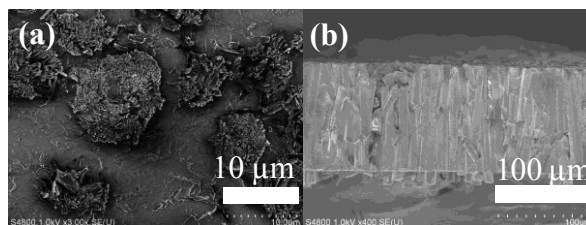


Fig.2 CF/PMMA TIM (60 wt%)

(a) Top view (b) Cross section

[1] Nihon graphite fiber, <http://www.ngfworld.com> [2] K. Uetani et al, Adv. Mater. 2014, 26, 5857.

Corresponding Author: S. Noda, Tel&Fax: +81-3-5286-2769, E-mail: noda@waseda.jp

Acknowledgement: This work was supported by JX Nippon Oil & Energy

Ultrathin graphene-based solar cells

Ya-Ping Hsieh¹, Chin-Fu Chen¹, Mario Hofmann²

¹Graduate Institute of Opto-Mechatronics, National Chung Cheng University and Advanced Institute of Manufacturing with High-Tech Innovations, Chiayi, 62102, Taiwan

²Department of Material Science and Engineering, National Cheng Kung University, Tainan, 70101, Taiwan

Decreasing the device thickness of multilayered heterojunction devices to atomic scales has many advantages. For example ultrathin solar cells [1] exhibit high transmittance, high mechanical flexibility, high conversion efficiency and low cost. The major issue that limits the thinning is an increase in leakage current due to the formation of pinholes.

We here demonstrate the use of graphene to lower the leakage current for enhanced device performance. We find that graphene electrodes can be safely suspended over voids that would cause leakage currents with traditionally deposited electrodes and a decrease in leakage current by 6 orders of magnitude was observed.

This ability enabled the fabrication of solid-state dye-sensitized solar cells with TiO₂ thicknesses between 5 nm and 100 nm, which represents some of the thinnest solar cells produced to date.

At those new length scales, unusual device characteristics were observed, such as two-dimensional dye loading and decreased interfacial charge compensation which highlight the limits of scaling ultrathin solar cells.

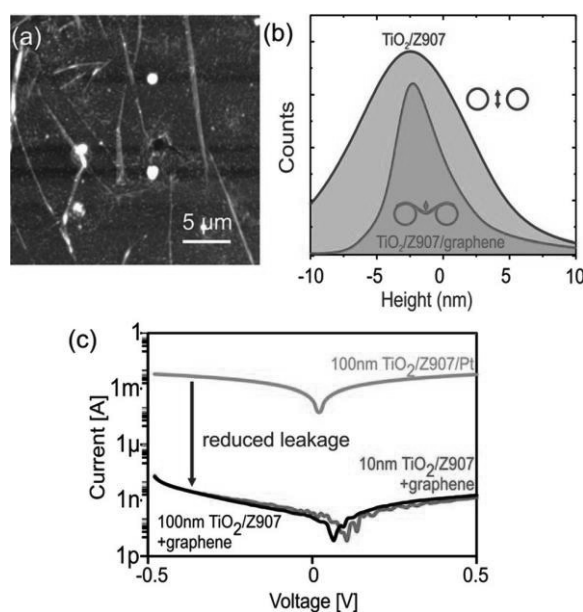


Fig.1(a) AFM image of graphene on 10 nm TiO₂/Z907, (b) height histogram before and after deposition of graphene on 10 nm TiO₂/Z907, (inset) depiction of origin of different roughness, (c) comparison of leakage currents for graphene on 10 nm and 100 nm TiO₂ and Pt on

Reference

[1] Hsieh, Ya-Ping, Bang-Jian Hong, Chu-Chi Ting, and Mario Hofmann. RSC Advances 5, no. 121, 99627-99631 (2015).

Preparation of methanofullerene derivatives: [70]PCBM and bis-[70]PCBM with high regioselectivity

○Takatoshi Ito¹, Yuta Inoue², Tetsuo Iwasawa², Fukashi Matsumoto¹, Toshiyuki Iwai¹, Kazuyuki Moriwaki¹, Yuko Takao¹, Takumi Mizuno¹, Toshinobu Ohno¹

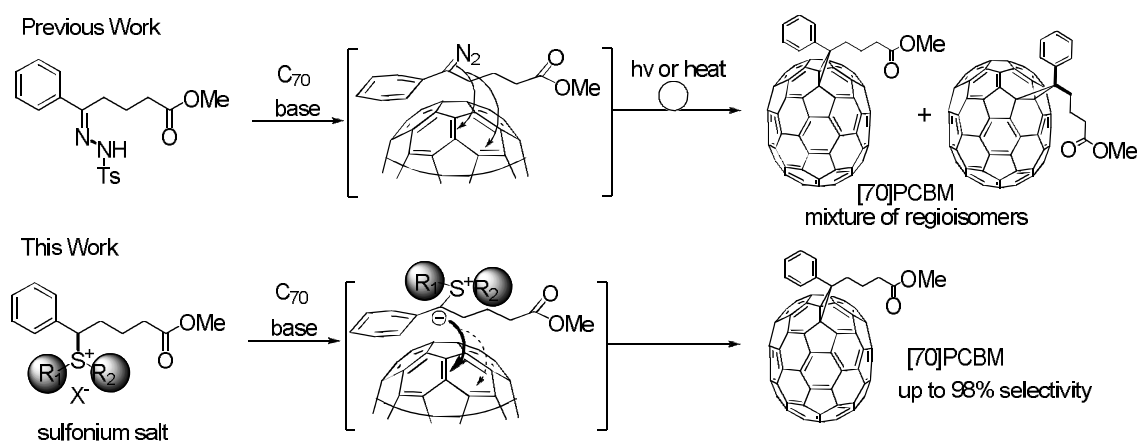
¹ Osaka Municipal Technical Research Institute, 1-6-50, Morinomiya, Joto-ku, Osaka 536-8553, Japan

² Faculty of Science and Technology, Ryukoku University, Otsu, Shiga 520-2194, Japan

Bulk heterojunction (BHJ) organic solar cells consisting of p-type conjugated polymers and n-type fullerene derivatives are considered to be attractive candidates for a low-cost sustainable energy source, and have become one of the most growing areas over the past decade. One of the most widely used electron acceptors in BHJ organic photovoltaic devices (OPVs) is fullerene derivatives, particularly [6,6]-phenyl-C₆₁/C₇₁-butyric acid methyl ester ([60]PCBM or [70]PCBM) [1].

The mono substitution toward C₆₀ fullerene gives single isomer, whereas mono addition of C₇₀ affords an isomeric product mixture in many cases due to the less symmetrical C₇₀ cage.

We recently reported facile synthesis of PCBMs by reaction of semi-stabilized sulfur ylides with C₆₀ and C₇₀, in which the desired [6,6]-isomer ([60]PCBM) was directly obtained without the generation of the corresponding [5,6]-open fulleroid [2]. Herein we wish to report extension of our study to regioselective synthesis of [70]PCBM (scheme 1).



Scheme 1. Synthetic protocols for [70]PCBM

Introducing two isopropyl groups with sulfur atom reached almost maximum values to afford α -type PC₇₁BM in high regioselectivity. Additionally, the use of excess sulfonium salt afforded bis-adducts (bis[70]PCBMs), in 57% yield, with a fairly high component ratio (*ca.* 97 : 3) compared to the conventional method.

[1] Hummelen, J. C.; Knight, B.W.; LePeq, F.; Wudl, F.; Yao, J.; Wilkins, C. L. *J. Org. Chem.* **1995**, *60*, 532.

[2] Ito, T.; Iwai, T.; Matsumoto, F.; Hida, K.; Moriwaki, K.; Takao, Y.; Mizuno, T.; Ohno, T. *Synlett.* **2013**, *24*, 1988.

Corresponding Author: Takatoshi Ito

Tel: +81-6-6963-8053, Fax: +81-6-6963-8049,

E-mail: ito@omtri.or.jp

Structure Determination of Saturn-Like Oligothiophene Macrocycle with $C_{61}H_2$ and C_{70}

○Hiroshi Okada,¹ Hideyuki Shimizu,² Shinobu Aoyagi,³ Biao Zhou,⁴
Masahiko Iyoda,² Yutaka Matsuo^{1,5}

¹ Department of Chemistry, School of Science, The University of Tokyo,
Tokyo, 113-0033, Japan

² Department of Chemistry, Graduate School of Science and Engineering,
Tokyo Metropolitan University, Hachioji, Tokyo 192-0397, Japan.

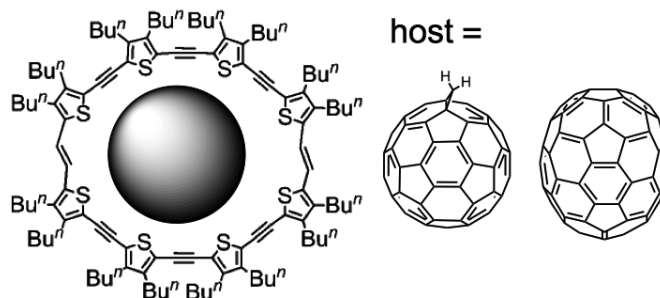
³ Department of Information and Biological Sciences, Nagoya City University,
Nagoya 467-8501, Japan

⁴ Department of Chemistry, College of Humanities and Sciences, Nihon University,
Sakurajosui 3-25-40, Setagaya-Ku, Tokyo 156-8550, Japan

⁵ University of Science and Technology of China, Anhui 230026, China

X-ray single crystallographic analysis for fullerenes such as fullerene derivatives, exotic metallofullerenes, and higher fullerenes is still one of powerful characterization tool to obtain precise structural information and structural properties. When we encounter difficulty of obtaining single crystals, we usually consider the use of supramolecular host molecules such as cobalt octaethylporphyrin to make co-crystals through non-covalent interaction for structural characterization.[1-3] These host molecules have been contributed to crystal structure determination of fullerenes that have been undetermined with ordinary crystallization methods. Furthermore, development of new good host molecules broadens opportunity for highly attractive structural, optical, and electronic properties of fullerene complexes.

Oligothiophene macrocycle is a promising candidate for supramolecular hosts for above-mentioned purpose. A Saturn-like complex of this macrocycle with C_{60} have been reported.[4] In this work, we chose dihydromethanofullerene, $C_{61}H_2$, as a guest fullerene derivatives that had not been crystallographically characterized even through $C_{61}H_2$ has a very simple structure.[5] Also we demonstrated complexation with C_{70} for detail examination of supramolecular formation.



References

- [1] K. Kurotobi and Y. Murata, *Science*. **2011**, 333, 613–616
- [2] S. Stevenson *et al.*, *Nature* **401**, 1999, 55–57
- [3] H. Ueno *et al.*, *Chem. Sci.*, **2016**, Advance Article, DOI: 10.1039/C6SC01209D
- [4] H. Shimizu *et al.*, *J. Chem. Am. Soc.* **2015**, 137, 3877–3885
- [5] Y. Zhang *et al.*, *J. Chem. Am. Soc.* **2011**, 133, 8086–8089.

Corresponding Author: H. Okada and Y. Matsuo

Tel: +81-3-5841-0978, E-mail: hokada@photon.t.u-tokyo.ac.jp; matsuo@photon.t.u-tokyo.ac.jp

Preparation of [C₆₀]Fullerene Nanowhisker-Silver Nanoparticle Composites and Their Catalytic Activity for Oxidation of Tetramethylbenzidine with Hydrogen Peroxide

○Jeong Won Ko¹, Weon Bae Ko^{1,2}

¹ Department of Convergence Science, Graduate School, Sahmyook University, Seoul 139-742, Korea

² Department of Chemistry, Sahmyook University, Seoul 139-742, Korea

Silver nanoparticles solution was prepared by dissolving trisodium citrate dihydrate (C₆H₅Na₃O · 2H₂O), sodium borohydride (NaBH₄), cetyltrimethyl ammonium bromide (CTAB, (C₁₆H₃₃)N(CH₃)₃Br), ascorbic acid (C₆H₈O₆) and silver nitrate (AgNO₃) in distilled water, and then the resulting solution was irradiated ultrasonication for 3 h. [C₆₀]Fullerene nanowhisker-silver nanoparticle composites were prepared using C₆₀-saturated toluene, silver nanoparticles solution and isopropyl alcohol by liquid-liquid interfacial precipitation method. The formation of [C₆₀]fullerene nanowhisker-silver nanoparticle composites was confirmed by X-ray diffraction, Raman spectroscopy, scanning electron microscopy, and transmission electron microscopy. The catalytic activity of [C₆₀]fullerene nanowhisker-silver nanoparticle composites for oxidation of tetramethylbenzidine (TMB) with H₂O₂ was confirmed by UV-vis spectroscopy.

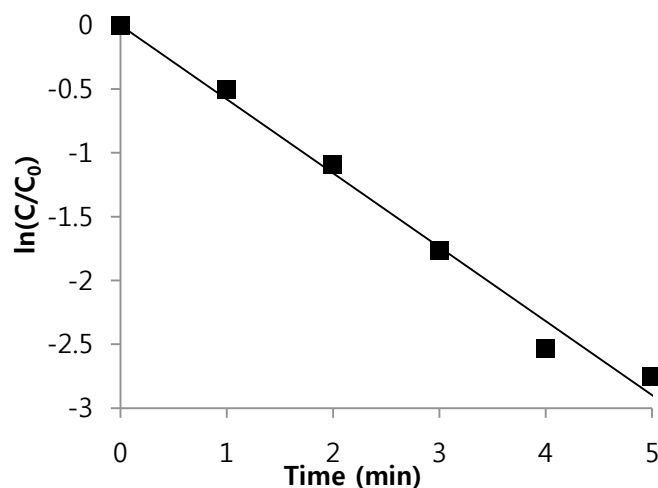


Fig. 1: Kinetics Study of Tetramethylbenzidine Oxidation with Hydrogen Peroxide using [C₆₀]Fullerene Nanowhisker-Silver Nanoparticle Composites.

[1] K. Miyazawa and K. Hotta, *J. Cryst. Growth*, **312**, 2764 (2010).

[2] J.W.Ko, J. Li and W.B. Ko, *Nanomater. Nanotechnol.*, **5**:37. doi: 10.5772/62086 (2015).

Corresponding Author: W. B. Ko

Tel: +82-2-3399-1700, Fax: +82-2-979-5318,

E-mail: kowb@syu.ac.kr

Color tuning of semitransparent organic solar cells using oxide/metal/oxide transparent anode

○Shunjiro Fujii¹ and Hiromichi Kataura¹

¹*Nanomaterials Research Institute, National Institute of Advanced Industrial Science and Technology (AIST), Ibaraki 305-8565, Japan*

Semitransparent organic solar cells (OSCs) have attracted a great attention for their potential applications such as power-generating windows for building-integrated photovoltaics and sun shading for automobiles. The former are especially interesting due to their multiple functions of light harvesting, lighting and indoor temperature control. However, the transmission spectra of semitransparent OSCs have been so far dominated by the materials used as the active layers. For the common bulk-heterojunction OSCs using poly(3-hexylthiophene):(6,6)-phenyl C61 butyric acid methyl ester (P3HT:PCBM), a red-purple color is observed because of a high absorbance at approximately 500 nm and the cut-off absorbance spectrum of P3HT:PCBM at 650 nm. Previously, we reported semitransparent OSCs based on a low-bandgap polymer of PTB7 and PC₇₁BM utilizing a MoO₃/Au/MoO₃ anode [1]. In this work we demonstrated the fabrication of color-tunable semitransparent PTB7:PC₇₁BM solar cells by adopting different metal layers in oxide/metal/oxide trilayer anode.

The device structure was Glass/ITO/PFN/PTB7:PC₇₁BM/MoO₃/thin metal/MoO₃ (Figure 1). For the thin metal layers sandwiched by the two transparent MoO₃ layers, Ag(20 nm), Au(20 nm) or Al(2 nm)/Cu(18 nm) were used, which acted as an optical spacer as well as electrode. Figure 2 shows the corresponding optical transmittance spectra for the semitransparent cells. By combining flat transmittance of PTB7:PC₇₁BM film with MoO₃(10 nm)/metals(Ag, Au or Al/Cu)/MoO₃ (20 nm) anodes, the colors of the semitransparent cells were broadly tuned to blue, green and gray, while maintaining a similar cell performance. The detailed device characteristics will be discussed. This work was supported by KAKENHI Nos. 16K17497, 25220602.

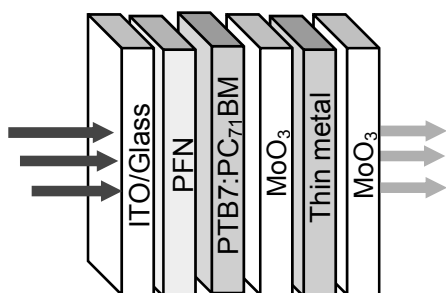


Figure 1 Schematic illustration of semitransparent solar cell.

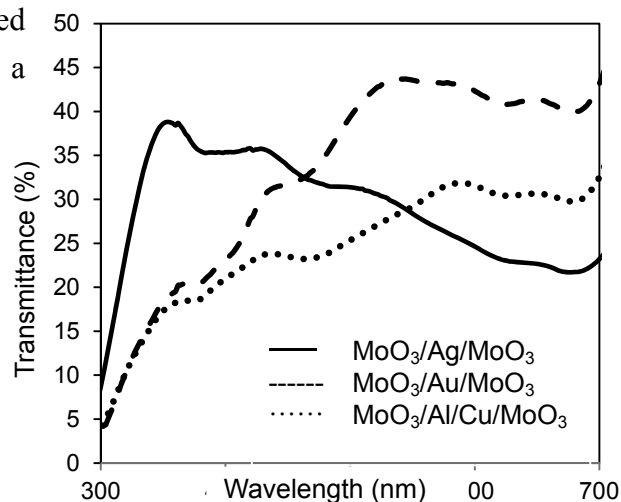


Figure 2 Optical transmittance spectra of semitransparent cells including ITO/glass substrate.

[1] S. Fujii et al., The 48th FNTG General symposium 2014, 1p-35
Corresponding Author: Hiromichi Kataura **E-mail:** h-kataura@aist.go.jp

Isolation of a missing fullerenes Gd@C_{2n} derivatives

○Ayano Nakagawa¹, Shinobu Aoyagi², Haruka Omachi¹, Zhiyong Wang¹,
Katsuma Ishino¹, Ryo Kitaura¹, and Hisanori Shinohara¹

¹ Department of Chemistry and Institute of Advanced Resaerch, Nagoya University, Nagoya
464-8602, Japan.

² Department of Information & Biological Science, Nagoya City University, Nagoya
467-8501, Japan.

The extraction of endohedral metallofullerenes M@C_{2n} (e.g., M = Y, La, or Gd etc., 2n = 60, 70, 72, or 74) has been a long-standing challenge in fullerene ever since the experimental discovery in 1985[1]. The high reactivity of these fullerenes has led to form their polymer, hindering the solvation in common organic solvents and the subsequent isolation process. Thus, no study has ever done on the elucidation of property and structure of these so called missing fullerenes.

Recently, our group has reported a new stabilization method of missing fullerenes by *in situ* functionalization of trifluoromethyl (CF₃) groups which enables their isolation[2]. Here, we demonstrated the separation of individual derivatives of Gd@C_{2n} missing fullerenes by chromatographic separation as shown in Fig. 1(a). MALDI- TOF mass spectra of an isolated derivative, as shown in Fig. 1(b), exhibits an intense peak of Gd@C₇₄(CF₃), indicating that mono-functionalization with CF₃ group has stabilized Gd@C₇₄ that allow its isolation. This isolation method of missing fullerenes will allow us to study their structure and property, significantly advancing the research of fullerenes.

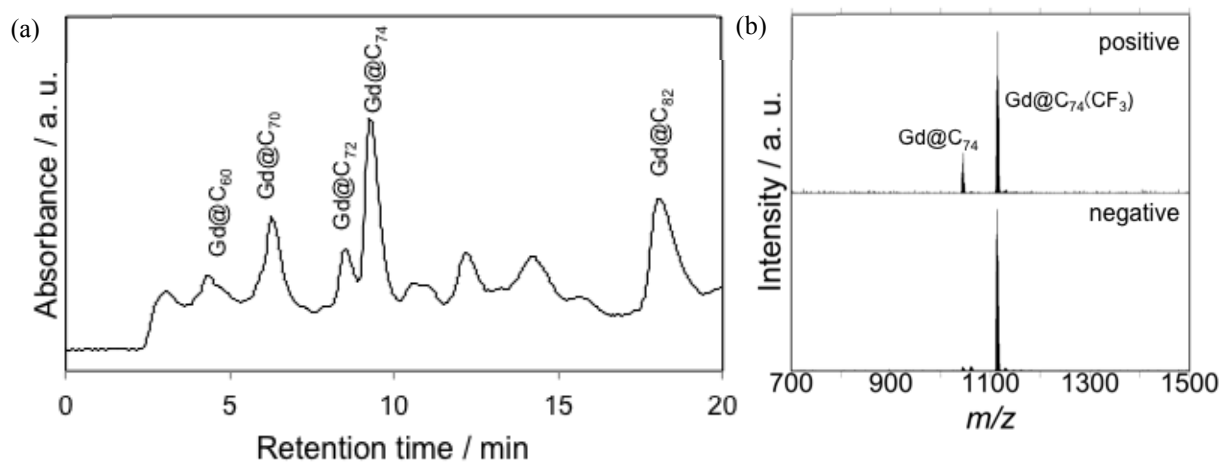


Fig.1 (a) First-stage HPLC chromatography of Gd@C_{2n} derivatives. (b) MALDI-TOF mass spectra of isolated Gd@C₇₄(CF₃)

[1] J. R. Heath *et al.*, *J. Am. Chem. Soc.*, **107**, 7779 (1985).

[2] (a) Z. Wang *et al.*, *Angew. Chem., Int. Ed.*, **52**, 11770 (2013). (b) Z. Wang *et al.*, *Angew. Chem., Int. Ed.*, **55**,199 (2016).

Corresponding Author: Hisanori Shinohara

Tel: +81-52-789-2482, Fax: +81-52-747-6442, E-mail: noris@nagoya-u.jp

***In-situ* TEM study on structure and optical emission during Joule heating of a multiwall carbon nanotube**

○Koushi Nishikawa, Koji Asaka, Hitoshi Nakahara, Yahachi Saito

Department of Quantum Engineering, Nagoya University, Furo-cho, Nagoya 464-8603

In previous study, some broad peaks in addition to the blackbody radiation spectrum during Joule heating of a multiwall carbon nanotube (MWNT) were observed in a scanning electron microscope [1]. However, the origin of the peaks has not been clarified yet. In this study, in order to make it clear, the structure of the MWNT during Joule heating of the MWNT was observed with simultaneous measurement of the optical emission.

MWNTs attached to an edge of a gold (Au) plate by dielectrophoresis were mounted on a specimen holder for *in-situ* transmission electron microscopy (TEM). An edge of a MWNT protruding from the Au plate was brought into contact with an Au-coated tungsten needle in TEM. The structure changes induced by Joule heating of the MWNT were observed by *in-situ* TEM. The bias voltage and current were measured simultaneously with the optical emission spectra.

Figures 1(a) and 1(b) show TEM images observed before and after the MWNT was fractured near the Au electrode by Joule heating, respectively. After the fracture, the diameter of the capped MWNT tip decreases, as shown in Fig. 1(b). The optical emission spectra before and after the fracture by the Joule heating are shown in Fig. 2(a) and 2(b). The intensity of the spectra continuously rises with the increase of the wavelength, indicating that the spectra include blackbody radiation components. Some peaks besides the blackbody radiation spectra are observed. After the fracture of the MWNT, the intensity of the peaks significantly increases. The peak energies are 1.40, 1.52, 1.70, 1.83 and 2.10 eV. The energies 1.40 and 1.52 eV are close to energy differences between van Hove singularities in a semiconducting carbon nanotube (CNT) with diameter 6.38 nm. The other peak energies correspond to CNTs with diameter 7.20, 4.73, and 5.55 nm, respectively. The peaks observed in optical emission spectra during Joule heating of the MWNT are considered to be attributed to the interband electron transitions in the MWNT.

[1] X. Cai *et al.* Thin Solid Films 464-465 (2004) 364-367.

Corresponding Author: Koushi Nishikawa

Tel: +81-52-789-3714, Fax: +81-52-789-3703, E-mail: nishikawa@surf.nuqe.nagoya-u.ac.jp

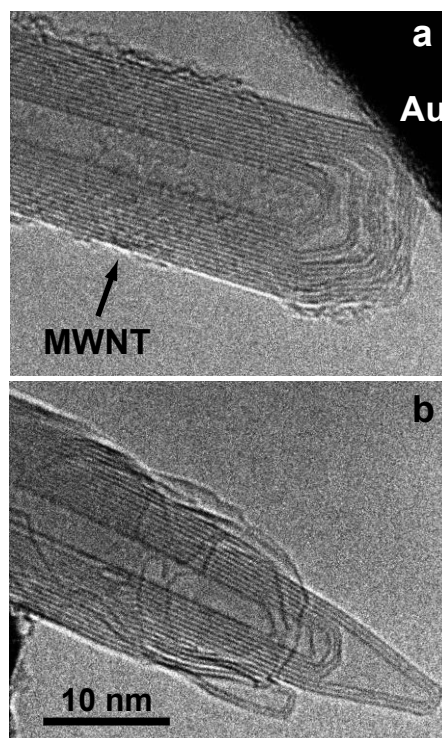


Fig.1 TEM images of a MWNT (a) before and (b) after the fracture of the MWNT near the Au electrode.

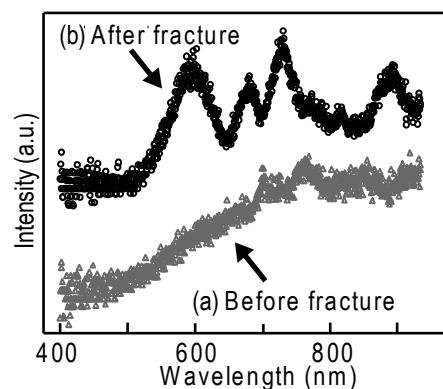


Fig. 2 Optical emission spectra during Joule heating of the MWNT at a power of $\sim 390 \mu\text{W}$. (a) before and (b) after fracture.

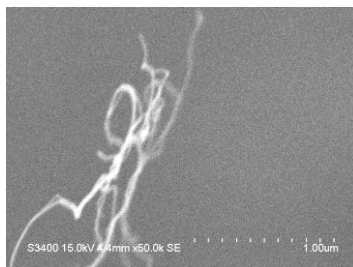
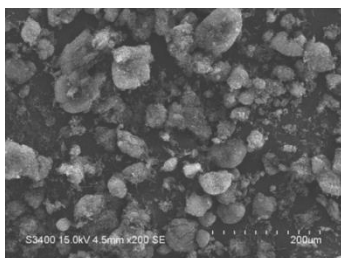
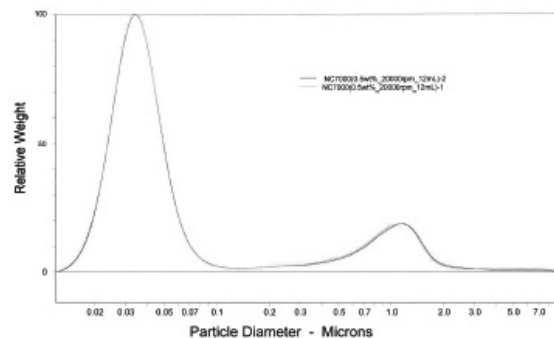
Novel Dispersion and Evaluation Method for CNTs by Using Ultrasonic Mixer, PR-1

○Takayuki Takatsuka
 THINKY Corporation, Tokyo 101-0021, Japan

Carbon nanotubes (CNTs) are strongly aggregated by van der Waals' force, and ultrasonic has been utilized to deagglomerate CNTs. Nano Premixer, PR-1 (Thinky, Tokyo) rotates CNTs in an enclosed vessel inside the ultrasonic bath and irradiates ultrasonic simultaneously from two directions, side and bottom, to disperse CNTs. With the combination of the rotation and the dual ultrasonic process, highly reproducible and stabilized CNT-dispersion can be obtained.

The evaluation result for CNT-dispersion is conventionally obtained by indirect approaches by using SEM and/or Four-terminal method; however, since the evaluation is based on powdered CNTs, the result does not reflect the actual dispersibility and stability of CNT-dispersion.

At this report, we will introduce the method to disperse several different CNTs with PR-1, and evaluate the dispersion using CPS Disc Centrifuge High Resolution Particle Size Analysis System.



Corresponding Author: Takayuki Takatsuka (THINKY)
 Tel: +81-3-5207-2717, Fax: +81-3-5289-3285
 E-mail: takatsuka@thinky.co.jp

THINKY

Pyrene dimer and monomer on single-walled carbon nanotubes

○Jinseok Baek¹, Tomokazu Umeyama¹, Yuta Sato², Kazu Suenaga², Hiroshi Imahori^{1,3}

¹ Department of Molecular Engineering, Kyoto University, Kyoto 615-8510, Japan

² National Institute of Advanced Industrial Science and Technology (AIST), AIST Central 5, Tsukuba 305-8565, Japan

³ Institute for Integrated Cell-Material Sciences (WPI-iCeMS), Kyoto University, Kyoto 615-8510, Japan

The close solid-state structure–property relationships of organic π -aromatic molecules have attracted interest due to their implications for the design of organic functional materials. In this regard, a dimeric structure is considered as a minimum unit for evaluating intermolecular interactions precisely. In this study, selective formation of the dimeric and monomeric π -aromatic units on an sp^2 carbon network of single-walled carbon nanotubes (SWNTs) was achieved using one- and two-step methods, i.e., direct addition of the pyrenylphenyl (PP) radical onto the SWNT sidewall (Py-1-SWNT) and stepwise addition consisting of first addition of the iodinephenyl (PI) radical onto the SWNT sidewall, followed by the second Suzuki coupling between the PI-functionalized SWNT and pyrene boronic ester (Py-2-SWNT) (Fig. 1) [1]. Py-2-SWNT presented monomeric pyrenes located on the SWNT sidewall, whereas dimeric pyrenes were formed on the SWNT sidewalls of Py-1-SWNT, as demonstrated both theoretically and experimentally. In particular, we successfully visualized for the first time the linking of dimeric molecules onto the outside of nanocarbon scaffolds at a single molecule level using the high-resolution transmission electron microscopy (HR-TEM) technique. Reflecting the unique orientation and separation distances between the two pyrene moieties, Py-1-SWNT exhibited an additional distinct band in the absorption spectrum and a photoinduced charge separation in the transient absorption (TA) spectrum, which is in marked contrast with Py-2-SWNT. The present methodology used to form and probe molecular dimers on SWNT is applicable to any organic molecules that contain aryl groups, including π -conjugated small molecules and oligomers. Thus, this method can be used to provide basic information regarding the close structure–property relationships existing within dimeric molecules of interest.

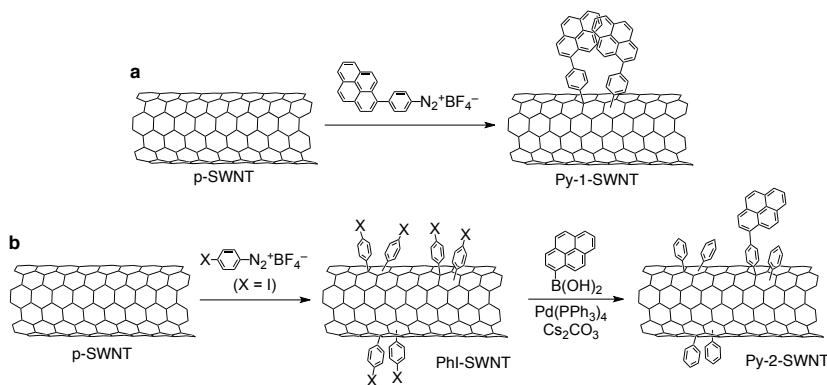


Fig. 1 Schematic representation of the functionalization of SWNTs with pyrene. (a) One-step functionalization. (b) Two-step functionalization.

[1] T. Umeyama, J. Baek, Y. Sato, K. Suenaga, F. Abou-Chahine, N. V. Tkachenko, H. Lemmetyinen and H. Imahori, *Nat. Commun.* **6**, 7732 (2015)

Corresponding Author: J. Baek

Tel: +81-75-383-2567, Fax: +81-75-383-2571,

E-mail: baek.jinseok.87e@st.kyoto-u.ac.jp

Electronic structure of CNT thin films with nanoscale interfaces under an electronic field

○Taketo Kochi and Susumu Okada

University of Tsukuba, 1-1-1 Tennodai, Tsukuba, Ibaraki, 305-8571 Japan

Carbon nanotubes (CNTs) are attracting much attention owing to their unique geometric and electronic properties. Because of the unusual physical properties, they are keeping a premier position in emerging materials for the future electronic devices. Indeed, it has been demonstrated that CNTs work as conducting channel of field effect transistors (FETs). In the FET, CNTs form a mat film structure in which CNTs intersect each other with nanometer scale interfaces. Although the CNT mat films can work as conducting channel in real devices, the microscopic mechanism of carrier accumulation in the CNT thin films under an external electric field is still unclear. Thus, in this manuscript, we aim to elucidate the fundamental electronic properties of CNT thin films with nanoscale interfaces among CNTs under an external electric field, which injects electrons/holes into the CNTs, using density functional theory with local density approximation. In this work, to simulate the CNT-FET device structure, we consider the CNT double-decker structure consisting of (10,0) and (11,0) CNTs which intersect each other with angles of 60, 75, and 90 degrees (Fig. 1). For both electron and hole doping, the accumulated carriers are mainly distributed on the CNT situated at the electrode side. In addition, under the particular conditions, the distribution of accumulated carriers shows the unusual feature, inducing the inversion electric field to the applied external electric field. We further investigate the capacitance of the CNTs.

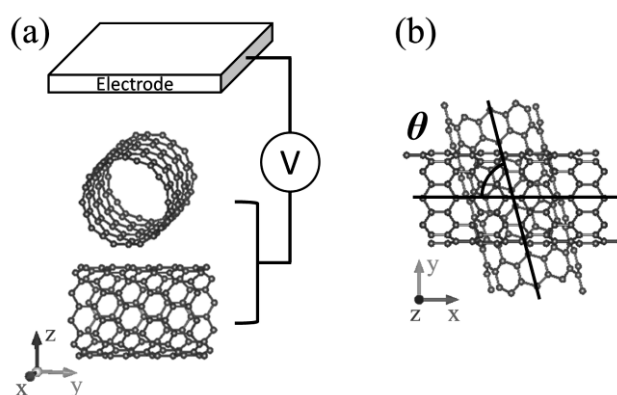


Fig. 1 (a) A structural model of CNT thin films in the FET structure under the electron field. (b) The top views of CNT thin films.

Voltage generation by movement of electrolyte solution on carbon nanotube thin film

○Tomohiro Yasunishi¹, Shigeru Kishimoto¹, and Yutaka Ohno^{1,2}

¹ Graduate school of Engineering, Nagoya University, Nagoya 464-8603, Japan.

² Institute of Materials and Systems for Sustainability, Nagoya University, Nagoya 464-8603, Japan.

Energy harvesting from environment energy sources is emerging technology for driving sensor devices for IoT. Recently, the voltage generation of a few millivolts from the movement of electrolyte solution have been demonstrated by using graphene [1, 2] and carbon nanotubes (CNTs) [3]. In this work, we fabricated the voltage generators using the single-walled CNT thin film on flexible substrate. Their characteristics such as the dependences on concentration of electrolyte solution and thickness of CNT thin film have been studied.

Highly-conductive CNT thin films were formed on polyethylenephthalate (PEN) substrate by the dry transfer process based on the floating-catalyst chemical vapor deposition. [4]. The size of the CNT thin film was 30 mm x 4 mm (Fig. 1 (a)). Ag-paste electrodes were formed on the both edges. 2-mol/l NaCl aqueous solution was used as the electrolyte. The droplet of the electrolyte solution was moved on the CNT thin film between two electrodes (Fig. 1 (b)). We measured open-circuit voltage by semiconductor device parameter analyzer.

Figure 2(a) and 2(b) show the voltage wave forms generated by moving electrolyte droplet for CNT film thickness of 40 and 10 nm, respectively. The CNT film thickness was measured by laser scanning confocal microscope. The maximum open circuit voltage was 220 μ V for the CNT film thickness of 40 nm (Fig. 2 (a)). Thinner CNT film of 10 nm generated higher voltage as 2.72 mV. This is probably due to the elimination of shunt current flowing through the underlayer CNTs.

[1] P. Dhiman *et al.*, *Nano Lett.* **11**, 3123, (2011).

[2] J. Yin *et al.*, *Nat. Nanotechnol.* **9**, 378, (2014).

[3] S. Ghosh *et al.*, *Science* **299**, 1042 (2003).

[4] A. Kaskela *et al.*, *Nano Lett.* **10**, 4349 (2010).

Corresponding Author: Y. Ohno

Tel&Fax: +81-52-789-5387,

E-mail: yohno@nagoya-u.jp

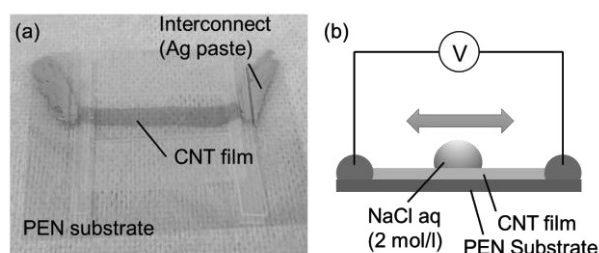


Fig. 1 (a) Photograph of fabricated device, (b) schematic of measurement system.

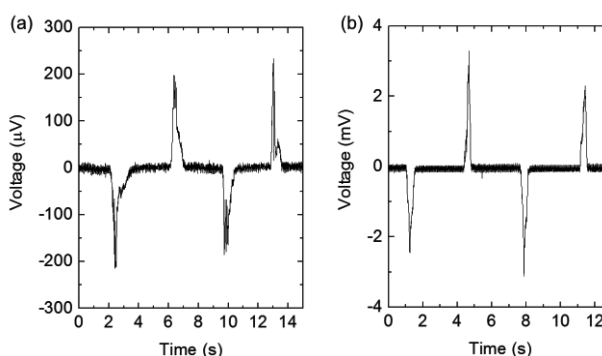


Fig. 2 Voltage wave forms generated by moving electrolyte droplet on CNT film. The thicknesses of CNT films are (a) 40 nm and (b) 10 nm, respectively.

Controlled n-type doping of carbon nanotube thin-film transistors with salt and crown ether

○Fumiya Nihey^{1,*}, Kei Endo^{1,2}, Jiang Pu^{1,3}, Noriyuki Tonouchi¹, Fusako Sasaki⁴, Yuki Kuwahara^{4,5}, Takeshi Saito^{4,5}, Hiroyuki Endoh¹

¹ IoT Devices Research Laboratories, NEC Corporation, Tsukuba 305-8501, Japan

² Graduate School of Engineering, Osaka University, Suita 565-0871, Japan

³ Department of Applied Physics, Waseda University, Shinjuku 169-8555, Japan

⁴ Technology Research Association for Single Wall Carbon Nanotubes, Tsukuba 305-8565

⁵ National Institute of Advanced Industrial Science and Technology, Tsukuba 305-8565

Carbon nanotubes (CNTs) have attracted much attention for various applications such as flexible, printable thin-film transistors (TFTs). CNT-TFTs generally show p-type behavior possibly due to unintentional hole doping by oxygen and/or water, so stable n-type doping has been anticipated especially for logic-circuit applications. Although organic molecules such as poly(ethylene imine) (PEI) and benzyl viologen have been reported as air-stable dopants, their stability is still controversial. Recently, Nonoguchi et al. proposed new n-type doping agents comprising salts and crown ether families that display prolonged air stability of negative Seebeck coefficients even under elevated temperatures [1]. Here, we have succeeded in controlling the electrical properties of CNT-TFTs with the salt and crown ether dopants. By changing the concentration of the dopant in solvent, CNT-TFTs changed from p-type to ambipolar, and eventually n-type characteristics.

Solution of 18-crown (0.1 mol/L) and KOH (saturated conc.) in N-methylpyrrolidone (NMP) was prepared. The solvent was diluted by NMP as needed. CNTs synthesized by using the enhanced direct-injection pyrolytic synthesis method [2] were used and enriched to semiconductive ones by using an electric-field-induced layer formation (ELF) method [3]. CNT-TFTs were fabricated on Si/SiO₂ substrates. The I_D - V_{GS} characteristics of the devices showed successive changes from p-type to n-type, depending logarithmically on the concentration of dopants.

Acknowledgment: This presentation is based on results obtained from a project subsidized by the New Energy and Industrial Technology Development Organization (NEDO).

References: [1] Y. Nonoguchi et al., Adv. Funct. Mater. 26, 3021 (2016). [2] T. Saito et al., J. Nanosci. Nanotechnol. 8, 6153 (2008). [3] K. Ihara et al., J. Phys. Chem. C 115, 22827 (2011).

***Corresponding Author:** Tel: +81-29-856-1168, E-mail: nihey@cd.jp.nec.com

High-yield fabrication of n-type carbon nanotube thin-film transistors on flexible plastic substrate

○Fu-Wen Tan¹, Jun Hirotani¹, Tomohiro Yasunishi¹, Shigeru Kishimoto¹, and Yutaka Ohno^{1,2}

¹Graduate School of Engineering, Nagoya University, Nagoya 464-8603, Japan

²Institute of Material and Systems for Sustainability, Nagoya University, Nagoya 464-8603, Japan

Carbon nanotube thin-film transistors (CNT TFTs) are envisioned to enable high-performance flexible electronic devices due to its highly desirable electrical and mechanical properties [1,2]. As-fabricated CNT TFT devices are normally p-type under ambient conditions, due to the chemical doping by adsorbing oxygen molecules. However, n-type TFTs are also required for constructing complementary metal-oxide-semiconductor (CMOS)-based circuits with low power consumption and good noise margins. In this work, we achieved a relatively high yield of 95.3 % for more than 800 n-type CNT TFTs on a flexible substrate.

Bottom-gate type TFTs were fabricated on a flexible and transparent poly(ethylene naphthalate) (PEN) substrate as shown in Fig. 1. Semiconductor-enriched CNTs were used for the channel material. Prior to n-type doping, we confirmed that all devices (831 devices) showed p-type behavior with on/off ratio of $\sim 10^4$ and rather uniform characteristics. Then, polyethyleneimine (PEI) (Sigma Aldrich, MW = 800) was spin-coated to achieve n-type doping. An Al_2O_3 passivation layer was formed by atomic layer deposition [3].

Figure 2 shows the transfer characteristics of 827 operational devices after PEI doping with Al_2O_3 passivation. 99.5% of 831 devices were converted to n-type behavior by the PEI doping method without significant degradation of on current and mobility. The other devices (4 devices) did not work after doping due to gate leakage current or damage during measurement. Although low on/off ratio and threshold voltage shift toward the normally-on condition were observed for a few percentages of devices, a majority of the TFTs maintained on/off ratio of $\sim 10^4$, with a small hysteresis width of 0.25 V on average.

[1] Q. Cao *et al.*, Nature **454**, 495 (2008).

[2] D.-M. Sun *et al.*, Nat. Nanotechnol. **6**, 156 (2011).

[3] T. Yasunishi, *et al.*, Jpn. J. Appl. Phys. **53**, 05FD01 (2014).

Corresponding Author: Y. Ohno

Phone & Fax: +81-52-789-5387,

E-mail: yohno@nagoya-u.jp

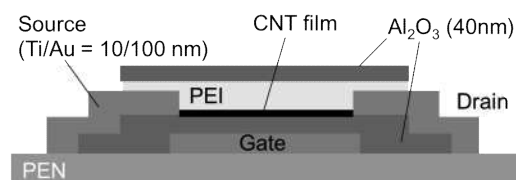


Fig.1 Schematic structure of n-type device.

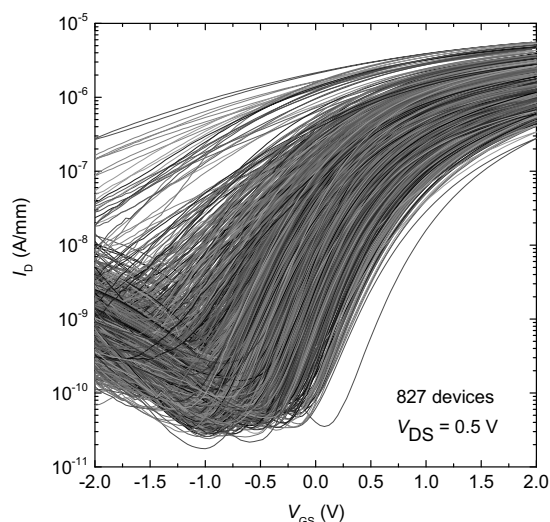


Fig. 2 I_D - V_{GS} characteristics at $V_{DS} = 0.5$ V of 827 CNT TFTs after PEI doping.

Response to pH of carbon nanotube thin-film transistors for sensor applications

○Kana Hasegawa¹, Nguyen Xuan Viet¹, Takuya Ushiyama¹,
Shigeru Kishimoto¹, Yutaka Ohno^{1,2}

¹Graduate School of Engineering, Nagoya University, Nagoya 464-8603, Japan

²Institute of Materials and Systems for Sustainability, Nagoya University, Nagoya 464-8603, Japan

Carbon nanotube field-effect transistors (CNT FETs) are promising platform as highly-sensitive electronic biosensors because of its excellent electrical property [1]. On the other hand, they lack in controlling the uniformity and mass production, causing large variation in characteristics. In our previous work, thin-film transistors (TFTs) based on a random CNT thin film are advantageous, compared to FETs based on individual CNTs from the viewpoint of uniformity and reproducibility [2]. In this study, we investigate sensor behavior of CNT TFTs to understand their operation in biological environments, which are typically electrolytic solutions.

CNT TFTs were fabricated in an electrolyte-gated transistor architecture, where single-walled CNT thin film connected two metal electrodes, source and drain (Fig. 1 (a)), and directly contacted with electrolytic solution. A liquid gate potential was applied to an Ag/AgCl (3-M NaCl) reference electrode respect to the grounded source electrode. The TFT was placed in a fluidic channel to avoid evaporation of test solution and make it easy to change solutions as shown in Fig. 1(b).

First, we examined the response to pH without varying the ion species and ion strength. Figure 2 shows the time-domain response measured at $V_{DS} = -0.05$ V and $V_{GS} = -0.1$ V when pH was varied between 6 and 8. Here, the electrolytic solution was 1-mM PBS and 10-mM NaCl solutions. The I_D exhibited linear dependence on pH as shown in the inset of Fig. 2. The response can be explained by ionization and deionization of functional groups on the CNT surface, depending on proton concentration [3].

[1] I. Heller *et al.* Nano Lett. **8**, 591 (2008).

[2] N.X. Viet *et al.* The 49th FNTG General Symp. 2P-7 (2015)

[3] T Haeberle *et al.* Appl. Phys. Lett. **101**, 223101 (2012).

Corresponding Author: Y. Ohno

Tel: +81-52-789-5387, Fax: +81-52-789-5387

E-mail: yohno@nagoya-u.jp

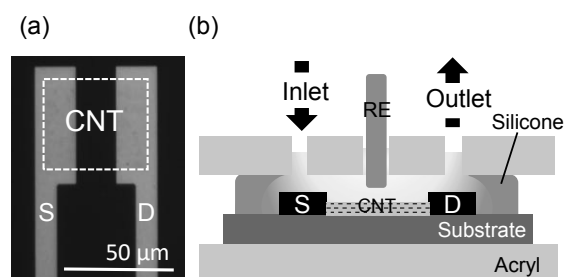


Fig. 1 (a) Fabricated CNT TFT, (b) schematic of measurement system.

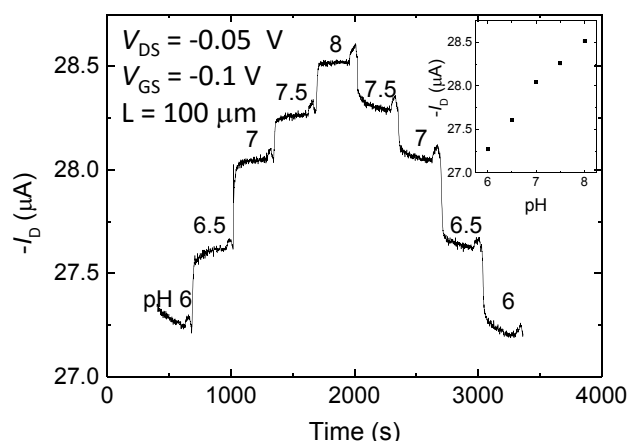


Fig. 2 Response to pH in 1-mM PBS and 10-mM NaCl solution. (inset) Drain current vs pH.

n-Type Thermoelectric Properties of Single-walled Carbon Nanotubes encapsulating 1,1'-Bis(diphenylphosphino)ferrocene

○Yu Iihara¹, Yoshiyuki Nonoguchi¹ and Tsuyoshi Kawai¹

¹Graduate School of Materials Science, Nara Institute of Science and Technology
8916-5 Takayama, Ikoma, Nara, 630-0192, Japan

n-Type single-walled carbon nanotubes (SWNTs) have been investigated for the development of flexible p-n junction devices including solar cells [1] and FETs [2]. n-Type SWNTs have been regarded as unstable under ambient condition, which has motivated us to improve air-stability by means of molecular doping. We have recently demonstrated that adsorption of phosphine derivatives alters the sign of majority carriers of SWNTs from p-type to n-type [3]. However, phosphine-SWNT composites showed limited stability in air.

In this work, we report on the n-type doping and the stabilization of n-type SWNTs using the encapsulation of phosphine derivatives in SWNTs. The internal space of nanotubes is expected to suppress the oxidation. We chose 1,1'-Bis(diphenylphosphino)ferrocene (dppf) as a dopant since it shows a stable redox behavior. We prepared SWNTs encapsulating dppf (dppf@SWNTs) by heating dppf/SWNTs composite films at 200 °C *in vacuo*.

TEM observation revealed that dppf was encapsulated into SWNTs (Fig 1). The conductivity of the dppf@SWNTs significantly enhanced compare to raw SWNTs, presumably due to the electron transfer from dppf to SWNTs. This composite showed comparatively high power factor ($195 \mu\text{W}/\text{mK}^2$) with the negative Seebeck coefficient ($-51 \mu\text{V}/\text{K}$) by encapsulation of dppf (Table 1). Moreover, we found this n-type film was stable over 120 h in air [4].

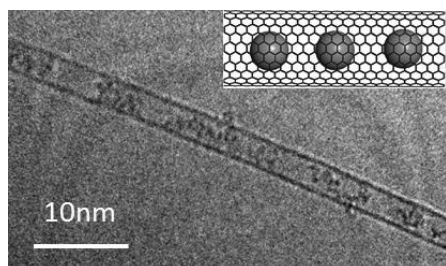


Figure 1. TEM micrograph of dppf@SWNTs

	Seebeck Coefficient ($\mu\text{V}/\text{K}$)	Conductivity (S/cm)	Power factor ($\mu\text{W}/\text{mK}^2$)
SWNTs	48	600	141
dppf/SWNTs	-4.6	596	1.5
dppf@SWNTs	-51	758	195

Table 1. Thermoelectric properties of SWNTs, dppf/SWNTs, dppf@SWNTs

[1] Taylor, A. D. *et al.* Nano Lett. **14**, 3388–3394 (2014).

[2] Dai, H. *et al.* J. Am. Chem. Soc. **123**, 11512–11513 (2001).

[3] Y. Nonoguchi *et al.* Sci. Rep. **3**, 3344 (2013).

[4] Y. Iihara *et al.* Chem. Asian. J. doi: 10.1002/asia.2016 00810 (2016).

Corresponding Author: Y. Nonoguchi

Tel: +81-743-72-6181, Fax: +81-743-72-6179,

E-mail: nonoguchi@ms.naist.jp

Gradual etching and long-length burning of metallic single-walled carbon nanotubes toward semiconducting nanotube arrays

○Taiki Inoue¹, Keigo Otsuka¹, Shohei Chiashi¹, Shigeo Maruyama^{1,2}

¹ *Department of Mechanical Engineering, The University of Tokyo, Tokyo 113-8656, Japan*

² *Energy NanoEngineering Lab., National Institute of Advanced Industrial Science and Technology (AIST), Ibaraki. 305-8564, Japan*

High carrier mobilities and finite band gaps of semiconducting (s-) single-walled carbon nanotubes (SWCNTs) make them a promising candidate for channel materials of future electronics. While random networks of separated s-SWCNTs have provided high enough performances for thin film transistor applications, high-purity and well-aligned s-SWCNT arrays are required for high-speed field-effect transistors (FETs) in logic circuit applications. Direct-growth of aligned SWCNTs together with long-length selective removal of metallic (m-) SWCNTs is a possible way for scalable fabrication of s-SWCNT arrays.

We developed methods for controlled etching as well as long-length removal of m-SWCNTs. Firstly, horizontal arrays of SWCNTs were grown on crystal quartz substrates by alcohol chemical vapor deposition [1] and transferred onto silicon with silicon dioxide substrates. Back-gated FET structures were fabricated by defining source and drain electrodes with 20 μm channel width and 5 - 20 μm channel lengths. Source–drain voltages were applied to SWCNT channels in various atmospheres, including ambient air, vacuum, water vapor, and oxygen with water vapor. Sequential application of increased voltages to SWCNTs in water vapor conditions was found to induce gradual extension of nanogaps in SWCNTs (Fig. 1) [2]. We also found that the long-lengths of m-SWCNTs were burnt away by applying voltages to polymer-coated SWCNTs under water vapor and oxygen conditions (Fig. 2).

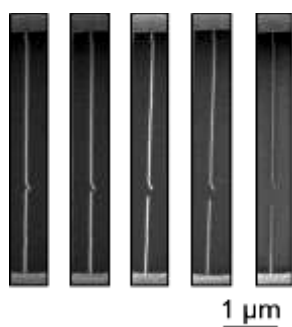


Fig.1: Gradual etching of SWCNTs.

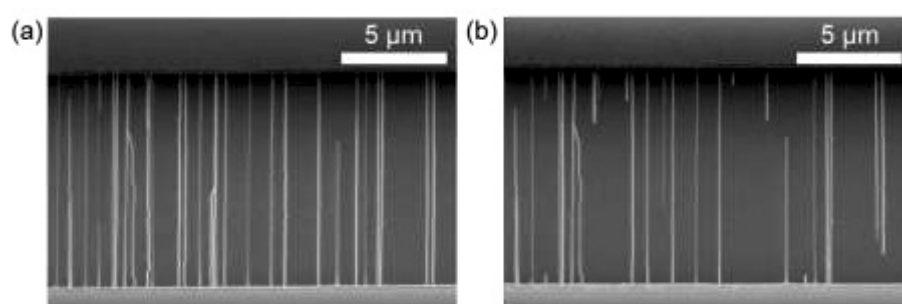


Fig.2: (a) Before and (b) after long-length selective burning of m-SWCNTs.

[1] S. Maruyama *et al.*, Chem. Phys. Lett., 360 (2002) 229.

[2] K. Otsuka *et al.*, submitted.

Corresponding Author: S. Maruyama

Tel: +81-3-5841-6421, Fax: +81-3-5800-6983

E-mail: maruyama@photon.t.u-tokyo.ac.jp

Effect of 7,8-substituents of Flavin Derivatives on Selective Separation of Single-Walled Carbon Nanotubes

Kanako Nishimura¹, Fumiya Toshimitsu¹, Naotoshi Nakashima^{1,2}

¹ Department of Applied Chemistry, Kyushu University, Fukuoka 819-0395, Japan

² WPI-F²CNER, Kyushu University, Fukuoka 819-0395, Japan

Single-walled carbon nanotubes (SWNTs) are classified to metallic (m-) or semiconducting (s-) SWNTs according to their chirality, which is expressed by chiral index (n,m). Separation of them is very important for use them in many applications. Several efficient sorting methods including gel chromatography method [1], density gradient ultracentrifugation method [2,3], use of oligo DNA [4], aqueous two-phase extraction method [5], use of dynamic coordination [6] and hydrogen polymer-based supramolecular chemistry [7] have been reported.

Recently, we found that a flavin derivative that has a long alkyl chain and an imidyl hydrogen can selectively sort s-SWNTs [8] by synthesizing various types of flavin derivatives by changing the length of an alkyl chain and replacing an imidyl hydrogen with a methyl group. It was revealed that the imidyl hydrogen and methyl group(s) on the 7,8-positions of the aromatic ring are essential for selective separation of s-SWNTs. However, it is not clear whether the substituents of 7,8-positions affect the selective separation or not. We now synthesized flavin derivatives that have a different substituent of 7,8-positions, and focus on the size and the electronic property of the substituents. From both experimental and simulations, we reveal important factors that recognize/sort s- and m-SWNT chirality.

This abstract is based on results obtained from a project commissioned by the New Energy and Industrial Technology Development Organization (NEDO).

- [1] H. Kataura *et al.*, *Nat. Commun.* **2011**, 2, 309.
- [2] M. C. Hersam *et al.*, *Nat. Nanotech.* **2006**, 1, 60.
- [3] R. B. Weisman *et al.*, *Nat. Nanotech.* **2010**, 5, 443.
- [4] M. Zheng *et al.*, *Nat. Mater.* **2003**, 2, 338.
- [5] M. Zheng *et al.*, *ACS Nano* **2015**, 9, 5377.
- [6] F. Toshimitsu and N. Nakashima, *Nat. Commun.* **2014**, 5, 5041.
- [7] F. Toshimitsu and N. Nakashima, *Sci. Rep.* **2015**, 5, 18066.
- [8] N. Nakashima *et al.*, *Chem. Lett.* **2015**, 44, 556.

Corresponding Author: N. Nakashima

Tel: +81-92-802-2840, Fax: +81-92-802-2840

E-mail: nakashima.naotoshi.614@m.kyushu-u.ac.jp

Efficient growth and chirality control of single-walled carbon nanotubes by extended alcohol catalytic chemical vapor deposition

○Bo Hou¹, Cheng Wu^{2,3}, Yoko Iizumi³, Takahiro Morimoto³, Toshiya Okazaki³, Taiki Inoue², Shohei Chiashi², Rong Xiang², and Shigeo Maruyama^{1,2}

¹ *Energy NanoEngineering Lab., Department of Energy and Environment, AIST, Tsukuba 305-8564, Japan*

² *Department of Mechanical Engineering, The University of Tokyo, Tokyo 113-8656, Japan*

³ *Nanotube Research Center, AIST, Tsukuba 305-8564, Japan*

Here we report the efficient growth of super-small diameter SWNTs, high-quality SWNTs ($G/D > 70$) and selective growth of SWNTs by extending the work window of conventional alcohol catalytic chemical vapor deposition (ACCVD). CVD temperature was varied from 350 °C to 1000 °C combined with the pressures range over 6 magnitudes. Scanning Raman with many laser lines, absorption, and photoluminescence (PL) were used to characterize the chirality and abundance of SWNTs. TEM was employed for examining the quality of SWNTs and for exploring the condition of catalysts around growth boundary. Super-small diameter SWNTs assigned as (6,4), (5,4), (5,3), (6,1) etc.. ($0.8 \text{ nm} > d_t > 0.52 \text{ nm}$) were obtained around 500 °C, 5 Pa, and their abundances were significantly increased comparing to previous reported works. At 850 °C, 65 Pa, high-quality SWNTs which is nearly no defect were obtained. In addition, growth mechanism is clarified through discussions on the experimental map of extended CVD.

Furthermore, effect of the carbon feedstocks [ethanol, dimethyl ether (DME) and acetonitrile] and catalysts (zeolite-supported Fe-Co, Cu-Co and W-Co) were studied in the extended CVD. Gas-phase thermal decomposition of ethanol, DME and acetonitrile were simulated using the chemical kinetic models under various SWNTs growth conditions. In addition, the different effects on the diameter and diameter distribution of SWNTs by ethanol, DME and acetonitrile were discussed. By using Fe-Co as the catalyst, the efficient growth of super-small diameter SWNTs was achieved in extended ACCVD. Cu-Co and W-Co were used to obtain chirality controlled SWNTs. Using Cu-Co catalysts, (6,5) became predominant at 500 °C. Growth of super-small diameter SWNTs, high-quality SWNTs and the chirality controlled SWNTs in extended ACCVD suggest the promising future works for application and fundamental understanding of growth of SWNTs.

Corresponding Author: Shigeo Maruyama

Tel: +81-29-861-2073, Fax: +81-29-851-7523,

E-mail: maruyama.nano@aist.go.jp

Growth of Single-Walled Carbon Nanotubes from Solid-Phase Cobalt Carbide Nanoparticles by Molecular Dynamics Simulations

○Ryo Yoshikawa^{1,2}, Hiroyuki Ukai¹, Yukai Takagi¹, Yann Magnin³, Shohei Chiashi¹, Christophe Bichara³, Shigeo Maruyama^{1,2}

¹ Department of Mechanical Engineering, The University of Tokyo, Tokyo 113-8656, Japan

² National Institute of Advanced Industrial Science and Technology, Ibaraki 305-8564, Japan

³ CINaM, Aix Marseille University, 13288 Marseille Cedex 9, France

Since single-walled carbon nanotubes (SWCNTs) grow from metal nanoparticles in catalytic chemical vapor deposition (CCVD) process, observation of metal nanoparticles is indispensable for understanding the mechanism of SWCNT growth. While it is difficult to observe nanoparticles in atomic scale experimentally, simulation is useful to observe them.

In this study, we performed molecular dynamics (MD) simulations to investigate the melting point of Co catalyst particle and the time evolution of SWCNT growth, using home-made Tersoff-type and Brenner-Tersoff potential. We put a Co nanoparticle at the center of 10-nm cubic cell and annealed it for 2 ns measuring the kinetic energy and the potential energy of the system, and then supplied carbon atoms into the cell. During the simulation, metal atoms were under Nosé-Hoover thermostat to keep the temperature of the system.

Figure 1 (a) shows the potential energy of pure Co nanoparticles depending on the cluster size and the temperature. We estimated the melting points from the energy jumps and confirmed that the melting point is a linear function of cubic root of the number of metal atoms (Fig. 1 (b)). Though pure Co₈₀ and Co₁₂₀ clusters are liquid at 1550 K, they formed solid carbide structure when carbon atoms were supplied to them. The particles remained solid carbide during and after the cap structures appeared (Fig. 2). Carbon atoms adsorbed and diffused on the surface of particles to reach the edge of SWCNTs, and then contributed to the SWCNT growth.

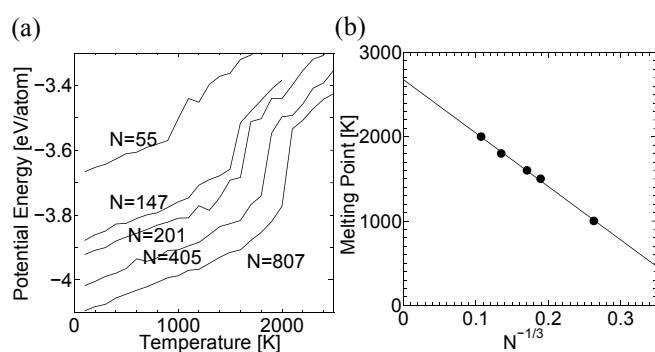


Fig. 1. (a) Energy jump of Co nanoparticles.

(b) Size dependence of melting points estimated from (a).

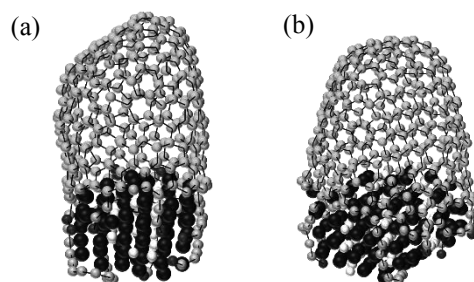


Fig. 2. Co carbide formation and SWCNT growth.

(a) Cubic carbide, 80 Co atoms, 1550 K.

(b) Layered carbide, 120 Co atoms, 1550 K.

Corresponding Author: S. Maruyama

Tel: +81-3-5841-6421 Fax: +81-3-5800-6983 E-mail: maruyama@photon.t.u-tokyo.ac.jp

In-Plane TEM Imaging of Bimetallic Catalyst for SWNT Growth

○Rong Xiang¹, Akihito Kumamoto², Hua An¹, Taiki Inoue¹, Shohei Chiashi¹, Yuichi Ikuhara², Shigeo Maruyama^{1,3}

¹ *Department of Mechanical Engineering, The University of Tokyo, Tokyo 113-8656, Japan*

² *Institute of Engineering Innovation, The University of Tokyo, Yayoi 2-11-16, Bunkyo-ku, Tokyo 113-8656, Japan*

³ *Energy NanoEngineering Laboratory, National Institute of Advanced Industrial Science and Technology (AIST), 1-2-1 Namiki, Tsukuba, 305-8564, Japan*

Catalyst is critical for the formation of single walled carbon nanotubes (SWNTs), while obtaining the intrinsic morphology and structure of these nano-sized particles at growth or near-growth conditions remains challenging. We propose an in-plane TEM approach, which enables a direct characterization of catalyst particles on a thin SiO₂ film. After optimization, collective information of many particles, as well as atomic resolution of catalyst structure can be obtained. With this new technique, we systematically investigated mono- and bi-metallic particles including Co, Fe, Ni, Pd, Pt, and W, and studied their behaviors at high temperatures.

In this work, we focus on two bimetallic catalyst systems that are recently proposed: Co-Cu and Co-W. The combination of Co-Cu was found to be able to produce all sub-nm vertically aligned SWNTs. [1] In-plane TEM clearly shows that, with addition of Cu, much smaller Co particles form epitaxially on Cu. This authoring effort contributes to the formation of high density small active growth sites. Co-W recently raises to be a promising catalyst for chirality-selective growth. [2] We used a sputtered Co-W and produced spatially uniform (12,6) SWNTs with enrichment of 50-70%. [3] An intermediate Co₆W₆C structure is unambiguously identified by selective area electron diffraction. High resolution TEM and high-angle annular dark-field (HAADF) STEM images reveal the details of this complex catalyst. We believe this in-plane TEM technique provides atomic yet statistic information that is so far the closest to a realistic growth process.

References:

[1] K. Cui et al., *Nanoscale* **8**, 1608 (2016).

[2] F. Yang et al., *Nature* **510**, 522 (2014).

[3] H. An et al, *Nanoscale*, (2016), in press.

Corresponding Author: Shigeo Maruyama

Tel: +81-3-5841-6421, Fax: +81-3-5800-6983

E-mail: maruyama@photon.t.u-tokyo.ac.jp

Oxidative Decomposition of Carbon Nanotubes and Extraction of Encapsulated Materials

○Miho Yamagishi¹, Haruka Omachi^{1,2}, Masachika Kato¹, Ryo Kitaura¹,
and Hisanori Shinohara^{1,3}

¹ Department of Chemistry, Graduate School of Science, Nagoya University, Nagoya
464-8602, Japan

² Research Center for Materials Science, Nagoya University, Nagoya, 464-8602, Japan

³ Institute for Advanced Research, Nagoya University, Nagoya, 464-8602, Japan

Carbon nanotubes (CNTs) have cylindrical structure which provide an ideal cavity to create one-dimensional (1D) nanomaterials. Recently, we have established synthesis of thin single-wall BN-nanotubes and diamantane polymers inside CNT [1,2]. However, since the synthesized 1D materials are remained inside CNTs, it is hard to reveal the actual properties of 1D materials. Hence, removal of the CNT shell is required to isolate encapsulated 1D nanomaterials.

In this research, we developed oxidative decomposition of CNTs under mild conditions. With the reaction progress, absorption spectra of CNTs were gradually decreased (Fig.1a). Most of peaks were finally disappeared after 24 hours. Interestingly, D/G ratio was improved in early stage of the reaction (Fig.1b). The decomposition was indicated to have high selectivity, as the reaction start from defects of the CNT shells. We then demonstrated the extraction of C₆₀ fullerene from C₆₀@SWCNT nano-peapod by using this CNT decomposition technology (Fig.1c). Isolation of other encapsulated 1D nanomaterials will also be reported in this presentation.

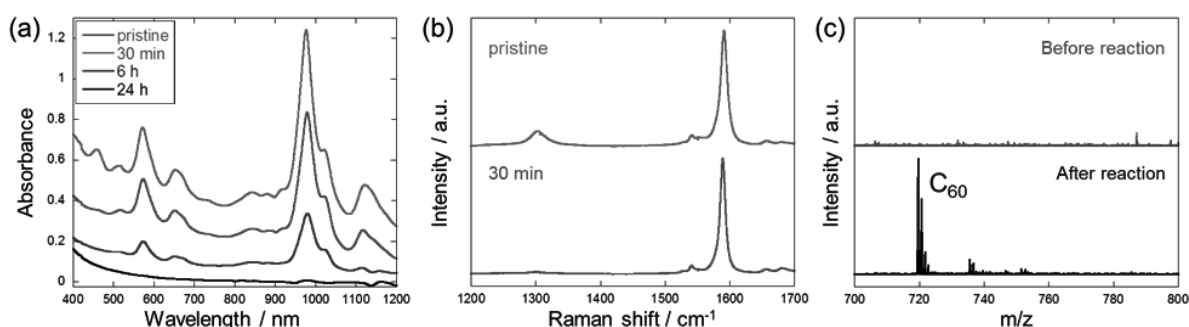


Fig. 1: (a) UV-Vis-NIR spectra and (b) Raman spectra of CNT dispersion at each reaction stage
(c) Mass spectra of toluene extraction before and after the decomposition treatment of C₆₀@SWCNT

[1] R. Nakanishi, *et al.*, *Sci. Rep.* **3**, 1385 (2013).

[2] Y. Nakanishi, *et al.*, *Angew. Chem., Int. Ed.*, **54**, 10802 (2015).

Corresponding Author: Haruka Omachi, Hisanori Shinohara

Tel: +81-52-789-2482, Fax: +81-52-747-6442

E-mail: omachi@chem.nagoya-u.ac.jp, noris@nagoya-u.jp

Growth of Single-Crystal Bi-Layer Graphene Using Alcohol CVD

○Masaki Sota¹ Mohamed Atwa^{1,2}, Kotaro Kashiwa¹, Naomasa Ueda¹, Xiao Chen¹,
Taiki Inoue¹, Rong Xiang¹, Shohei Chiashi¹, Shigeo Maruyama^{1,3}

¹ Department of Mechanical Engineering, The University of Tokyo, Tokyo 113-8656, Japan

² Department of Integrated Devices and Circuits, Royal Institute of Technology, Stockholm
SE-164 40 Kista, Sweden

³ Energy NanoEngineering Lab., National Institute of Advanced Industrial Science and
Technology (AIST), Ibaraki 305-8564, Japan

Graphene, an sp^2 -bonded single-layer carbon sheet, is an attractive material due to its extraordinary mechanical, thermal, and electrical properties. However, single-layer graphene (SLG) is the zero band-gap material and unsuitable for some applications which need finite energy gaps. Several groups reported that a bandgap up to 250 meV can be opened by an external electric field in AB-stacked bi-layer graphene (BLG) [1]. Therefore, efficient synthesis of BLG is essential for electronic applications of graphene. Chemical vapor deposition (CVD) is a reliable method for the synthesis of large-scale graphene. Since grain boundaries in polycrystal graphene degrade its superior properties, many efforts have been focused on enlarging the size of single-crystal graphene. As a result, single-crystal SLG of centimeter sizes has been synthesized using CVD, but the size of single-crystal BLG domains is still limited.

In this study, we investigated the method for the single-crystal BLG synthesis and succeeded in synthesizing BLG domains of several hundreds of micrometers. Graphene was synthesized using alcohol catalytic chemical vapor deposition (ACCVD) [2]. We used a copper foil as the catalyst and oxidized and folded it into a pocket before synthesis. CVD was performed at 1065 °C with various pressures of Ar/H₂ and ethanol. We found that SLG, BLG, and multi-layer graphene can be grown by controlling the total pressure of the CVD condition. Figure 1 shows large-size single-crystal BLG together with SLG. Figure 2 is the relationship between the graphene size and the growth time. This revealed that there is an incubation time for BLG growth after starting alcohol supply.

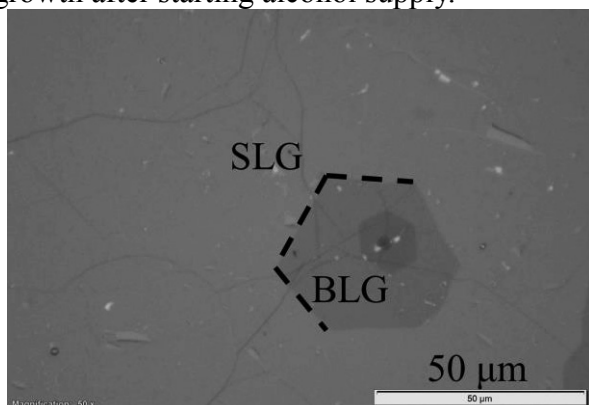


Fig. 1 Optical image of SLG and BLG.

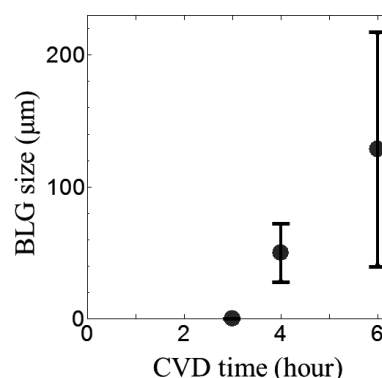


Fig. 2 Relationship between BLG size and growth time.

[1] Y. Zhang *et al.* Nature **459**, 820 (2009).

[2] X. Chen *et al.* Carbon, (2016) in press.

Corresponding Author: S. Maruyama

Tel: +81-03-5841-6421, Fax: +81-03-5841-6421,

E-mail: maruyama@photon.t.u-tokyo.ac.jp

Effects of nanobar-catalyst types on structure of graphene nanoribbon grown with advanced plasma CVD

○Yuta Wato, Hiroo Suzuki, Toshiro Kaneko, and Toshiaki Kato

Department of Electronic Engineering, Tohoku University, Sendai 980-8579, Japan

Graphene nanoribbons (GNR) combine the unique electronic and spin properties of graphene with a transport gap that arises from quantum confinement and edge effects. Although GNR can be made in a variety of ways, the reliable site and alignment control of GNR with high on/off current ratios remains a challenge.

Up to now, we have developed a novel method based on the advanced plasma CVD with nano scale Ni catalyst (Ni nanobar) for directly fabricating suspended GNR devices [1, 2]. Although this method has outstanding advantages in terms of precise site and alignment controlled growth of suspended GNR, there still remain a space to be studied about this method, especially for the structural controllability of GNR such as layer number, width, and length. At the current state, the dominant GNR structures are few layered GNR with ~10 nm width and relatively short length (~500 nm). Monolayer GNR with narrower width and longer length should be useful for the optoelectrical applications of suspended GNRs with higher performance.

In this study, we attempted to elucidate the effects of catalyst types with nanobar structures on the structure of GNRs. Based on our previous study about the growth model of GNR, it is found that the nanobar structure becomes liquid phase under the high temperature condition during the GNR growth and the wettability of liquid phase nanobar is very important to grow suspended GNR [2]. Then, we systematically carried out the growth of GNR with various types of catalysts such as Ni, Cu, and those of bi-metals with different mixture ratios. The averaged GNR length grown with Cu nanobar becomes longer than that grown with Ni nanobar, which can be explained by the difference of carbon solubility, wettability, and thermal stabilities of Cu nanobar. GNR grown with Cu nanobar shows the relatively higher on/off ratio, this can imply the layer number of GNR can be reduced by using Cu nanobar.

[1] T. Kato and R. Hatakeyama, *Nature Nanotechnology* **7**, 651 (2012).

[2] H. Suzuki, T. Kaneko, Y. Shibuta, M. Ohno, Y. Maekawa and T. Kato, *Nature Communications* **7**, 11797 (2016).

Corresponding Author: Y. Wato

Tel: +81-22-795-7046, E-mail: yuta.wato.s8@dc.tohoku.ac.jp

Enhancement of laser-induced water decomposition by 2D sheets studied by first-principles simulations II

○Yoshiyuki Miyamoto¹, Hong Zhang², Xinlu Cheng³ Angel Rubio⁴

¹ *Research Center for Computational Design of Advanced Functional Materials, AIST, Umezono, 1-1-1 Central 2, Tsukuba 305-0685, Japan*

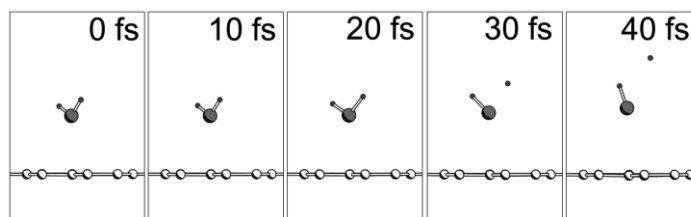
² *College of Physical Science and Technology, Sichuan University, Chengdu 610065, China*

³ *Key Laboratory of High Energy Density Physics and Technology of Ministry of Education; Sichuan University, Chengdu, 610064, China*

⁴ *Max Planck Institute for the Structure and Dynamics of Matter and Center for Free-Electron Laser Science, Luruper Chaussee 149, 22761 Hamburg, Germany*

This work was motivated by recent report of metal-free photocatalysis consisting of graphitic carbon nitride (gC₃N₄) [1,2] and we have proposed usage of high-intensity pulse laser as an alternative to ordinary light-source for achieving higher yield of H₂O decomposition. Continuing to our presentation in the last meeting, we are still investigating property of 2D material in enhancement of laser-induced H₂O decomposition by means of the first-principles simulation. Here we present updated results; 1) We have compared threshold laser intensity of H₂O decomposition for an isolated molecule and for molecules above 2D-sheets, and we will present dependence of pulse-width of the laser. 2) We have proposed an idea to combine electrical hole-doping in graphene and pulse-laser H₂O decomposition for higher yield of H and OH generation.

We have obtained significantly lower threshold laser-intensity of H₂O decomposition when H₂O is above 2D sheets. [3] The cause of the threshold lowering is attributed as a field enhancement effect by the 2D sheets studied by this work. The threshold is further decreased when we extended the full-width-of-half-maximum (FWHM) from 10 fs to 20fs, yet the estimated laser fluence for the H₂O becomes larger with wider FWHM. The details of the computational method, results, and potential application for generating hydrogen fuel will be discussed. The figure shows snapshot of the H₂O dynamics which was strongly bind to graphene under electrical hole-doping condition. (At the beginning, the O-side of water is closer to graphene due to polar nature of the H₂O molecule.)



Snapshots of H₂O dynamics upon pulse-laser illumination (FWHM=10fs, 800nm) with laser field intensity 7V/Å.

This work is supported by the fund from MEXT, Japan, Grant-in-Aid for Scientific Research on Innovative Areas "Science of Atomic Layers (SATL)" (Project No.16H00925)

[1] X. Wang *et al*, Nature Mat. **8**, 76 (2009).

[2] J. Liu *et al*, Science **347**,970 (2015).

[3] Paper in preparation.

Corresponding Author: Y. Miyamoto

Tel: +81-29-849-1498, Fax: +81-29-851-5428,

E-mail: yoshi-miyamoto@aist.go.jp

Size separation of graphene nanosheets by gel chromatography

○Shunichi Ishiguro, Takaaki Tomai, Yuta Nakayasu, Naoki Tamura, Itaru Honma

*Institute of Multidisciplinary Research for Advanced Materials, Tohoku University,
Sendai 980-8577, Japan*

Top-down graphene production via the exfoliation from graphite produces a mass of graphene, but with structural variations in layer number, sheet size, edge type, and defect density, which strongly affect the electronic structure of graphene. For the useful application, the subsequent structural separation of graphene is mandatory.

In this study, we demonstrated simple separation of graphene using multicolumn gel chromatography [1]. The graphene dispersed in the aqueous surfactant solution was separated via flowing through the allyl dextran-based gel columns in series (Fig. 1).

At the first column, by the filtering effect, the unexfoliated graphite fragments are separated out, and the unbound fragment consisted of thin graphene sheets. By the chromatographic separation at the subsequent columns, it was observed that the large-size graphene tends to be unbound by the gel (Table 1). In this chromatographic separation, the surfactant affinity affects the adsorption priority on the gel. The reduction of surfactant absorption density on the graphene caused by the structural disorder, in-plane defect and edge, will result in the preferential attachment of small-size graphene on the gel surface [2, 3]. This scalable simple separation method will contribute to the further precise separation of graphene structure, and promote the industrial application of graphene.

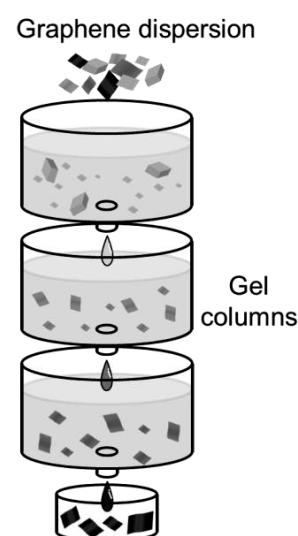


Fig.1 Schematic diagram of gel chromatography

Table 1. The average sheet sizes of the unbound graphene for each column

Column Number	1	3	10
Sheet Size [nm]	56.70	71.12	142.5

[1] H. Liu *et al.*, *Nat. Commun.* **2**, 309 (2011).

[2] A. G. Hsieh *et al.*, *J. Phys. Chem. B* **117**, 7950 (2013).

[3] A. J. Glover *et al.*, *J. Phys. Chem. C* **116**, 20080 (2012).

Corresponding Author: T. Tomai

Tel: +81-22-217-5818, Fax: +81-22-217-5828

Email: ishiguro@mail.tagen.tohoku.ac.jp

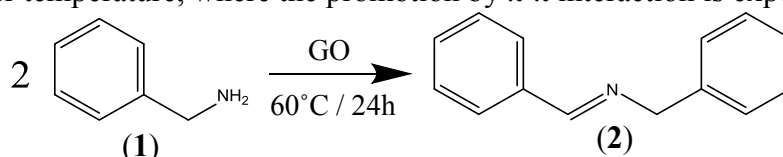
Evaluation of GO Catalyst regarding oxidative amine coupling reaction

○Takuya Isaka¹, Kentaro Tajima¹, Tomoki Yamashina¹, Yutaka Ohta², Kazuyuki Takai^{1,2}

¹Graduate School of Science and Engineering, Hosei University, Tokyo 184-8584, Japan

²Department of Chemical Science and Technology, Hosei University, Tokyo 184-8584, Japan

Graphene oxide (GO) having oxygen-containing groups is expected as metal-free and environment-compatible catalyst. The research on GO catalyst progressed [1][2], although the detail mechanism for GO catalytic activity is not clear yet. Investigating GO properties before / after the catalytic reaction is a promising strategy for clarification of the mechanism. Our previous study found that the synthesis of a xanthene derivative in water solvent might relate with the functional group of C=O and COOH in GO [3]. But the simultaneous structural changes by a thermal reduction was problem. In this study, we conduct the oxidative amine coupling reaction of benzylamine (**1**) to *N*-benzylidenebenzylamine (**2**) using GO progressing even at the lower temperature, where the promotion by π - π interaction is expected.



Scheme 1 Oxidative amine coupling reaction of benzylamine to *N*-benzylidenebenzylamine

The following reaction using GO synthesized by Hummers method was conducted (Scheme 1). A mixture of (**1**) (3 mL) and GO (0.1 g) was stirred at 60°C for 24 hours after pre-ultrasonication. After filtration of GO from the reaction media and washing with ethanol, the reaction media was characterized by GC-MS. The chemical structure of GO before / after the reaction was evaluated by FTIR.

The GC-MS yields for (**2**) in the condition with / without GO were 15% and 2%, respectively. According to the FTIR spectrum for oxidative amine coupling reaction (Fig.1), the reduction of oxygen-containing functional groups of GO does not occur in the control condition (only GO and water), while those are considerably reduced after oxidative amine coupling reaction. In contrast, the spectra for the reaction in water solvent are almost same in the control condition and after reaction. It was suggested that the reaction mechanism for oxidative amine coupling reaction significantly differs from that for the reaction in water solvent, where GO works as Brönsted acid.

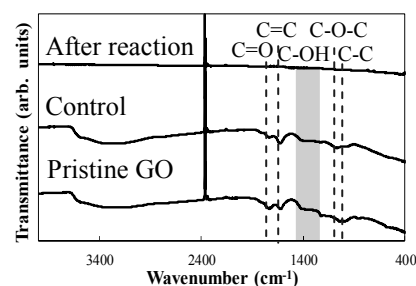


Fig.1 FTIR for GO on oxidative amine coupling reaction

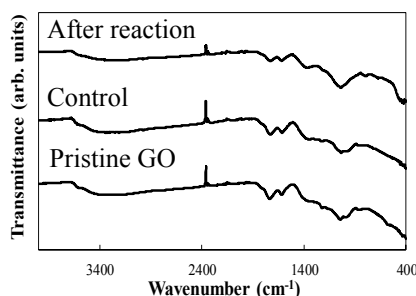


Fig.2 FTIR for GO on the synthesis reaction of a xanthene derivative

[1]C. Su, M. Acik, K. Takai *et al. Nat. Commun.*, **3**, 1298, (2012)

[2]A. Shaabani, M. Mahyari, and F. Hajishaabanha, *Res. Chem. Intermed.*, **40**, 8, 2799–2810 (2014)

[3]FNTG50 conference, T. Isaka *et al*

Corresponding Author: Kazuyuki Takai

Tel: +81-42-387-6138, Fax: +81-42-387-7002, E-mail: takai@hosei.ac.jp

Magnetic Characterization of NO_x adsorption by Nanographene Host Material

Satomi Nishijima¹, Asataro Yamada¹, Kazuyuki Takai^{1,2}

¹ Graduate School of Science and Engineering, Hosei University, Tokyo 184-8584, Japan

² Department of Chemical Science and Technology, Hosei University, Tokyo 184-8584, Japan

NO_x are one of the major chemical species causing acid rain pollution, where NO molecule is major species at the source of pollution. To eliminate gaseous NO_x diluted in huge volume of air, adsorption by activated carbon fibers (ACFs) is investigated as a promising strategy [1]. However, the details mechanism of NO_x adsorption has been not well known yet. In microscopic view point, ACFs consists of 3D random network of nanographenes, which is interesting host material having nanospace between nanographenes and the localized spins originating from the electronic states at edge part. In this study, adsorption properties and chemical reactivity of NO and its derivatives in activated carbon fibers as nanographene host material is investigated in terms of spin magnetism.

Gaseous NO molecule was adsorbed into activated carbon fibers (FR-20, Kuraray) vacuum-heat-treated in advance. The magnetic susceptibility was measured by SQUID magnetometer (MPMS-1 Quantum Design) at 1 T in the range of 2 – 300 K, where the magnetization was measured in the field of 0 – 1 T at 2 K. X-band ESR measurement was performed by using JEOL FA-300. The temperature dependence of the susceptibility indicates the significant reduction in the localized spin density N_s of ACFs upon adsorption of 5.7 kPa of NO gas (N_s = 7.9 × 10¹⁹ to 3.3 × 10¹⁹ spin g⁻¹), where the Weiss temperature θ decreases from -7 to -2. The reduction in the exchange interactions between spins is also confirmed by the magnetization curve at 2 K. This is well explained by the NO pressure dependence of ESR for ACFs (Fig. 1). The rapid reduction of ESR linewidth and g-value upon even slight amount of NO molecule indicates strong antiferromagnetic interactions between edge-state spins and NO spins caused by adsorption of NO molecule on the edge of nanographene. On the other hand, the ESR intensity gradually reduces at the lower NO pressure but becomes increasing and decreasing again at the higher pressure, suggesting the termination of the edge-state spins by NO chemisorption on the edge of nanographene with simultaneous physisorption of magnetic NO molecules and their dimerization at the higher NO pressure. The mechanism of elimination NO by ACFs are revealed as the fast chemisorption process on the edges of nanographene followed by physisorption into nanospace among nanographene in ACFs in by investigation in terms of spin magnetism as probe.

[1] T. Shimohara et al, *J. Jpn. Soc. Atmospheric Env.*, **48**, 65-73 (2013) [2] T. Enoki and K. Takai, *Solid State Comm.*, **149**, 1144-1150 (2009).

Corresponding Author: Kazuyuki Takai

Tel: +81-42-387-6138, Fax: +81-42-387-7002,

E-mail: takai@hosei.ac.jp

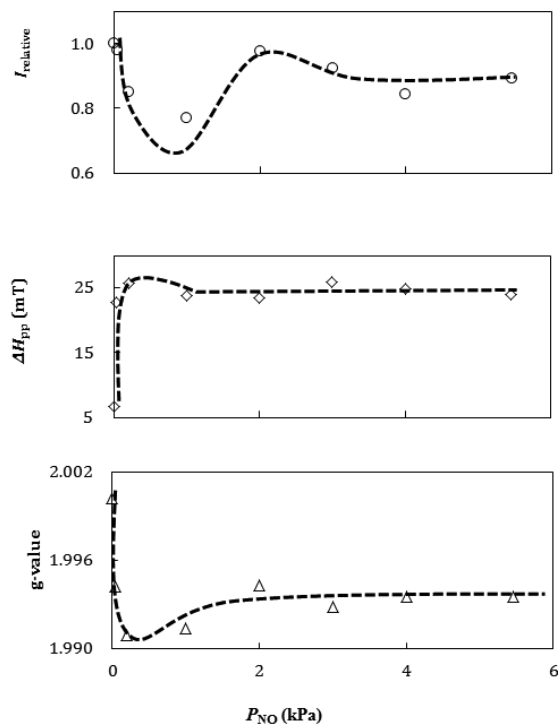


Fig. 1 NO pressure dependence of ESR intensity (a), linewidth (b), and g-value (c)

Electrochemical grafting of aryl molecules onto graphene on Au

○Shun Tanno¹, Yusuke Sato², Ryota Kumagai³, Koji Nakashima³,
Masaru Kato^{1,2}, Satoshi Yasuda³, Kei Murakoshi³, Ichizo Yagi^{1,2}

¹Graduate School of Environmental Science, Hokkaido University, Sapporo 060-0810, Japan

²Faculty of Environmental Earth Science, Hokkaido University, Sapporo 060-0810, Japan

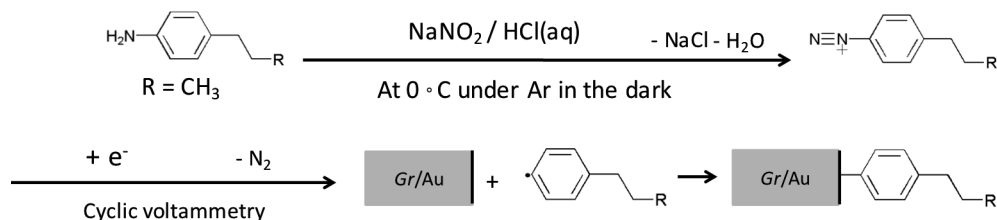
³Department of Chemistry, Faculty of Science, Hokkaido University, Sapporo 060-0810, Japan

Graphene has been expected to be used as electronic device materials thanks to its high mechanical strength and electroconductivity. Graphene surfaces can be modified to control its electronic properties and interactions with other materials. Aryl molecules are chemically grafted to graphene monolayers on SiO₂ and Al₂O₃ (sapphire) substrates.^[1] To make tunnel junctions, we need to graft molecules densely packed and highly oriented on graphene electrodes.

Herein, we report electrochemical grafting of aryl molecules onto graphene on polycrystalline Au, Au(poly). Graphene was grown on Au(poly) substrates by chemical vapor deposition.^[2] Electrochemical grafting of 4-propylphenyl group onto the graphene surface was performed by electrochemical reduction of *in situ* generated aryldiazonium cations.^[3, 4] Graphenes before and after molecular grafting were characterized by Raman spectroscopy.

Raman spectra showed that a few layers of graphene covered Au(poly). D band intensity over G band intensity ratios (I_D/I_G) of graphene were determined to be 0.438 and 2.66 before and after grafting, respectively. This result indicated that 4-propylphenyl groups may be grafted onto edges and defects of graphene on Au(poly). We will also discuss electrochemical grafting of aryl molecules onto graphene on Au(111).

Scheme 1: Electrochemical reduction of in-situ generated aryldiazonium cations on gold.



[1] Q. H. Wang, *et al.*, *Nature Chem.*, **4**, 724, (2012). [2] S. Yasuda, *et al.*, *J. Phys. Chem. Lett.*, **6**, 3403, (2015).

[3] T. Breton, *et al.*, *Langmuir*, **24**, 8711, (2008). [4] S. Boland, *et al.*, *Langmuir*, **24**, 6351, (2008).

Corresponding Author: S. Tanno

Tel: +81-11-706-2258, Fax: +81-11-706-4529,

E-mail: shuntanno@ees.hokudai.ac.jp

Fabrication of Graphene Composite Plasmon-Active Photoelectrode

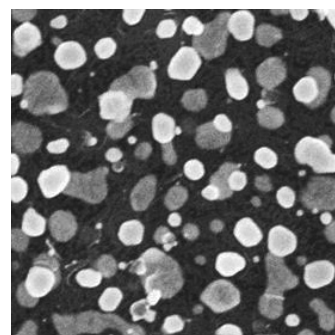
○Kensuke Yasuda, Hiro Minamimoto, Zhou Ruifeng, Satoshi Yasuda, Kei Murakoshi

*Department of Chemistry, Faculty of Science, Hokkaido University,
Sapporo 060-0810, Japan*

It is well known that Au nano-structures supported on TiO₂ (Au / TiO₂) substrate generate photocurrent under near-infrared light illumination due to the excitation of localized surface plasmon resonance. Although it is possible to improve the usability of light beyond the intrinsic limits of the materials, the photoelectronic conversion efficiency is still low for the application in photovoltaic devices. In order to enhance the photoelectronic conversion efficiency of this system, it can be expected that the formation of nano multi-layer structures using thin materials is one of the effective way. Graphene, which has good mechanical, electrical, and optical properties, can be considered as an appropriate material for the system. In this study, we tried to fabricate the graphene composite Au / TiO₂ photoelectrode for high efficiency photoelectric conversion devices. In addition, micro Raman measurement was also carried out for the analysis of its properties.

Plasmon active Au nano structures were deposited on an n-type TiO₂ substrate. Single graphene layer synthesized by CVD method was transferred onto the Au / TiO₂. Then, Au nano structures were deposited on the graphene layer again (Au / Graphene / Au / TiO₂). SEM image of the prepared substrate is shown in Fig. 1. From the image, the formation of Au / Graphene / Au layer structure was confirmed. Additionally, through the photoelectrochemical measurements, it was found that the photocurrent response was completely different from Au / TiO₂ substrates. As the next step, *in-situ* electrochemical Raman measurements were performed as shown in Fig. 2. Consequently, we have succeeded in evaluating the career transfer process and electronic state of the Au / Graphene / Au / TiO₂ system.

Corresponding Author: K. Murakoshi
TEL: +81-(0)11-706-2704, FAX: +81-(0)11-706-4810
E-mail: kei@sci.hokudai.ac.jp



— 200 nm

Fig. 1. SEM image of the Au / Graphene / Au / TiO₂ substrate.

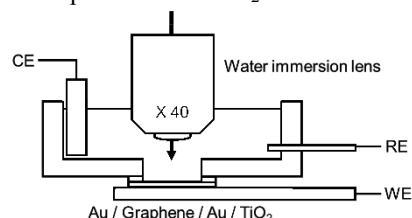


Fig. 2. Schematic illustration of the system for *in-situ* electrochemical Raman spectroscopy. C.E.: Pt wire, R.E.: Ag/AgCl (sat. KCl), electrolyte solution: 0.5 M Na₂SO₄. Excitation wavelength was 785 nm.

Direct observation of ultrafast carrier dynamics in graphene on SiC(000 $\bar{1}$) studied by time- and angle-resolved photoemission spectroscopy

○T. Someya¹, H. Fukidome², H. Watanabe³, T. Yamamoto¹, M. Okada¹, H. Suzuki⁴, Y. Ogawa¹, T. Iimori¹, N. Ishii¹, T. Kanai¹, K. Tashima², B. Feng¹, S. Yamamoto¹, J. Itatani¹, F. Komori¹, K. Okazaki¹, S. Shin¹ and I. Matsuda¹

¹ Institute for Solid State Physics, The University of Tokyo, Kashiwa 277-8581, Japan

² Research Institute of Electrical Communication, Tohoku University, Sendai 980-8577, Japan

³ Department of Physics, Osaka University, Suita 565-0871, Japan

⁴ Department of Physics, The University of Tokyo, Bunkyo-ku 113-0033, Japan

Because of its broadband absorption, high carrier mobility, and ultrafast optical response, graphene attracts the attention of many researchers as a promising material for next-generation optoelectronic devices. Nowadays, many graphene-based optoelectronic devices are test-manufactured and demonstrated to have a certain practical capability. However, contrary to this fact, the most elementary phenomena, i.e., the photo-excited carriers in graphene, is not exactly understood. Therefore, uncovering the carrier dynamics in graphene is essential not only for designing graphene-based optoelectronic devices but also for improving their performance.

In this study, we performed time- and angle-resolved photoemission spectroscopy (TRARPES) on graphene epitaxially grown on a SiC(000 $\bar{1}$) C-terminated surface to reveal underlying relaxation mechanisms of photo-excited graphene carriers. TRARPES has been one of the most powerful experimental techniques to trace a transient distribution of photo-excited carriers owing to its simultaneous accessibility to both momentum and energy spaces. As an example, Figure 1 shows the TRARPES spectra of the C-face graphene taken at several delay times ($h\nu_{\text{pump}} = 1.55 \text{ eV}$, $660 \mu\text{J}/\text{cm}^2$, 300 K). In the poster session, we will show the pump fluence and lattice temperature dependence of the obtained transient electronic temperatures and discuss the possible decay scheme of the photo-excited graphene carriers.

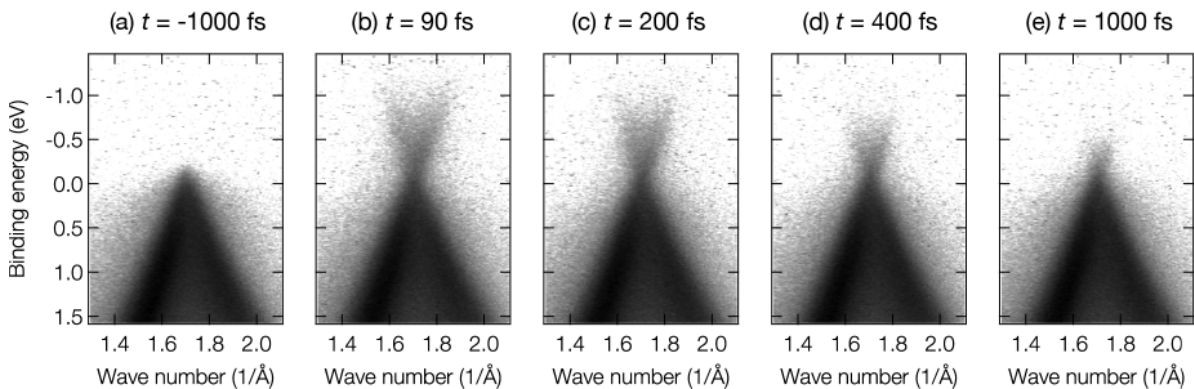


Figure 1. TRARPES spectra of the C-face graphene taken near \bar{K} point at pump-probe delays of (a) -1000fs, (b) 90 fs, (c) 200 fs, (d) 400 fs and (e) 1000 fs, respectively.

Corresponding Author: I. Matsuda

Tel: +81-(0)4-7136-3402,

E-mail: imatsuda@issp.u-tokyo.ac.jp

Work function modulation of edge functionalized graphene nanoflakes

Remi Taira, Ayaka Yamanaka, and Susumu Okada

University of Tsukuba, 1-1-1 Tennodai, Tsukuba, Ibaraki, 305-8571 Japan

Electronic structure of graphene nanoflakes is sensitive to their sizes, edge atomic structure, and edge functionalized groups. Graphene nanoribbons with hydrogenated edges are known to be either metals or semiconductors depending on their width and edge morphology. According to their tunable electronic structure by the morphology and chemical modification, graphene nanoflakes are keeping a premier position in emerging materials for various functional devices in the wide areas of the modern technology. Therefore, in the present work, we aim to investigate how the work function and electronic structure of the graphene nanoflakes depend on the functionalized groups using the density functional theory with the local density approximation. To investigate the effect of the functionalized groups attached to the graphene edges, we consider the graphene nanoribbon with width of 1.5 nm and zigzag edges of which edges are asymmetrically terminated by H and functionalized groups R , where R are -O, -OH, -COH, and -COOH. Figure 1 shows the electrostatic potential of the asymmetrically terminated graphene ribbons on the plane normal to the ribbon direction. For all functionalized groups except OH, the work function at the edge functionalized by these groups is larger than that at the H-terminated edge. In contrast, the edge with OH functionalization exhibits opposite nature: The calculated work function at the OH-terminated edge is smaller than that at the H-terminated edge.

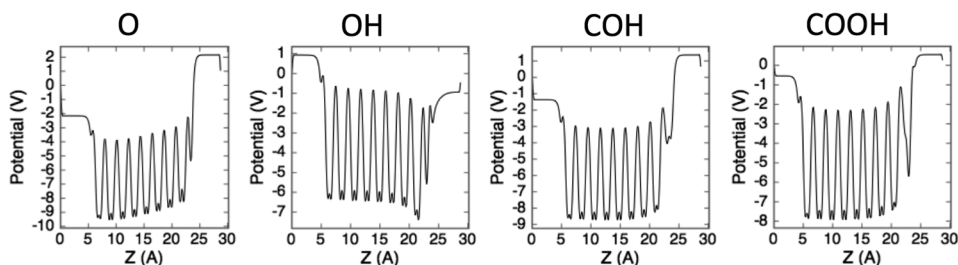


Fig. 1: Electrostatic potential of asymmetrically edge functionalized graphene ribbons with O, OH, COH, and COOH groups.

Corresponding author: R. Taira (resoccermi222@gmail.com)

Charge/Covalent Interactions at the Interface between Graphene and Electrolyte

○Daisuke Suzuki¹, Kazuyuki Takai^{1,2}

¹ Graduate School of Science and Engineering, Hosei University, Tokyo 184-8584, Japan

² Department of Chemical Science and Technology, Hosei University, Tokyo 184-8584, Japan

Phenomena at the interface between carbon electrode and electrolyte such as storage and degradation mechanism, Solid Electrolyte Interphase (SEI) formation are crucial for the performance of energy storage devices. However the phenomena are still unclear because of complicated structure of conventional carbon electrode materials. In this study, the electrochemical interactions at the interface between graphene electrode as the model structure of carbon electrode materials and electrolyte solution is investigated in order to clarify the phenomena in energy storage devices.

Gate voltage dependence of the conductivity was measured for graphene FET on SiO₂ substrate with the bipolar electrochemical configuration, where the graphene channel and Pt wire in the electrolyte were applied as working and counter electrodes, respectively. 1 M KCl and 1 M LiCl aqueous solution and 1 M LiBF₄ organic solution (EC/DMC) were used as electrolyte solution. Raman spectroscopy (532 nm) was carried out under an atmospheric condition. A reversible behavior of the transfer curve and an irreversible behavior of the electrochemical currents upon cycles of sweeping top gate voltage were observed in both KCl and LiCl solutions. In the case of LiBF₄ organic electrolyte solutions, increment of electrochemical current below -2 V becomes suppressed after cycles of gate sweeping (Fig.1). This is attributed to SEI formation by the reaction between graphene and EC/DMC [1] [2]. In either condition, the position of G band and 2D band didn't change in Raman spectroscopy, indicating the absence of chemical doping. On the other hand, D band appeared at only edge parts in graphene in 2D-Raman mapping after electrochemical cycles in LiBF₄ (Fig.2). SEI formation occurs by the reaction between chemically active graphene edges and EC/DMC, suggesting significant roles of edge of carbon electrode in actual energy storage devices.

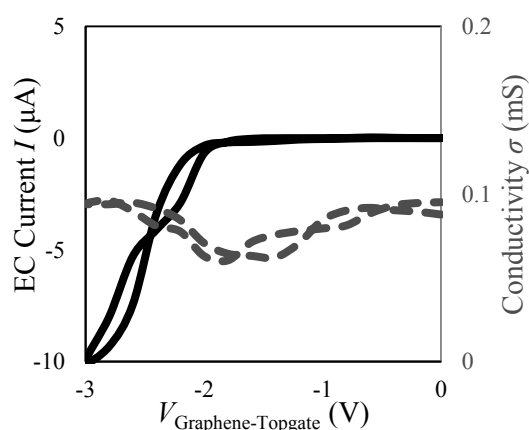


Fig.1 Gate voltage dependence of Conductivity in FET with LiBF₄ organic electrolyte

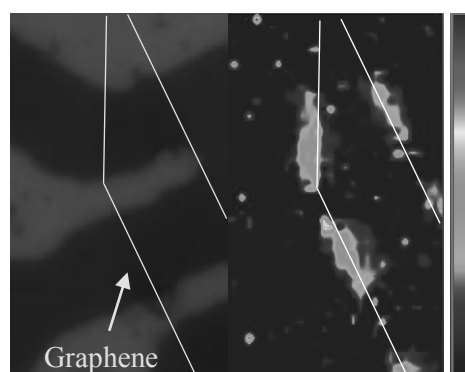


Fig.2 D band mapping of graphene after electrochemical cycles

[1] Elad Pollak *et al*, Nano.lett. **10**, 3386 (2010) [2] Jingshu Hui *et al*, ACS.Nano. **10**, 4248 (2016)

Corresponding Author: Kazuyuki Takai

Tel: +81-42-387-6138, Fax: +81-42-387-7002, E-mail: takai@hosei.ac.jp

Growth and optical properties of Nb-doped WS₂ monolayers

○Shogo Sasaki¹, Yu Kobayashi¹, Zheng Liu^{2,3}, Kazutomo Suenaga³
Yutaka Maniwa¹, Yuhei Miyauchi⁴, Yasumitsu Miyata^{1,5}

¹Department of Physics, Tokyo Metropolitan University, Hachioji 192-0397, Japan

²Inorganic Functional Materials Research Institute, AIST, Nagoya, 463-8560, Japan

³Nanomaterials Research Institute, AIST, Tsukuba, 305-8565, Japan

⁴Institute of Advanced Energy, Kyoto University, Uji 611-0011, Japan

⁵JST, PRESTO, Kawaguchi 332-0012, Japan

For atomic layers of transition metal dichalcogenides, alloying is one of the most useful ways to control their physical properties. To date, several groups have been reported that composition dependence of bandgap on monolayer Mo_{1-x}W_xS₂ alloys [1, 2]. In contrast, it is still an important issue to understand the effects of substitutional doping of the other elements to create impurity states and modulate carrier densities. To solve this issue, we have developed a growth method of monolayer Nb-doped WS₂ and investigated its optical properties [3]. In this presentation, we report the nonlinear behavior of photoluminescence (PL) intensity in monolayer Nb-doped WS₂.

Monolayer Nb-doped WS₂ crystals were grown on SiO₂/Si substrates by halide-assisted chemical vapor deposition (CVD) [4] using WO₃, Nb and NaCl powders at 800 ~ 850 °C under argon/sulfur atmosphere. Scanning transmission electron microscope observation reveals that the Nb atoms were substituted into the W site at a rate of 0.5%. Nb-doped samples have new PL peaks (L) at 1.4-1.6 eV with free excitons peak (X) at room temperature (Fig. 1a). The intensities of peak L show a saturation behavior with the increase in excitation power (Fig. 1b). We found that this behavior can be reproduced by the rate equation model for a three-level system consisted of free excitons (X), localized excitons (L), and ground states (Fig. 1b). These results indicate that the observed PL peaks are assignable to the emission from impurity states generated by the substitution of Nb as shown in Fig. 1c.

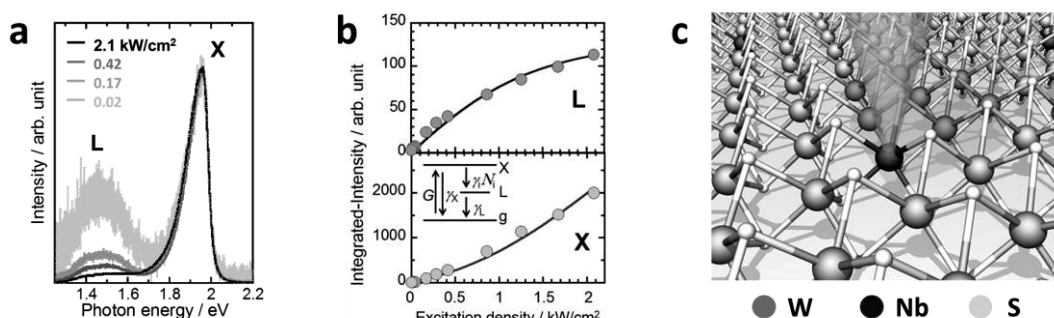


Fig. 1 (a) Normalized PL spectra of Nb-doped WS₂ measured at four different laser powers. (b) PL intensities of L (upper panel) and X (lower panel) peaks plotted as a function of excitation density. Solid lines indicate the fitting results. The inset shows a schematic of the three-level system of doped WS₂. (c) Schematic illustration of PL from an Nb-doped site in monolayer WS₂.

- [1] Y. Chen *et al.* ACS Nano **7**, 4610–4616 (2013). [2] Y. Kobayashi *et al.* Nano Res. **8**, 3261–3271 (2015).
[3] S. Sasaki *et al.* Appl. Phys. Express **9**, 071201 (2016). [4] S. Li *et al.* Appl. Mater. Today **1**, 60–66 (2015).
Corresponding Author: Yasumitsu Miyata, Tel: +81-42-677-2508, E-mail: ymiyata@tmu.ac.jp

Layer number controlled synthesis of integrated WS₂ array

○Chao Li, Toshiro Kaneko, Toshiaki Kato

Department of Electronic Engineering, Tohoku University, Sendai 980-8579, Japan

Recently, relatively new type of two-dimensional (2D) nano materials such as graphene and transition metal dichalcogenide (TMD) initiate new avenue in electronic science domain as their atomically thin thickness, superior electrical, mechanical and optical properties [1-4].

As one of the promising nano-materials, graphene possesses high carrier mobility and high optical transmittance, which can be a potential candidate for next generation electrical devices with high performance. Nevertheless, it is very difficult to be straightly applied for the semiconducting device fields due to its zero band gap. Layered TMD that is well known as its excellent semiconducting properties, which can be tuned from indirect band gap to direct band gap by controlling its layer number from multilayer to monolayer. However, there still remain lots of issues we have to conquer for the practical applications with TMD-based devices. Above all, position, crystal size, orientation, and layer number controlled synthesis are regarded as crucial issues at the current production stage.

In our research group, we have developed a unique method, which can realize the position controlled synthesis of monolayer and single-crystal WS₂ in large scale with Au dot as a nucleation guide [5]. In this research, we improved the previous method and realized layer number controlled synthesis of the integrated WS₂ array by adjusting the growth condition. Since the suitable layer number of TMD crystal strongly depends on the type of applications, layer number control for the integrated WS₂ is very important subject. We explored that the Ar gas flow rate is very sensitive to the layer number of WS₂ grown from gold dot. With Ar gas flow rate ranging from low to high, layer number of WS₂ can be controlled from monolayer to few-layer, which may attribute to the difference of growth speed ratio of vertical to lateral direction within the range of Ar flow rate used in our study.

[1] T. Kato and R. Hatakeyama, ACS Nano **6** (2012) 8508.

[2] T. Kato and R. Hatakeyama, Nature Nanotechnology **7** (2012) 651.

[3] T. Kato and T. Kaneko, ACS Nano **8** (2014) 12777.

[4] H. Suzuki, T. Kaneko, Y. Shibuta, M. Ohno, Y. Maekawa, and T. Kato, Nature Communications, **7** (2016) 11797.

[5] T. Takahashi, T. Kato, T. Kaneko, Abstract of the 50th Fullerenes-Nanotubes-Graphene General Symposium p. 178, 2016.

Corresponding Author: Chao Li

Tel: +81-22-795-7046, Fax: +81-22-263-9225,

E-mail: li15@ecei.tohoku.ac.jp

Polarization-resolved photoluminescence spectroscopy on monolayer transition metal dichalcogenides under electrostatic gating

○Wenjin Zhang, Yusuke Hasegawa, Shinichiro Mouri, Kazunari Matsuda, and Yuhei Miyauchi

Institute of Advanced Energy, Kyoto University, Uji, Kyoto 611-0011, Japan

Mono- and few-layers of transition-metal dichalcogenides (TMDs) MX_2 , where M and X are a transition metal (typically Mo, W, Ta) and a chalcogen (typically S, Se or Te), respectively, have recently emerged as two dimensional (2D) semiconductors promising for future electronics and optoelectronics applications beyond graphene [1-6]. Their hexagonal lattice structures are similar to those of graphene, but unlike graphene with zero band gap, some monolayer (1L) TMDs have finite direct band gaps; this facilitates semiconductor device applications of these 2D materials. In 1L TMDs such as MoS_2 and WSe_2 , there are two inequivalent valleys, K and K', in momentum space. The strong spin-orbit interaction and the intrinsic structural inversion asymmetry enable a mutual conversion between valley polarized states and circularly polarized photons [3, 4]; this unique property further makes these materials attractive, especially for exploiting new families of devices relying on valley degree of freedom in signal processing, called valleytronics. However, relaxation of the polarized valley state is very fast, and it has been strongly desired to clarify the valley relaxation mechanism and prolong the valley lifetimes in 1L-TMDs.

Here we examine the effect of carrier density on the polarized photoluminescence (PL) properties reflecting the valley polarization states and lifetimes of excitons (and trions) to understand the valley relaxation mechanism in 1L-TMDs. Fig. 1 shows the source-drain current (I_{ds}) versus gate voltage (V_{g}) measured on a 1L- MoS_2 field-effect transistor (FET) device (inset) fabricated to modulate the carrier density. Effects of the electrostatic gating on the polarization-resolved photoluminescence spectra at low temperature conditions will be discussed.

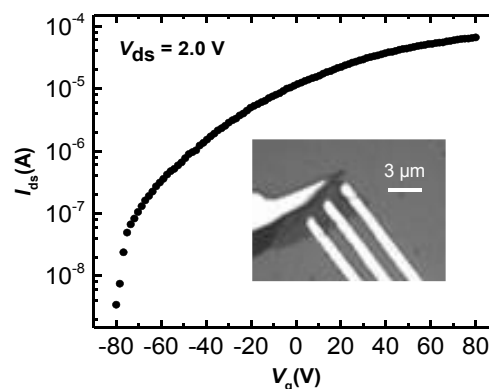


Fig. 1. Source-drain current (I_{ds}) versus gate voltage (V_{g}) measured on the fabricated monolayer MoS_2 FET device. Inset shows a picture of the device.

- [1] S. Koirala *et al.*, *Phys. Rev. B.* **93**, 075411 (2016)
- [2] S. Mouri, Y. Miyauchi, and K. Matsuda, *Nano Lett.* **13**, 5944 (2013)
- [3] K. F. Mak *et al.*, *Nat. Nanotechnol.* **7**, 494 (2012)
- [4] D. Xiao *et al.*, *Phys. Rev. Lett.* **108**, 196802 (2012)
- [5] K. F. Mak *et al.*, *Nat. Mater.* **12**, 207 (2013)
- [6] C. Chakraborty *et al.*, *Nat. Nanotechnol.* **10**, 507 (2015)

Corresponding Author: Y. Miyauchi

Tel/Fax: +81-774-38-3463/+81-774-38-4567

E-mail: miyauchi@iae.kyoto-u.ac.jp

Electron beam lithography induced strain in MoS₂ crystal

○Masahiro Matsunaga¹, Ayaka Higuchi¹, Guanchen He², Tetsushi Yamada¹, Peter Krüger¹
Jonathan P. Bird^{1,2}, Yuichi Ochiai¹ and Nobuyuki Aoki^{1,3}

¹ Graduate School of Advanced Integration Science, Chiba University,
Chiba 263-8522, Japan

² Department of Electrical Engineering, University at Buffalo, SUNY,
Buffalo, New York 14260-1920, USA

³ JST-PRESTO, Kawaguchi, Saitama 332-0012, Japan

In recent studies, molybdenum disulfide, MoS₂, which has layered structure, has been attracted lots of interests because of its properties [1]. Typically, it exhibits semiconducting properties having a band gap of 1.8 eV in the monolayer structure. Therefore, it has been studied so as to be utilized as a field effect transistor (FET). In our study, we use scanning gate microscopy (SGM) to examine characteristic of MoS₂. SGM can visualize local transport properties in semiconducting materials using a metallic coated cantilever as a mobile top gate.

Single layer MoS₂ crystals which were directly grown on SiO₂/Si substrates by chemical vapor deposition and provided by the Ajayan group at Rice University [2]. Source and drain electrodes (Cr/Au) were patterned by electron beam lithography [3].

In our previous study [4], we reported that unusual SGM response was observed inside the channel. In addition, huge potential drop was occurred at the same position where SGM response was observed. We concluded that a different electric property was induced by electron beam exposure.

Here, we measured photoluminescence and Raman mapping of MoS₂ crystal having exposed and unexposed region. From the results, compressive strain is induced by electron beam exposure. Moreover, the exposed region has slightly wider band gap than the unexposed (usual) one. Therefore, a small potential barrier is formed at the boundary between the exposed and the unexposed MoS₂ and then it behaves active in the SGM image.

Furthermore, we calculated the relationship between a band gap shift and an induced biaxial strain to estimate by a first principle DFT calculation. We estimated that ~0.3 % strain is induced by electron beam exposure.

The work was supported in part by JST-PRESTO and the Science of Atomic Layers, a Grant in Aid for Scientific Research from MEXT.

[1] Q. H. Wang *et al.*, Nature Nanotech. **7**, 699 (2012).

[2] Y. Zhan *et al.*, Small **8**, 966 (2012).

[3] G. He *et al.*, Nano lett. **13**, 4212 (2015).

[4] A. Higuchi *et al.*, The 50th FNTG General Symposium 1P-38 (2016).

Corresponding Author: N. Aoki

Tel: +81-43-290-3430, Fax: +81-43-290-3427

E-mail: n-aoki@faculty.chiba-u.jp

Optimization of Preparation Conditions for Fibrous Aggregates of Single-Walled Carbon Nanohorns

○Ryota Yuge¹, Fumiyuki Nihey¹, Kiyohiko Toyama¹, and Masako Yudasaka^{2,3}

¹*IoT devices Research Laboratories, NEC Corporation, Tsukuba 305-8501, Japan*

²*National Institute of Advanced Science and Technology (AIST), Tsukuba, 305-8565, Japan*

³*Graduate School of Science and Technology, Meijo University, Nagoya 468-8502, Japan*

Single-walled carbon nanohorns (SWCNHs) usually assemble in spherical forms [1], and they are attractive having high dispersibility in solutions and large specific surface area. However, for example, when used for electrical capacitors, the low electrical conductivity has been a drawback. Recently, we have succeeded in preparing SWCNHs aggregated in a fibrous form, named as carbon nanobrushes [2]. The carbon nanobrushes have high dispersibility in solutions, large specific surface areas, and high electrical conductivity [3]. Therefore, they are highly expected to show the high performance when used in various electrical devices. The carbon nanobrushes are prepared by CO₂ laser ablation of iron-containing carbon target at room temperature. Currently, the yield of carbon nanobrushes is small and the major products are the spherical aggregates of SWCNHs. In this study, we have optimized the iron-concentration in carbon target to achieve the high yield of carbon nanobrushes. Their structure and electrical properties were also characterized.

In the experiments, the various iron concentrations in the target were tested. The target of 30 mm in diameter and 60 mm in length was rotated at 2 rpm for 30 second during the laser ablation. The CO₂ laser was operated at the power of 3.5 kW in the continuous-wave mode. The buffer gas was nitrogen, and its pressure and flow rate in the growth chamber were kept at about 760 Torr and 10 L/min, respectively, by controlling the evacuation rate.

From SEM and STEM observation of the obtained samples, the ratio of the carbon nanobrushes in samples depended strongly on the iron concentration in carbon targets. Especially, we found that a lot of carbon nanobrushes were prepared at the 1 at %. The TGA measurements showed that combustion temperature of carbon nanobrushes and spherical SWCNHs was almost same. From EDX and XPS measurements, the iron particles were found in carbon nanobrushes, and they were metal iron. The details will be shown in the presentation.

[1] S. Iijima *et al.* Chem. Phys. Lett. **309**, 165 (1999).

[2] R. Yuge *et al.* Ad. Mater. in press.

Corresponding Author: R. Yuge

Tel: +81-29-850-1566, Fax: +81-29-856-6137

E-mail: r-yuge@bk.jp.nec.com

Ambipolar transistors based on random networks of WS₂ nanotubes

○Mitsunari Sugahara¹, Hideki kawai¹, Yohei Yomogida¹, Yutaka Maniwa¹, Susumu Okada², and Kazuhiro Yanagi¹

¹ *Department of Physics, Tokyo Metropolitan University, Tokyo 192-0397, Japan*

² *Pure and Applied Sciences, Tsukuba University, Ibaraki 305-8577, Japan*

Tungsten disulfide (WS₂) nanotubes, which have a cylindrical structure of two-dimensional WS₂ sheet, can exhibit various unique properties because of their quantum conditions along circumference direction. In contrast to single walled carbon nanotubes, which are well-known nanotube materials and have not only semiconducting but also metallic types, WS₂ nanotubes exhibit only semiconducting characteristics regardless of how the sheet is rolled, and thus have great advantages for semiconductor device application such as transistors. However, the random networks of WS₂ nanotubes have not yet shown evidence of suitable electronic properties for applications. For example, previously reported electronic characteristics, such as opto-electronic and field-effect properties, are limited only to a single rope of the WS₂ nanotubes. [1] In this study, we investigated capability of carrier injections on WS₂ nanotubes networks through electrolyte gating approaches, and investigated the potential of WS₂ nanotubes films as semiconducting channels [2]. First, we fabricated WS₂ nanotube random network film on the PTFE-membrane-filter by filtration processes. Then we fabricated a WS₂ nanotube film on a channel between the source and drain electrodes by a transfer process, and compared field-effect transistor characteristics with carrier injections using ionic liquid gating and SiO₂ gating (Fig. 1). In the case of SiO₂ gating, we couldn't observe any field-effect on the source-drain current. However, in the case of ionic liquid gating, we could observe the ambipolar characteristic. Here carriers were injected to WS₂ nanotubes through formation of electric double layers on their surfaces by electrolyte gating. In addition, hole and electron carrier injections were also confirmed by Raman measurements, supporting FET transistor results.

[1] R. Levi et al., Nano Lett. 13, 3736 (2013) [2] M. Sugahara et al., Appl. Phys. Express 9, 075001 (2016)

Corresponding Author: Kazuhiro Yanagi e-mail: yanagi-kazuhiro@tmu.ac.jp

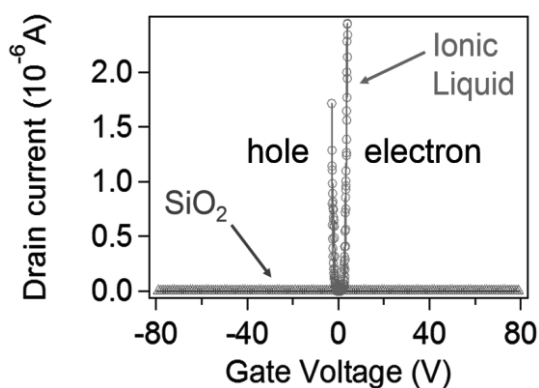


FIG1: Transport properties of electrolyte gating and back-gating on WS₂ nanotube networks

Self-assembled nanofibers of fluorinated bisanthene derivatives○Hironobu Hayashi¹, Hiroko Yamada¹¹ Graduate School of Materials Science, Nara Institute of Science and Technology (NAIST),
8916-5, Takayama-cho, Ikoma, Nara 630-0192

Nanographenes, small pieces of graphene, are regarded as promising fluorescent materials for sensor and bioimaging.¹ There are mainly two ways to prepare nanographenes, that is, top down and bottom-up methods. A bottom-up method has an advantage to synthesize atomically precise nanographenes, which is important for fine-tuning the physical property and understanding the structure-property relationships. A bisanthene is regarded as the smallest type of nanographene with the peak at 650 nm in concentrated sulfuric acid.² While a pristine bisanthene has a fascinating zigzag edged graphene nanoribbon (GNR) character which shows low band gap compared with arm-chaired GNR character,³ it is highly unstable due to the high highest occupied molecular orbital energy level. Therefore, the highly stable bisanthene derivatives are desirable for practical applications.

On the other hand, fluorine has unique properties such as the second smallest van der Waals radius and the largest electronegativity. Therefore, fluorination is known as the powerful method to tune the stability, solubility, redox potential, optical property, and solid state packing of compounds. Here we report the synthesis of *meso*-substituted bisanthene derivatives with different degree of fluorine substitution on bisanthene core. Triisopropylsilyl(TIPS)ethynyl group and phenyl group were introduced at *meso*-position to enhance the stability of the electron rich bisanthene. The effect of fluorine substitution on the physical property and the supramolecular architecture were also investigated.

Briefly, fluorine substitution on bisanthene core effectively tuned the physical properties. The absorption and emission maxima were blue-shifted with increasing the degree of fluorination. It should be noted that TIPSethynyl substituted octafluoro-bisanthene derivative (F8) displayed strong fluorescence at 657 nm with high fluorescence quantum yield (84%) and excellent photostability. We also found that F8 strongly stacked in the solid state and self-assembled into bundles of crystalline-like long nanofibers.

[1] J. Shen, Y. Zhu, X. Yang, C. Li, Chem. Commun. **48**, 3686 (2012).

[2] S. M. Arabei, T. A. Pavich, J. Appl. Spectrosc. **67**, 236 (2007).

[3] A. Konshi, Y. Hirao, K. Matsumoto, H. Kurata, R. Kishi, Y. Shigeta, M. Nakano, K. Tokunaga, K. Kamada, T. Kubo, J. Am. Chem. Soc. **135**, 1430 (2013).

Corresponding Author: H. Hayashi

Tel: +81-743-72-6136, Fax: +81-743-72-6042,

E-mail:hhayashi@ms.naist.jp

Synthesis of Sulfur-doped Graphene Oxides

○Haruka Omachi,^{1,2} Zois Syrgiannis,³ Yasuhiro Kinno,² Maurizio Prato³
and Hisanori Shinohara^{2,4}

¹ *Research Center for Materials Science, Nagoya University, Nagoya, 464-8602, Japan.*

² *Department of Chemistry, Graduate School of Science, Nagoya University.*

³ *Centre of Excellence for Nanostructured Materials (CENMAT), INSTM, Dipartimento di Scienze Chimiche e Farmaceutiche, Università di Trieste, Italy.*

⁴ *Institute for Advanced Research, Nagoya University.*

Sulfur-doped graphene oxide provides an emerging applications such as the material for lithium ion battery, dye-sensitized solar cells and the composition with metal nanoparticles. However, reported methods of sulfur-doping to graphene oxide have employed some harsh reaction conditions such as thermal annealing with sulfur reagents [1].

Here we present synthesis of sulfur-doped graphene oxide by the reaction with Lawesson's reagent. Graphene oxide, prepared by using a modified Hummers method [2], was refluxed with Lawesson's reagent in THF solvent. Resultant sulfur-doped graphene oxide was observed by transmission electron microscopy (TEM) (Figure 1). Energy dispersive X-ray spectrometry (EDX) measurement and X-ray photoelectron spectroscopy (XPS) analysis revealed successful sulfur-doping to graphene oxide. Other characterizations will also be reported in this presentation.

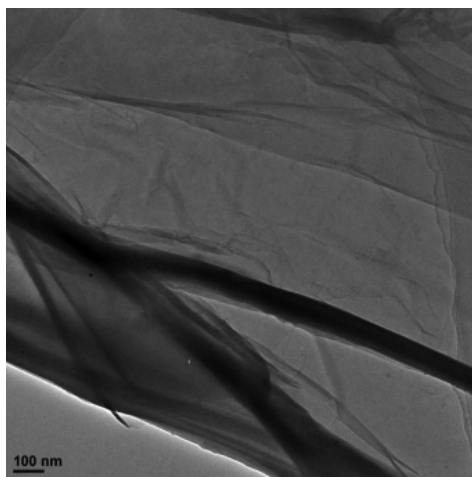


Figure 1. TEM image of synthesized sulfur-doped graphene oxide

[1] (a) Z. Yang *et al.*, *ACS Nano*, **6**, 205 (2012). (b) H. L. Poh *et al.*, *ACS Nano*, **7**, 5262 (2013).

[2] (a) W. S. Hummers *et al.*, *J. Am. Chem. Soc.*, **80**, 1339 (1958). (b) E. L. K. Chng *et al.*, *Chem. Eur. J.*, **19**, 8227 (2013).

Corresponding Author: Haruka Omachi, Hisanori Shinohara

Tel: +81-52-789-2482, Fax: +81-52-747-6442

E-mail: omachi@chem.nagoya-u.ac.jp, noris@nagoya-u.jp

著者索引
Author Index

Author Index

Bold number: Speaker

< A >

Abe, Fumiyoshi	2P-25
Abe, Shuhei	2-11
Abuillan, Wasim	1P-4
Ajiki, Hiroshi	1S-3
Akasaka, Takeshi	2-4
Akita, Seiji	1P-23, 1P-25, 2P-11, 2P-13
An, Hua	2-2 , 3P-19
Anno, Yuki	1P-23, 1P-25
Aoki, Nobuyuki	1-10, 3P-35
Aoshima, Hisae	1P-3
Aoyagi, Shinobu	3P-2, 3P-5
Arie, Takayuki	1P-23, 1P-25, 2P-11, 2P-13
Ariga, Katsuhiko	2P-2
Asaka, Koji	3P-6
Atwa, Mohamed	3P-21
Awaya, Keisuke	1P-28

< B >

Baba, Takuma	1P-12
Baek, Jinseok	3-4, 3P-8
Bairi, Partha	2P-2
Bandow, Shunji	2P-20
Bichara, Christophe	3P-18
Bird, Jonathan P.	1-10, 3P-35
Burk, Alexandra	1P-4

< C >

Chao, Liu	2P-2
Chen, Chin-Fu	2P-39
Chen, Xiao	3P-21
Cheng, Xinlu	3P-23

Chiashi, Shohei	1P-14, 2-2, 3P-15, 3P-17, 3P-18, 3P-19, 3P-21
-----------------	---

Chiu, Yi-Jing	1P-40
Cuong, Nguyen Thanh	1P-27

< D >

D'Arcié, Lorenzo	2-6
De Feyter, Steven	3-5
Dresselhaus, Mildred S.	2P-33

< E >

Eda, Junko	1P-8
Edo, Michiko	2P-16
En, Lim	1P-36
Endo, Kei	3P-11
Endo, Morinobu	1P-24
Endoh, Hiroyuki	3P-11
Esconjauregui, Santiago	2-6

< F >

Fei, Wenxi	2P-35
Feng, Baojie	3P-29
Fujigaya, Tsuyohiko	1P-11
Fujii, Shunjiro	2-3, 2-5, 3P-4
Fujii, Takayuki	1P-18
Fujimoto, Yoshitaka	1-11 , 2-1
Fujita, Takeshi	3-3
Fujita, Yasuhiko	3-5
Fujiwara, Kyosuke	1P-21, 2P-21
Fukidome, Hirokazu	3P-29
Furukawa, Ko	1P-5
Furutani, Sho	1P-6
Futaba, Don	1-4, 1P-10, 2S-5 , 2P-17
Futagoishi, Tsukasa	2P-5

< G >

Gao, Weilu 1P-31
 Gao, Yanlin **1P-34**
 Gorgoll, Ricardo 1P-4
 Greenwood, John 3-5
 Guo, Huaihong 2P-33

< H >

Hano, Shigeki 1P-10
 Harada, Yoichi **1P-31**
 Harano, Koji **1-12**, 1P-4, 2P-2
 Harigai, Toru 1-13
 Hasdeo, Eddwi H. 1P-31, 1P-32
 Hasegawa, Kana **3P-13**
 Hasegawa, Syun **2P-22**
 Hasegawa, Yusuke **2P-30**, 3P-34
 Hashima, Yuki **1P-38**
 Hashimoto, Yoshio 1P-24
 Hashizume, Daisuke 1P-9
 Hata, Kenji 1-4, 1P-10, 2P-10,
 2P-17
 Hatakeyama, Kazuto 1P-26, 1P-28, **2-10**
 Hayami, Shinya 2-10
 Hayashi, Hironobu **3P-38**
 He, Guanchen 1-10, 3P-35
 Higo, Yuji 2P-36
 Higuchi, Ayaka 1-10, 3P-35
 Hill, Jonathan P. 2P-2
 Hiraiwa, Atsushi 2-11
 Hirano, Atsushi 2-3, 2-5, **2P-6**
 Hirano, Masahiro 2P-23, 2P-25
 Hirano, Yu 2P-35
 Hirotani, Jun 1P-17, 3P-12
 Hisakuni, Tomohiko **2P-36**
 Hisashi, Hideyuki **3S-6**
 Hofmann, Mario 1P-40, 2P-39
 Homma, Tatsuya 1P-4
 Honda, Shin-ichi 2P-36

Honma, Itaru 3P-24
 Hou, Bo **3P-17**
 Hsieh, Ya-Ping 1P-40, 2P-39
 Huang, Shengxi 2P-33

< I >

Ideue, Toshiya 1P-9
 Igarashi, Keisuke 2-11
 Iida, Tamio 1-13
 Iihara, Yu **3P-14**
 Iijima, Sumio 2P-15
 Imori, Takushi 3P-29
 Iizumi, Yoko 2P-15, 2P-37, 3P-17
 Ikeda, Keiichiro 3-6
 Ikeda, Tomohiro **1P-13**
 Ikuhara, Yuichi 3P-19
 Ikuma, Naohiko **1P-2**, 2P-1
 Imahori, Hiroshi 2-4, 3-4, 3P-8
 Inaba, Masafumi **2-11**, 2P-35
 Inaba, Saori 2P-1
 Inose, Tomoko 3-5
 Inoue, Daishi 1P-9
 Inoue, Taichi **1P-25**
 Inoue, Taiki 1P-14, 2-2, **3P-15**,
 3P-17, 3P-19, 3P-21
 Inoue, Yuta 3P-1
 Isaka, Takuya **3P-25**
 Ishiguro, Shunichi **3P-24**
 Ishii, Nobuhisa 3P-29
 Ishii, Rieko 2P-6
 Ishikawa, Yasuaki 1P-38
 Ishino, Katsuma 3P-5
 Ishizawa, Sachiko 2P-17
 Isobe, Shigehito **2-7**
 Itatani, Jiro 3P-29
 Ito, Masayuki 1P-3
 Ito, Takatoshi **3P-1**
 Ito, Yoshikazu 3-3

Ivasenko, Oleksandr	3-5			Kiribayashi, Hoshimitsu	1P-18		
Iwai, Toshiyuki	3P-1			Kishimoto, Shigeru	2P-14,	3P-10,	3P-12,
Iwasa, Yoshihiro	1P-9				3P-13		
Iwasawa, Tetsuo	3P-1			Kitaura, Ryo	1P-17,	1P-20,	3P-5,
Iwashita, Kazuki	2P-6				3P-20		
Iwata, Tadao	2P-36			Ko, Jeong Won	3P-3		
Iyoda, Masahiko	3P-2			Ko, Weon Bae	3P-3		
Izumi, Hirokazu	2P-36			Kobashi, Kazufumi	1-4		
				Kobayashi, Daiki	2P-13		
< J >				Kobayashi, Hayato	1P-14		
Jeon, Il	1-3,	2P-3		Kobayashi, Keita	1-7		
Jintoku, Hirokuni	1P-39			Kobayashi, Shiho	1P-23		
				Kobayashi, Yu	1P-22,	1P-35,	2P-28,
< K >					2P-32,	2P-34,	3P-32
Kameda, Tomoshi	2P-6			Kochi, Taketo	3P-9		
Kanai, Teruto	3P-29			Koh, Shinji	2P-23,	2P-24,	2P-25
Kaneko, Toshiro	1-5,	2P-18,	3P-22,	Koinuma, Michio	1P-26,	1P-28,	1P-30,
	3P-33				2-8,	2-10	
Kashiwa, Kotaro	3P-21			Kokubo, Ken	1P-1,	1P-2	
Kataoka, Yosuke	1P-7,	2P-19		Komori, Fumio	3P-29		
Kataura, Hiromichi	2-3,	2-5,	3P-4	Konabe, Satoru	1P-35		
Kato, Azusa	2P-5			Kono, Junichiro	1S-1,	1P-31	
Kato, Masachika	3P-20			Kozawa, Akinari	2P-15		
Kato, Masaru	2-9,	3P-27		Krüger, Peter	3P-35		
Kato, Tatsuhisa	1P-5,	2P-5		Kumagai, Ryota	3P-27		
Kato, Toshiaki	1-5,	2P-18,	3P-22,	Kumamoto, Akihito	1-12,	3P-19	
	3P-33			Kunisada, Yuji	2P-22		
Kauppinen, Esko	1P-14			Kurogi, Ruriko	1P-26		
Kawai, Hideki	3P-37			Kuwahara, Yuki	3P-11		
Kawai, Tsuyoshi	1P-13,	3P-14					
Kawano, Saki	2P-4			< L >			
Kawano, Yukio	2P-12,	3-3		Laszczyk, Karolina	1-4		
Kawarada, Hiroshi	2-11.	2P-35		Li, Chao	3P-33		
Kida, Tetsuya	2-10			Li, Juxian	3-3		
Kihara, Hideyuki	1P-39			Ling, Xi	2P-33		
Kikitsu, Tomoka	1P-9			Liu, Zheng	3P-32		
Kimura, Hiroe	1P-10						
Kinno, Yasuhiro	3P-39						

< M >

Maddala, Sai Prakash	1P-4	Miyauchi, Yuhei	1-9, 1P-36, 2P-30,
Maeda, Yutaka	1-2		2P-31, 2P-37, 3P-32,
Maekawa, Yuki	1-5	Mizobuchi, Kyohei	3P-34
Magnin, Yann	3P-18	Mizuno, Takumi	2P-25
Maniwa, Yutaka	1P-22, 1P-35, 2P-28,	Mori, Shohei	3P-1
	2P-32, 2P-34, 3P-32,	Morimoto, Shingo	2P-32
	3P-37	Morimoto, Shingo	1P-24
Maruyama, Mina	2P-29	Morimoto, Takahiro	3P-17
Maruyama, Shigeo	1-3, 1P-14, 2-2,	Moriwaki, Kazuyuki	3P-1
	3P-15, 3P-17, 3P-18,	Mouri, Shinichiro	2P-30, 3P-34
	3P-19, 3P-21	Murakami, Shinichi	2-8
Maruyama, Takahiro	1P-18, 1P-21, 2P-15,	Murakoshi, Kei	1P-15, 3P-27, 3P-28
	2P-21	Murata, Yasujiro	2P-5
Masuda, Hideki	2P-35	Muto, Marika	2-9
Matsubara, Manaho	2P-27		
Matsuda, Iwao	3P-29	< N >	
Matsuda, Kazunari	1-9, 1P-36, 2P-30,	Nagase, Shigeru	1-2, 2-4
	2P-31, 2P-37, 3P-34	Nakagawa, Ayano	1P-5, 3P-5
Matsumae, Takashi	1P-33	Nakagawa, Noritoshi	2P-23, 2P-24, 2P-25
Matsumoto, Fukashi	3P-1	Nakagawa, Takafumi	2P-3
Matsumoto, Morihiko	3-6	Nakahara, Hitoshi	3P-6
Matsumoto, Naoyuki	2P-17	Nakamura, Eiichi	1-12, 1P-4, 2P-2
Matsumoto, Yasumichi	1P-26, 1P-28, 1P-30,	Nakamura, Yasushi	1-13
	2-8, 2-10	Nakanishi, Terunobu	1P-20
Matsunaga, Masahiro	1-10, 3P-35	Nakanishi, Waka	2P-2
Matsuno, Yutaka	1-6, 1P-29	Nakashima, Koji	3P-27
Matsuo, Yutaka	1-3, 2P-3, 3-8,	Nakashima, Naotoshi	1P-11, 1P-19, 2P-7,
	3P-2		3P-16
Matsuzawa, Yoko	1P-39	Nakashima, Yuki	1P-11
Minami, Kosuke	2P-2	Nakayasu, Yuta	3P-24
Minami, Shun	1-2	Naramura, Takuro	2-11
Minamimoto, Hiro	3P-28	Naritsuka, Shigeeya	1P-18, 1P-21, 2P-15,
Miyamoto, Yoshiyuki	3-1, 3P-23		2P-21
Miyata, Yasumitsu	1S-2, 1P-17, 1P-22,	Nihey, Fumiyuki	3P-11, 3P-36
	1P-35, 2P-28, 2P-32,	Niibe, Masahito	2P-36
	2P-34, 3P-32	Nishijima, Satomi	3P-26
		Nishikawa, Koushi	3P-6
		Nishimura, Kanako	3P-16

Nishimura, Tomoaki	1P-24	Omachi, Haruka	1P-17, 3P-5, 3P-20,
Nishino, Akane	1-2		3P-39
Niwase, Keisuke	2P-36	Omori, Kengo	2-7
Noda, Suguru	2P-16, 2P-38	Onitsuka, Hisashi	2P-7
Nonoguchi, Yoshiyuki	1P-13, 3P-14	Osawa, Toshio	2P-38
Nouchi, Ryo	3-6	Oshima, Azusa	2P-17
Nugraha, Ahmad R.T.	1P-31, 1P-32, 2P-9	Oshima, Shuntaro	2P-8
		Oshima, Takumi	1P-2
		Otsuka, Keigo	3P-15
		Ozono, Keita	1P-19
< O >		< P >	
Ochiai, Yuichi	1-10, 3P-35	Prassides, Kosmas	3-9
Oda, Shunri	2P-12, 3-3	Prato, Maurizio	3P-39
Ogata, Chikako	1P-26 , 1P-30	Pu, Jiang	3P-11
Ogata, Hironori	1P-7, 1P-24 , 2P-4,		
	2P-19	< Q >	
Ogawa, Seigo	1P-18	Qian, Yang	2-2
Ogawa, Shun	1P-22 , 2P-28	Qin, Feng	1P-9
Ogawa, Yu	3P-29	< R >	
Ogumi, Keisuke	2P-3	Robertson, John	2-6
Ohba, Hironori	1P-16	Rubio, Angel	3P-23
Ohfuchi, Mari	3-1		
Ohno, Munekazu	1-5	< S >	
Ohno, Toshinobu	3P-1	Saida, Takahiro	1P-18, 2P-15
Ohno, Yutaka	1P-17, 2P-14, 3P-10,	Saito, Naoto	3S-7
	3P-12, 3P-13	Saito, Riichiro	1-1 , 1P-31, 1P-32,
Ohta, Yutaka	3P-25		2-5, 2P-9, 2P-33
Ohyama, Shinnosuke	2-2	Saito, Susumu	1-11, 2-1 , 2P-8
Okada, Hiroshi	3P-2	Saito, Takeshi	3P-11
Okada, Masaru	3P-29	Saito, Tetsuki	1P-35, 2P-34
Okada, Susumu	1-8, 1P-6, 1P-27,	Saito, Yahachi	3P-6
	1P-34, 1P-37, 2P-27,	Sakaguchi, Norihito	2P-22
	2P-29, 3P-9, 3P-30,	Sakaguchi, Takahiro	1P-14
	3P-37	Sakai, Yuji	1P-31
Okada, Toshihiko	2P-1	Sakuraba, Shun	2P-6
Okamoto, Naofumi	1P-38	Sakurada, Ryuji	1P-35
Okazaki, Kozo	3P-29		
Okazaki, Toshiya	2P-15, 2P-37, 3P-17		
Okochi, Takeshi	1P-14		
Okudaira, Saki	2P-37		

Sakurai, Hidehiro	1P-1,	2P-1	Sugime, Hisashi	2-6,	2P-16,	2P-38
Sakurai, Shunsuke	1-4,	1P-10	Suko, Hiroki	1P-14		
Sandhaya, Koirala	1P-36		Sundaram, Rajyashree	2P-10		
Sano, Masahito	1-6,	1P-29	Suzuki, Daichi	2P-12,	3-3	
Sasaki, Fusako	3P-11		Suzuki, Daisuke	3P-31		
Sasaki, Shogo	2P-28,	2P-32,	3P-32	Suzuki, Hakuto	3P-29	
Sato, Hikaru	1-6,	1P-29	Suzuki, Hiroo	1-5,	3P-22	
Sato, Naomichi	2-5		Suzuki, Mitsuaki	1-2,	2-4	
Sato, Nozomi	1P-1		Suzuki, Seiya	3-2		
Sato, Yusuke	3P-27		Syrgiannis, Zois	3P-39		
Sato, Yuta	3P-8					
Sato, Yutaka	1P-7,	1P-24	< T >			
Sato, Yu-uya	1-6,	1P-29	Taguchi, Eiji	2P-36		
Sekiguchi, Atsuko	1-4,	2P-10	Taguchi, Tomitsugu	1P-16		
Shi, Wu	1P-9		Taira, Remi	3P-30		
Shibata, Masanobu	2-11		Tajima, Kentaro	3P-25		
Shibata, Naoya	1-12		Takabayashi, Yasuhiro	3-9		
Shibuta, Yasushi	1-5		Takada, Tomoya	1P-12		
Shigekawa, Hidemi	1P-20,	1P-35,	2P-32	Takagi, Yukai	3P-18	
Shih, Ching-Hua	1P-40		Takai, Kazuyuki	3P-25,	3P-26,	3P-31
Shima, Hiroyuki	1-13		Takano, Yuta	2-4		
Shimizu, Hideyuki	3P-2		Takao, Yuko	3P-1		
Shin, Shik	3P-29		Takashima, Kengo	1P-35,	2P-26	
Shinohara, Hisanori	1P-5,	1P-17,	1P-20,	Takatsuka, Takayuki	3P-7	
	3P-5,	3P-20,	3P-39	Takehana, Yuya	1-2	
Shintani, Yukihiro	2-11		Takei, Kuniharu	1P-23,	1P-25,	2P-11,
Shiozawa, Hidetsugu	3-7			2P-13		
Shiraki, Kentaro	2P-6		Takeuchi, Osamu	1P-20,	1P-35	
Shiraki, Tomohiro	2P-7		Takeuchi, Takahiro	2P-32		
Shrestha, Lok Kumar	2P-2		Takezaki, Hiroki	2-2		
Someya, Takashi	3P-29		Takikawa, Hirofumi	1-13		
Sorimachi, Jun-ya	1P-37		Tamura, Naoki	3P-24		
Sota, Masaki	3P-21		Tan, Dezhi	1-9		
Srinivasan, Sanjay K.	1P-31		Tan, Fu-Wen	3P-12		
Suda, Yoshiyuki	1-13		Tanaka, Fumiaki	1-4		
Suenaga, Kazutomo	2P-32,	3P-8,	3P-32	Tanaka, Motomu	1P-4	
Suga, Tadatomo	1P-33		Tanaka, Takeshi	2-3,	2-5,	2P-6
Sugahara, Mitsunari	3P-37		Taniguchi, Takaaki	1P-26		

Taniguchi, Takashi	1P-35, 2P-34	Wang, Zhiyong	3P-5
Tanno, Shun	3P-27	Watanabe, Hiroshi	3P-29
Tashima, Keiichiro	3P-29	Watanabe, Kenji	1P-35, 2P-34
Tashita, Ryo	2-4	Watanabe, Takayuki	1P-10
Tatsumi, Yuki	2P-33	Wato, Yuta	3P-22
Tenne, Reshef	1P-9	Wei, Xiaojun	2-3, 2-5
Terasawa, Mititaka	2P-36	Wu, Cheng	3P-17
Thendie, Boanerges	1P-17		
Tobe, Yoshito	3-5	< X >	
Tomai, Takaaki	3P-24	Xiang, Rong	1P-14, 2-2, 3P-17,
Tonouchi, Noriyuki	3P-11		3P-19 , 3P-21
Toshimitsu, Fumiyuki	1P-19, 3P-16	Xu, Bin	2P-18
Toyama, Kiyohiko	3P-36		
Toyoda, Masayuki	2P-8	< Y >	
Tsuchiya, Bun	2P-20	Yagi, Ichizo	2-9, 3P-27
Tuan Hung, Nguyen	2P-9	Yamada, Asataro	3P-26
		Yamada, Hiroko	3P-38
< U >		Yamada, Jumpei	1P-21, 2P-21
Uchibori, Yosuke	1P-15	Yamada, Junya	1-12
Ue, Hitoshi	1-13	Yamada, Michio	1-2
Ueda, Naomasa	3P-21	Yamada, Ryo	2P-38
Ueda, Yuki	1P-21 , 2P-21	Yamada, Takeo	1-4, 2P-10
Uenuma, Mutsunori	1P-38	Yamada, Tetsushi	3P-35
Uji-i, Hiroshi	3-5	Yamagishi, Miho	3P-20
Ukai, Hiroyuki	3P-18	Yamaguchi, Takahisa	1P-5
Ukhtary, M. Shoufie	1P-31, 1P-32	Yamakoshi, Yoko	3S-8
Umeyama, Tomokazu	3-4 , 3P-8	Yamamoto, Daichi	1P-21, 2P-21
Uraoka, Yukiharu	1P-38	Yamamoto, Hiroyuki	1P-2
Ushiyama, Takuya	2P-14 , 3P-13	Yamamoto, Shunya	1P-16
		Yamamoto, Susumu	3P-29
< V >		Yamamoto, Takahiro	1P-35, 2P-26
Viet, Nguyen	3P-13	Yamamoto, Takashi	3P-29
		Yamanaka, Ayaka	1-8 , 3P-30
< W >		Yamanaka, Tomoki	1-10
Wang, Guowei	2-3	Yamaoka, Takao	1P-36
Wang, Minjie	1P-31	Yamashina, Tomoki	3P-25
Wang, Xiaofan	1-9, 2P-31	Yamashita, Ichiro	1P-38
Wang, Zhipeng	1P-24	Yanagi, Kazuhiro	1P-8, 3P-37

Yanai, Kouhei	2P-23, 2P-24
Yang, Teng	2P-33
Yasuda, Hidehiro	1-7
Yasuda, Kensuke	3P-28
Yasuda, Masaaki	2P-11
Yasuda, Satoshi	1P-15, 2-7, 3P-27, 3P-28
Yasunishi, Tomohiro	3P-10 , 3P-12
Yokokura, Eita	1P-7, 2P-19
Yomogida, Yohei	1P-8 , 2-5, 3P-37
Yoshida, Masaro	1P-9
Yoshida, Masaru	1P-39
Yoshida, Shoji	1P-20, 1P-35, 2P-32
Yoshida, Takahiro	2P-20
Yoshikawa, Ryo	3P-18
Yoshimura, Masamichi	3-2
Yoshimura, Shintaro	2P-28
Yoshitake, Haruhiko	1P-24
Yudasaka, Masako	2P-37, 3P-36
Yuge, Ryota	3P-36
Yumura, Motoo	1P-10

< **Z** >

Zadik, Ruth H.	3-9
Zak, Alla	1P-9
Zhang, Hong	3P-23
Zhang, Jin	2S-4
Zhang, Wenjin	3P-34
Zheng, Liu	2P-32
Zhou, Biao	3P-2
Zhou, Ruifeng	3P-28

複写をご希望の方へ

フラーレン・ナノチューブ・グラフェン学会は、本誌掲載著作物の複写に関する権利を一般社団法人学術著作権協会に委託しております。

本誌に掲載された著作物の複写をご希望の方は、(社)学術著作権協会より許諾を受けて下さい。但し、企業等法人による社内利用目的の複写については、当該企業等法人が社団法人日本複写権センター((社)学術著作権協会が社内利用目的複写に関する権利を再委託している団体)と包括複写許諾契約を締結している場合にあっては、その必要はございません(社外頒布目的の複写については、許諾が必要です)。

権利委託先：一般社団法人学術著作権協会

〒107-0052 東京都港区赤坂 9-6-41 乃木坂ビル 3階

電話：03-3475-5618 FAX：03-3475-5619 E-Mail：info@jaacc.jp

注意：複写以外の許諾(著作物の引用、転載・翻訳等)に関しては、(社)学術著作権協会に委託致していません。直接、フラーレン・ナノチューブ・グラフェン学会へお問い合わせください。

Reprographic Reproduction outside Japan

- ・ Making a copy of this publication

Please obtain permission from the following Reproduction Rights Organizations (RROs) to which the copyright holder has consigned the management of the copyright regarding reprographic reproduction.

- ・ Obtaining permission to quote, reproduce; translate, etc.

Please contact the copyright holder directly.

Users in countries and regions where there is a local RRO under bilateral contract with Japan Academic Association for Copyright Clearance(JAC) are requested to contact the respective PROs directly to obtain permission.

Users in countries or regions in which JAC has no bilateral agreement are requested to apply for the license to JAC.

Japan Academic Association for Copyright Clearance (JAC)

Address : 9-6-41 Akasaka, Minato-ku, Tokyo 107-0052 Japan

Website : <http://www.jaacc.jp/>

E-mail : info@jaacc.jp TEL : 81-3-3475-5618 FAX : 81-3-3475-5619

2016年9月7日発行

第51回フラーレン・ナノチューブ・グラフェン総合シンポジウム 講演要旨集

<フラーレン・ナノチューブ・グラフェン学会>

〒113-8656 東京都文京区本郷 7-3-1

東京大学大学院工学系研究科 機械工学専攻

丸山研究室内

Tel : 03-3830-4848

Fax : 03-3830-4848

E-mail : fntg@photon.t.u-tokyo.ac.jp

URL : <http://fullerene-jp.org>

印刷 / 製本 北海道大学生生活協同組合 印刷・情報サービス部

GRAND ARM

Atomic Resolution electron Microscope

JEM-ARM300F

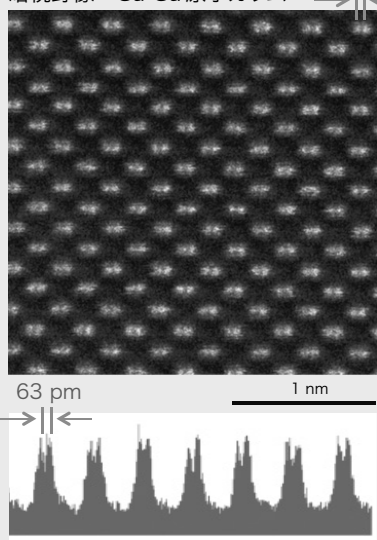
JEM-ARM300Fは、JEM-ARM200Fで培った高安定化技術を基に開発された装置です。

冷陰極電界放出電子銃を標準搭載し、STEMおよびTEMに球面収差補正装置が

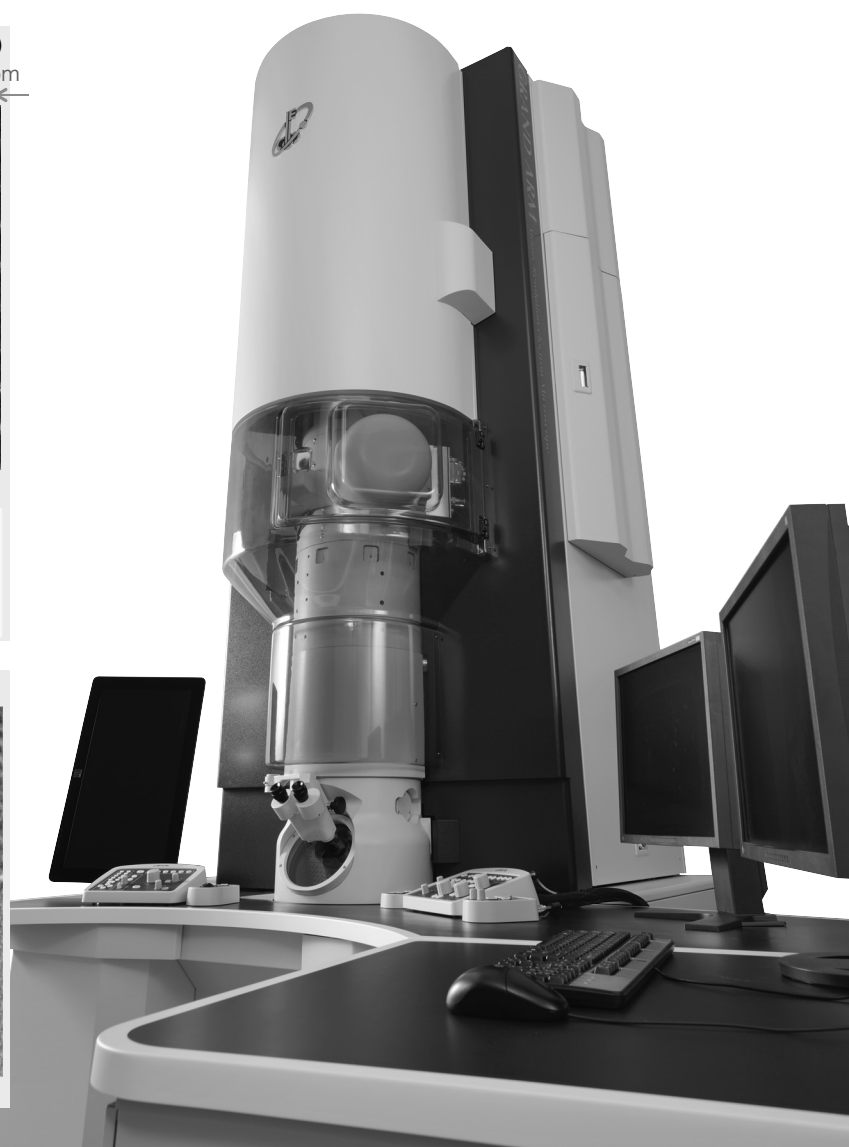
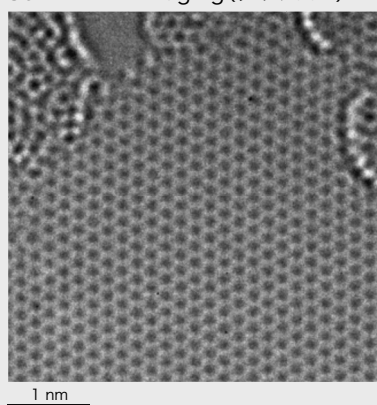
搭載可能な最高加速電圧300 kVの世界最高峰の超高分解能電子顕微鏡です。

300 kV STEM Imaging (GaN[211])

暗視野像 Ga-Ga 原子カラム 63 pm



80 kV TEM Imaging (グラフェン)



JEOL 日本電子株式会社

本社・昭島製作所 〒196-8558 東京都昭島市武蔵野3-1-2 TEL:(042)543-1111(大代表) FAX:(042)546-3353
www.jeol.co.jp ISO 9001・ISO 14001 認証取得

JEOLグループは、「理科学・計測機器」「産業機器」「医用機器」の3つの事業ドメインにより事業を行っております。

「理科学・計測機器事業」電子光学機器・分析機器・計測検査機器 「産業機器事業」半導体関連機器・産業機器 「医用機器事業」医用機器

“はかる”技術で未来を創る

ResiTest8400 比抵抗/ホール測定システム

高感度測定で 次世代半導体を評価

「ResiTest8400型」は、東陽テクニカが開発した《ACホール起電圧測定法》と米国LakeShore社開発の《低ノイズ電圧アンプ》を採用する事により、従来のResiTest8300型よりも、60倍高感度のホール測定を可能にしました。

特長

- ホール移動度 : $0.001\text{cm}^2/\text{V}\cdot\text{s}$ 以上
(端子間抵抗 $10^8\Omega$ 以下)
- 比抵抗 : $10^{-8}\Omega\text{cm}\sim 10^9\Omega\text{cm}$
(試料厚み=1 μm)
- 幅広い温度範囲: 4.2K \sim 1073K(800 $^{\circ}\text{C}$)

アプリケーション例

- 太陽電池材料 : a-Si、p-Si、CIGS
- 透明電極 : IGZO、グラフェン
- パワー半導体 : GaN、SiC
- ワイドバンドギャップ半導体
- 有機物半導体

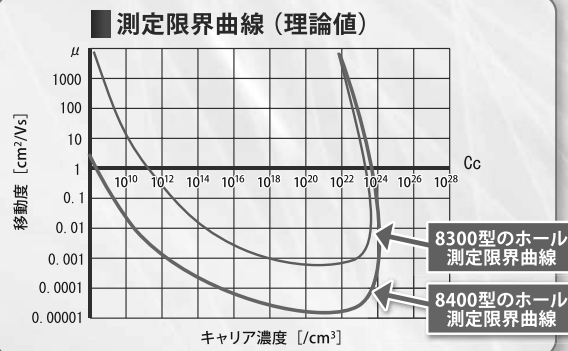


ResiTest8400型
(ResiTest8300型後継機種)

米国 LakeShore 社との
共同開発により
ホール起電圧測定感度が
従来の60倍に!

測定例 太陽電池材料のHall測定結果

	測定結果
ホール移動度 [cm^2/Vs]	1.40E+00
キャリアタイプ	P
キャリア濃度 [$/\text{cm}^3$]	1.48E+12
ホール係数 [cm^3/C]	4.22E+06
抵抗率 [Ωcm]	3.02E+06
シート抵抗 [$\Omega\Box$]	3.02E+10



 **東陽テクニカ** [www.toyo.co.jp / material /](http://www.toyo.co.jp/material/)

 **Lake Shore**
CRYOTRONICS

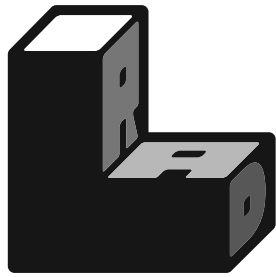
株式会社 東陽テクニカ
理化学計測部

〒103-8284 東京都中央区八重洲1-1-6
TEL.03-3279-0771 E-Mail: lakeshore@toyo.co.jp

本カタログに記載された商品の機能・性能は 断り無く変更されることがあります。

大阪支店 〒532-0003 大阪府大阪市淀川区宮原1-6-1 (新大阪ブリックビル) TEL.06-6399-9771
名古屋営業所 〒465-0095 愛知県名古屋市名東区高社1-263 (一社中央ビル) TEL.052-772-2971
宇都宮営業所 〒321-0953 栃木県宇都宮市東宿郷2-4-3 (宇都宮大塚ビル) TEL.028-678-9117

未採択の申請書 を利用した オープンイノベーションプラットフォーム



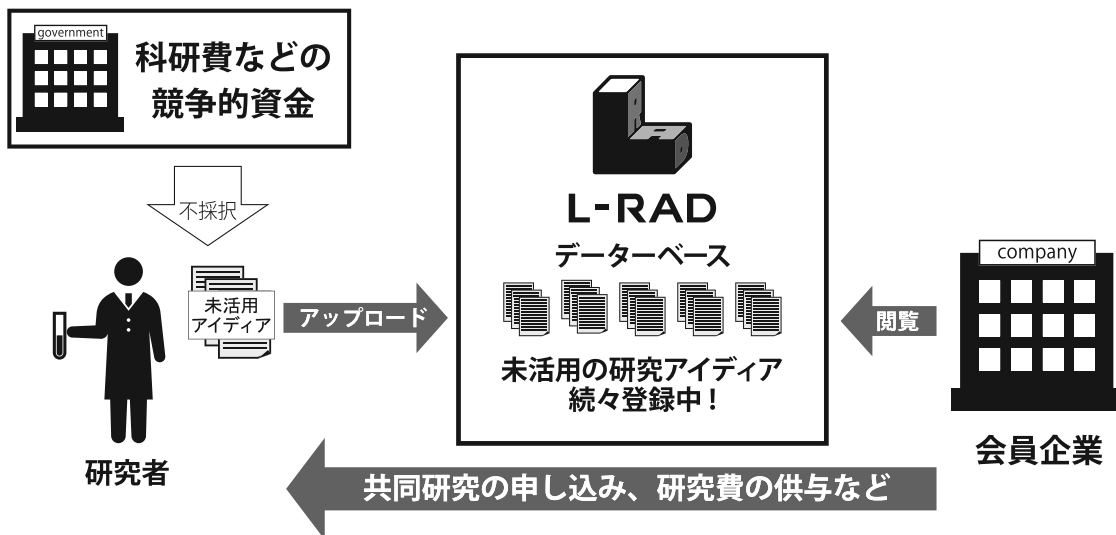
- エルラド -

L-RAD

リバネス - 池田 研究開発促進システム powered by COLABORY

L-RAD に登録して 研究費を獲得しませんか？

「L-RAD(エルラド)」は研究者と企業の共同研究を支援するオープンイノベーションプラットフォームです。研究予算がつかなかった未活用のアイデアを登録することにより、企業の資金を獲得する機会を得られます。



詳細はコチラ！

 株式会社 池田理化

<http://www.ikedarika.co.jp>

本社

〒101-0044 東京都千代田区鍛冶町1-8-6 神田KSビル
TEL:03-5256-1811 FAX:03-5256-1818

八王子支店 TEL:042-642-0570
小金井支店 TEL:0422-39-5441
鶴見支店 TEL:045-501-5881
横浜支店 TEL:045-983-0491
藤沢支店 TEL:0466-54-0300
平塚支店 TEL:0463-37-4711
三島支店 TEL:055-975-0975
藤枝支店 TEL:054-644-5551
名古屋支店 TEL:052-249-8350

大阪支店 TEL:06-6136-1255
岩国支店 TEL:0827-21-6701
千葉支店 TEL:043-290-4055
つくば支店 TEL:029-836-6611
埼玉支店 TEL:049-245-7831
高崎支店 TEL:027-320-7735
宇都宮支店 TEL:028-610-3722
仙台支店 TEL:022-217-7037
札幌支店 TEL:011-208-2822

Hitachi Koki

HITACHI

Inspire the Next

カーボンナノチューブの
分離・精製に

日立の超遠心機シリーズ!

バイオ研究 & ナノ粒子研究 の強い味方 世界トップクラスの高性能、床置き・卓上、日立なら選べます!

小形超遠心機

エコでスリムな
床置きタイプ

himac CS-FNX

Series

世界最高速150,000rpm* (CS150FNX)
世界最大遠心加速度1,050,000×g* (CS150FNX)
クラス最静音45dB(A)*
省スペース床置きタイプの小形超遠心機は日立だけ!

特長

- 世界標準の安全規格CEマーキング適合製品
- サンプルのバランスは目分量でOK!
- ロータは全て載せるだけ! (ロータクイックセッティング方式)
- エコ対応省エネモデル
- 7mlスイングロータ(S50ST)が回せます。
- 2012年度グッドデザイン賞受賞!

仕様

形名	CS150FNX	CS120FNX	CS100FNX
最高回転速度 (rpm)	150,000	120,000	100,000
最大遠心加速度 (xg)	1,050,000	771,000	571,000
サイズ (W×D×H mm)	440×520×910		
質量 (kg)	105		
標準価格 (税別)	¥5,500,000	¥4,900,000	¥4,300,000



卓上超遠心機

コンパクトなボディに
世界トップクラスの性能

himac CS150NX

世界最高速150,000rpm*
世界最大遠心加速度1,050,000×g*
世界最小コンパクトサイズ*
クラス最静音45dB(A)*

特長

- 短い真空待ち時間
- サンプルのバランスは目分量でOK!
- ロータは全て載せるだけ!
- 7mlスイングロータが回せます。

仕様

形名	CS150NX
最高回転速度 (rpm)	150,000
最大遠心加速度 (xg)	1,050,000
サイズ (W×D×H mm)	590×582×408
質量 (kg)	97
標準価格 (税別)	¥6,000,000



* (2016年6月現在
当社調べによる)



ロータ仕様

形名	S110AT	S50A	S50ST
最高回転速度 (rpm)	110,000	50,000	50,000
容量 (ml) × 本数 (本)	5.0×8	30.0×6	7.0×4
標準価格 (税別)	¥1,100,000	¥950,000	¥1,500,000

形名	S140AT	S58A	S55A2
最高回転速度 (rpm)	140,000	58,000	55,000
容量 (ml) × 本数 (本)	2.0×10	13.5×8	1.5×12
標準価格 (税別)	¥1,290,000	¥1,000,000	¥750,000

バイオ研究 & ナノ粒子研究 のスタンダード

超遠心機



遠心分離が楽しくなる
機能満載!

himac CP-NX

Series

クラス最高速100,000rpm* (CP100NX)
クラス最大遠心加速度803,000×g* (CP100NX)
* (2016年6月 現在当社調べによる)

特長

- 離れていても運転状況がわかるLEDインジケータ搭載!
- ロータ寿命自動管理と寿命延長機能搭載 (RLMアダプタ付ロータ)
- カラー液晶タッチパネルを操作しやすい前面に配置
- ユーザー支援ソフト「himac ASSIST」標準装備
- 2014年度グッドデザイン賞受賞!

仕様

形名	CP100NX	CP90NX	CP80NX
最高回転速度 (rpm)	100,000	90,000	80,000
最大遠心加速度 (xg)	803,000	700,000	615,000
サイズ (W×D×H mm)	790×690×880 (テーブルまでの高さ863)		
質量 (kg)	390		
標準価格 (税別)	¥11,000,000	¥9,500,000	¥8,000,000



ロータ仕様

形名	P100AT2	P70AT	P45AT	P21A2	P40ST	P32ST	P28S
最高回転速度 (rpm)	100,000	70,000	45,000	21,000	40,000	32,000	28,000
呼称容量 (ml) × 本数 (本)	6.5×8	40×8	94×6	230×6	13×6	40×6	40×6
標準価格 (税別)	¥2,250,000	¥2,200,000	¥2,350,000	¥1,800,000	¥2,490,000	¥2,480,000	¥2,350,000

※本広告に掲載した以外にもロータを取り揃えております。最寄りの営業所へお気軽にお問い合わせください。

【製造・販売・保守】

日立工機株式会社 ライフサイエンス機器事業部

東日本地区 03-6738-0860

西日本地区 0798-23-4125

日立遠心機お客様相談センター ☎ 0120-024125

受付時間 9:00~12:00 / 13:00~17:00 (土・日・祝日・弊社休業日除く)

URL <http://www.hitachi-koki.co.jp/himac/>

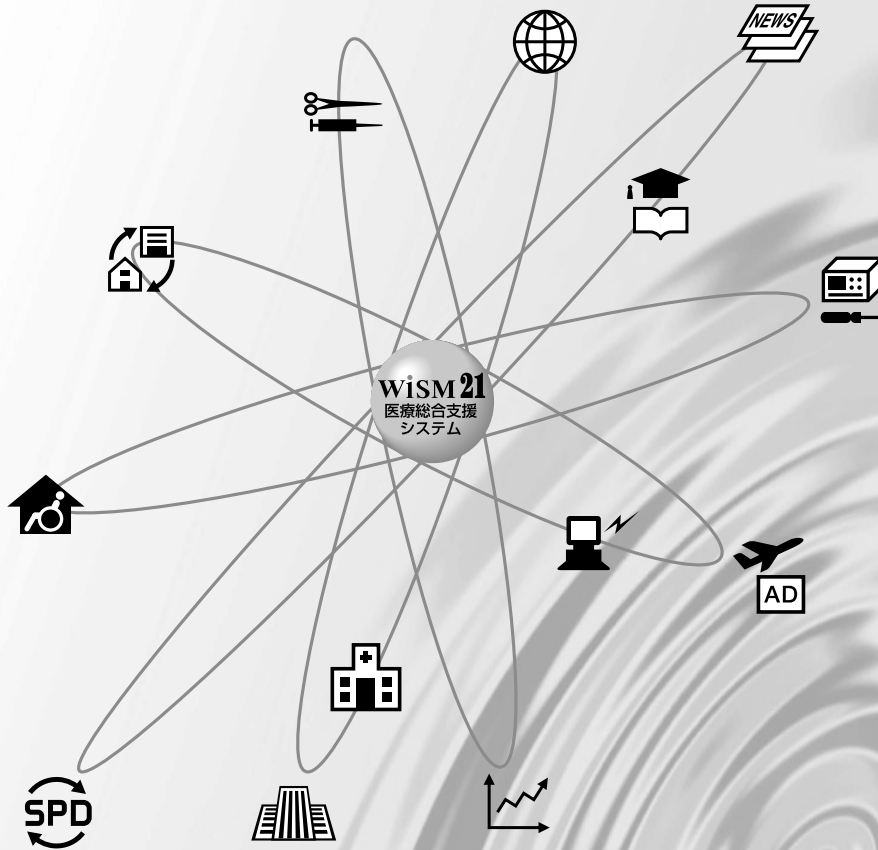
- 製品の仕様、外観および価格は、改善のため予告なく変更する場合があります。
- 標準価格は仕様や構成により異なります。
- 全て税別価格となります。
- 安全のために使用環境、使用条件、据付条件が制限される場合があります。



WISM 21 ウィズム21
ムトウの医療総合支援システム

WISM 21は、21世紀の医療をトータルでサポートし、お客様のニーズと共に成長するシステムです。

病院の近代化が進むなか、取り巻く環境が厳しさを増しつつある医療施設において、WISM 21は医療の変化に対応すべく、お客様のためにご用意させていただいた医療総合支援システムです。必要な時に必要なシステムを選び、ご利用ください。



- 医療・理化学機器の販売・アフターフォロー
- 最新医療情報の提供
- 医療機器の設置・メンテナンス・保守契約
- 学会イベントの企画・運営
- 旅行・広告代理
- 情報システムの提案・開発
- 経営分析・診断・改善
- 資金計画・償還計画・物件調査及び建築
- 大型プロジェクトコンサルティング
- SPNシステム
- 在宅医療・福祉
- 通信販売
- 貿易

総合医療機器商社

WISM 株式会社 ムトウ

取扱品目 医療機器・理化学機器・ME機器・病院設備・放射線機器
メディカルコンピューター・貿易業務・歯科機器・福祉機器・介護用品

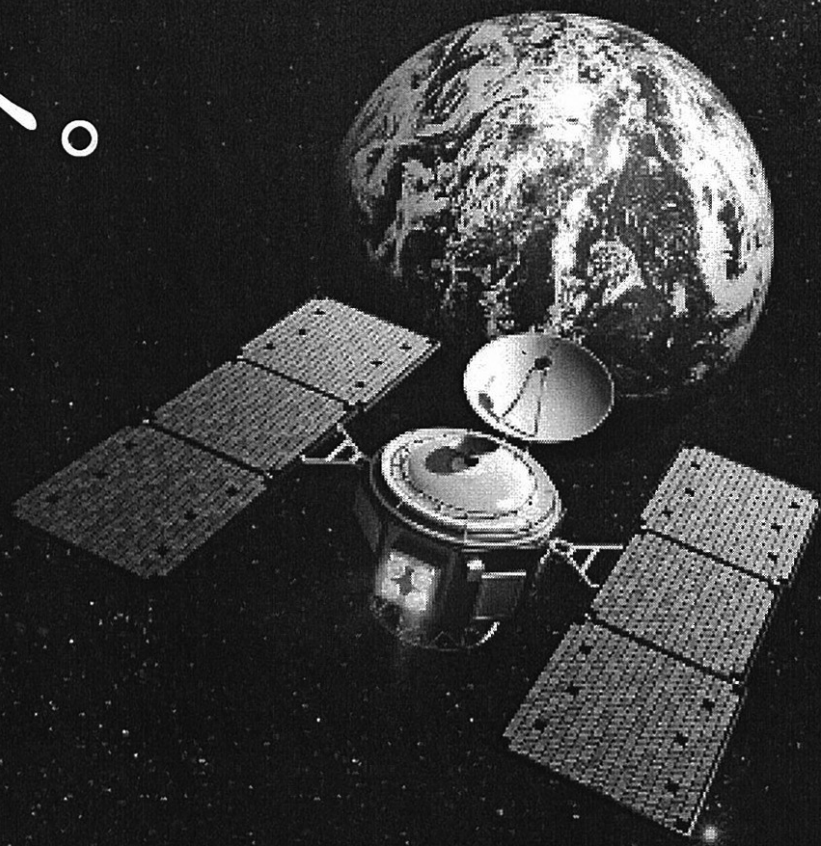
- | | |
|----------------------------|--|
| 札幌本社(北海道事業本部) / 〒001-0011 | 札幌市北区北11条西4丁目1番15号
TEL 011-746-5111 |
| 東京本社(東京事業本部) / 〒110-8681 | 東京都台東区入谷1丁目19番2号
TEL 03-3874-7141 |
| 名古屋支社(名古屋事業本部) / 〒465-0014 | 名古屋市名東区上菅2丁目1108番地
TEL 052-799-3011 |
| 大阪支社(大阪事業本部) / 〒537-0002 | 大阪市東成区深江南2丁目13番20号
TEL 06-6974-0550 |
| 福岡支社(福岡事業本部) / 〒812-0044 | 福岡市博多区千代4丁目29番27号
TEL 092-641-8161 |

支店 / 札幌中央・札幌西・札幌白豊・新札幌・旭川・函館・釧路・帯広・北見・遠紋・八雲・室蘭・苫小牧・日高・小樽・千歳・岩見沢・空知
名士・稚内
秋田・仙台・いわき・群馬・栃木・日立・水戸・茨城・熊谷・埼玉東・埼玉・埼玉中央・所沢・東京西・本郷・城北・城西・城南・城東
多摩・多摩西・武蔵野・練馬・柏・千葉西・千葉・鴨川・神奈川・横浜・横須賀・横浜市大前・川崎・川崎北・相模・成田・名古屋南
伊勢志摩・北大阪・南大阪・西大阪・奈良・広島・鳥取・小倉・飯塚・筑豊・大川・久留米・佐賀・大牟田・唐津

営業所 / 青森・島根
出張所 / 鹿島

<http://www.wism-mutoh.co.jp/>

未来へ。



宇宙の夢と、エア・ウォーター。

たとえば、当社のエンジニアも参加した、国産ロケットH1の開発プロジェクト。

そこで学んだのは「精細なガスコントロール技術」と「絶対にあきらめないスピリッツ」。

その後、世界でこれまでになかった「オンサイト型高純度窒素発生装置-V1シリーズ」の開発に成功。

宇宙の夢と地球の夢をつなげました。

また現在、惑星探査機のイオンエンジンの推進剤として使われる

「キセノンガス」は国内では唯一、当社が製造販売を手がけている貴重な産業ガス。

宇宙の夢とエア・ウォーターはつながっています。

産業ガスのソリューション。広がる事業のイノベーション。
エア・ウォーター



エア・ウォーター株式会社

〒542-0083 大阪市中央区東心斎橋1丁目20番16号
TEL.06-6252-5411 FAX.06-6252-3965
<http://www.awi.co.jp>



北海道エア・ウォーター株式会社

札幌産業支店 市場開発グループ

〒003-0805 札幌市白石区菊水5条2丁目3番12号
TEL.011-811-8822 FAX.011-811-8828
info-hawi-west@awi.co.jp

モデルチェンジ ～スマートなデザインに簡単操作～

BRANSON 超音波ホモジナイザー

長くご愛顧いただいておりますBRANSON超音波ホモジナイザーで新たなモデルが誕生しました。

主な特長

- 1.電気エネルギーから超音波振動への変換効率が95%以上
→ 無駄なエネルギーロスが小さく、安定した振幅が得られる。
- 2.通常では、液体の種類によって振幅が安定し難い。
→ 条件を変えても一定の振幅を保つ機能がついている。
- 3.ジュール (watt/sec) による発振制御が可能
→ Total何ジュールでこの処理が完了するという情報が論文に掲載できる。

20kHz超音波ホモジナイザー
BRANSON SONIFIER SFX250,550

40kHz超音波ホモジナイザー
BRANSON SONIFIER SFX150HH



主なアプリケーション

分散

カーボンナノチューブ 有機顔料 無機顔料 セラミック セメント 感光体 記録材料
磁性粉 粉末冶金 酸化鉄 金属酸化物 シリカ アルミナ カーボンブラック
ポリマー ラテックス 製紙 ファンデーション
研磨剤 電池 フィラー 光触媒 触媒 ワクチン 体外診断薬 歯磨き粉 シャンプー
半導体 電子基盤 液晶 貴金属 金属 宝石 タイヤ 発酵菌類 その他

乳化

エマルジョン製剤 農薬 トナー ラテックス 界面活性剤 クリーム 乳液 その他

日本総代理店

株式会社 **セントラル** 科学貿易

URL <http://www.cscjp.co.jp/>

本社 111-0052 東京都台東区柳橋1-8-1
Tel 03-5820-1500 Fax 03-5820-1515
大阪支店 533-0031 大阪府大阪市東淀川区西淡路1-1-36 新大阪ビル
Tel 06-6325-3171 Fax 06-6325-5180
福岡営業所 812-0016 福岡県福岡市博多区博多駅南1-2-15 事務機ビル
Tel 092-482-4000 Fax 092-482-3797
札幌出張所 001-0911 北海道札幌市北区新琴似11条7-13-2
Tel 011-764-3611 Fax 011-764-3612

心豊かな 地球環境の創造

科学技術・バイオ研究の発展と共に歩み続けます

機器のアフターサービスに於いても
絶大な信頼をいただいております。

S-COOS

Smart - Communication Online and Ordering System

[バイオ関連試薬、機器・理化学分析機器]

 **北海道和光純薬株式会社**

本社 / 〒001-0015 札幌市北区北15条西4丁目
TEL011-747-2811 FAX011-747-2934

営業所 / 旭川・函館・道央・苫小牧

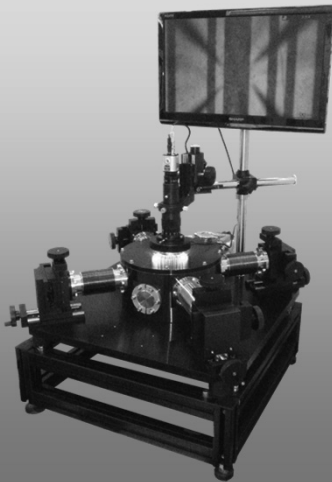
ご注文専用アドレス hokkaido@hwako.com
当社ホームページ <http://www.hwako.com>
S-COOS <http://www.s-coos.com>

Life3S

たえず進歩し続けるテクノロジーがめざすもの、もたらすものは何か？
科学技術 (Study) ・医療分野 (Support) ・地球環境 (Safety) の
それぞれに携わることで、得られた結論=生命 (Life)。



真空<低温>プローバシステム



■低温・高温オプションにて 極低温から高温まで温度を選択可能

■標準構成

- 1) システムチャンバー
- 2) マニピュレーター 2式
- 3) CCDカメラ&モノスコープ
- 4) 液晶モニター
- 5) アルミ製スタンド

■標準仕様

温度範囲: 室温
プローブ数: 2本
コネクタ: BNCコネクタ

■オプション

- 1) 低温・高温オプション
 - ・液体窒素冷却ユニット(80K~500K)
 - ・高温ユニット(室温~500K)
 - ・スターリング冷凍機ユニット(50K~室温)
 - 2) 温調器ユニット
 - 3) マニピュレーター追加(最大2式)
 - 4) ロードロック機構
- その他オプション、アクセサリは
お問い合わせください。

0.1Wトップロード冷凍機システム



■AC100V・空冷式コンプレッサーを採用 ■サンプル交換が容易なトップロードシステム

■構成

- 1) コールドヘッド
- 2) コンプレッサー
- 3) Heガスホース
- 4) クライオスタット
- 5) サンプルロッド
- 6) システムスタンド

■仕様

最低到達温度: 4K台
温度範囲: 4K台~300K
冷凍機能力: 0.1W@4.2K
サンプルスペース: φ22mm
入力電源: 100V
冷却方式: 空冷式

冷凍機・プローバシステムの改造も承っております!
(改造例)・トップロード冷凍機システム ・再凝縮クライオスタット ・冷凍機プローバシステム など

◆ 詳細は Website まで <http://www.systembrain.co.jp>

販売



SystemBrain

株式会社システムブレイン

本社 〒003-0021 北海道札幌市白石区栄通9-5-8
電話 011-851-9944 FAX 011-851-9969
東京営業所 〒333-0831 埼玉県川口市木曾呂681-4
電話 048-494-0348 FAX 048-494-1431
システム機器部 〒305-0043 茨城県つくば市大角豆638-2
電話 029-860-8001 FAX 029-860-8002
support@systembrain.co.jp http://www.systembrain.co.jp

製造



Thermal Block Company

株式会社サーマルブロック

本社・工場
〒333-0831 埼玉県川口市大字木曾呂681-4
電話 048-430-7545 FAX 048-430-7546
support@thermalblock.co.jp http://thermalblock.co.jp

エイジングケアの最高峰 “フラーレン”

【特徴】

- ・抗酸化力はビタミンCの250倍以上
- ・多くの活性酸素を満遍なく除去し、その効果は長時間続く
- ・発見者はノーベル化学賞を受賞
- ・著名研究者との共同研究による豊富なエビデンス

水溶性フラーレン：ラジカルスポンジ



表示名称：フラーレン、PVP、BG、水

- 強くて持続性のある抗酸化力
- あらゆる製品へ容易に配合可能
- 採用実績「No.1！」



油溶性フラーレン：リポフラーレン



表示名称：フラーレン、スクワラン

- 強くて持続性のある抗酸化力
- 植物性スクワラン使用
- 「オイルリッチな製品」に最適



パウダー状フラーレン：ヴェールフラーレン



表示名称：フラーレン、シリカ

- 肌の外側で抗酸化力を発揮
- フラーレンの「美容効果」がある粉末原料
- メイクアップ・スキンケアパウダー製品等を差別化



リポソーム化用フラーレン：モイストフラーレン



表示名称：フラーレン、水添レシチン、フィトステロールズ、BG

- 抗酸化力に「保湿と浸透性」をプラス
- 肌なじみの良いテクスチャー
- オリジナルカプセル処方差別化



お問い合わせ先：

ビタミンC60バイオリサーチ株式会社

<http://www.vc60.com/>

〒103-0028 東京都中央区八重洲1-3-19 辰沼建物9F

TEL: 03-3517-3251 FAX: 03-3517-3260

E-mail: info@vc60.com

超安定型マウントPolaris™シリーズ

精密アライメントを追求した光学マウント

特長

- 温度変化による光軸ズレを最小限に抑制
- 真空用途 10^{-9} Torr以下にも対応*
- 標準型、SMネジ付き、低歪み、ピエゾアジャスタ付き、固定式のミラーマウントのほか、プラットフォームマウントをラインナップ
- ポストやクランプアームなど専用アクセサリも充実 *一部対応していない製品もございます。



■ Polarisシリーズのラインナップ (抜粋)



● Polarisシリーズの全ラインナップは当社ウェブサイトをご参照ください。

仕様のカスタマイズやOEM用途にも対応いたします。詳細は当社までお問い合わせください。

www.thorlabs.co.jp

E-mail: sales@thorlabs.jp

THORLABS

ソーラボジャパン株式会社

〒170-0013 東京都豊島区東池袋2-23-2 TEL : 03-5979-8889 FAX : 03-5979-7285



その未来、ゼオン。

みんなの夢を、独創的な技術でスピーディに実現してゆくこと。

世界が驚く新素材を開発し、社会に貢献してゆくこと。

それが、私たちゼオンの使命です。

自動車をはじめ、航空機、デジタル家電、エネルギー、医療…

世界中のさまざまな分野で私たちの製品は活躍しています。

あなたが見つめる未来、ゼオンが化学の力で今日にします。

化学の力で未来を今日にする

ZEON



世界最速、最高画質のラマン分光イメージング。

Nanophoton products | Laser Raman Microscope

高速・高分解能レーザーラマン顕微鏡

RAMAN touch

極板上の成分分散を、高速・高分解能でラマンイメージング

- 微細な物質分布を鮮明に捉える、350nmの空間分解能。
- レーザー走査により、ステージやセルを動かさずにイメージング。
- ライン照明による超高速イメージング機能搭載。

Other products

視野を広げた、新しいラマンイメージング。



広視野ラマンスコープ

RAMAN view

- Larger field of view.
- Deeper depth of focus.
- Longer working distance.

前人未達のナノイメージングの世界へ。



先端増強ラマン散乱顕微鏡

TERSsense

- 10 nm spatial resolution.
- Probe is delivered with performance guarantee.

Visit our website for more information: www.nanophoton.jp